Water Waves

Numerical study of the generalized Korteweg-de Vries equations with oscillating nonlinearities and boundary conditions

--Manuscript Draft--

Manuscript Number:	WAWA-D-22-00002R1
Full Title:	Numerical study of the generalized Korteweg-de Vries equations with oscillating nonlinearities and boundary conditions
Article Type:	Original Article
Funding Information:	
Abstract:	The focus here is upon the generalized Korteweg-de Vries equation, $u_t + u_x + p_1 (u^p)_x + u_{xxx} = 0$, where $p = 2, 3, \cdots$. When $p \geq 5$, it is thought that the equation is not globally well posed in time for L^2-based Sobolev class data. Various numerical simulations carried out by multiple research groups indicate that solutions can blowup in finite time for large, smooth initial data. This is known to be the case in the critical case $p = 5$, but remains a conjecture for supercritical values of p. Studied here are methods for controlling this potential blow up. Sev- eral candidates are put forward; the addition of dissipation or of higher order dispersion are two obvious candidates. However, these appar- ently can only work for a limited range of nonlinearities. However, the introduction of high frequency temporal oscillations appear to be more effective. Both temporal oscillation of the nonlinearity and of the bound- ary condition in an initial-boundary-value configuration are considered. The bulk of the discussion will turn around this prospect in fact.
Corresponding Author:	JERRY L. BONA, Ph.D. University of Illinois at Chicago Chicago, Illinois UNITED STATES
Corresponding Author Secondary Information:	
Corresponding Author's Institution:	University of Illinois at Chicago
Corresponding Author's Secondary Institution:	
First Author:	JERRY L. BONA, Ph.D.
First Author Secondary Information:	
Order of Authors:	JERRY L. BONA, Ph.D.
	Youngjoon Hong, Ph.D.
Order of Authors Secondary Information:	
Author Comments:	Our funding sources are listed at the end of the ms. Neither of them turns up in your dropdown box in ms. data. There is no award number for one of the sources, so I cannot enter it. The only way your system goes forward is to pretend there are no funding sources.
Response to Reviewers:	This is all in our response to the referee reports.

Numerical study of the generalized Korteweg-de Vries equations with oscillating nonlinearities and boundary conditions

Jerry Bona[1*] and Youngjoon Hong[2†]

[1*]Department of Mathematics, Statistics, and Computer Science, University of Illinois at Chicago, Chicago, IL, USA.
[2]Department of Mathematics, Sungkyunkwan University, Suwon, South Korea.

*Corresponding author(s). E-mail(s): jbona@uic.edu;
Contributing authors: hongyj@g.skku.edu;
†These authors contributed equally to this work.

Abstract

The focus here is upon the generalized Korteweg-de Vries equation,

$$u_t + u_x + \frac{1}{p}\left(u^p\right)_x + u_{xxx} = 0,$$

where $p = 2, 3, \cdots$. When $p \geq 5$, it is thought that the equation is not globally well posed in time for L_2-based Sobolev class data. Various numerical simulations carried out by multiple research groups indicate that solutions can blowup in finite time for large, smooth initial data. This is known to be the case in the critical case $p = 5$, but remains a conjecture for supercritical values of p. Studied here are methods for controlling this potential blow up. Several candidates are put forward; the addition of dissipation or of higher order dispersion are two obvious candidates. However, these apparently can only work for a limited range of nonlinearities. However, the introduction of high frequency temporal oscillations appear to be more effective. Both temporal oscillation of the nonlinearity and of the boundary condition in an initial-boundary-value configuration are considered. The bulk of the discussion will turn around this prospect in fact.

Keywords: generalized Korteweg-de Vries equations, blow up phenomena, Fouier-spectral method, Legendre-Galerkin method, time-oscillating nonlinearity, time-oscillating boundary condition.

1 Background and motivation

The Korteweg-de Vries equation,

$$u_t + u_x + uu_x + u_{xxx} = 0,$$

written here in scaled, dimensionless variables, was originally derived by Boussinesq in 1877 [27]. It was put forward by him as a model for unidirectional long wavelength surface water waves of small amplitude. Rederived by Korteweg and his student de Vries in 1895 [54], it went unremarked by the European schools of hydrodynamics for decades.

This changed in the 1950's when this equation also appeared as the continuum limit of a mass and string model studied by Fermi, Pasta and Ulam with help from Tsingou [35, 41]. It also arose a little later in a plasma physics model derived by Gardner and Morikawa [43]. The advent of the inverse scattering method for solving the Korteweg-de Vries equation in the middle 1960's by Gardner, Greene, Kruskal and Miura, and with later help from Su, (see the review article of Miura [55]) brought this equation and its relatives into a central position in the mathematical firmament. Subsequent laboratory and field studies as well as theoretical work have shown the efficacy of Korteweg-de Vries type models in describing surface water waves (see, for example [18], [45], [46], [78]). Since the time of its ascendancy in the scientific world, the Korteweg-de Vries equation has appeared as a model for a considerable variety of other real world phenomena.

One of these is in internal wave theory. In the idealized format of a two-fluid system with a lighter layer resting upon a denser lower layer, the so called extended Korteweg-de Vries equation (also known as the Gardner equation)

$$u_t + u_x + auu_x + u^2u_x + u_{xxx} = 0$$

arises at a low level of approximation (see [64]). Here, a is a constant dependent upon various details of the physical situation. In particular, at a certain critical ratio of depths and densities, the dominant nonlinear term is no longer quadratic, but is instead cubic. One can view this as an invitation to the study of what is known as the generalized Korteweg-de Vries equation, namely

$$u_t + u_x + \frac{1}{p}\left(u^p\right)_x + u_{xxx} = 0, \tag{1}$$

where $p = 2, 3, \cdots$. (It must be confessed that for larger values of p, this equation arose first in mathematical investigations of the interaction between nonlinearity and dispersion and not as a model of a physical situation (see for example [3])).

In the critical case when $p = 5$, the pure initial-value problem for (1) on the whole line is known to have solutions that blow up in finite time (see the sustained and detailed work of Merle and his several collaborators, starting with [59]). It is an open question whether or not the Cauchy problem for the generalized Korteweg-de Vries equation (gKdV equation henceforth) with a supercritical nonlinearity $p \geq 6$ has global solutions for large, smooth initial data. Numerical simulations (*e.g* [10, 12]) indicate probably not, but rigorous results attesting to this have not yet been forthcoming.

There are several possible ways of controlling the singularity formation that seems to occur when $p > 5$. One of these might be to append dissipation, so leading to an equation of the form

$$u_t + u_x + \frac{1}{p}\left(u^p\right)_x + u_{xxx} - \delta u_{xx} = 0,$$

where $\delta > 0$. In fact, as seen in [13], this does not appear to stop the blow up occurring for large initial data. More precisely, for given initial data that blows up in the absence of dissipation, there is a critical positive value δ_c of δ such that for $\delta > \delta_c$, the solution is global and uniformly bounded. However, for $\delta < \delta_c$, the solution continues to blow up in finite time. One might suppose that the failure of the $-u_{xx}$ term to control the singularity formation is because it is a lower-order term in the equation. Appending a term of the form νu_{xxxx} instead might do the trick. However, this also appears not to work as the remarks in [15] indicate.

Another way the blow up might be controlled is to add higher-order dispersion, *e.g.* something like

$$u_t + u_x + \frac{1}{p}\left(u^p\right)_x + u_{xxx} + \delta u_{xxxxx} = 0,$$

where $\delta \neq 0$. This, does indeed manage the blow up as long as $p < 8$. However, numerical experiments show that for $p > 9$, blow up reasserts itself.

A third possibility is based on recent theoretical studies that have shown that a time-dependent oscillation added to the nonlinearity can avert blow-up. Indeed, the solution converges in the limit of large-frequency oscillation to a global solution of a certain limiting problem. It is our purpose here to study this latter phenomenon numerically in the situation where the problem is posed as a periodic initial-value problem. We also study a related problem, namely a boundary-value problem for the supercritical gKdV equation with oscillating boundary conditions. It is found here also that large frequency oscillation can kill potential blow-up phenomena.

For the intial-value problem, (1) is modified by the addition of temporal modulation of its nonlinearity, *viz.*

$$u_t + g_1(\omega t)\frac{1}{p}(u^p)_x + u_{xxx} = 0, \quad p > 5, \tag{2}$$

where $\omega \gg 1$ and g_1 is a mean-zero periodic function used to manage the nonlinearity. In this situation, posed as an initial-value problem on the entire real line $\mathbb{R}$, the solution is known to be global for large values of ω (see [28], [31], [63] and [61] for the case $p = 2$). In particular, Panthee and Scialom showed in [63] that solutions to the initial-value problem (IVP in what follows) associated to (2) converges to a limit problem as $\omega \to \infty$ (see (5) in Section 2). (Note that for the pure initial-value problem, the convective term u_x can be dispensed with by moving to traveling coordinates. This is not the case for the boundary-value problem to be discussed presently.)

For the pure initial-value problem, a Fourier spectral method is put forward, tested for accuracy and convergence and used in our study. Approximate solutions to the boundary-value problem are obtained via a spectral element method.

The present, quantitative appraisal of the initial-value problem for (2) is placed in a periodic context rather than on the whole real line $\mathbb{R}$. The practice of approximating KdV-type equations on $\mathbb{R}$ by associated periodic problems is commonplace and goes back to the work of Zabusky and others in the 1960's. However, it is worth noting that rigorous theory asserting the validity of this procedure on finite, but long time intervals may be found in [32] (and see also [8]).

A related issue arises for the gKdV equation posed as a non-homogeneous problem, *viz.*

$$\begin{cases} u_t + \dfrac{1}{p}(u^p)_x + u_x + u_{xxx} = 0, \quad 0 < x < L, \\ u(0,t) = g_2(\omega t), \\ u(L,t) = u_x(L,t) = 0, \\ u(x,0) = 0, \end{cases} \tag{3}$$

where the solution is forced from the left-hand boundary. Here, g_2 is again a periodic function. While there is no theory showing this problem to be globally well posed in time, the approximate solutions computed here indicate that there is again no blow up for large values of ω whereas the addition of dissipaton or higher order dispersion has only limited success in this aspect.

The overall conclusion derived from this study is that high frequency oscillation can mitigate the effects of supercritical nonlinearity, thereby resulting in a problem that is globally well posed.

Theory for the initial-value problem for real-valued solutions of the gKdV equations has a long history, starting with the case $p = 2$ in the 1970's (see [19], [48]). In the ensuing years, the theory for these equations has become

quite subtle (see for example the monograph [72] of Tao or the nice review lectures of Erdogan and Tzirakis [39], but the reader is cautioned that there are many, many references). However, in the present essay, we will only need the relatively elementary results derived already by Kato in [49] (and see also [3]). These state that the IVP for the gKdV equation (1) is globally well posed in the L_2-based Sobolev space H^k if $k \geq 1$ and $p = 2, 3, 4$. If $p = 5$, the problem is globally well posed provided the L_2-norm of the initial data is not too large. The same is true for $p > 5$, but now under the assumption that the H^1-norm of the initial data is not too large. These results apply equally to the problem posed on the whole real line and to the periodic initial-value problem.

For initial-boundary-value problems (IBVP) such as (3), much less is available in the literature. Problems such as these for the KdV equation ($p = 2$) itself have been studied, but for higher power nonlinearities, not much is known. The articles [22, 23] provide a guide to the available literature.

Considerable effort has also been made to develop numerical methods for studying solutions of the KdV and gKdV equations. The extensive literature in this area includes finite difference, finite element, finite volume and spectral methods for the KdV equation itself (see e.g. [2, 4, 5, 38, 71] and the references therein). More recently, discontinuous Galerkin methods have been adapted to the gKdV equations and related models [9, 60, 75, 76]. These have the great advantage that local spatial refinement is very easily implemented, which helps especially with solutions that appear to be blowing up. For the gKdV equations, a fully discrete scheme for the (periodic) initial-value problem using the finite element method for the spatial approximation and a diagonally implicit Runge-Kutta method for the time stepping was introduced in [10–12]. These works provided numerical evidence of the existence of solutions that blow up in finite time. More recent numerical contributions to the study of gKdV equations may be found in the works of C. Klein and his collaborators (see [37], [52]) and [53]).

In the present paper, a Fourier spectral method is implemented to solve the periodic initial-value problem (2), whereas a spectral element and a collocation method are used to investigate the initial-boundary-value problem (3). For dispersive equations posed as periodic initial-value problems, the spectral method has the advantage of achieving high accuracy with a relatively coarse spatial discretization. Such methods have been studied in [44], [56] and [69], for example. In the presence of non-periodic and non-homogeneous boundary conditions, Chebyshev collocation methods for KdV-type equations were proposed in [62, 67], and Legendre-Gelerkin methods were developed in [57, 66]. Both of these methods have been implemented for the spatial discretization of the gKdV equation (3) in the presence of a time-oscillating boundary condition. However, details of this work are only reported here for the spectral element method. The convergence of the two methods has been tested and both are found to achieve spectral accuracy in space and the appropriate algebraic convergence rate in time. As they produced very similar results, only the details of the spectral element method are presented.

The plan of the paper is to first investigate the time-oscillating nonlinearity in Section 2. This will include details of our numerical scheme as well as convergence and accuracy tests. Once the computer code is deemed satisfactory, it is used in an exploratory mode to understand in more detail the route to global well posedness despite the presence of a supercritical nonlinearity. A similar pattern is followed in Section 3, which deals with the oscillating non-homogeneous boundary-value problem. A short conclusion follows Section 3.

A final comment concerns investigations of other equations in the setting of time-oscillating nonlinearities. We point to the works of Abdullaev *et al.*, Konotop and Pacciani, and Zharnitsky *et al.* [1, 51, 77], respectively, in the context of Bose-Einstein condensates as well as investigations of the influence of time-oscillation on nonlinear Schrödinger equations by Goubet and collaborators in [34, 36], Gabitov and Lushnikov in [42], and that of Cazenave and Scialom [28].

2 Oscillating nonlinearities

The focus in this section is the periodic initial-boundary-value problem,

$$\begin{cases} u_t + g(\omega t)\dfrac{1}{p}(u^p)_x + u_{xxx} = 0, \quad -M \le x \le M, \\ u(x,0) = u_0(x), \end{cases} \tag{4}$$

which is (2), repeated here for convenience. The function u_0 is a smooth, periodic function with period $2M > 0$, $g = g(\tau)$ is a periodic function of τ while the parameter ω is positive and will eventually be taken large. Attention is given to the supercritical cases $p = 6$ and 7. (The reason for choosing both an even and an odd value of p will appear presently. As mentioned earlier, the initial-value problem for (4) has a satisfactory local existence theory.)

In [63], the authors showed that as $\omega \longrightarrow \infty$, the solution u of (4) converges to the solution U of

$$U_t + U_{xxx} + \frac{m(g)}{p}(U^p)_x = 0, \tag{5}$$

with the same initial value, uniformly on bounded time intervals. Here, if Ω is the period of g, then

$$m(g) := \frac{1}{\Omega}\int_0^{\Omega} g(t)dt \tag{6}$$

is its temporal average. The concern here is not with issues of how rough u_0 or g can be taken and still have a satisfactory theory of this sort. Indeed, to justify rigorously the convergence of our numerical schemes in reasonably strong spaces, a fair amount of smoothness is required.

Notice that regardless of the choice of g, the L^2-norm of solutions is conserved, which is to say

$$\frac{1}{2}\frac{d}{dt}\|u(\cdot,t)\|_{L^2}^2 = 0. \tag{7}$$

It is straightforward to deduce that as long as the L^∞-norm of a solution remains bounded on bounded time intervals, then the solution is global, as the L^∞-bound allows the local existence theory to be successfully iterated, achieving a solution which is bounded on bounded time intervals in whatever space the initial data allows. Hence, singularity formation can be tested by monitoring the L^∞-norm of a solution.

It is at this point that the difference between even and odd values of p presents itself. For even values, the sign in front of the nonlinear term does not matter and solutions blow up with either sign. This is no longer true for odd values of p. Indeed, if p is odd and there is a minus sign in front of the nonlinear term, the solution are global no matter how large the initial data and despite the supercriticality of the nonlinearity. This is the so-called defocusing case. The global well posedness subsists on the conservation law,

$$\frac{d}{dt}\int_{-\infty}^{\infty} u_x^2 + \frac{2}{p(p+1)}u^{p+1}dx \;=\; 0.$$

Together with the invariance of the L^2-norm, this implies the H^1-norm to be uniformly bounded and hence that the solution is uniformly bounded. As remarked, this implies the solution is global in time.

The next subsection describes and tests a Fourier-spectral method for approximating solutions of (4). A sequence of numerical experiments is then presented which casts more light on the results in [63].

2.1 Fourier-spectral scheme

A change of the spatial variable puts (4) on the interval $[0, 2\pi]$ and the problem becomes

$$u_t + \frac{g(\omega t)\pi}{Mp}(u^p)_x + \frac{\pi^3}{M^3}u_{xxx} = 0, \quad 0 \le x \le 2\pi. \tag{8}$$

Taking the discrete Fourier transform of this equation yields

$$\widehat{u_t} + g(\omega t)\frac{ik\pi}{Mp}\widehat{(u^p)} - \frac{ik^3\pi^3}{M^3}\widehat{u} = 0, \tag{9}$$

where $\widehat{u}$ is the Fourier transform in space of u. A standard problem now arises, namely that the linear dispersion relation features high frequencies (large wave numbers k corresponding to very short wavelengths), thereby leading to a very stiff system of ordinary differential equations when a time-stepping is implemented. Indeed, the CFL stability condition would mandate very small

time steps indeed. To ameliorate this issue, introduce an integrating factor as in [30, 74]. Setting

$$\widehat{U} = \exp\left(-\frac{ik^3\pi^3}{M^3}t\right)\widehat{u},$$

there obtains

$$\widehat{U_t} + g(\omega t)\frac{ik\pi}{Mp}\exp\left(-\frac{ik^3\pi^3}{M^3}t\right)\widehat{(u^p)} = 0, \tag{10}$$

while the initial data remains unchanged. The stiff term is thereby removed. In numerical computations, Equation (10) is discretized in the form

$$\widehat{U_t} + g(\omega t)\frac{ik\pi}{Mp}e^{-\beta t}\mathcal{F}\left(\left(\mathcal{F}^{-1}(e^{\beta t}\widehat{U})\right)^p\right) = 0, \tag{11}$$

where $\mathcal{F}$ is the discrete Fourier transform operator (see *e.g.* [68, 74]) and $\beta = ik^3\pi/M^3$. The standard fourth-order Runge-Kutta method is employed for the temporal discretization.

Since exact solutions of (4) are not available, non-homogeneous equations of the form

$$\begin{cases} u_t + g(\omega t)\dfrac{1}{p}(u^p)_x + u_{xxx} = f, \quad -M \le x \le M, \\ u(x,0) = a\,\mathrm{sech}^2(x). \end{cases} \tag{12}$$

with a source term f are considered. Choosing

$$u(x,t) \;=\; a\,\mathrm{sech}^2(x-4t), \tag{13}$$

the corresponding forcing function f is easily computed. Of course, the solution (13) is not periodic in space. However, since u converges to 0 exponentially rapidly as $\mathsf{x} \to \infty$, the initial-value problem on the whole line can be considered as a periodic initial-value problem for $x \in (-M, M)$. As long as the solution does not have significant amplitude at the boundaries (see again [32]), these two problems yield essentially the same answer on the spatial interval $[-M, M]$.

To test the numerical convergence, define the relative L^2-error

$$\frac{\|u_{ex} - u_{num}\|_{L^2}}{\|u_{ex}\|_{L^2}}, \tag{14}$$

where u_{ex} is the exact solution (13) and u_{num} is the numerical approximation of (12). Since the L_2-norm is preserved up to roundoff error in the code, it seems wise to also calculate the relative error

$$\frac{\|\partial_x(u_{ex} - u_{num})\|_{L^2}}{\|\partial_x u_{ex}\|_{L^2}}, \tag{15}$$

in the H^1-seminorm. For the tests whose resulting errors are recorded below, the following oscillation function and parameters are used:

$$a = 2, \quad g = \sin(100\pi t), \quad M = 30, \quad \Delta t = 10^{-4}, \tag{16}$$

and the simulations were carried out up to a final time $t = 1$. Tables 2.1 and 2.2 display the performance of the numerical method when $p = 6$ and 7. Notice the spectral convergence in space and the fourth-order convergence in time.

Δt	N	p	Relative L^2-error
10^{-4}	200	6	2.5561×10^{-7}
10^{-4}	300	6	1.3523×10^{-10}
10^{-4}	400	6	2.3967×10^{-13}
10^{-4}	500	6	6.2168×10^{-16}

Δt	N	p	Relative L^2-error
10^{-4}	200	7	3.2924×10^{-6}
10^{-4}	300	7	2.4056×10^{-9}
10^{-4}	400	7	1.6526×10^{-12}
10^{-4}	500	7	3.7814×10^{-15}

Table 1: Relative L^2-error as a function of the spatial discrietization of the Fourier-spectral approximation of the forced problem (12), with exact solution (13) and parameter values (16). Here, N is the number of Fourier modes being kept in the simulation and the errors are reported at $t = 1$. Notice the spectral accuracy.

Δt	N	p	Relative L^2-error	Order	Relative H^1-error	Order
1.2×10^{-4}	500	6	1.7154×10^{-11}	N.A.	1.2998×10^{-10}	N.A.
1.0×10^{-4}	500	6	8.2729×10^{-12}	3.9998	6.2735×10^{-11}	3.9955
0.8×10^{-4}	500	6	3.3935×10^{-12}	3.9935	2.6192×10^{-11}	3.9144
0.6×10^{-4}	500	6	1.0817×10^{-12}	3.9743	8.9588×10^{-12}	3.7292
1.2×10^{-4}	500	7	2.2062×10^{-10}	N.A.	3.6241×10^{-9}	N.A.
1.0×10^{-4}	500	7	1.0657×10^{-10}	3.9912	1.7509×10^{-9}	3.9901
0.8×10^{-4}	500	7	4.4679×10^{-11}	3.8957	7.3520×10^{-10}	3.8887
0.6×10^{-4}	500	7	1.4887×10^{-11}	3.8202	2.4702×10^{-10}	3.7912

Table 2: The relative L^2- and H^1-seminorm errors at $t = 1$ obtained by approximating (2.9) with exact solution (2.10) and the parameter choices in (2.12).

2.2 The supercritical case $p = 6$

Reported first is a sequence of numerical simulations of the gKdV equation with time-oscillating nonlinearity as in (4) for the supercritical case $p = 6$. The auxiliary specifications used in these simulations are

$$\begin{aligned} &u_0 = 2.5\,\mathrm{sech}^2(x), \quad \Delta t = 0.5 \times 10^{-6}, \\ &N = \text{number of Fourier modes} = 2500, \quad M = 50. \end{aligned} \tag{17}$$

As mentioned in (7), the L^2-norm of solutions is invariant in time. Setting $g(t) = \sin(200\pi t)$, the change in the L^2-norm of the numerical solution is around 6×10^{-11} from $t = 0$ to $t = 5$, another check on the computer code.

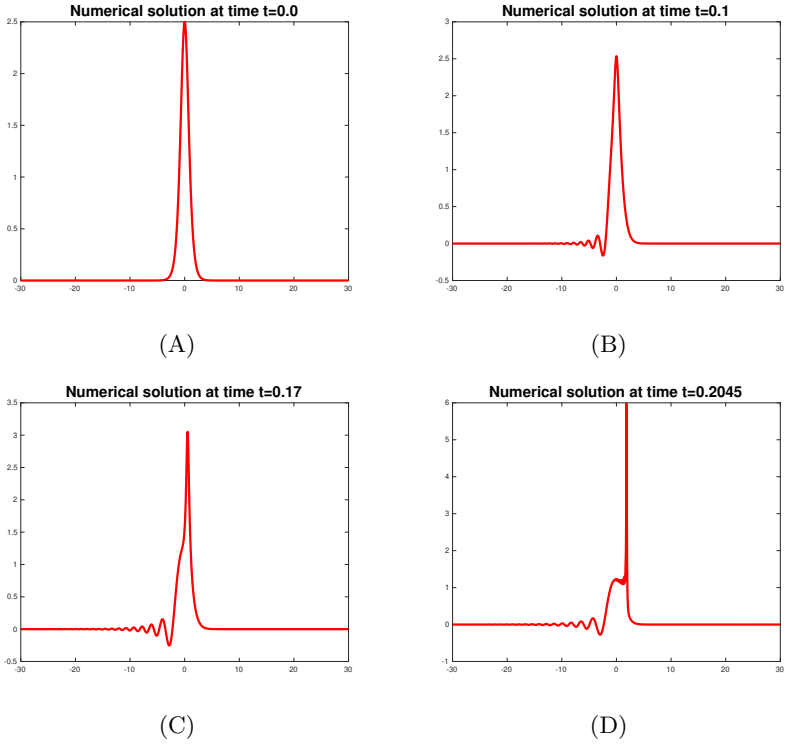

Fig. 1: Numerical solution to the gKdV equation (4) where $p = 6$ and $g = \sin(\pi t)$ with the parameters shown in (17). (A) $t = 0.0$; (B) $t = 0.1$; (C) $t = 0.17$; (D) $t = 0.2045$.

Figures 1 to 3 each display spatial traces of the numerical approximations at increasing times of various simulations of (4) with the specifications in (17). The different figures correspond to different choices of time-oscillating functions g and choices of the oscillation frequency ω. As anticipated, with a low frequency parameter (e.g. $\omega = \pi$), the numerical approximations appear to blow-up for both supercritical values $p = 6, 7$. The oscillation is slow enough that it does not have time to effect the solution before it has already gone into blowup mode. Moreover, the structure of the blowing-up peak is very much like what is observed without the oscillation (see our Figure 1 and compare to Figures 6 and 7 in [12]). (N.B. the value of p in [12] corresponds to $p - 1$ in our notation.)

However, numerical approximations associated with larger values of ω show a different behavior. For instance, when the associated oscillation is $g(\omega t) = \sin(\omega t)$ and ω is large, there is no indication of singularity formation, though of course one does see the effect of the oscillation – see Figures 2 and 3 below. In fact, the L^∞-norm of the approximate solution appears to decrease more or less monotonically as a function of t in both of these simulations. This result is explained by the theory in [63]. From (6) with $g(\tau) = \sin(\omega\tau)$, it is clear that $m(g) = 0$. Thus, for large frequencies, it is expected that the solution will resemble a purely dispersive solution of the linearized KdV equation. In fact, Figure 4 shows just how similar the oscillating solution is to the solution of the linear KdV equation with the same initial data.

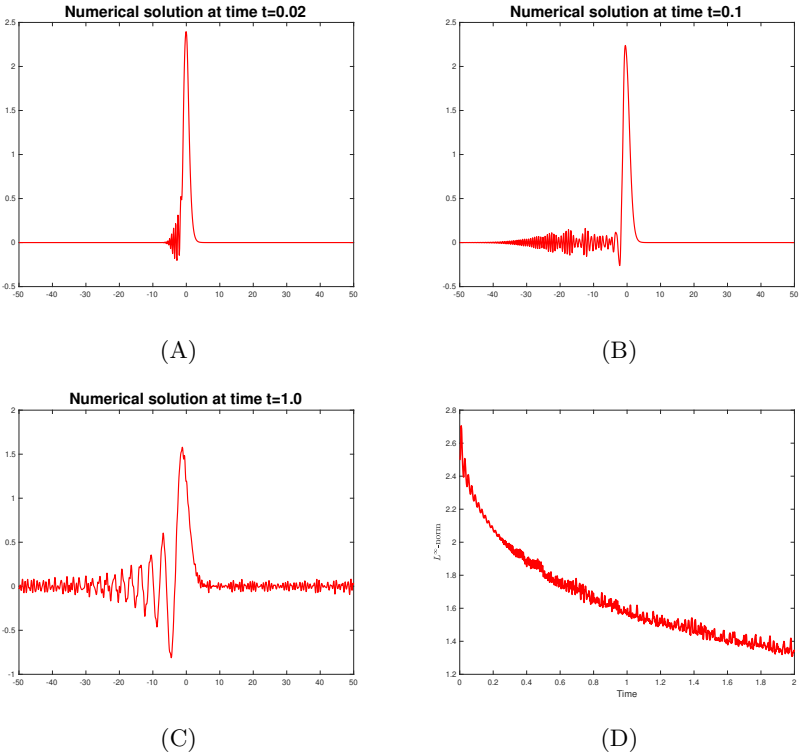

Fig. 2: Numerical solution to the gKdV equation (4) with $\omega = 100\pi$ where $p = 6$ and $g = \sin(\omega t)$ with the parameters as displayed in (17). (A) $t = 0.02$; (B) $t = 0.1$; (C) $t = 1.0$; (D) a plot of the L^∞-norm of the numerical solution as a function of time.

On the other hand, if the oscillation takes the form $g(\omega t) = \cos^2(\omega t)$, the numerical results tell another story. From (6) with this latter specification of g, one calculates that $m(g) = 1/2$. Thus, blowup is to be expected, at least

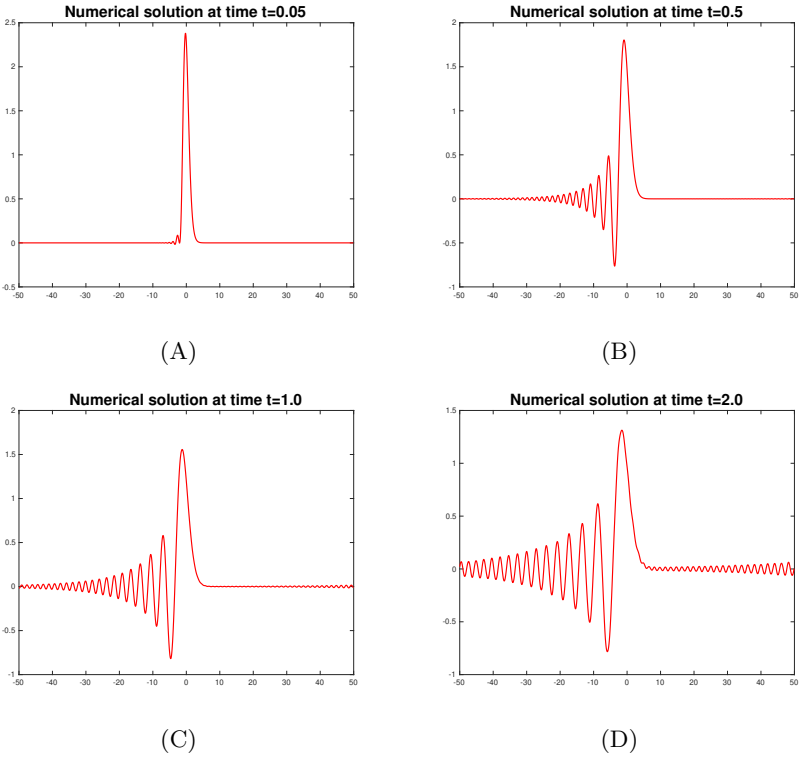

Fig. 3: Numerical solution to the gKdV equations (4) with high frequency $\omega = 10^5$ where $p = 6$, again with $g = \sin(\omega t)$ and the specifications in (17). (A) $t = 0.05$; (B) $t = 0.5$; (C) $t = 1.0$; (D) $t = 2.0$.

for large values of ω. When $\omega = \pi$ and the auxiliary data shown in (17) is used, Figure 5 displays the same sort of blowup seen with the oscillation $\sin(\pi t)$. However, for quite a large middle range, roughly ω in the interval $[19.5\pi, 4292\pi]$, the solutions no longer appear to blow up. In these cases, the time-oscillation parameter ω is apparently not large enough that the solution is modeled well by the solution of

$$u_t + \frac{1}{2}(u^6)_x + u_{xxx} = 0. \tag{18}$$

But, it does appear that it is large enough to control the blowup. An example is shown in Figure 6 where $\omega = 100\pi$. As theory assures, for truly large values of ω, say $\omega = 10^5$, the numerical solution again blows up in finite time and the blowup structure is that observed for (18) in Figure 7. At present, we do not have an explanation for this somewhat counterintuitive behavior in the middle range of frequency of oscillation.

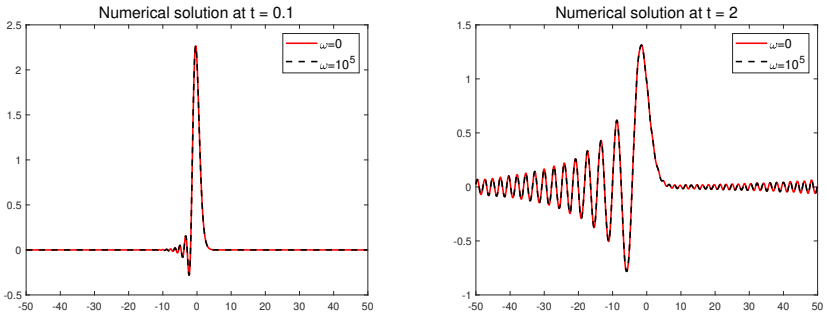

(A) (B)

Fig. 4: Numerical solution of (4) where $p = 6$ and $g = \sin(\omega t)$ with the parameters as displayed in (17). The red solid line displays the solution of the linear KdV equation, i.e. $\omega = 0$, and the dotted black line superimposes the solution of (4) with $\omega = 10^5\pi$; (A) $t = 0.1$; (B) $t = 2.0$.

2.3 The supercritical case $p = 7$

In this section, numerical experiments are reported for $p = 7$ in (4). Even and odd powers of the nonlinearity are different. Even powers do not depend on the sign in front of the nonlinearity, whereas odd ones do. More precisely, if p is odd and the gKdV equation

$$u_t - (u^p)_x + u_{xxx} = 0$$

features a minus sign in front of the nonlinear term, the so-called defocusing case, then solutions of the initial-value problem are global and remain uniformly bounded, no matter how large is p. If p is even, the change of variables $u \mapsto -u$ effectively changes the sign in front of the nonlinearity, leading to the conclusion that the sign is not important as far as singularity formation is concerned. This point is investigated in some of the simulations discussed now. The specifications

$$\begin{aligned} &u_0 = 2.5\,\mathrm{sech}^2(x), \quad \Delta t = 0.5 \times 10^{-6}, \\ &N = \text{number of Fourier modes} = 2500, \quad M = 50, \end{aligned} \tag{19}$$

are used in what follows in this subsection.

Simulations were made with $g(t) = \sin^2(\omega t)$ where $\omega = \pi$, 200π, and 10^5. Just as for the case $p = 6$, two different regimes were detected. When the value of ω was small, the solutions blew up quickly, though not so quickly as did the case $p = 6$ with $g(t) = \cos^2(\omega t)$ because this time the oscillation starts at 0 instead of 1. The blow up occurred at $t \sim 0.343$. It also blew up in a very similar way to the case $p = 6$ when $\omega = 10^5$. The other regime was for intermediate values such as $\omega = 200\pi$, where a bounded, slowly dispersing solution was

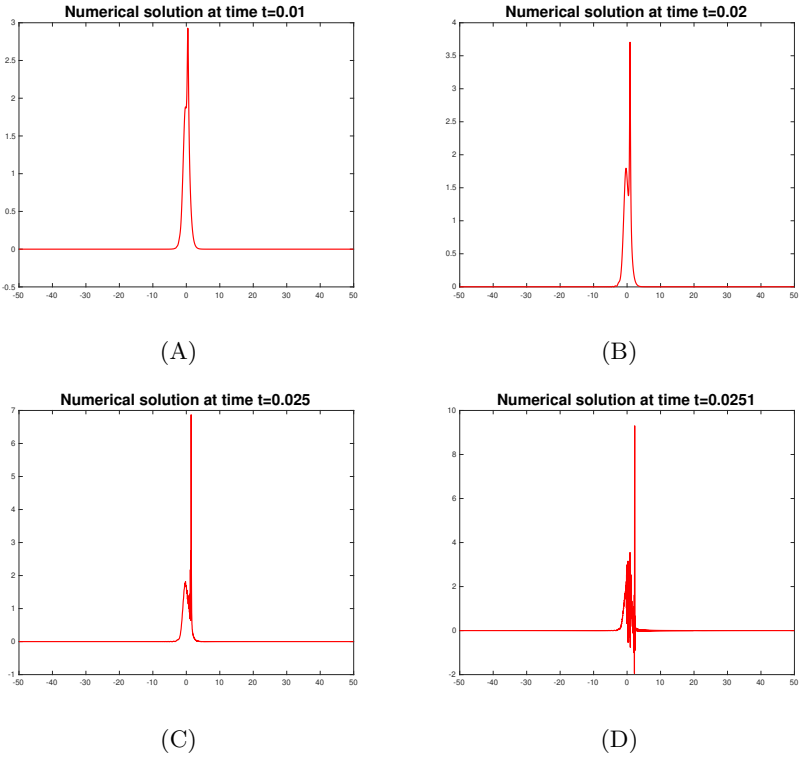

Fig. 5: Numerical solution to the gKdV equations (4) where $p = 6$ and $g(t) = \cos^2(\pi t)$ with (17). (A) $t = 0.01$; (B) $t = 0.02$; (C) $t = 0.025$; (D) $t = 0.0251$.

observed. Figure 8 presents the outcome of three simulations, shown in pairs on single graphs. The inputs are identical except for the frequencies, which took the values $\omega = 18.75\pi, 19\pi$ and 19.25π. As the oscillation is $\sin(\omega t)$ again, we know already that for small values of ω, blowup is expected whereas for large values the solution should be global. Here, a transition is exhibited. Blowup appears for $\omega = 18.75$ which transitions to a solution at $\omega = 19.25$ where blowup seems about to manifest itself, but can't quite beat the dispersive effect of the oscillation.

If p is even and the time oscillation is non-positive so that $g(t) \leq 0$, the defocusing gKdV-type equations are presented. The defocusing nature of the equation guarantees the global well-posedness corresponding to quite reasonable classes of initial data u_0; for more theoretical details, see e.g. [70, 73]. In Figure 9, the outcome of a numerical simulation using $g(t) = -\sin^2(\pi t)$ is displayed. The numerical results show slowly decreasing solutions corresponding to the order one value $\omega = \pi$, on account of the defocusing nature of the forcing.

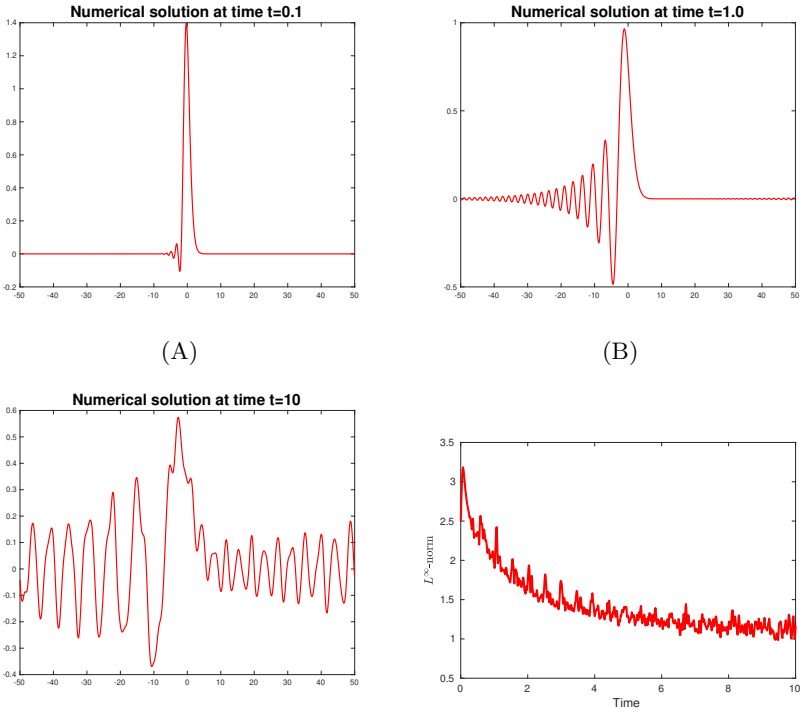

Fig. 6: Numerical solution to the oscillating gKdV equation (4) with $\omega = 100\pi, p = 6$ and $g(t) = \cos^2(\omega t)$ with auxiliary specifications (17). (A) $t = 0.1$; (B) $t = 1.0$; (C) $t = 10.0$; (D) L^∞-norms of the numerical solution against time.

3 Boundary oscillation

A new aspect of control of singularity formation is dealt with in this section. The context is the initial-boudary-value problem (3) with $p = 6$ and 7. The original mathematical problem that arose when trying to check the accuracy of the KdV approximation is the half-line problem,

$$\begin{cases} u_t + \dfrac{1}{p}(u^p)_x + u_x + u_{xxx} = 0, \quad x \geq 0, \\ u(0,t) = g_1(\omega t), \\ u \ \text{ bounded as } \ x \to +\infty, \\ u(x,0) = 0. \end{cases} \tag{20}$$

Boundary-value problems of this sort have arisen when modeling long-crested waves generated by a wavemaker. In such a situation, the function $g(t)$ is

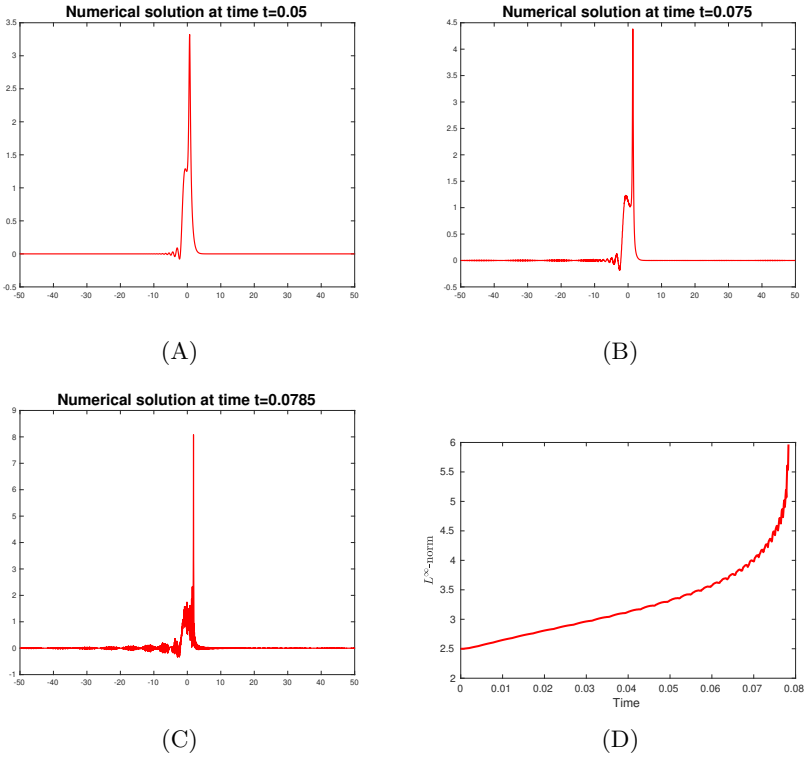

Fig. 7: Numerical solution to the oscillating gKdV equations (4) with high frequency $\omega = 10^5$, $p = 6$ and $g(t) = \cos^2(\omega t)$ with the specifications (17). (A) $t = 0.05$; (B) $t = 0.075$; (C) $t = 0.0785$; (D) L^∞-norms of the numerical solution against time.

determined from a measurement taken at a single spatial point as a function of time at one end of the medium of propagation (see [18, 46, 78]). Just as for the pure initial-value problem (2), the solution of the two-point boundary-value problem (3) is known to approximate well the solution of (20), when the latter is restricted to the spatial interval $[0, L]$, on a time interval of order L (see [32]). As remarked earlier, the convective term u_x cannot be eliminated by a traveling change of variables as the left-hand boundary is then deformed. In this problem, the time-oscillating parameter ω appears in the left-hand boundary condition, $u(0, t) = g_1(\omega t)$ where g_1 is a periodic function.

The theory for either of the problems (3) and (20) is somewhat more complicated than for the initial-value problem. For $p = 2$, the Korteweg-de Vries equation itself, there is a global theory in [24, 25] of smooth solutions for (20) provided the initial- and boundary-data satisfy certain obvious compatibility conditions at $(x, t) = (0, 0)$ (the number of compatibility conditions depends upon the smoothness class in which one is seeking a solution). Such smooth

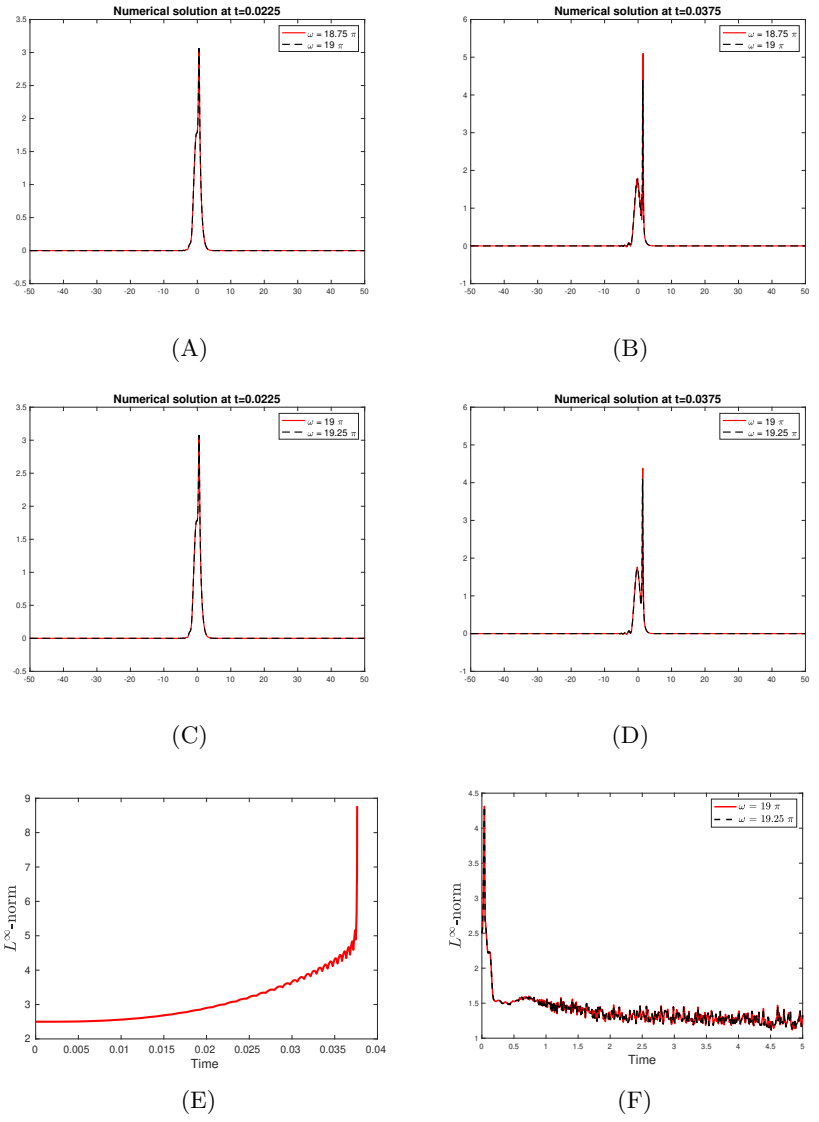

Fig. 8: Numerical solution to the gKdV equations (4) where $p = 6$ and $g(t) = \sin(\omega t)$ with the specifications in (19). In (A) and (B), we compare $\omega = 18.75\pi$ (red solid line) with $\omega = 19\pi$ (black dotted line) at two times. For (C) and (D), we compare $\omega = 19\pi$ (red solid line) with $\omega = 19.25\pi$ (black dotted line) at the same two times. For (E), the L^∞-norm of the numerical solution as a function of t with $\omega = 18.75\pi$ is displayed, while (F) shows the L^∞-norms of the solutions for $\omega = 19\pi$ and $\omega = 19.25\pi$.

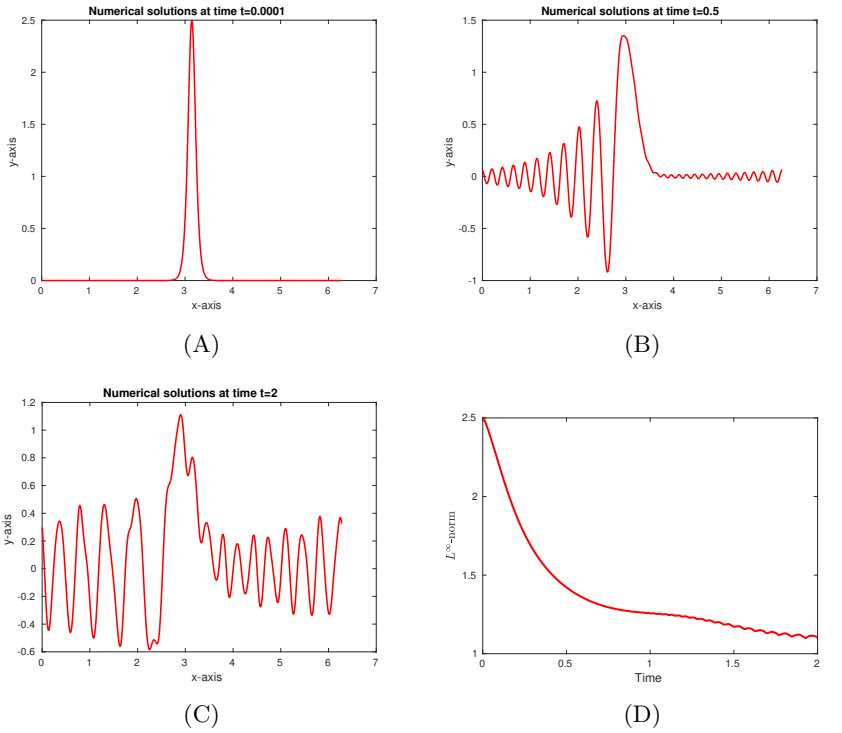

Fig. 9: Numerical solution to the oscillating gKdV equations (4) with a negative time oscillating nonlinearity $g(t) = -\sin^2(\pi t)$ with the auxiliary specifications (19) and $p = 7$. (A) $t = 0.0001$; (B) $t = 0.5$; (C) $t = 2$; (D) L^∞-norms of the numerical solution against time. (Compare with Figure 8 where signs of blowup are evident.)

solutions can be approximated by the numerical techniques to be introduced presently. Rigorous theory to this effect for the numerical approximations can be set in order, but this is not pursued here. The theory does depend upon the smoothness of the solutions of course. No smoothness means no approximation in continuous function spaces, for example. Later works slightly generalized these results (see for example [17] and [40] and especially the references to the Russian literature in the paper of Faminski). Using a clever reduction to a forced problem, Colliander and Kenig [33] dealt with general positive integer values of p, but obtained only very weak solutions. So far as we are aware, there is not even a local theory of strong solutions in the literature for nonhomogeneous boundary-value problems for the generalized KdV equation (1), let alone for the oscillatory problems under consideration here. In what follows, we shall assume that strong solutions obtain for smooth, compatible initial data, at least locally in time.

Two spectral methods were implemented for the spatial discretization of the gKdV equation in the presence of lateral boundaries; the Chebyshev-collocation method and the Legendre-Galerkin method. Using exact solutions, the convergence of these two methods was tested and both achieve spectral accuracy in space and fourth-order accuracy in time. Only the Legendre-Galerkin results are reported here, as those for the Chebyshev method produced very similar outcomes. A large number of experiments were then initiated, some of which will be described after preliminary discussion of the accuracy of the scheme.

A simple change of the spatial variable puts the problem in the form

$$\begin{cases} u_t + \dfrac{1}{p}(u^p)_x + u_x + u_{xxx} = 0, & -1 < x < 1, \\ u(-1,t) = g(\omega t), & t \geq 0, \\ u(1,t) = u_x(1,t) = 0, \\ u(x,0) = u_0(x), \end{cases} \tag{21}$$

where p is a positive integer, $g(\tau)$ is a periodic function and $\omega > 0$. This problem has different characteristics from those of the initial-value problem. For a start, energy is not preserved here, as the wavemaker (represented by the left-hand boundary condition) may be introducing or extracting energy from the system.

3.1 Description of spectral approximations

The spectral element method to approximate solutions of (21) is introduced now. Before describing the method, it is convenient to homogenize the boundary conditions. Define

$$v := u - g(t)r(x), \quad \text{where} \quad r(x) = (1-x)^2/4. \tag{22}$$

In the new variable v, the initial-boundary-value problem (21) becomes

$$\begin{cases} v_t + \dfrac{1}{p}[(v+gr)^p]_x + v_x + v_{xxx} = f := -g_t r - g r_x, & -1 < x < 1, \\ v(-1,t) = 0, & 0 \leq t, \\ v(1,t) = v_x(1,t) = 0, \\ v(x,0) = u_0(x) - g(0)r(x). \end{cases} \tag{23}$$

Notice that we are implicitly presuming that $u_0(-1) = g(0)$, otherwise there is a mismatch at $(0,0)$. This is in fact the lowest level compatibility condition that was mentioned earlier. Since homogeneous boundary conditions are imposed in (23), the standard framework of spectral methods is available for this problem.

The Legendre Galerkin spectral element method

The numerical scheme proposed here is based on the ideas in [44, 57, 66]. The scheme actually approximates the solution of the homogenized equation (23) and the solution to the oscillating boundary gKdV equation (21) is retrieved by reversing the change of variables (22).

For the temporal discretization, a Crank-Nicolson/leapfrog scheme scheme is employed, *viz.*

$$\frac{v^{n+1}-v^{n-1}}{2\Delta t}+\frac{1}{p}\left[(v^n+rg^n)^p\right]_x+\frac{v_x^{n+1}+v_x^{n-1}}{2}+\frac{v_{xxx}^{n+1}+v_{xxx}^{n-1}}{2}=f^n, \quad (24)$$

where $v^n(\cdot)$ is the approximation of $v(\cdot,t_n)$ with $t_n = n\Delta t$. The scheme is initiated by using an implicit Euler method with Picard iteration for the first time step. This comprises an unconditionally stable scheme.

Let $\mathcal{P}_N$ denote the linear space spanned by the Legendre polynomials of degree at most N. The subspaces

$$\begin{aligned}\mathcal{V}_N &= \{v\in\mathcal{P}_N : v(\pm1)=v_x(1)=0\},\\ \mathcal{V}_N^* &= \{v\in\mathcal{P}_N : v(\pm1)=v_x(-1)=0\},\end{aligned} \quad (25)$$

are natural for the spatial situation of interest here. Let T be the final time to which the simulation is aimed. The problem then devolves to finding $v_N^k\in\mathcal{V}_N$, $k=0,1,\cdots K=T/\Delta t$ such that for any $w\in\mathcal{V}_N^*$,

$$\begin{aligned}&(v_N^{n+1},w)+\Delta t(\partial_x v_N^{n+1},w)+\Delta t(\partial_x v_N^{n+1},\partial_{xx}w)\\ &=(v_N^{n-1}-\Delta t\partial_x v_N^{n-1}-\Delta t\partial_{xxx}v_N^{n-1}+2\Delta t f_N^n,w)-\frac{2\Delta t}{p}(\partial_x I_C H(N_k^n),w).\end{aligned} \quad (26)$$

Here, v_N^n is the approximation of $v(\cdot,n\Delta t)$, I_C is the interpolation operator at the Chebyshev-Gauss-Lobatto points, and the operator $H(v_N^n):=(v_N^n+rg^n)^p$ has the nonlinearity.

A convenient set of basis functions in this situation is

$$\begin{aligned}\phi_n(x)&=L_n(x)-\frac{2n+3}{2n+5}L_{n+1}(x)-L_{n+2}(x)+\frac{2n+3}{2n+5}L_{n+3}(x),\\ \psi_n(x)&=L_n(x)+\frac{2n+3}{2n+5}L_{n+1}(x)-L_{n+2}(x)-\frac{2n+3}{2n+5}L_{n+3}(x),\end{aligned} \quad (27)$$

which satisfy the boundary conditions

$$\phi_n(\pm1)=\psi_n(\pm1)=\phi_n'(1)=\psi_n'(-1)=0. \quad (28)$$

The function $L_n(x)$ is the standard Legendre polynomial satisfying

$$(1-x^2)L_n^{''}(x) - 2xL_n'(x) + n(n+1)L_n(x) = 0 \tag{29}$$

with the usual normalization $L_n(1) = 1$. For $N \geq 3$, we have

$$\begin{aligned} \mathcal{V}_N &= \text{span}\{\phi_0, \phi_1, ..., \phi_{N-3}\}, \\ \mathcal{V}_N^* &= \text{span}\{\psi_0, \psi_1, ..., \psi_{N-3}\}. \end{aligned} \tag{30}$$

Taking $w = \psi_m$, $m = 1, \cdots N-3$ and writing v_N in terms of this basis, *viz* $v_N = \sum_{k=0}^{N-3} \tilde{v}_k \phi_k$, the scheme just outlined can be written in matrix form in the usual way.

The convergence of this numerical scheme is tested by creating an exact solution of (23). We use

$$v(x,t) = \sin(\pi x)(1-x)\cos(\pi t), \quad \text{with} \quad g(t) = \cos(\pi t). \tag{31}$$

The function v satisfies the three homogeneous boundary conditions, and while it does not satisfy the equation, a relevant forcing term is easily calculated.

Table 3 displays the relative L^2- and H^1-errors of the Legendre-Galerkin spectral method just outlined for solving (23) versus the time discretization Δt with $p = 2$ and $p = 6$. The relative L^2- and H^1-errors are defined just as in (14) and (15). Seen clearly is the second-order convergence rate one associates to Crank-Nicholson time stepping. Table 4 shows the relative L^2- and H^1-errors of the Legendre-Galerkin spectral method for solving (23) versus the number N of modes being kept in the simulation, again for $p = 2$ and $p = 6$. Note the spectral accuracy that obtains.

Δt	N	p	L^2-error	H^1-error
10^{-1}	64	2	6.2672×10^{-2}	1.9344×10^{-1}
10^{-2}	64	2	5.9216×10^{-4}	1.8935×10^{-3}
10^{-3}	64	2	5.9342×10^{-6}	1.8973×10^{-5}
10^{-4}	64	2	5.9354×10^{-8}	1.8976×10^{-7}
Δt	N	p	L^2-error	H^1-error
10^{-1}	64	6	6.1074×10^{-2}	1.9062×10^{-1}
10^{-2}	64	6	5.7470×10^{-4}	1.8576×10^{-3}
10^{-3}	64	6	5.7583×10^{-6}	1.8611×10^{-5}
10^{-4}	64	6	5.7594×10^{-8}	1.8615×10^{-7}

Table 3: Relative L^2- and H^1-error (14) of our Legendre-Galerkin approximation of (23) versus the time discretization Δt with $p = 2$ and $p = 6$ at final time $T = 1$.

Δt	N	p	L^2-error	H^1-error
10^{-4}	10	2	8.5206×10^{-4}	9.7093×10^{-3}
10^{-4}	12	2	6.9948×10^{-6}	9.9190×10^{-5}
10^{-4}	14	2	1.3594×10^{-7}	2.1230×10^{-6}
10^{-4}	16	2	5.9424×10^{-8}	1.9874×10^{-7}
Δt	N	p	L^2-error	H^1-error
10^{-4}	10	6	1.4316×10^{-3}	6.5726×10^{-3}
10^{-4}	14	6	6.5849×10^{-5}	3.4664×10^{-4}
10^{-4}	18	6	4.3757×10^{-6}	1.7848×10^{-5}
10^{-4}	22	6	4.5503×10^{-8}	5.7194×10^{-7}

Table 4: Relative L^2- and H^1-error, (14), of our Legendre-Galerkin approximation of (23) versus the number of modes N with $p = 2$ and $p = 6$ at final time $T = 1$.

3.2 The supercritical case $p = 6$

In this section, numerical results for the gKdV equations in a finite domain (21) with oscillating boundary conditions are presented. To begin, take $p = 6$ and

$$N = 100, \quad \Delta t = 10^{-4}. \tag{32}$$

Numerical approximations of (21) with $p = 6$ and the specifications (32) and several choices of boundary conditions and frequencies ω at the left-hand side of the interval were run. Figure 10 shows a typical outcome when $\omega = \pi$ and $g(t) = 3\sin(\omega t)$. With this low temporal frequency, the numerical solution appears to blow up. The singularity formation starts to show itself near the left-hand boundary which is not surprising. For example, the amplitude of the solution shown in Figure 10 goes from about 4.5 to almost 300 in the last time interval of length 0.005. A very similar result obtained when $\omega = \pi$ and $g(t) = 3\sin^2(\omega t)$. The display is redundant and so is omitted. Notice the blow-up structure for this boundary forced problem is different from that of the pure initial-value problem for $p = 6$ (see the case $p = 5$ in [12]).

However, when the frequency ω of the boundary data is increased, the numerical approximations no longer show indications of blowing up. Instead their L_2-norm appears to stabilize around something like a limit cycle. This is true for both the mean-zero boundary data $3\sin(20\pi t)$ (see Figure 11)) and the positive-mean boundary oscillation $3\sin^2(60\pi t)$ (see Figure 13). This stabilization of the L_2-norm continued far beyond $t = 1$. Indeed, as seen in Figure 12, the solution itself gives way to a structure that is periodic in t. This is perhaps not surprising in hindsight, as it is known experimentally [18] that real water waves in a channel forced periodically by a wavemaker become periodic in time at each point down the channel. It is also known rigorously that the KdV and the BBM equation on the half line, forced periodically from the left, yields a solution that is asymptotically periodic in time at each spatial point (see [18, 21, 26]).

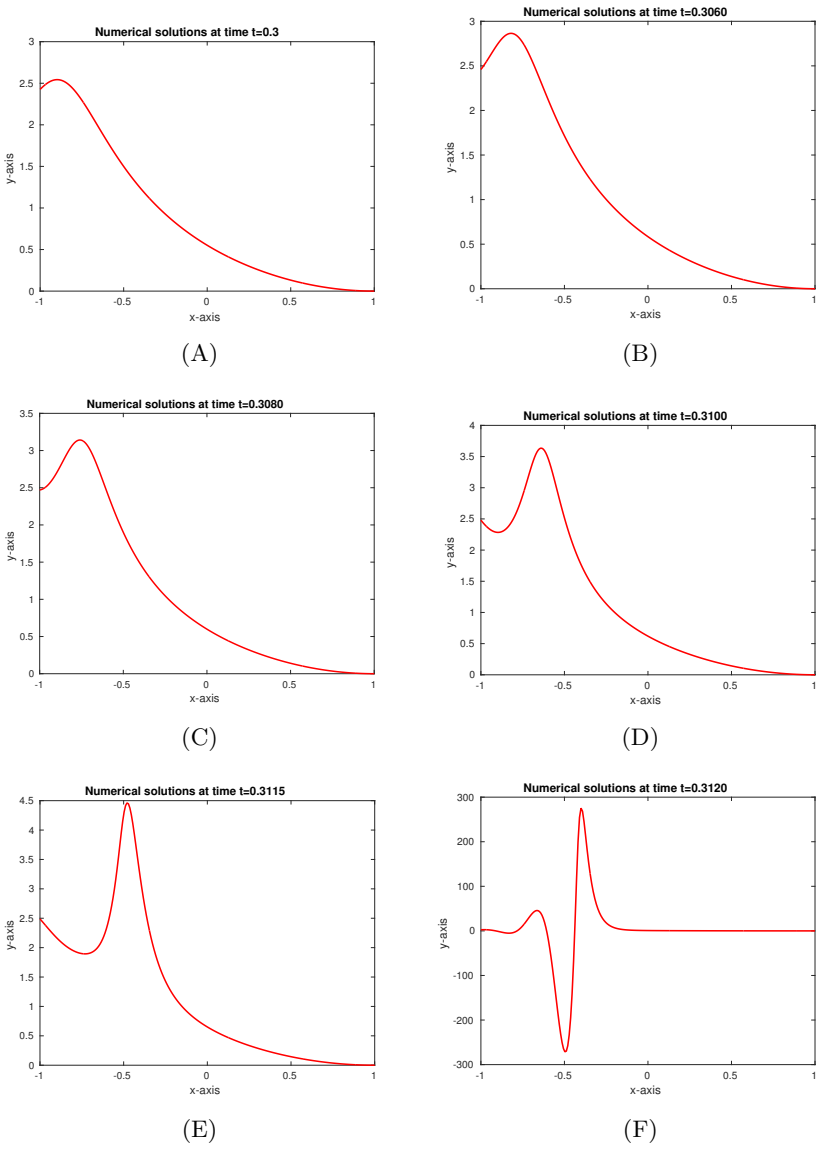

Fig. 10: Blow-up pattern of the numerical solution to the gKdV equations (21) with (32) where $p = 6$ and $g = 3\sin(\pi t)$. (A) $t = 0.3$; (B) $t = 0.3060$; (C) $t = 0.3080$; (D) $t = 0.31$; (E) $t = 0.3115$; (F) $t = 0.312$.

Figure 13 displays the stable numerical solution of the gKdV equation with higher time frequency parameter $\omega = 60\pi$. Since the boundary condition is non-negative, it requires higher time-oscillatory frequencies than the previous case in Figure 11 to obtain bounded numerical solutions. In Figure 13 (A), the

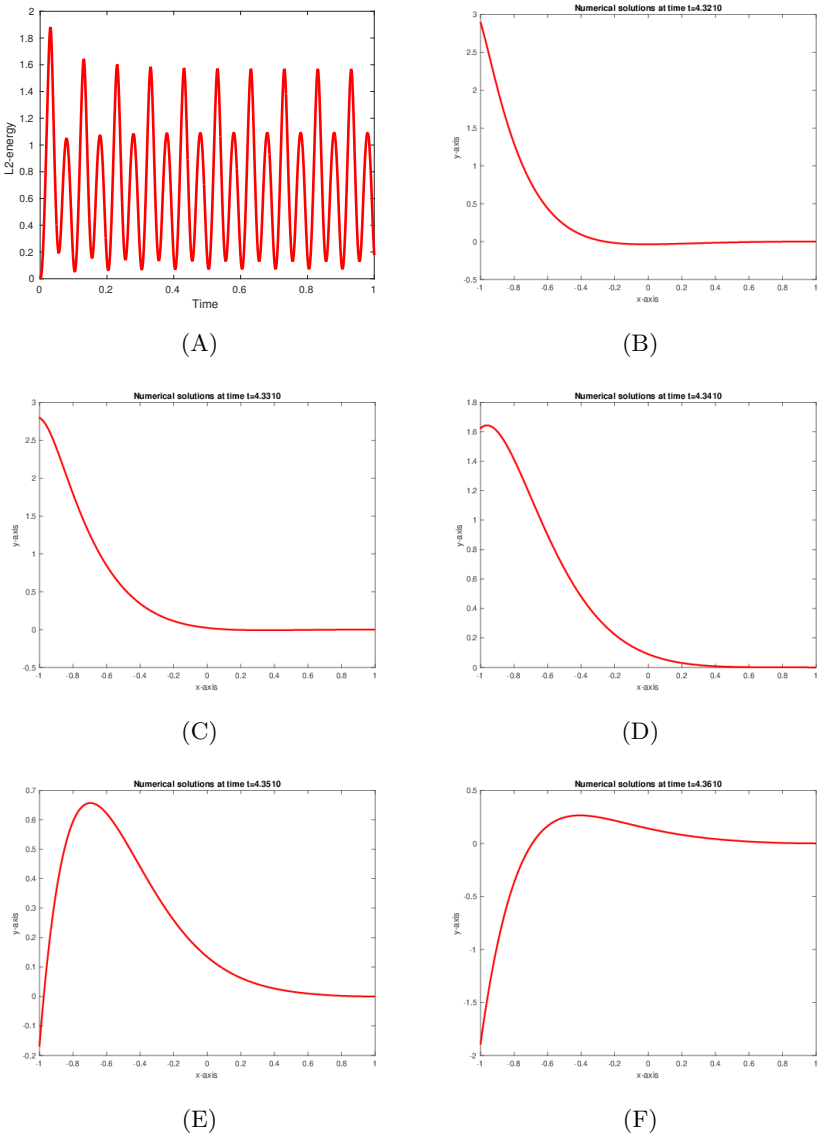

Fig. 11: Numerical solutions to the gKdV equations (21) with specifications (32) where $p = 6$ and $g(t) = 3\sin(20\pi t)$. (A) L^2-norm of the numerical solution as a function of t; (B)-(F) graphs of the numerical solution at increasing times.

stabilization of the L^2-energy of the numerical solution is shown from $t = 0$ to $t = 1$. This stabilization of the L_2-norm appears to continue indefinitely. Figure 13 (B) displays the numerical approximation at $t = 5$.

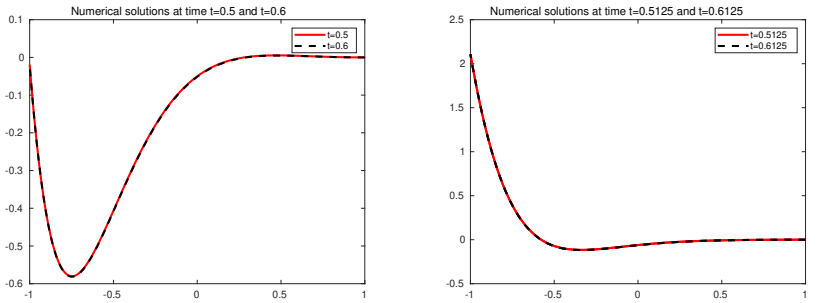

(A) (B)

Fig. 12: Manifestation of periodic solutions of Figure 11. (A) comparison at t=0.5 and 0.6; (B) comparison at t=0.5125 and 0.6125.

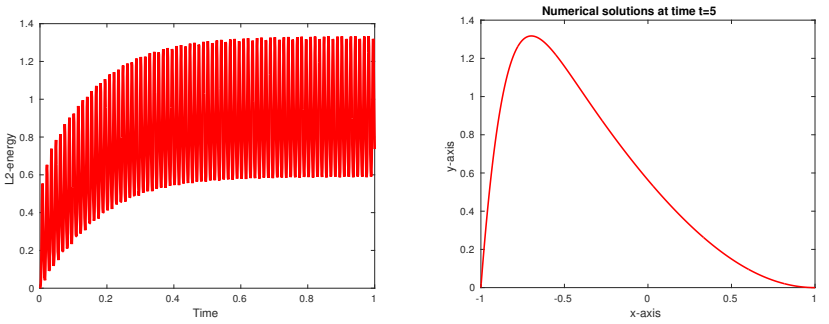

(A) (B)

Fig. 13: Numerical solutions to the gKdV equations (21) where $p = 6$ and $g = 3\sin^2(60\pi t)$ with (32). (A) L^2-norm of the numerical solution; (B) Numerical solution at $t = 5$.

3.3 The supercritical case $p = 7$

The numerical experiments are repeated with an odd power $p = 7$ of the nonlinearity. The Legendre-Galerkin approximation continues to be used in the investigation, though one finds the same results using the Chebyshev-collocation method. The following specifications were used:

$$N = 100, \quad \Delta t = 10^{-4}, \quad p = 7, \quad g(t) = 2.5\sin(\omega t). \tag{33}$$

In Figure 14, the numerical solution appears to be forming a singularity when $\omega = \pi$. The blow-up pattern is the same as in the case $p = 6$. However, when ω is increased to 20π, the numerical solution of the gKdV equation shows no signs of unbounded behavior. Figure 15 (A) displays the L^2-energy of the

numerical solutions from $t = 0$ to $t = 1$; for $t > 1$, the same pattern is observed. Figure 15 (B) shows the numerical solution at $t = 5$. When considering positive boundary conditions (e.g. $\sin^2(\omega t)$) the same results as in $p = 6$ are observed. The display of the solution in this example is again redundant and so is also omitted.

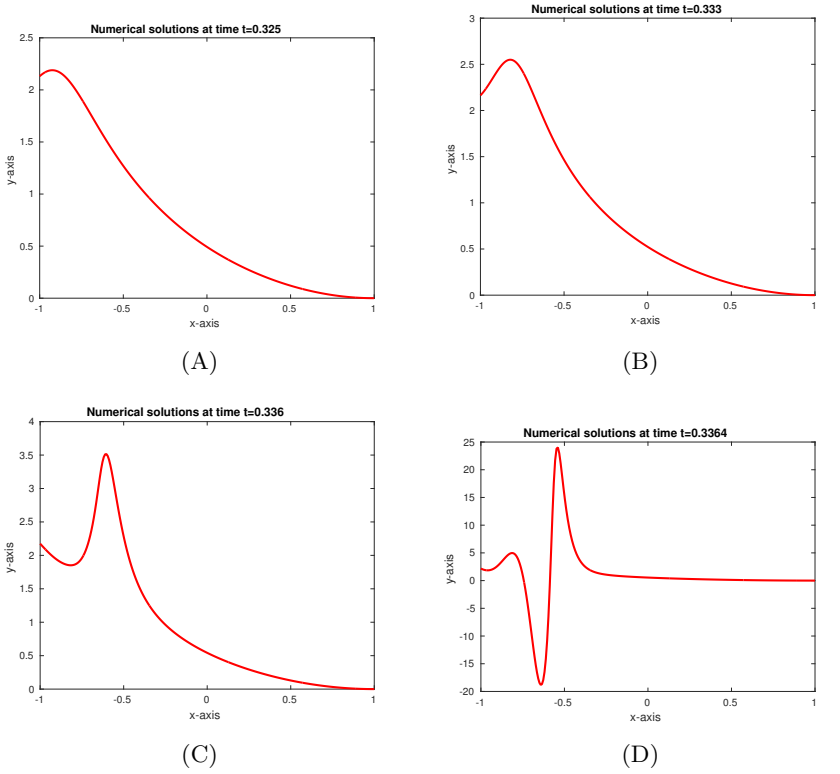

Fig. 14: Blow-up pattern of the numerical solution to the gKdV equations (21) where $p = 7$ and $g = 2.5\sin(\pi t)$ with (33). (A) $t = 0.3250$; (B) $t = 0.3330$; (C) $t = 0.3360$; (D) $t = 0.3364$.

4 Conclusion

Numerical studies of the supercritical gKdV equations adorned with high frequency oscillations are presented. In Section 2, the IVP associated to the supercritical gKdV equation (4) with a temporal oscillation attached to the nonlinearity was considered. As the frequency of the time-oscillation increases, the numerical solution resembles more and more the solution of the limit problems (5) in which the oscillation is replaced by its mean value. This is consistent

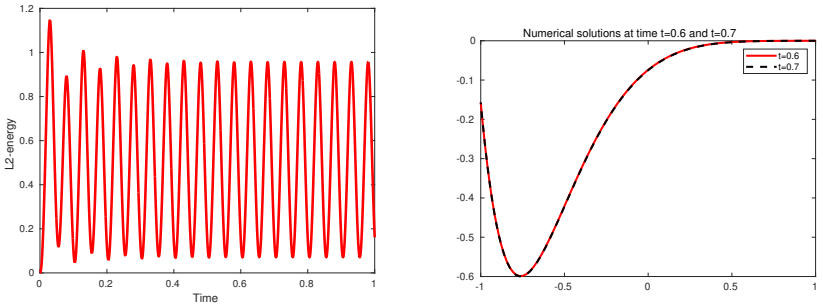

(A) (B)

Fig. 15: Numerical solutions to the gKdV equations (21) where $p = 7$ and $g = 2.5\sin(20\pi t)$ with (33). (A) L^2-norm of the numerical solution; (B) Manifestation of periodic solutions: numerical solutions at $t = 0.6$ and $t = 0.7$.

with the theoretical results [63]. When p is odd, the defocusing case can appear with the correct sign of the forcing. When this is simulated, there are no signs of singularities. This provides evidence that the blow-up solutions observed in other circumstances are not caused by instabilities connected with the oscillations. In Section 3, the supercritical gKdV equations (21) have been studied in a finite domain with zero boundary conditions at the right and an oscillating boundary condition at the left. Due to the non-homogeneous boundary conditions, mathematical studies of the gKdV equations (21) are technically more difficult and relatively little progress has been made in this direction. For numerical experiments, an accurate spectral collocation method and spectral element method were implemented and tested. Applying the numerical scheme, a blow-up structure, which started to appear near the oscillating boundary, was found. As the temporal frequency of the boundary oscillation was increased, non-explosive numerical solutions of (21) are observed. In the case of boundary oscillation, the mean-zero aspect does not appear to play a role.

Several interesting avenues of investigation present themselves as a consequence of what has been observed. The question of what other equations can be managed by way of oscillations in their nonlinearity is an obvious line of development. As far as boundary-value problem are concerned, this is largely virgin territory, both analytically and numerically. This also seems worth further investigation.

Acknowledgements

This work was partially supported by a research grant from the University of Illinois at Chicago. The work of Y. Hong was supported by the Basic Science Research Program through the National Research Foundation of Korea (NRF), funded by the Ministry of Education (NRF-2021R1A2C1093579).

References

[1] Fatkhulla Kh. Abdullaev, Jean Guy Caputo, Robert A. Kraenkel, and Boris A. Malomed. Controlling collapse in Bose-Einstein condensates by temporal modulation of the scattering length. *Phys. Rev. A*, 67:013605 (2003).

[2] Kanji Abe and Osamu Inoue. Fourier expansion solution of the Korteweg-de Vries equation. *J. Comput. Phys.*, 34(2) 202–210 (1980).

[3] J. P. Albert, J. L. Bona and M. Felland. A criterion for the formation of singularities for the generalized Korteweg-de Vries equation. *Mat. Aplic. Comp.* 5(1) 3–11 (1988).

[4] M. E. Alexander and J. Ll. Morris. Galerkin methods applied to some model equations for non-linear dispersive waves. *J. Comput. Phys.*, 30(3) 428–451 (1979).

[5] G. A. Baker, V. A. Dougalis, and O. A. Karakashian. Convergence of Galerkin approximations for the Korteweg-de Vries equation. *Math. Comp.*, 40(162) 419–433 (1983).

[6] T. B. Benjamin, J. L. Bona, and J. J. Mahony. Model equations for long waves in nonlinear dispersive systems. *Philos. Trans. Roy. Soc. London Ser. A*, 272(1220) 47–78 (1972).

[7] B. Boczar-Karakiewicz, J. L. Bona, W. Romanczyk and E. G. Thornton. Modeling the dynamics of the bar system at Duck, N.C., USA. In *Proc. 26th International Conference on Coastal Engr.* (Copenhagen) American Soc. Civil Engrs., New York, pp. 2877–2887, 1998.

[8] J. L. Bona. Convergence of periodic wave trains in the limit of large wavelength. *Appl. Sci. Res.* 37 21–33 (1981).

[9] J. L. Bona, H. Chen, O. A. Karakashian, and Y. Xing. Conservative, discontinuous Galerkin-methods for the generalized Korteweg-de Vries equation. *Math. Comp.*, 82(283) 1401–1432 (2013).

[10] J. L. Bona, V. A. Dougalis, and O. A. Karakashian. Fully discrete Galerkin methods for the Korteweg-de Vries equation. *Comput. Math. Appl. Ser. A*, 12(7) 859–884 (1986).

[11] J. L. Bona, V. A. Dougalis, O. A. Karakashian, and W. R. McKinney. Computations of blow-up and decay for periodic solutions

of the generalized Korteweg-de Vries-Burgers equation. *Appl. Numer. Math.*, 10(3-4) 335–355 (1992). *A Festschrift to honor Professor Garrett Birkhoff on his eightieth birthday.*

[12] J. L. Bona, V. A. Dougalis, O. A. Karakashian, and W. R. McKinney. Conservative, high-order numerical schemes for the generalized Korteweg-de Vries equation. *Philos. Trans. Roy. Soc. London Ser. A*, 351(1695) 107–164 (1995).

[13] J. L. Bona, V. A. Dougalis, O. A. Karakashian, and W. R. McKinney. The effect of dissipation on solutions of the generalized Korteweg-de Vries equation. *J. Comp & Applied Math.* 74 127–154 (1996).

[14] J. L. Bona, H. Chen, S.-M Sun and B.-Y. Zhang. Comparison of quarter-plane and two-point boundary value problems: The KdV equation. *Discrete Continuous Dynamical Systems - Series B* 7(3) 465–49 (2007).

[15] J. L. Bona, H. Chen and Y. Hong. Blowup in the face of higher-order dissipation for the generalized Korteweg - de Vries equation. In preparation.

[16] J. L. Bona and J. Lenells. The KdV Equation on the half line: Time periodicity and mass transport. *SIAM J. Math. Anal.* 52(2) 1009–1039 (2020).

[17] J. L. Bona and L. Luo. A generalized Korteweg-de Vries equation in a quarter plane. *Contemp. Math.* 221 59–125 (1999).

[18] J. L. Bona, W. G. Pritchard and L. R. Scott. An evaluation of a water wave model. *Phil. Trans. Roy. Soc. London Ser. A* 302 457–510 (1981).

[19] Jerry L. Bona and R. Smith. The initial-value problem for the Korteweg-de Vries equation. *Phil. Trans. Roy. Soc. London Ser. A 278* 555-601 (1975).

[20] J. L. Bona, P. E. Souganidis, and W. A. Strauss. Stability and instability of solitary waves of Korteweg-de Vries type. *Proc. Roy. Soc. London Ser. A*, 411(1841) 395–412 (1987).

[21] J. L. Bona, S.-M. Sun and B.-Y. Zhang. Forced ocsillations of a damped Korteweg-de Vries equation in a quarter plane. *Commun. Contemporary Math.* 5(3) 369–400 (2003).

[22] J. L. Bona, S.-M. Sun, and B.-Y. Zhang. A nonhomogeneous boundary-value problem for the Korteweg-de Vries equation posed on a finite domain. *Comm. Partial Differential Eq.*, 28(7-8) 1391–1436 (2003).

[23] J. L. Bona, S.-M. Sun, and B.-Y. Zhang. A non-homogeneous boundary-value problem for the Korteweg-de Vries equation posed on a finite domain. II. *J. Differential Equations*, 247(9) 2558–2596 (2009).

[24] J. L. Bona and R. Winther. The Korteweg-de Vries equation, posed in a quarter plane. *SIAM J. Math. Anal.* 14(6) 1056-1106 (1983).

[25] J. L. Bona and R. Winther. The Korteweg-de Vries Equation, posed in a quarter plane, continuous dependence results. *Differential Integral Eq.* 2(2) 228-250 (1989).

[26] J. L. Bona and J. Wu. Temporal growth and eventual periodicity for dispersive wave equations in a quarter plane. *Discrete Continuous Dynamical Sys.* 23 (4) 1141–1168 (2009).

[27] J. Boussinesq. Essai sur la theorie des eaux courantes. *Memoires presentes par divers savants l'Acad. des Sci. Inst. Nat. France,* XXIII 1–680, 1877.

[28] T. Cazenave, and M. Scialom. A Schrödinger equation with time-oscillating nonlinearity. *Revista Matemática Complutense*, 23 321-–339 (2010).

[29] Cl. Canuto, M. Yousuff Hussaini, A. Quarteroni, and T. A. Zang. *Spectral methods in fluid dynamics.* Springer Series in Computational Physics. Springer-Verlag, New York, 1988.

[30] T. F. Chan and T. Kerkhoven. Fourier methods with extended stability intervals for the Korteweg-de Vries equation. *SIAM J. Numer. Anal.* 22(3) 441–454 (1985).

[31] X. Carvajal, M. Panthee, and M. Scialom. On the critical KDV equation with time-oscillating nonlinearity. *Differential Integral Eq.* 24(5-6) 541–567 (2011).

[32] H. Chen. Long period limit of nonlinear, dispersive waves. *Differential Integral Eq.* 19(4) 463-480 (2006).

[33] J. E. Colliander and C. E. Kenig. The generalized Korteweg-de Vries equation on the half line. *Comm. Partial Differential Eq.* 27(11-12) 2187–2266 (2002).

[34] I. Damergi and O. Goubet. Blow-up solutions to the nonlinear Schrödinger equation with oscillating nonlinearities. *J. Math. Anal. Appl.* 352(1) 336–344 (2009).

[35] T. Dauxois. Fermi, Pasta, Ulam, and a mysterious lady. *Physics Today* Jan. 2008, 56–57.

[36] L. Di Menza and O. Goubet. Stabilizing blow up solutions to nonlinear Schrödinger equations. *Commun. Pure Appl. Anal.* 16(3) 1059–1081 (2017).

[37] B. Dubrovin, T. Grava, and C. Klein. Numerical study of breakup in generalized Korteweg-de Vries and Kawahara equations. *SIAM J. Appl. Math.* 71(4) 983–1008 (2011).

[38] V. A. Dougalis and O. A. Karakashian. On some high-order accurate fully discrete Galerkin methods for the Korteweg-de Vries equation. *Math. Comp.* 45(172) 329–345 (1985).

[39] M. B. Erdogan and N. Tzirakis. Lecture Notes II: On local and global theory for the KdV equation. Published online at https://faculty.math.illinois.edu/ tzirakis/KdV.pdf

[40] A. V. Faminskii. An initial boundary-value problem in a half-strip for the Korteweg– de Vries equation in fractional-order Sobolev spaces *Comm. Partial Differential Equations* 29 1653–1695 (2004).

[41] E. Fermi, J. Pasta and S. Ulam. Studies of nonlinear problems *Document LA-1940. Los Alamos National Laboratory* (1955).

[42] I.R. Gabitov and P.M. Lushnikov. Nonlinearity management in a dispersion-managed system *Optics Letters* 27(2) 113–115 (2002)

[43] C. S., Gardner and G. K. Morikawa. Similarity in the asymptotic behavior of collision-free hydromagnetic waves and water waves. Report MF-2, NYO-9080, Courant Institute of Mathematical Sciences, New York University (1960).

[44] B.-Y. Guo. *Spectral methods and their applications.* World Scientific Publishing Co., Inc., River Edge, NJ, 1998.

[45] J. L. Hammack A note on tsunamis: their generation and propagation in an ocean of uniform depth. *J. Fluid Mech.* 60(4) 769–799 (1973).

[46] J. L. Hammack and H. Segur. The Korteweg-de Vries equation and water waves. Part 2. Comparison with experiments. *J. Fluid*

Mech. 65(2) 289–314 (1974).

[47] W. Heinrichs. Spectral approximation of third-order problems. *J. Sci. Comput.* 14(3) 275–289 (1999).

[48] T. Kato. On the Korteweg-de Vries equation. *Manuscripta mathematica* 28 89—99 (1979).

[49] T. Kato. On the Cauchy problem for the (generalized) Korteweg-de Vries equation. In *Studies in Applied mathematics*, volume 8 of *Adv. Math. Suppl. Stud.* pp. 93–128. Academic Press, New York, 1983.

[50] C. E. Kenig, G. Ponce, and L. Vega. Well-posedness and scattering results for the generalized Korteweg-de Vries equation via the contraction principle. *Comm. Pure Appl. Math.* 46(4) 527–620 (1993).

[51] V. V. Konotop and P. Pacciani. Collapse of solutions of the nonlinear Schrödinger equation with a time-dependent nonlinearity: Application to Bose-Einstein condensates. *Phys. Rev. Lett.*, 94:240405 Jun (2005).

[52] C. Klein and R. Peter. Numerical study of blow-up and dispersive shocks in solutions to generalized Korteweg-de Vries equations. *Phys. D*, 304/305 52–78 (2015).

[53] C. Klein and J.-C. Saut. Numerical study of blow up and stability of solutions of generalized Kadomtsev-Petviashvili equations. *J. Nonlinear Sci.*, 22(5) 763–811 (2012).

[54] D. J. Korteweg and G. de Vries. On the change of form of long waves advancing in a rectangular canal, and on a new type of long stationary waves. *Philosophical Magazine*. 39 (240) 422–443 (1895).

[55] R. M. Miura. The Korteweg–de Vries equation: a survey of results. *SIAM Rev.* 18(3) 412–459 (1976).

[56] Y. Maday and A. Quarteroni. Error analysis for spectral approximation of the Korteweg-de Vries equation. *RAIRO Modél. Math. Anal. Numér.* 22(3) 499–529 (1988).

[57] Heping Ma and Weiwei Sun. A Legendre-Petrov-Galerkin and Chebyshev collocation method for third-order differential equations. *SIAM J. Numer. Anal.* 38(5) 1425–1438 (2000).

[58] Laurent Di Menza and Olivier Goubet. Stabilizing blow up solutions to nonlinear Schrödinger equations. *Commun. Pure Appl. Anal.* 16(3) 1059–1081 (2017).

[59] F. Merle. Existence of blow-up solutions in the energy space for the critical generalized KdV equation. *J. American Math. Soc.* 14(3) 555–578 (2001).

[60] D. Levy, C.-W. Shu, and J. Yan. Local discontinuous Galerkin methods for nonlinear dispersive equations. *J. Comput. Phys.* 196(2) 751–772 (2004).

[61] W. V. L. Nunes. Global well-posedness for the transitional Korteweg-de Vries equation. *Appl. Math. Lett.* 11(5) 15–20 (1998).

[62] D. Pavoni. Single and multidomain Chebyshev collocation methods for the Korteweg-de Vries equation. *Calcolo* 25(4) 311–346 (1989).

[63] M. Panthee and M. Scialom. On the supercritical KdV equation with time-oscillating nonlinearity. *NoDEA Nonlinear Differential Equations Appl.* 20(3) 1191–1212 (2013).

[64] E. Pelinovsky, O. Polukhina, A. Slunyaev and T. Talipova. Internal solitary waves. Ch. 4 of *WIT Transactions on State of the Art in Science and Engineering* Vol 9, WIT Press, Southhampton, U.K. (2007).

[65] A. C. Scott, F. Y. F. Chu, and D. W. McLaughlin. The soliton: a new concept in applied science. *Proc. IEEE* 61 1443–1483 (1973).

[66] Jie Shen. A new dual-Petrov-Galerkin method for third and higher odd-order differential equations: application to the KdV equation. *SIAM J. Numer. Anal.* 41(5) 1595–1619 (2003).

[67] Jan Ole Skogestad and Henrik Kalisch. A boundary value problem for the KdV equation: comparison of finite-difference and Chebyshev methods. *Math. Comput. Simulation* 80(1) 151–163 (2009).

[68] Jie Shen and Tao Tang. *Spectral and high-order methods with applications*, volume 3 of *Mathematics Monograph Series*. Science Press Beijing, Beijing, 2006.

[69] Jie Shen, Tao Tang, and Li-Lian Wang. *Spectral methods*, volume 41 of *Springer Series in Computational Mathematics*. Springer, Heidelberg, 2011. Algorithms, analysis and applications.

[70] Stefan Steinerberger. Dispersion dynamics for the defocusing generalized Korteweg–de Vries equation. *Proc. Amer. Math. Soc.* 143(2) 789–800 (2015).

[71] Thiab R. Taha and Mark J. Ablowitz. IST numerical schemes for nonlinear evolution equations of physical interest. In *Numerical approximation of partial differential equations (Madrid, 1985)*, volume 133 of *North-Holland Math. Stud.* 425–433 North-Holland, Amsterdam, 1987.

[72] Terrance Tao. Nonlinear dispersive equations: local and global analysis. CBMS Regional Conference Series in Mathematics 106 American Math. Soc., Providence, 2006.

[73] Terence Tao. Two remarks on the generalised Korteweg-de Vries equation. *Discrete Contin. Dyn. Syst.* 18(1) 1–14 (2007).

[74] Lloyd N. Trefethen. *Spectral methods in MATLAB*, volume 10 of *Software, Environments, and Tools*. Society for Industrial and Applied Mathematics (SIAM), Philadelphia, PA (2000).

[75] Nianyu Yi, Yunqing Huang, and Hailiang Liu. A direct discontinuous Galerkin method for the generalized Korteweg-de Vries equation: energy conservation and boundary effect. *J. Comput. Phys.* 242 351–366 (2013).

[76] Jue Yan and Chi-Wang Shu. A local discontinuous Galerkin method for KdV type equations. *SIAM J. Numer. Anal.* 40(2) 769–791 (2002).

[77] V. Zharnitsky, E. Grenier, Christopher K. R. T. Jones, and S. K. Turitsyn. Stabilizing effects of dispersion management. *Phys. D* 152/153 794–817 (2001).

[78] N. J. Zabusky and C. Galvin. *J. Fluid Mech.* 47(4) 811–824 (1971).

Click here to access/download Figure;bloww_compare_002.pdf

Numerical solutions at time t=0.02

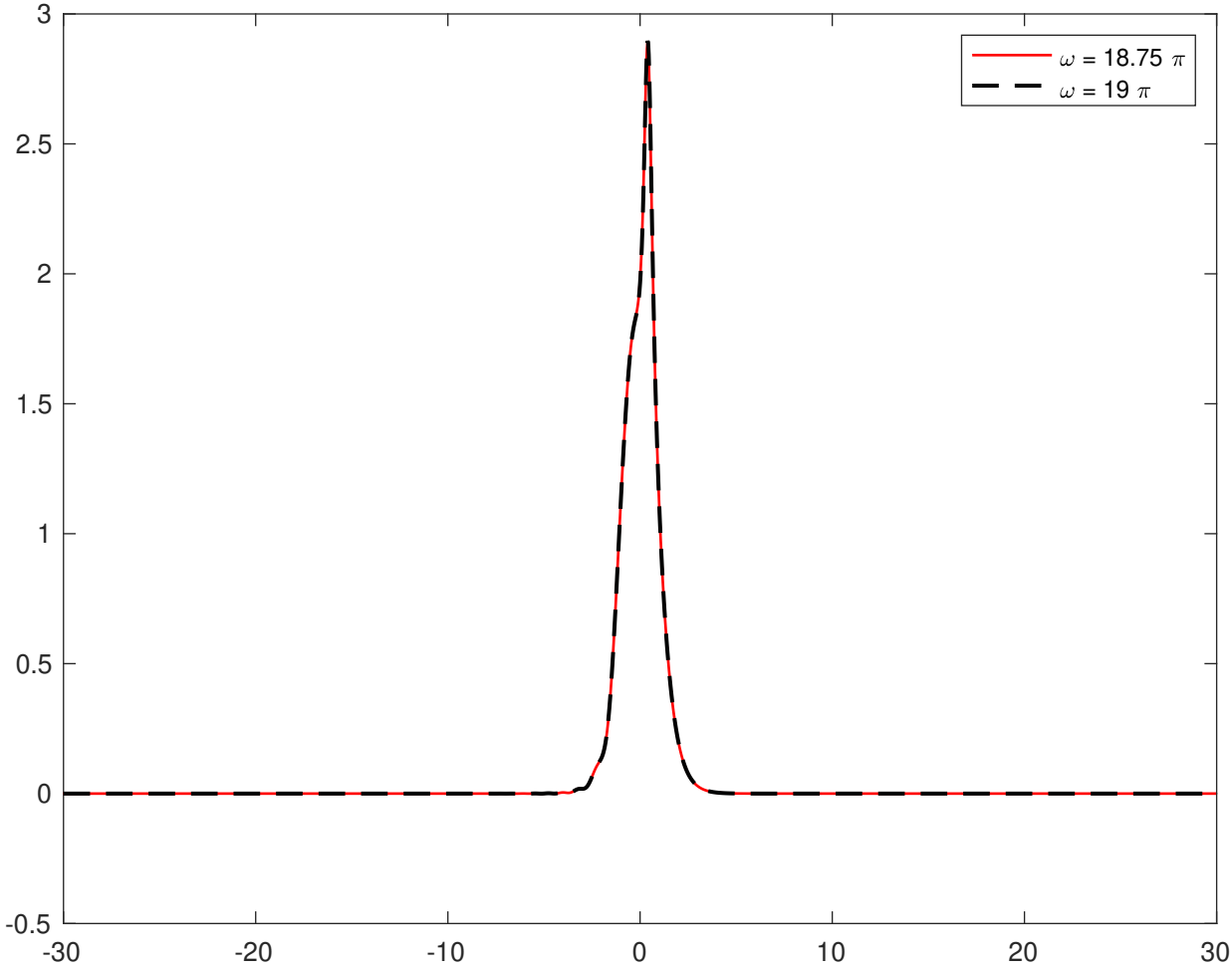

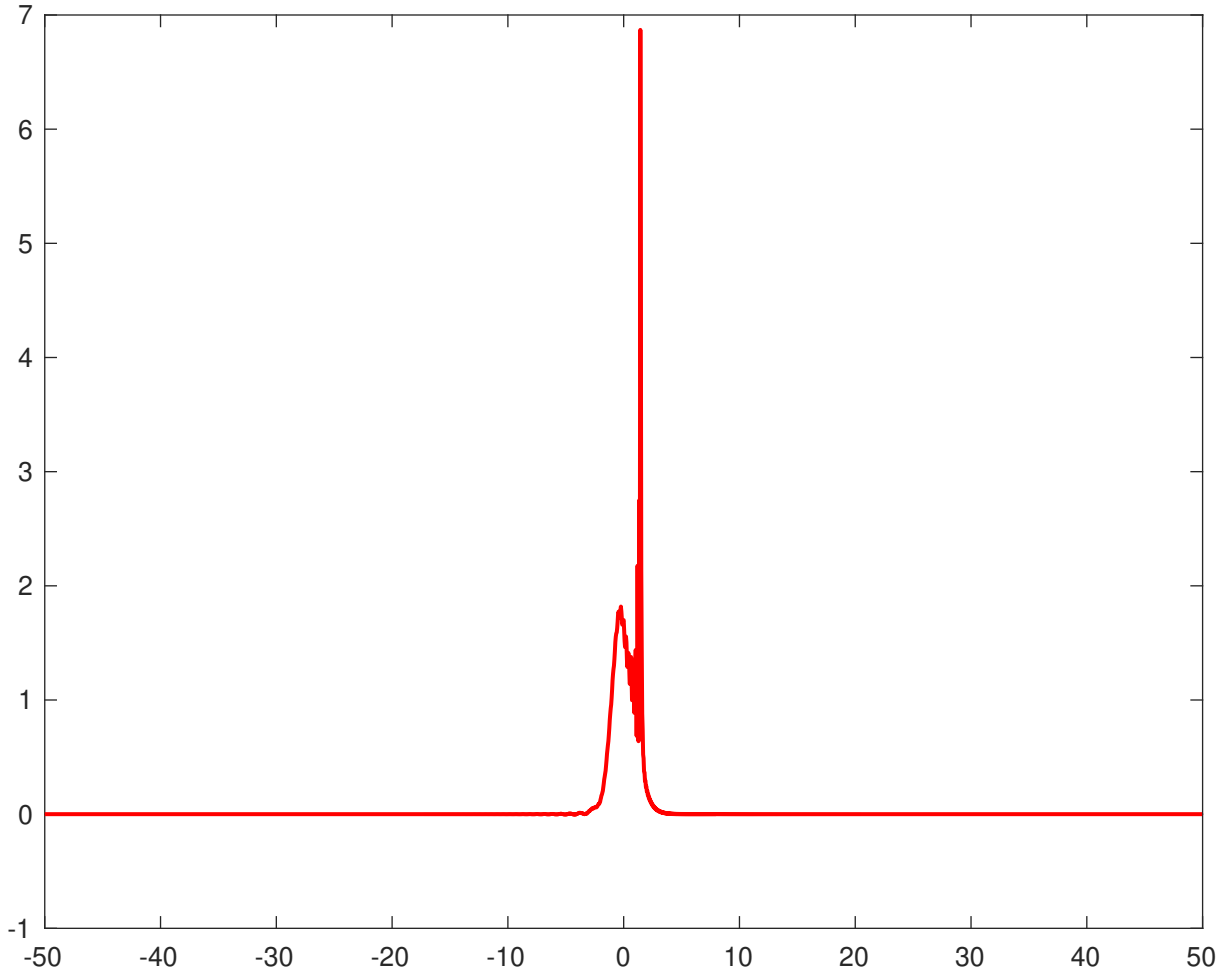

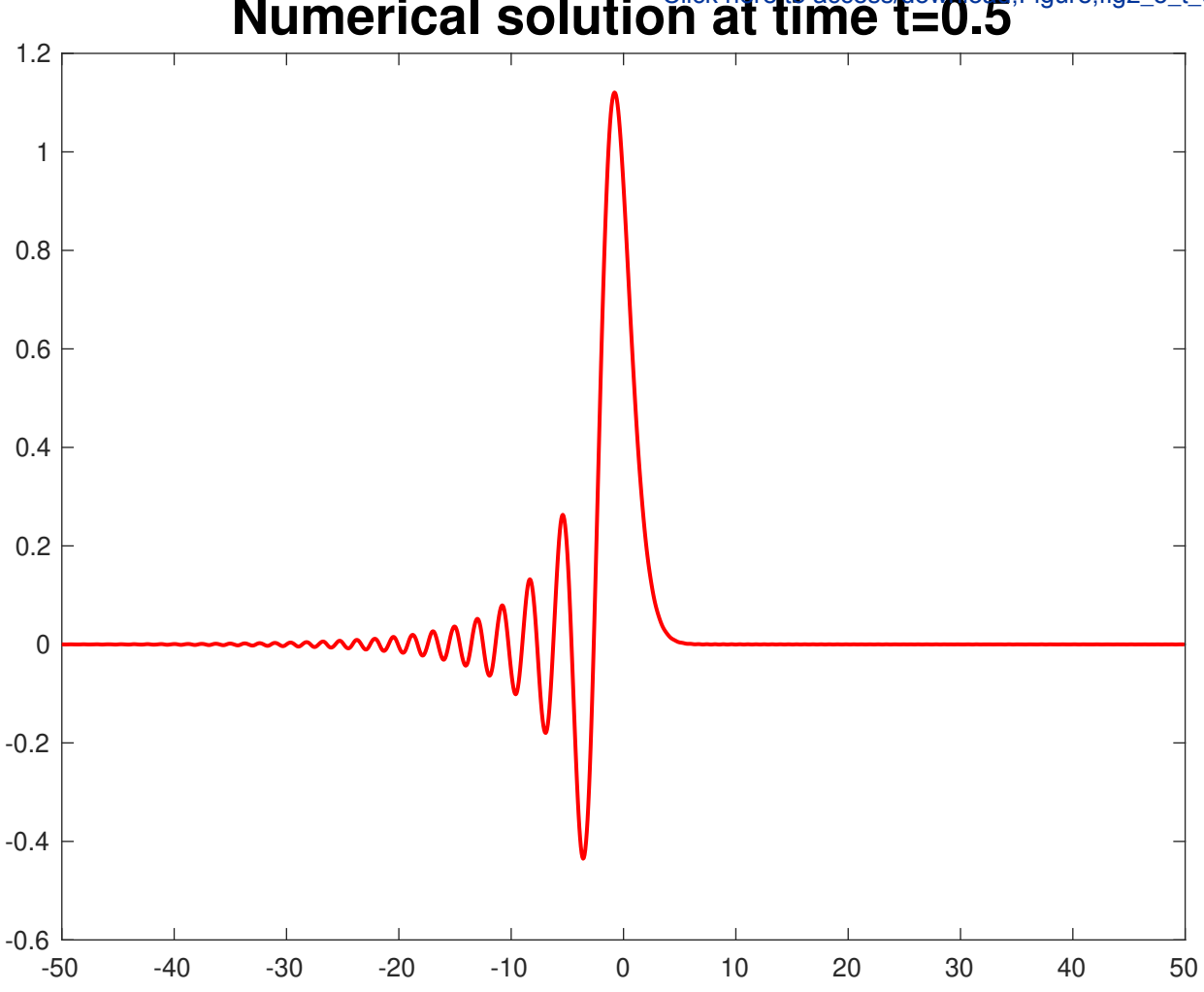

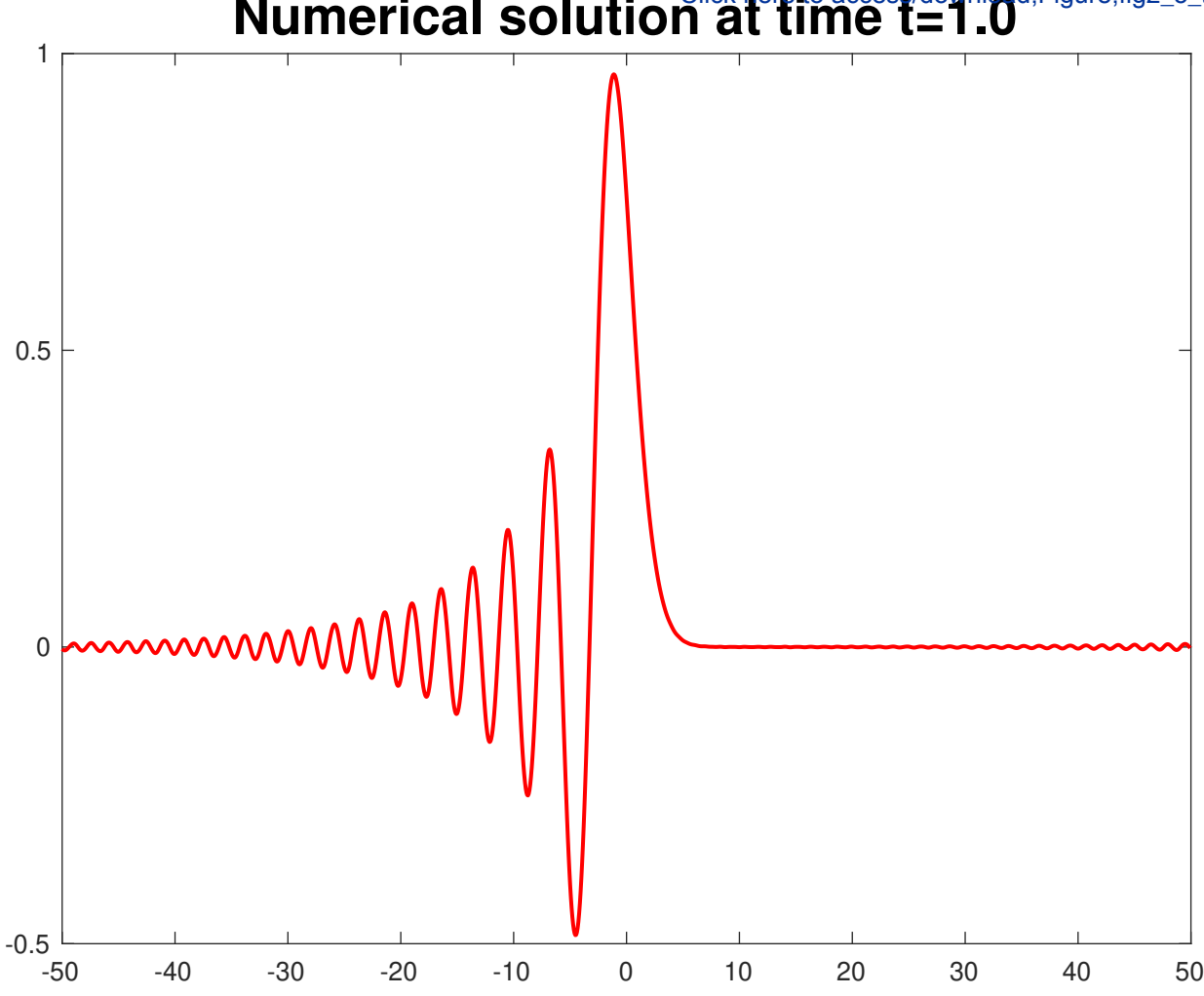

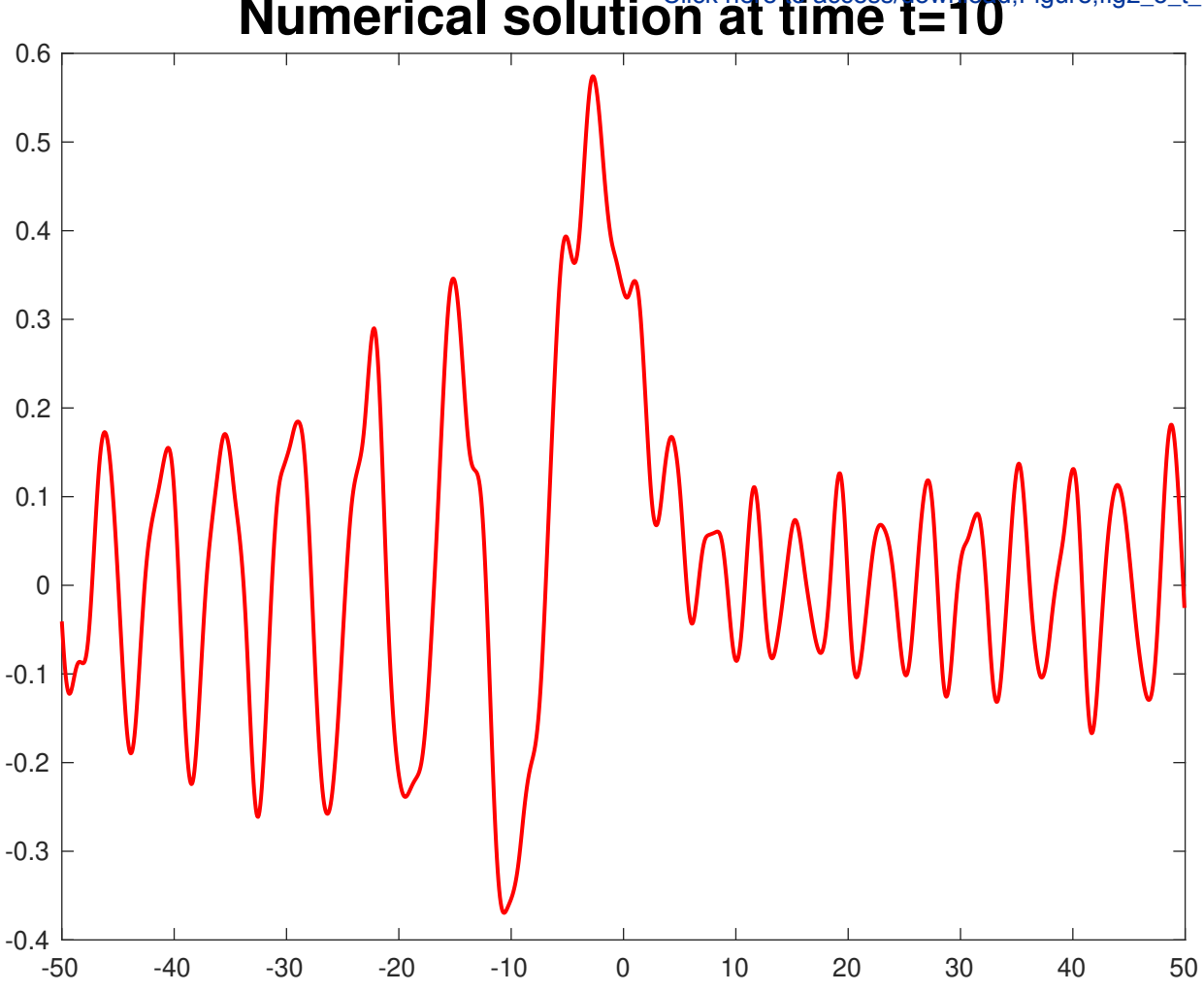

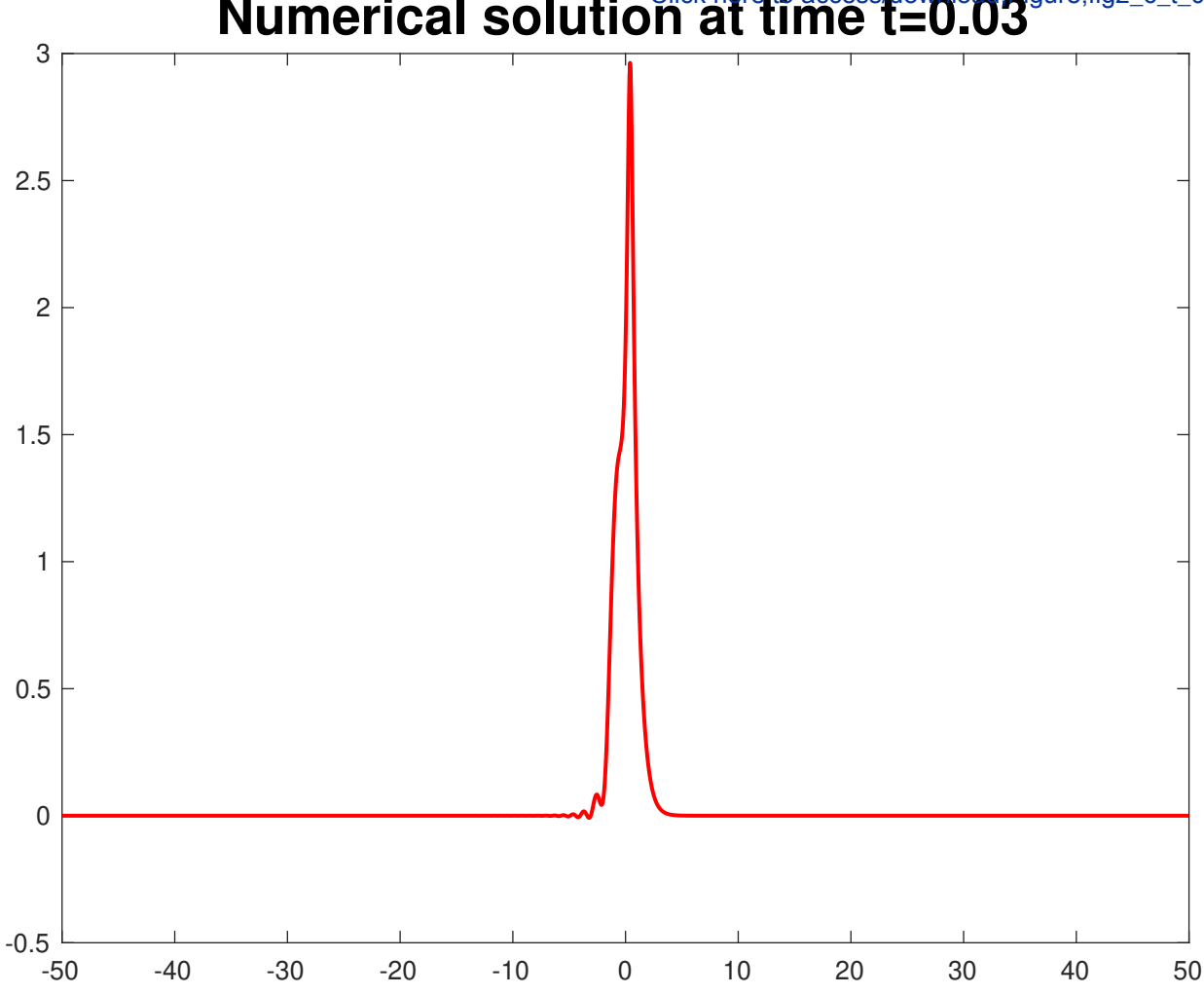

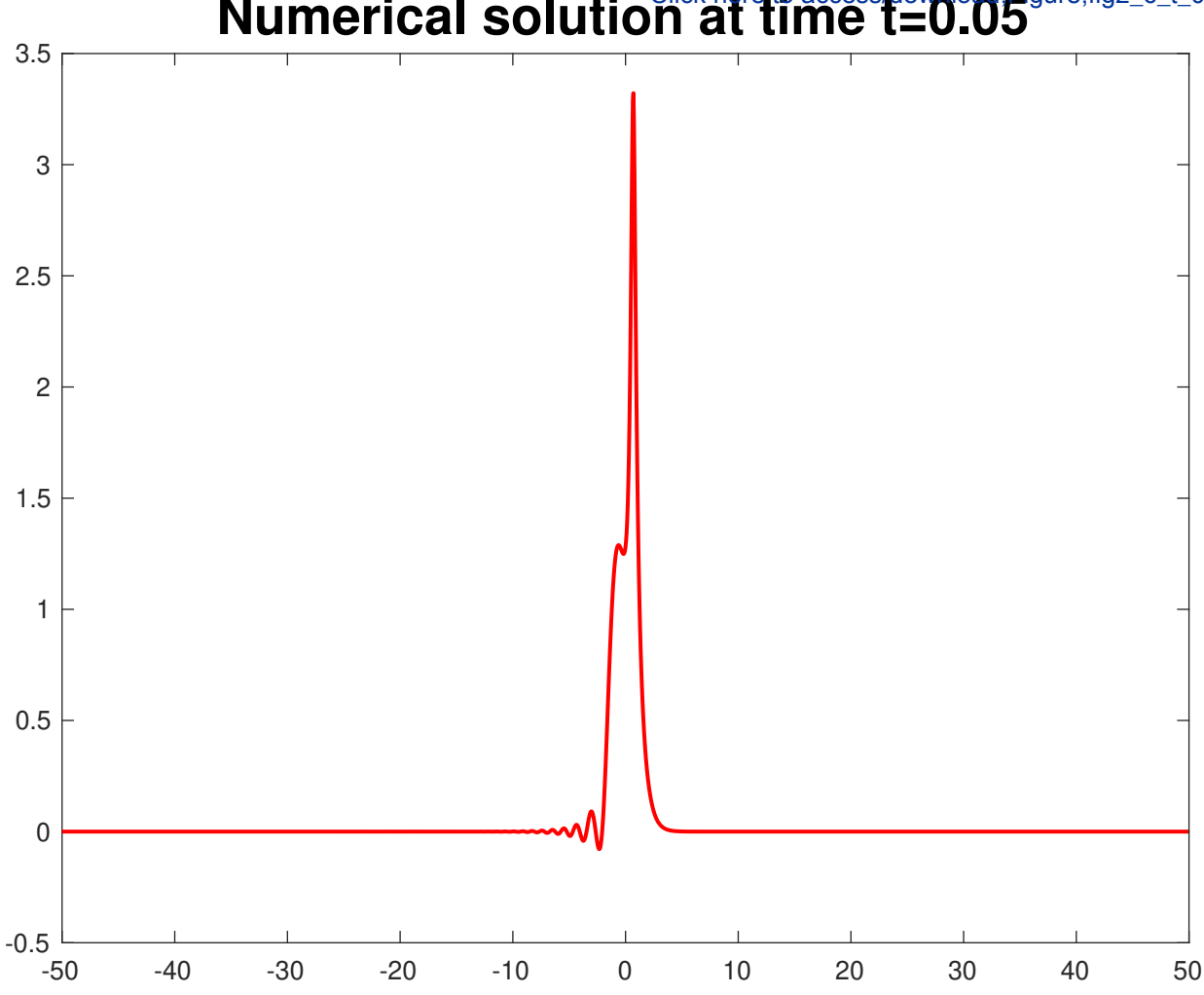

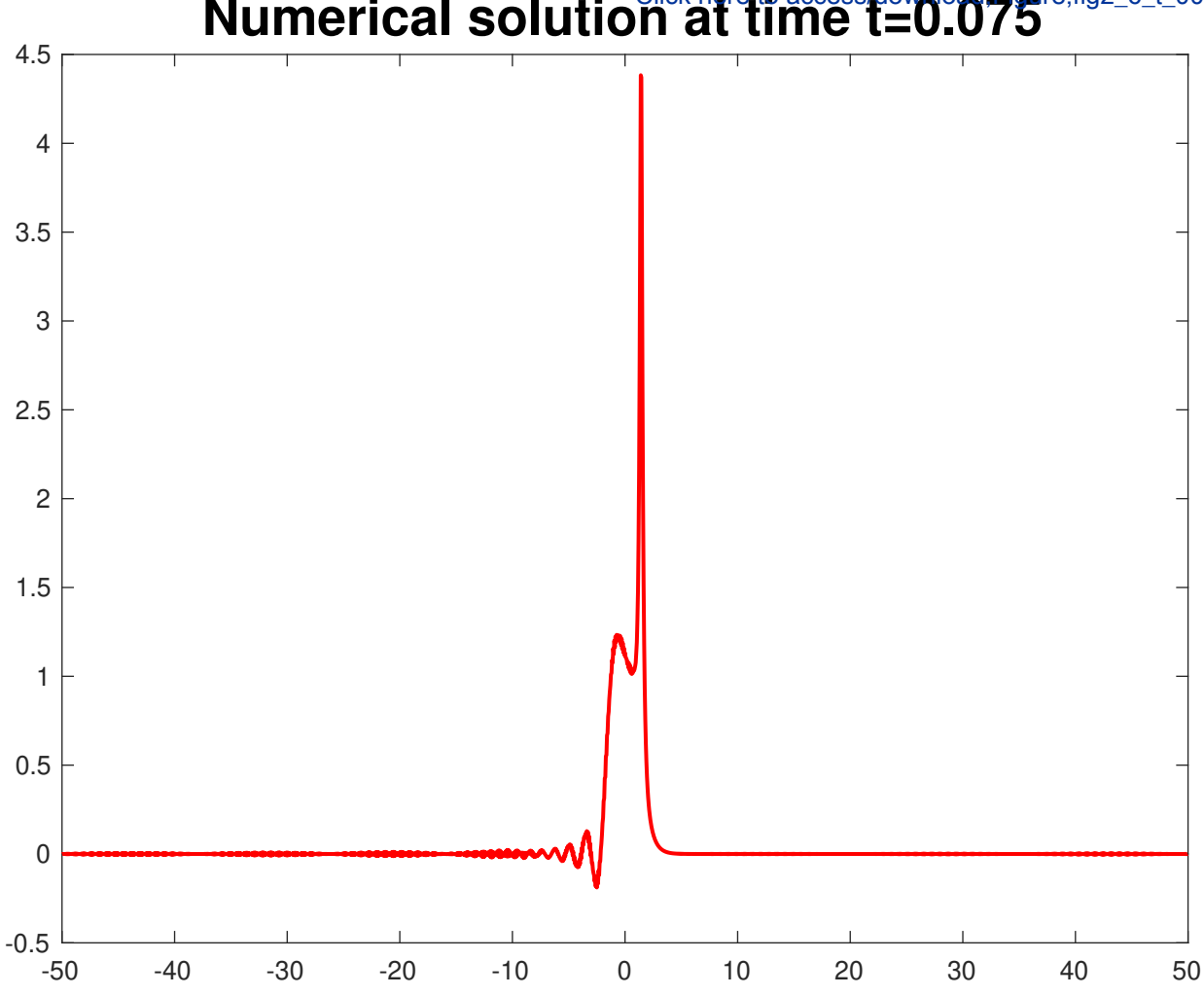

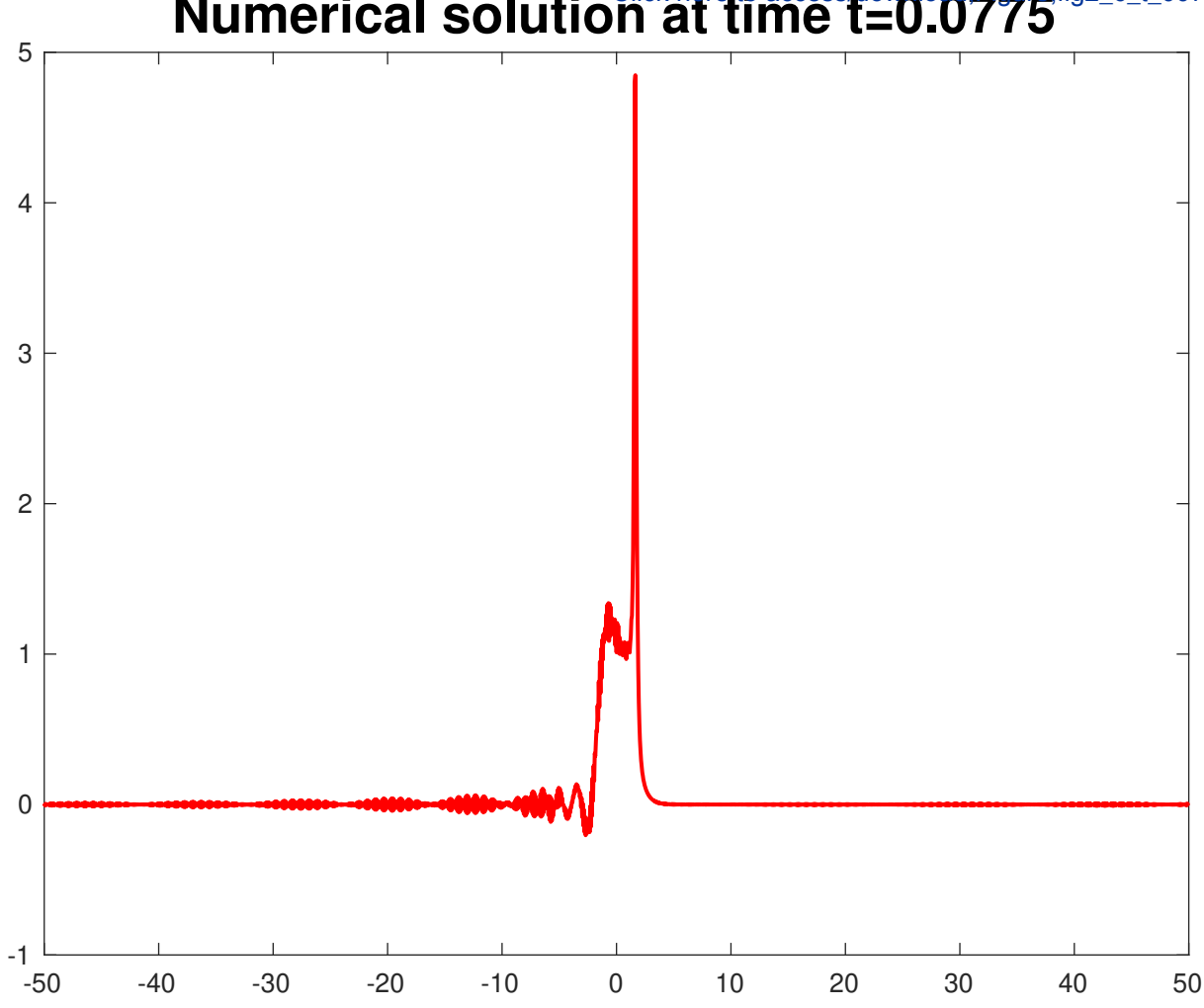

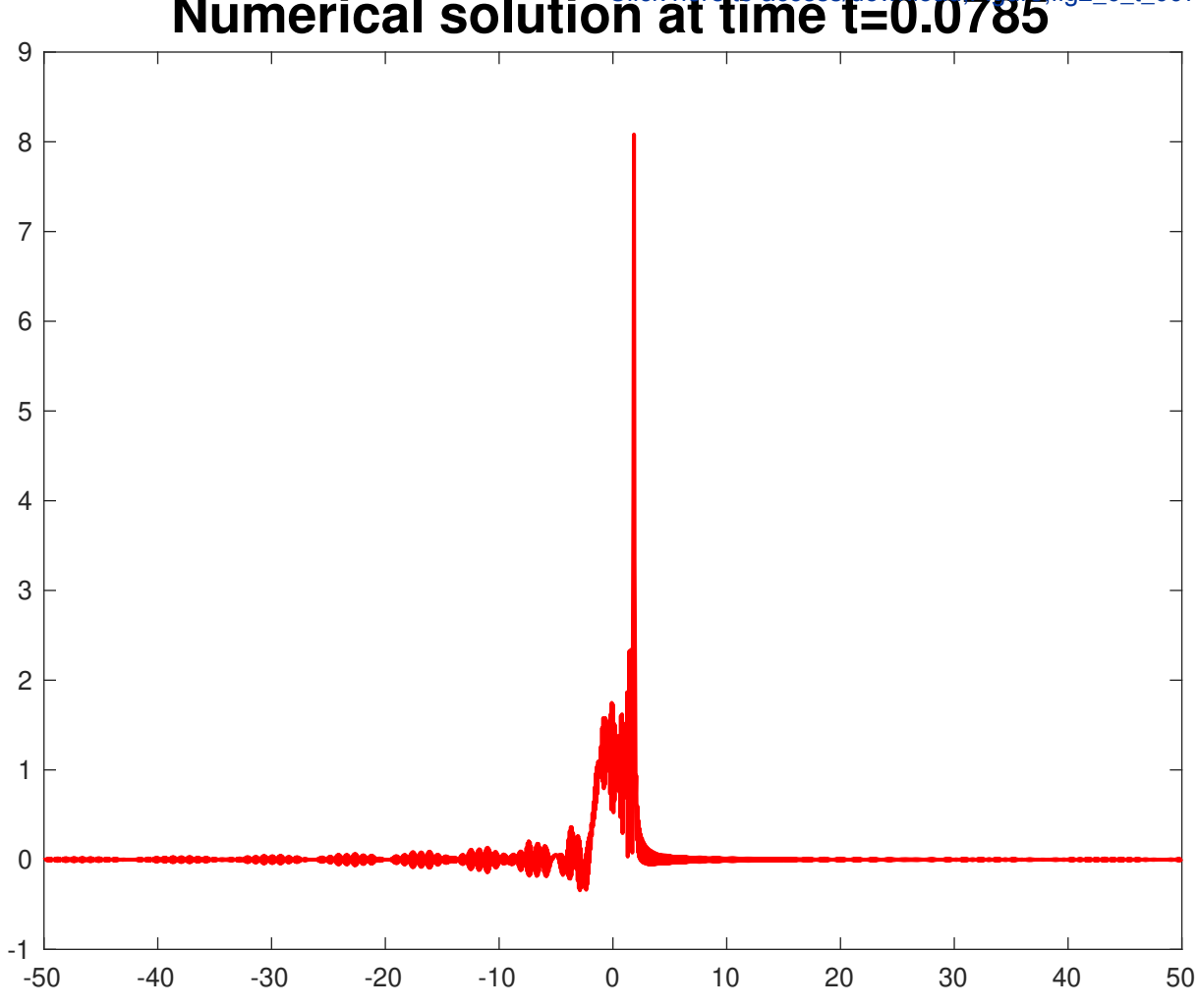

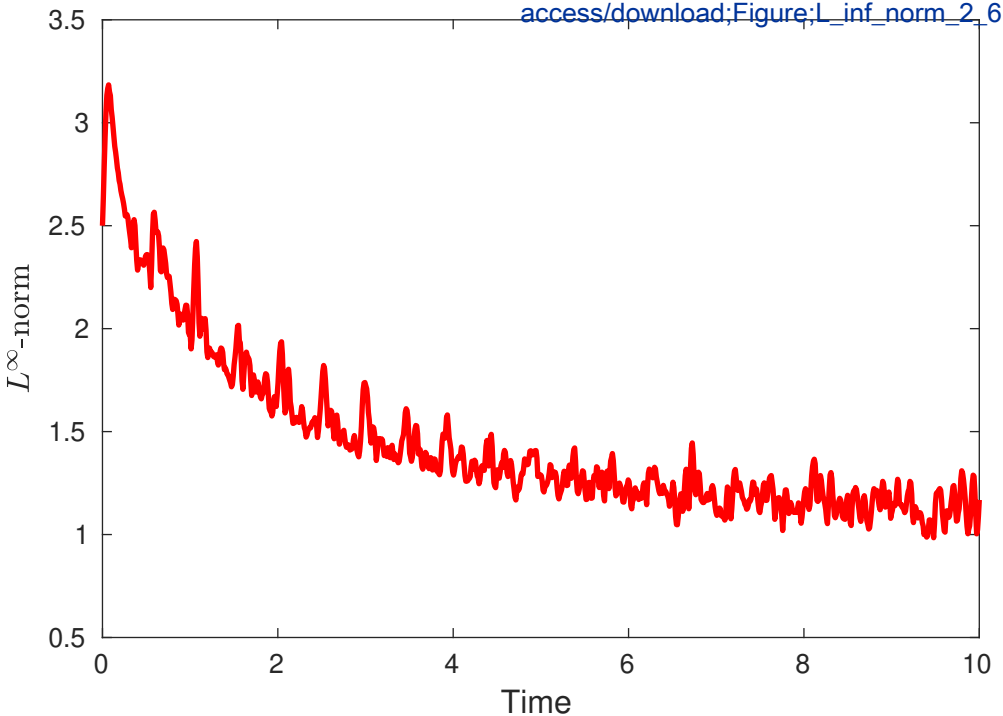

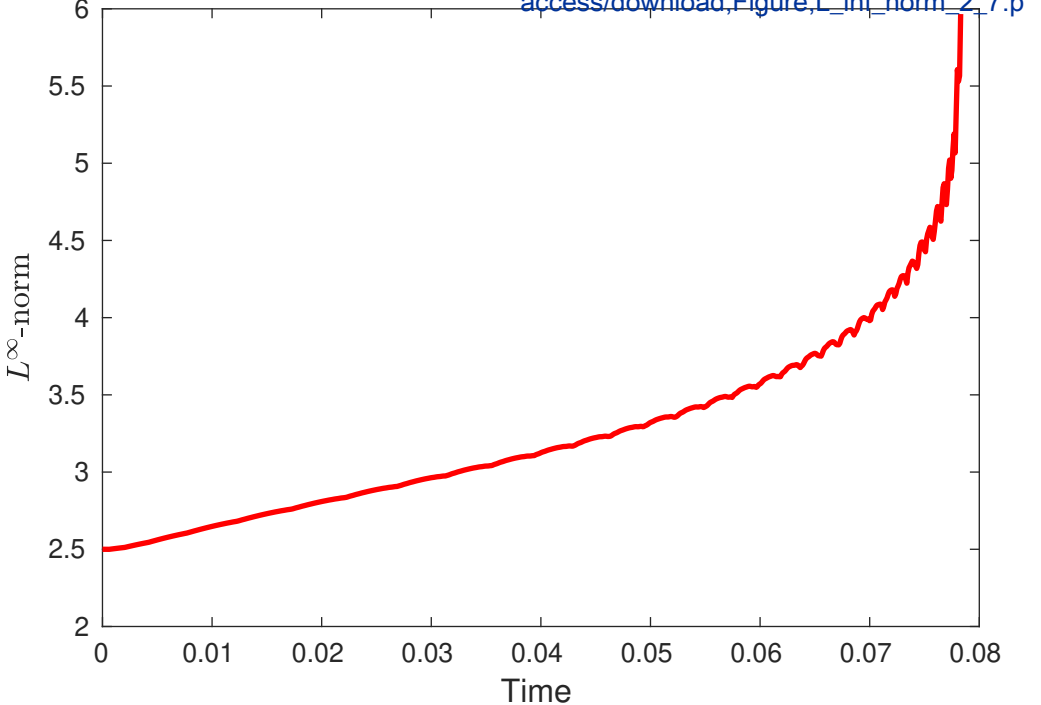

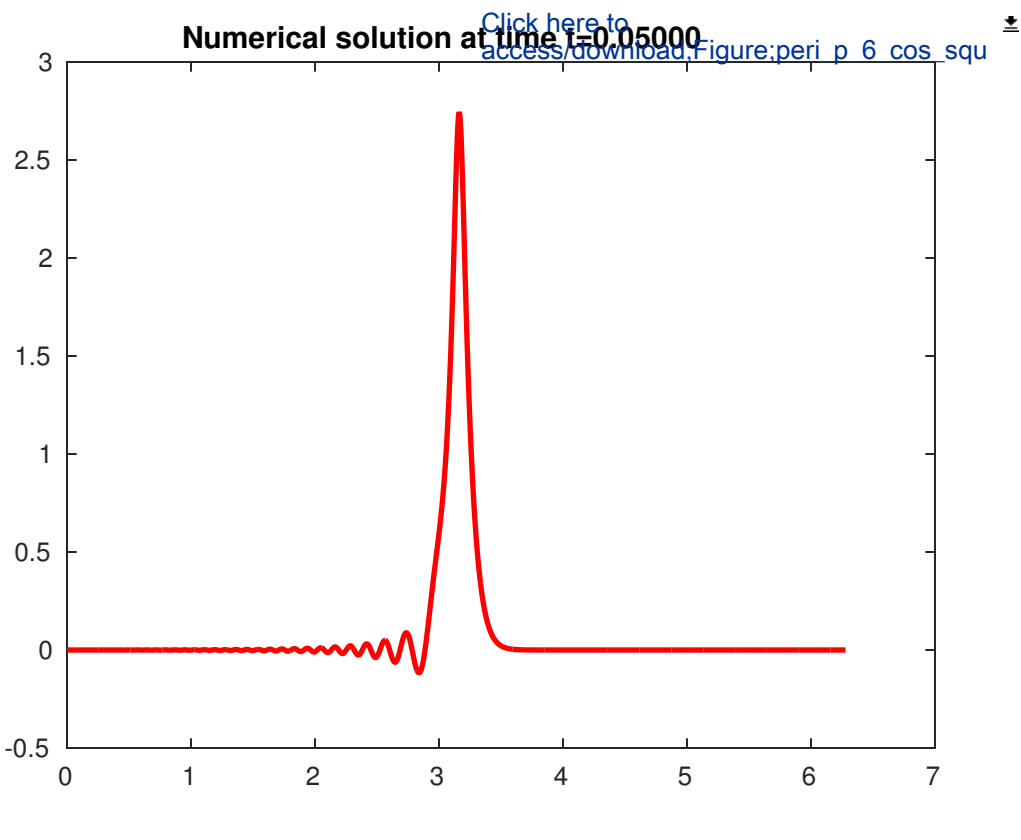
Numerical solution at time t=0.05000
Click here to access/download;Figure;peri_p_6_cos_squ
3
2.5
2
1.5
1
0.5
0
-0.5
0
1
2
3
4
5
6
7

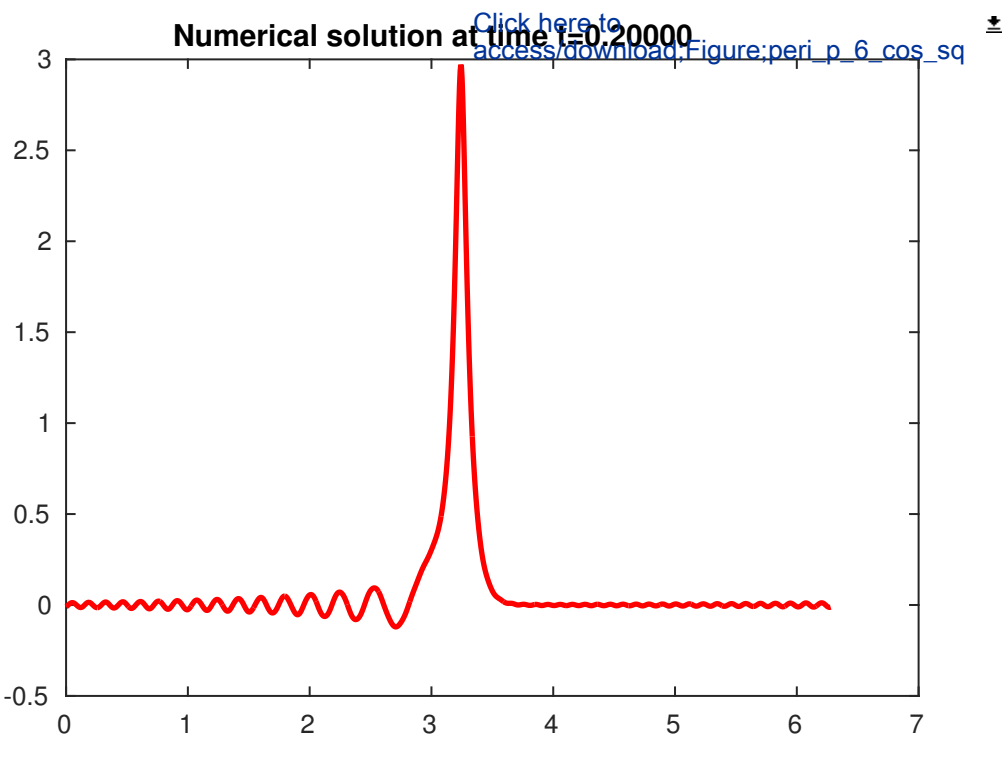
Numerical solution at time t=0.20000
Click here to access/download;Figure;peri_p_6_cos_sq
3
2.5
2
1.5
1
0.5
0
-0.5
0
1
2
3
4
5
6
7

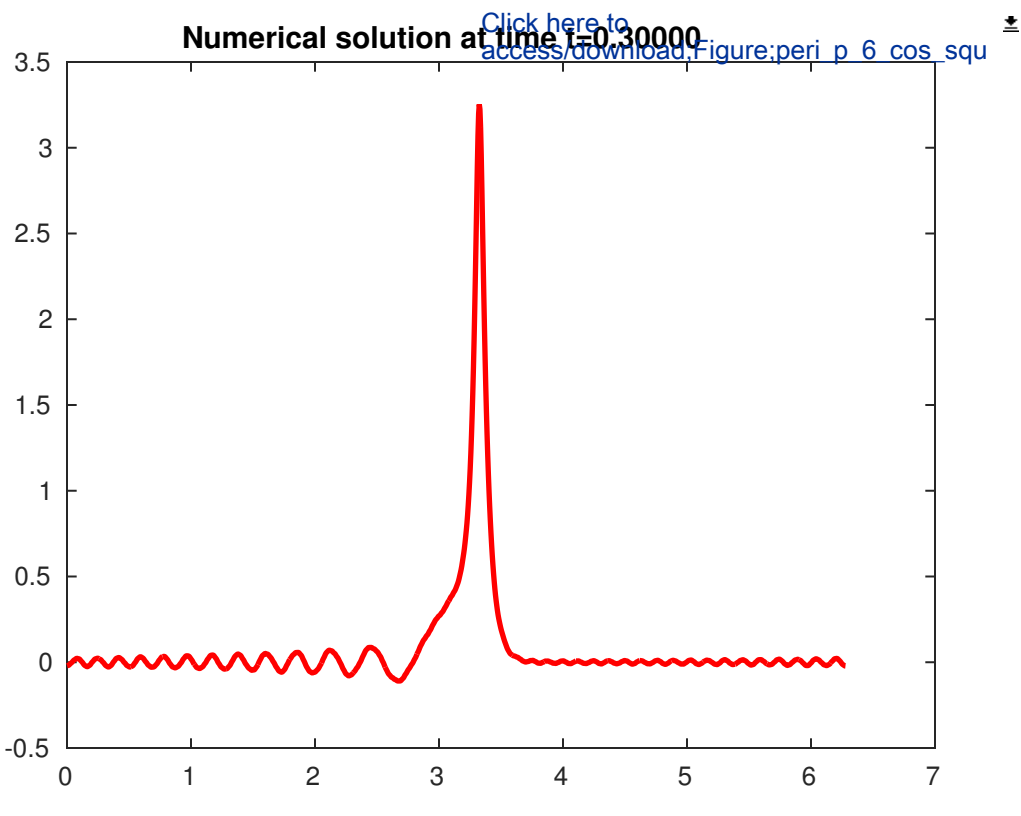
Click here to
access/download;Figure;peri_p_6_cos_squ
Numerical solution at time t=0.30000
3.5
3
2.5
2
1.5
1
0.5
0
-0.5
0
1
2
3
4
5
6
7

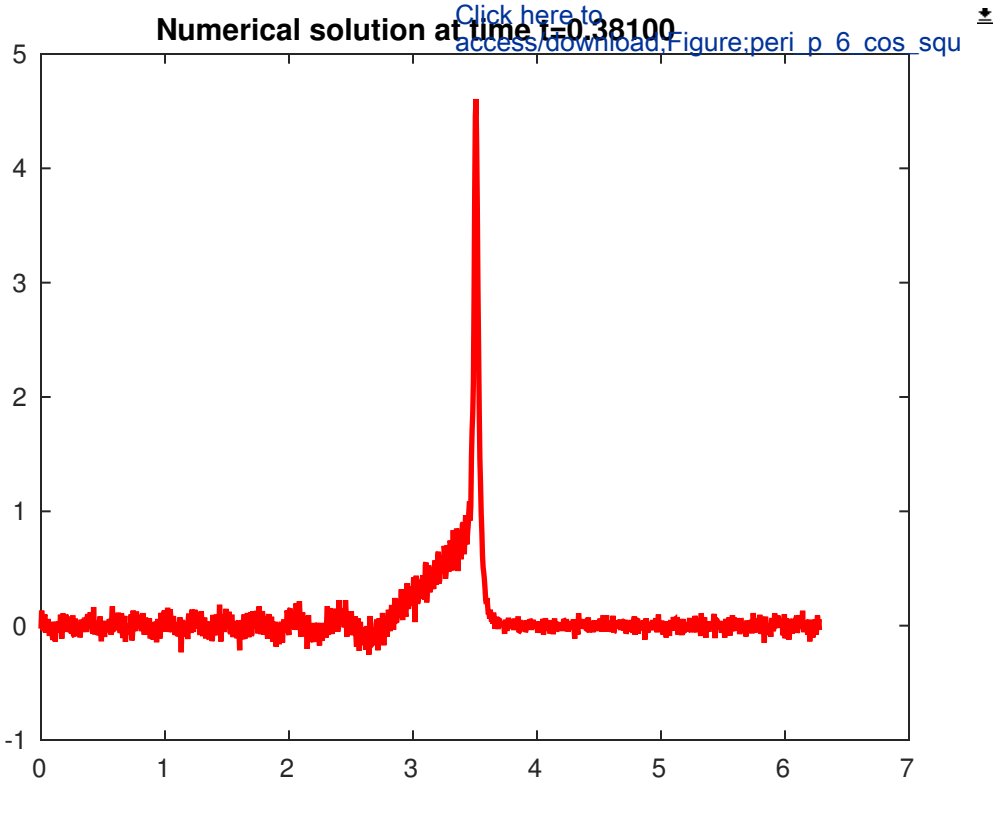
Numerical solution at time t=0.38100
Click here to access/download;Figure;peri_p_6_cos_squ
5
4
3
2
1
0
-1
0
1
2
3
4
5
6
7

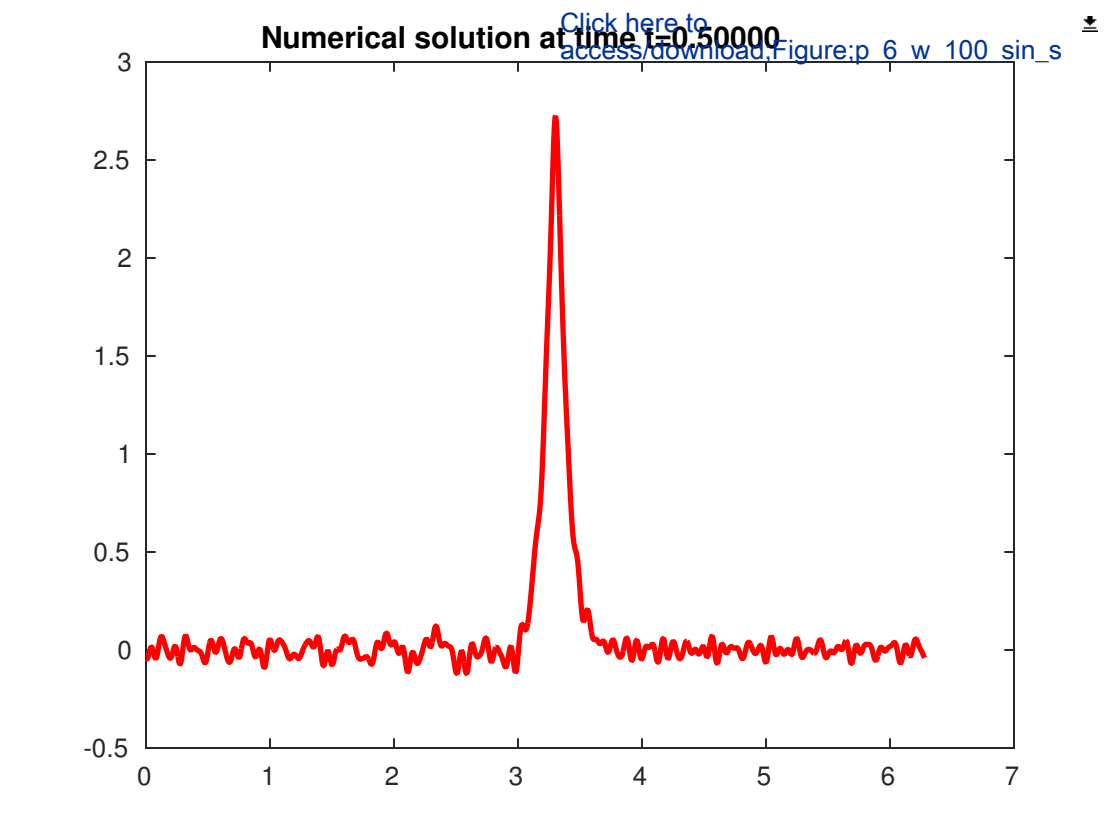
Numerical solution at time t=0.50000
Click here to access/download;Figure;p_6_w_100_sin_s
3
2.5
2
1.5
1
0.5
0
-0.5
0
1
2
3
4
5
6
7

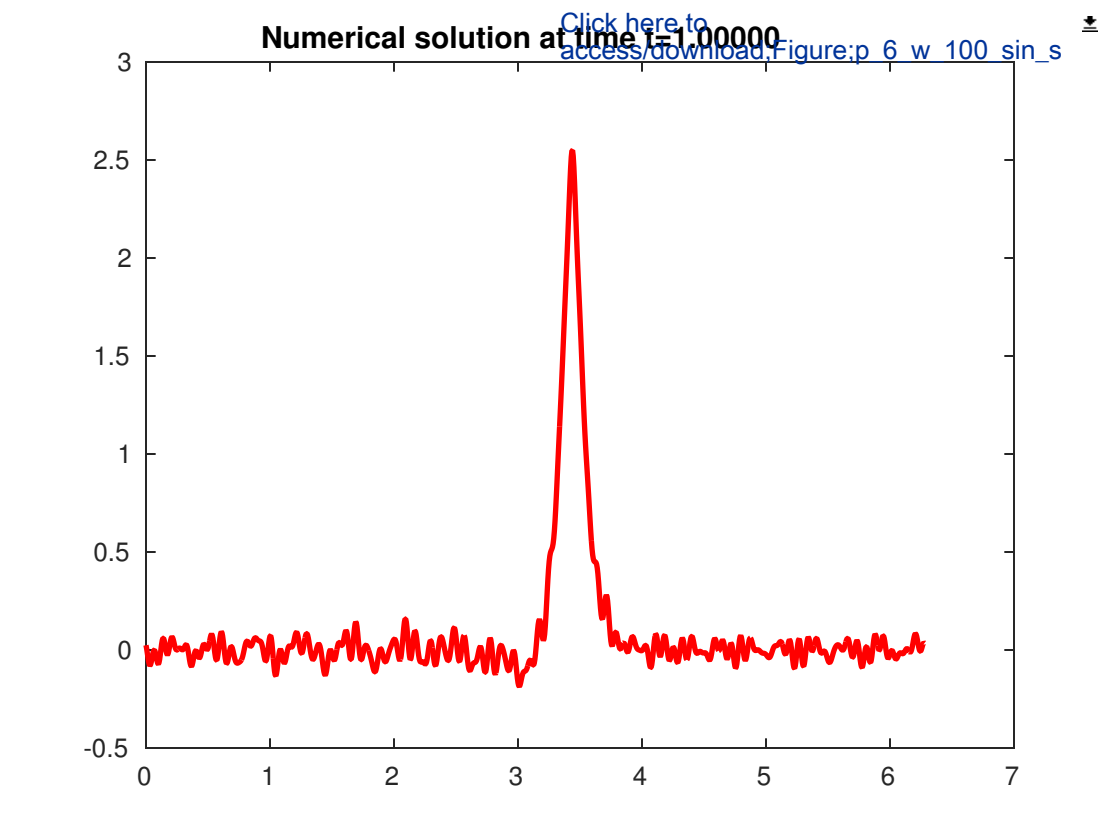
Click here to
access/download;Figure;p_6_w_100_sin_s
Numerical solution at time t=1.00000
3
2.5
2
1.5
1
0.5
0
-0.5
0
1
2
3
4
5
6
7

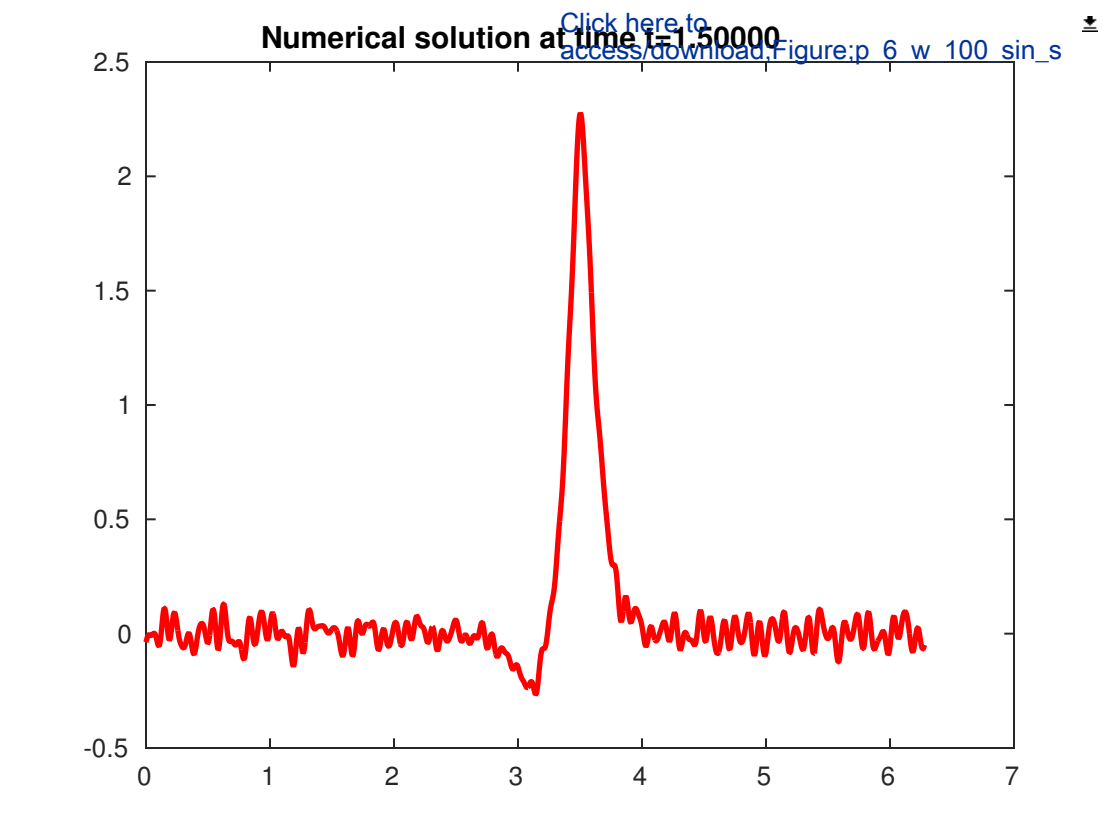
Numerical solution at time t=1.50000
Click here to access/download;Figure;p_6_w_100_sin_s
2.5
2
1.5
1
0.5
0
-0.5
0
1
2
3
4
5
6
7

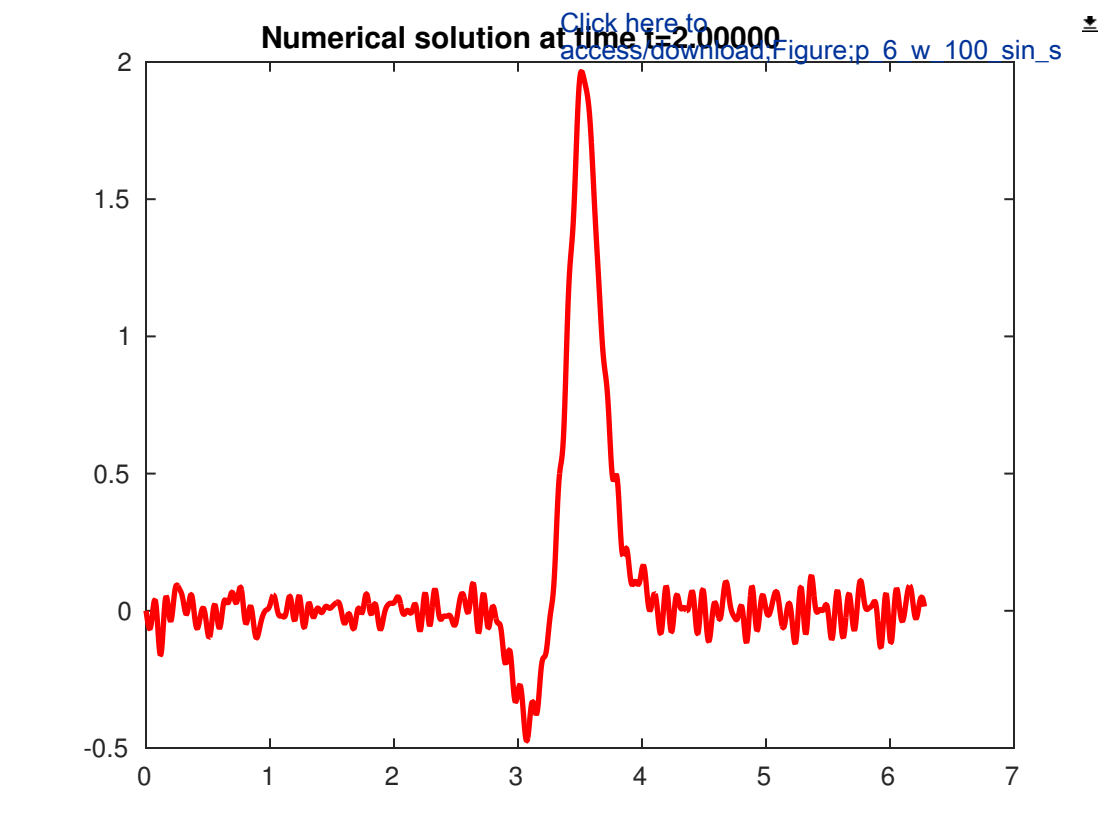
Numerical solution at time t=2.00000
Click here to access/download;Figure;p_6_w_100_sin_s
2
1.5
1
0.5
0
-0.5
0
1
2
3
4
5
6
7

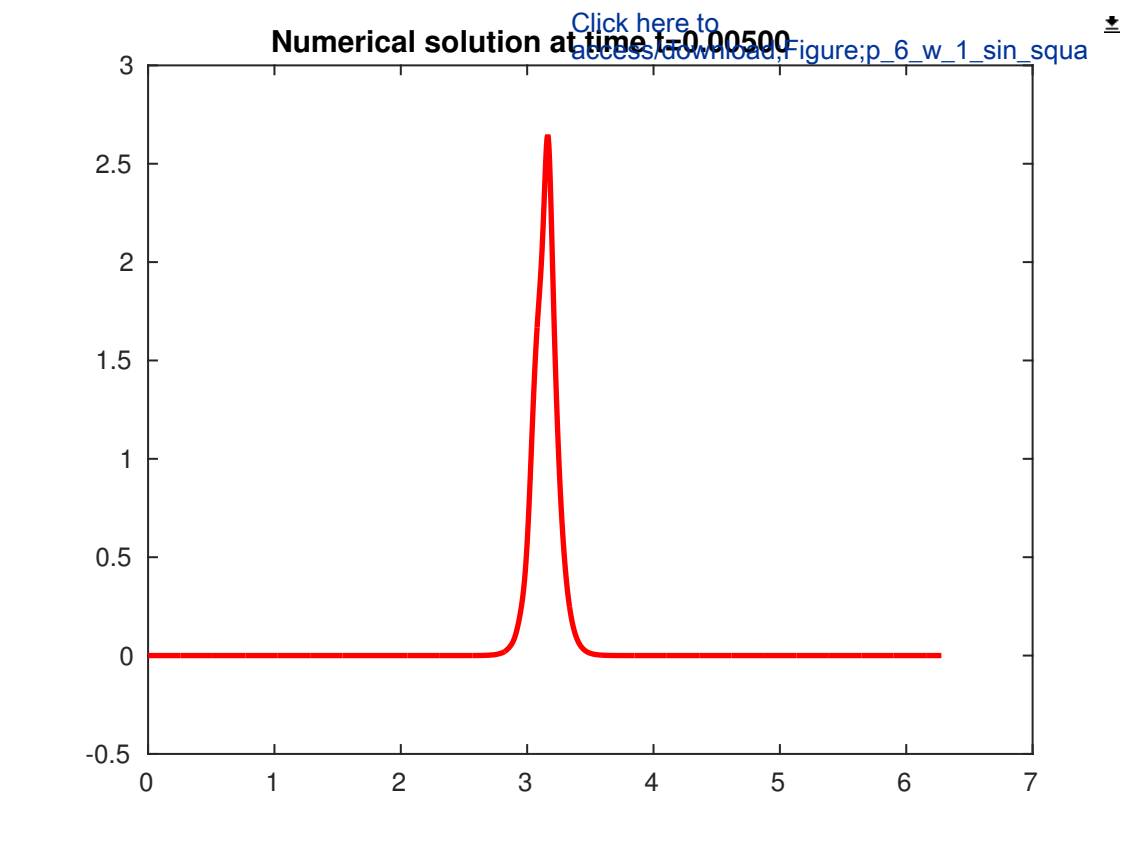
Numerical solution at time t=0.00500
Click here to
access/download;Figure;p_6_w_1_sin_squa
3
2.5
2
1.5
1
0.5
0
-0.5
0
1
2
3
4
5
6
7

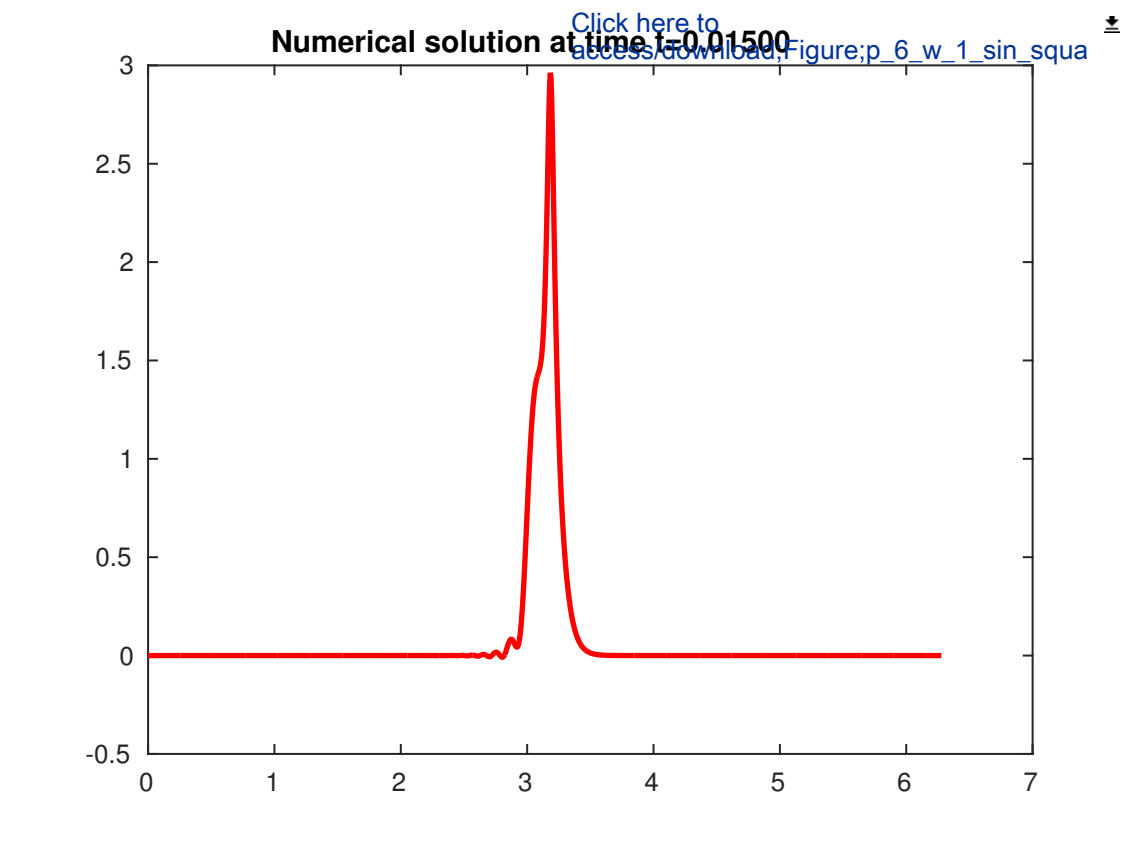
Numerical solution at time t=0.01500
Click here to
access/download;Figure;p_6_w_1_sin_squa
3
2.5
2
1.5
1
0.5
0
-0.5
0
1
2
3
4
5
6
7

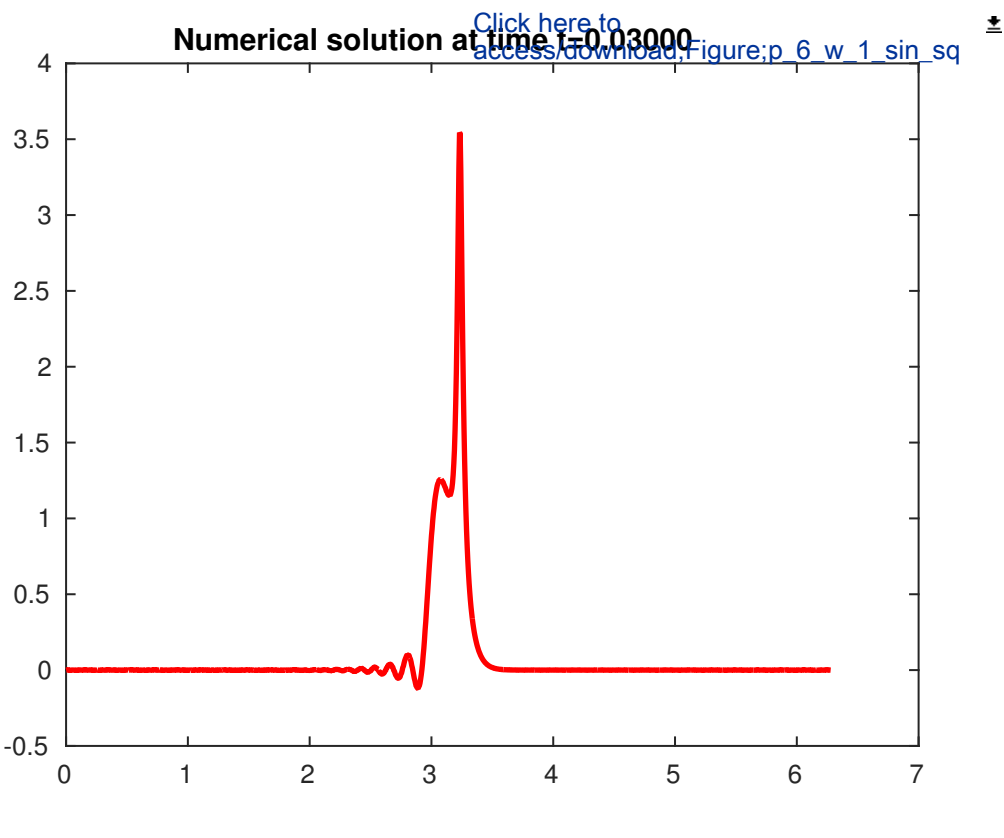
Numerical solution at time t=0.03000
Click here to access/download;Figure;p_6_w_1_sin_sq
4
3.5
3
2.5
2
1.5
1
0.5
0
-0.5
0
1
2
3
4
5
6
7

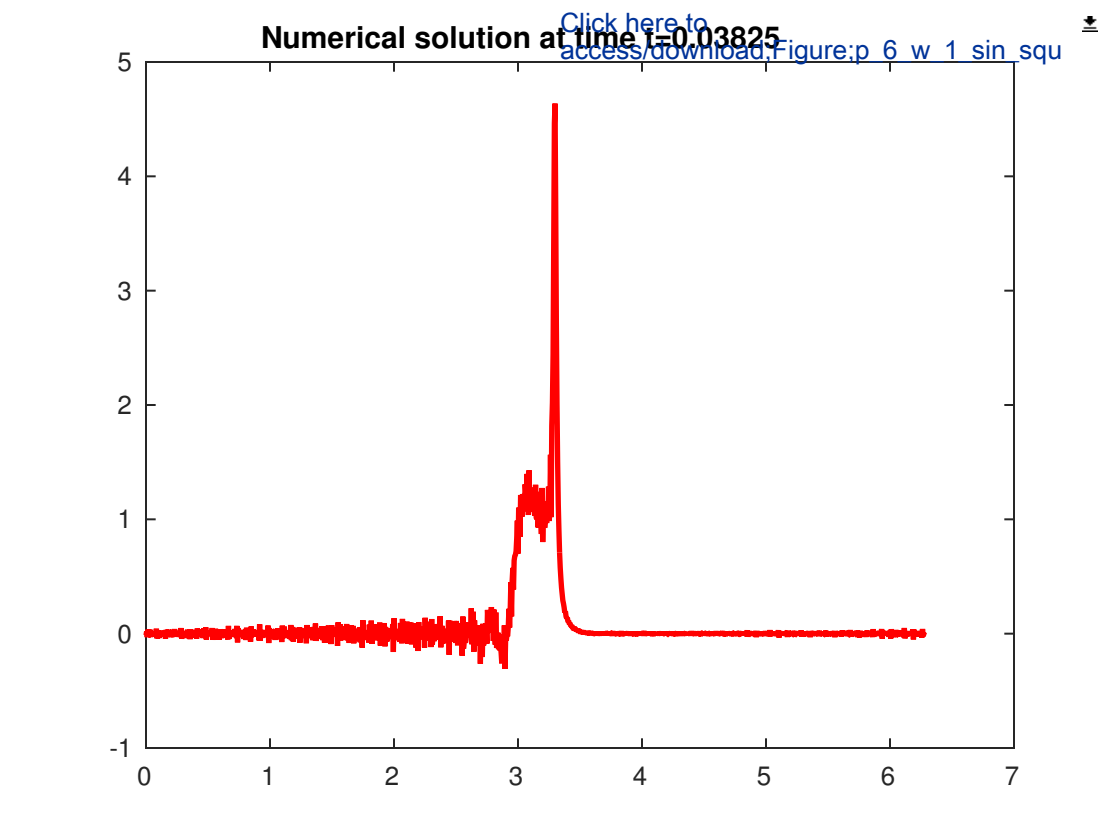
Numerical solution at time t=0.03825
Click here to access/download;Figure;p_6_w_1_sin_squ
5
4
3
2
1
0
-1
0
1
2
3
4
5
6
7

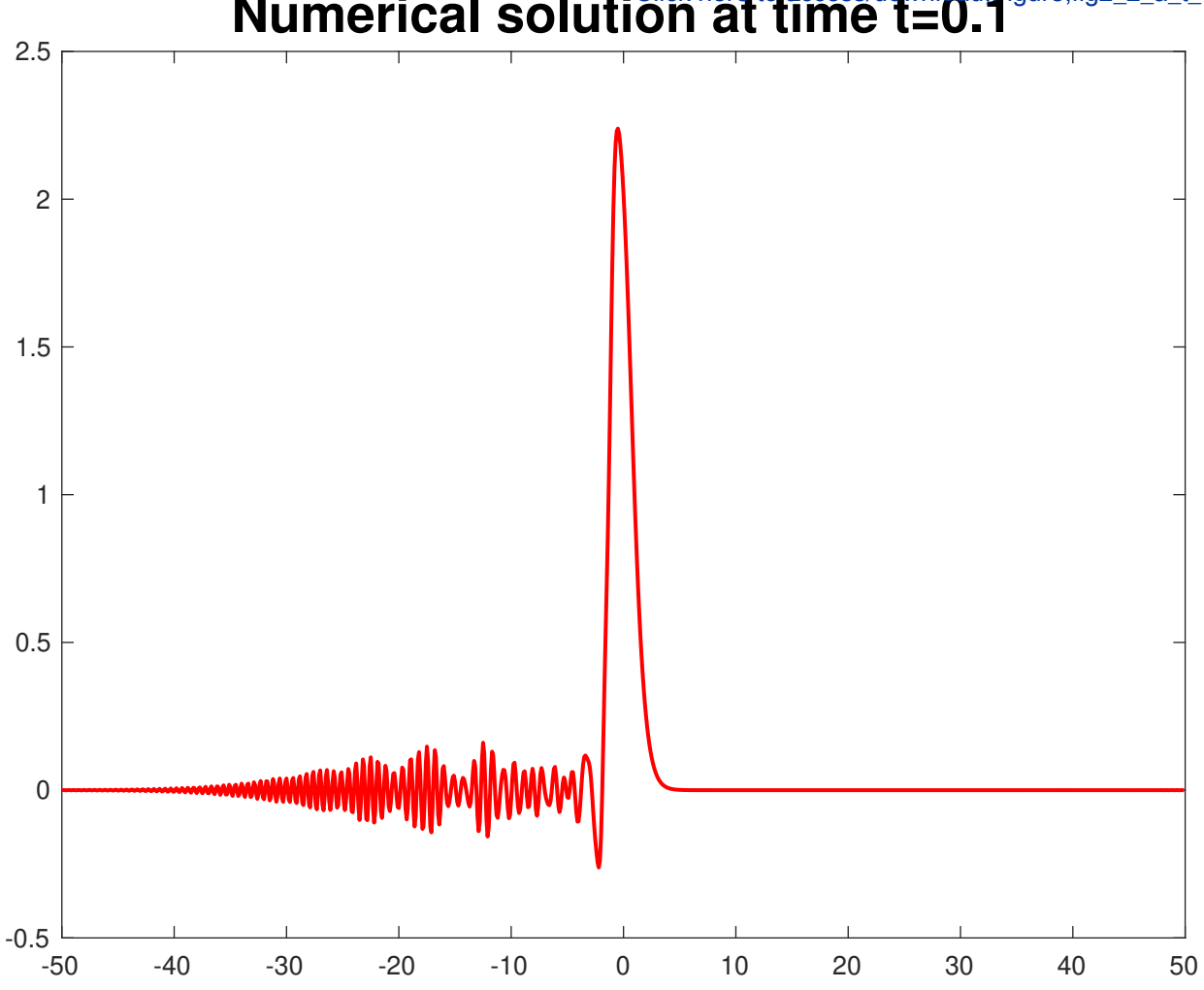

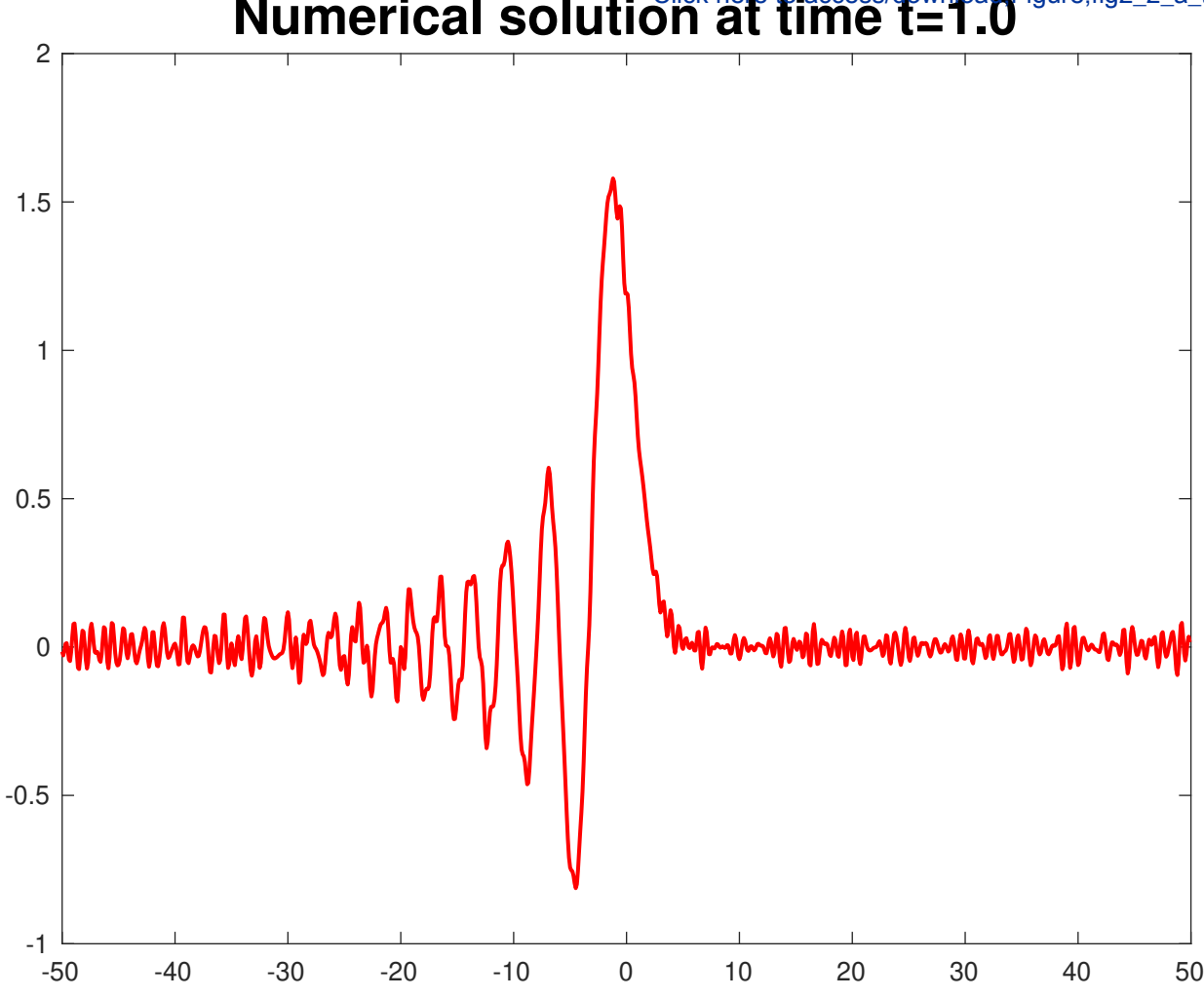

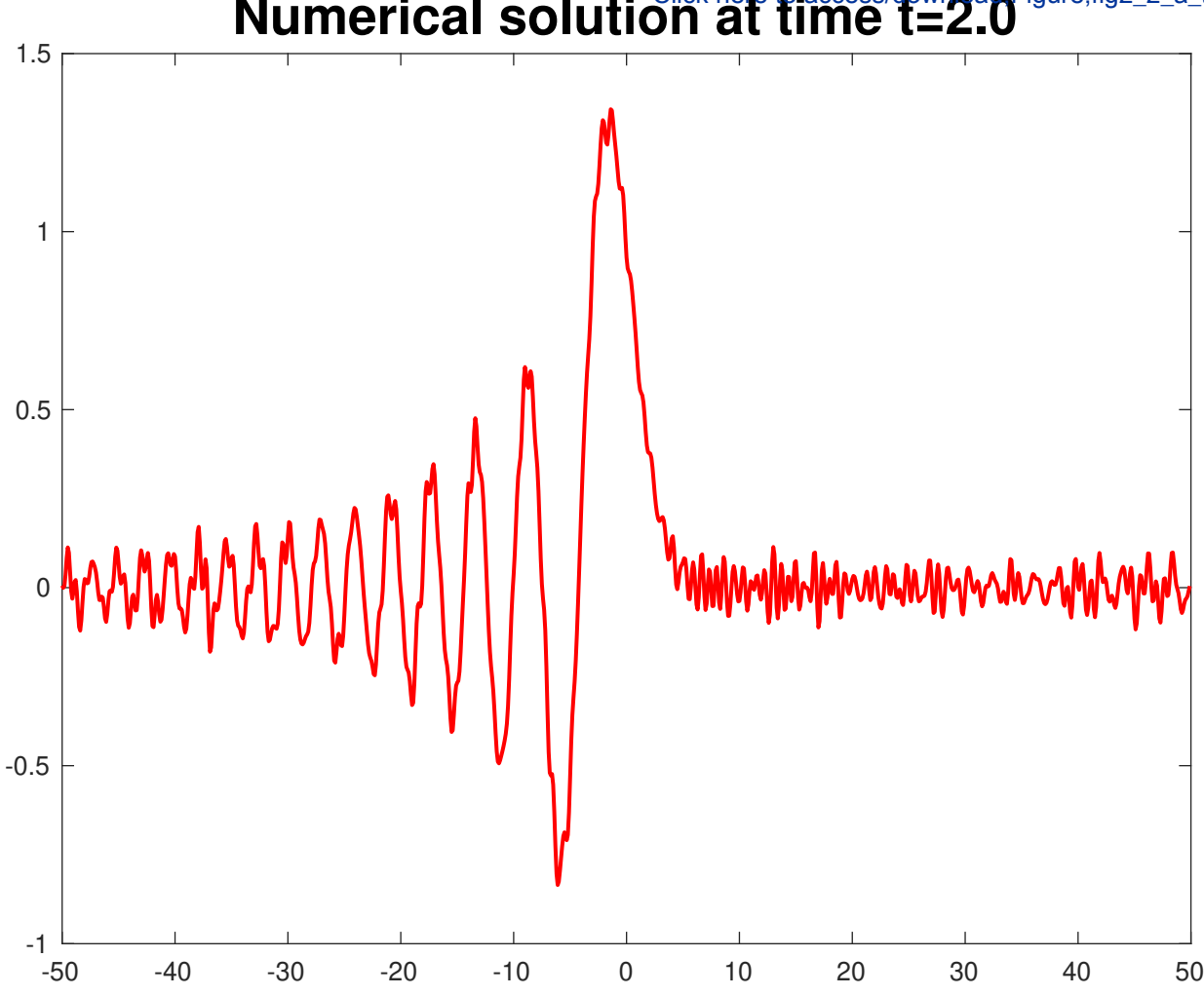

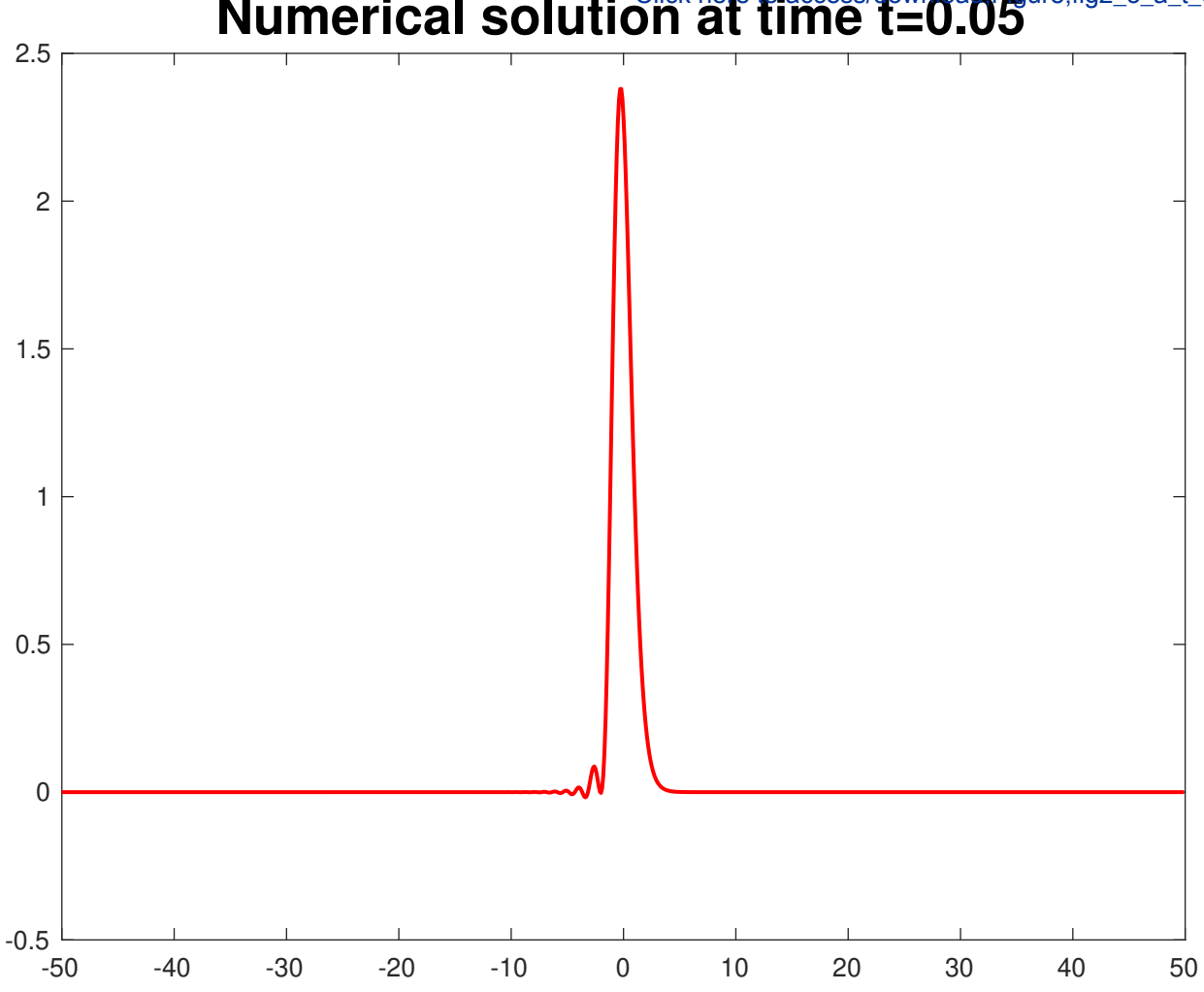

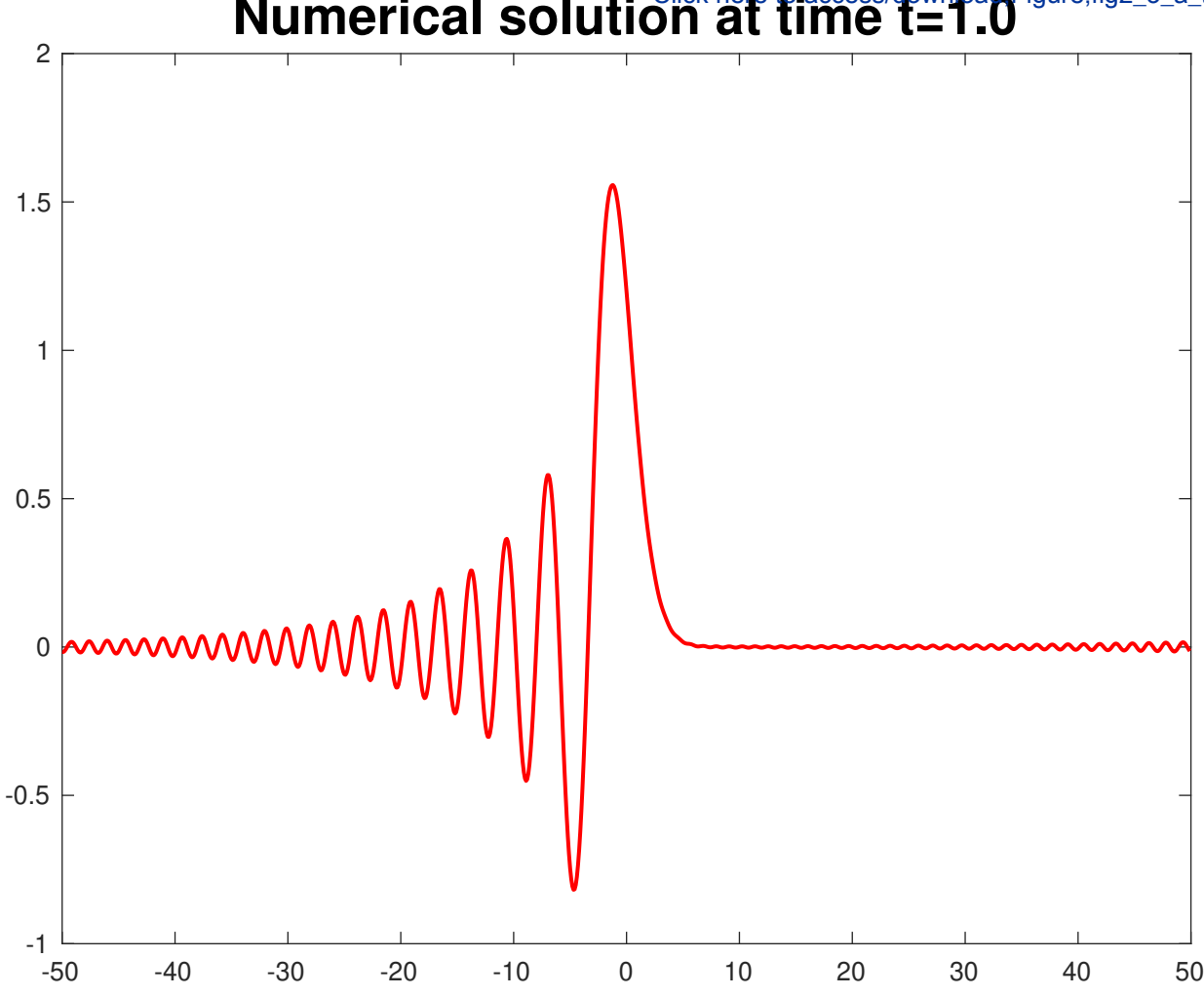

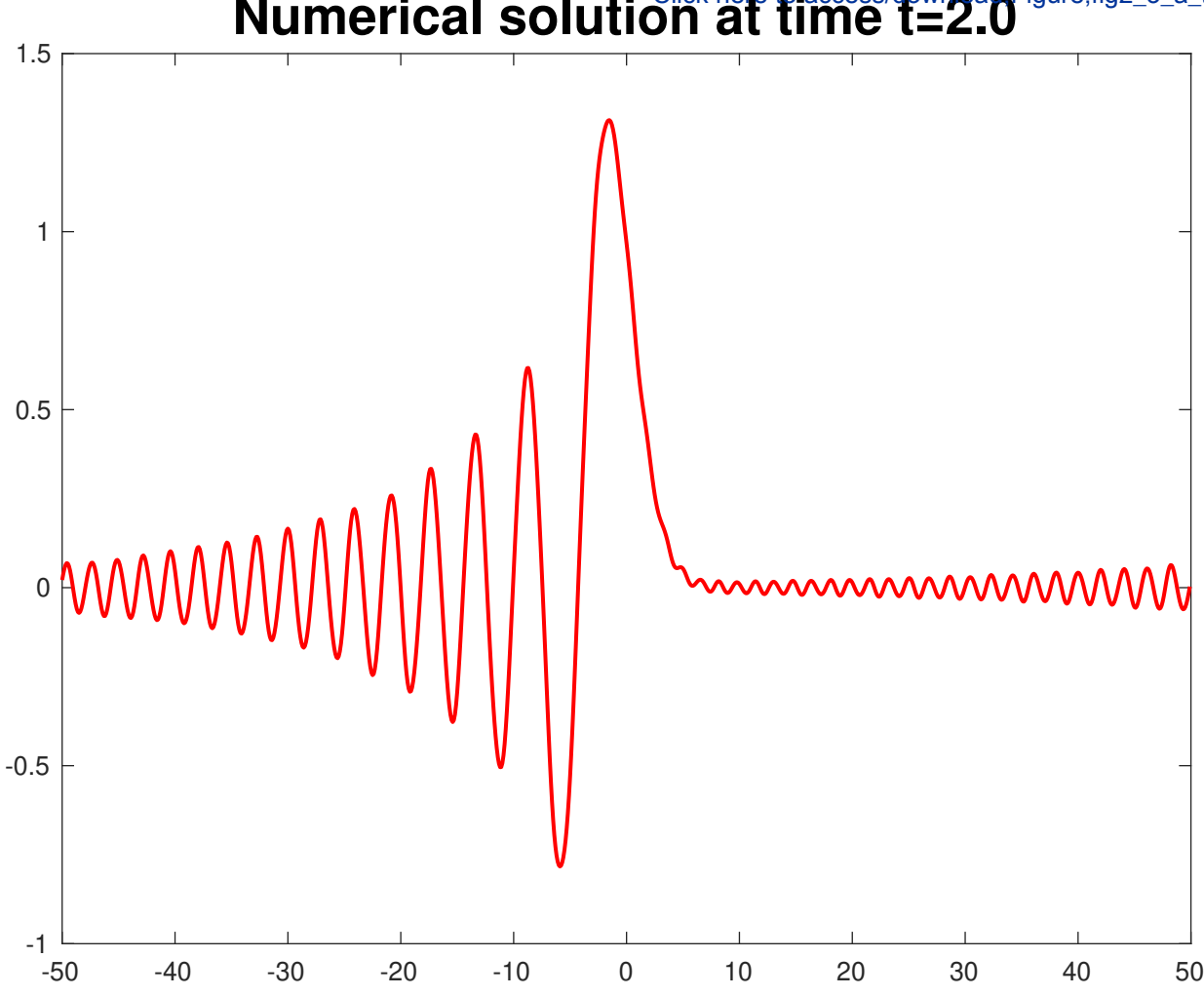

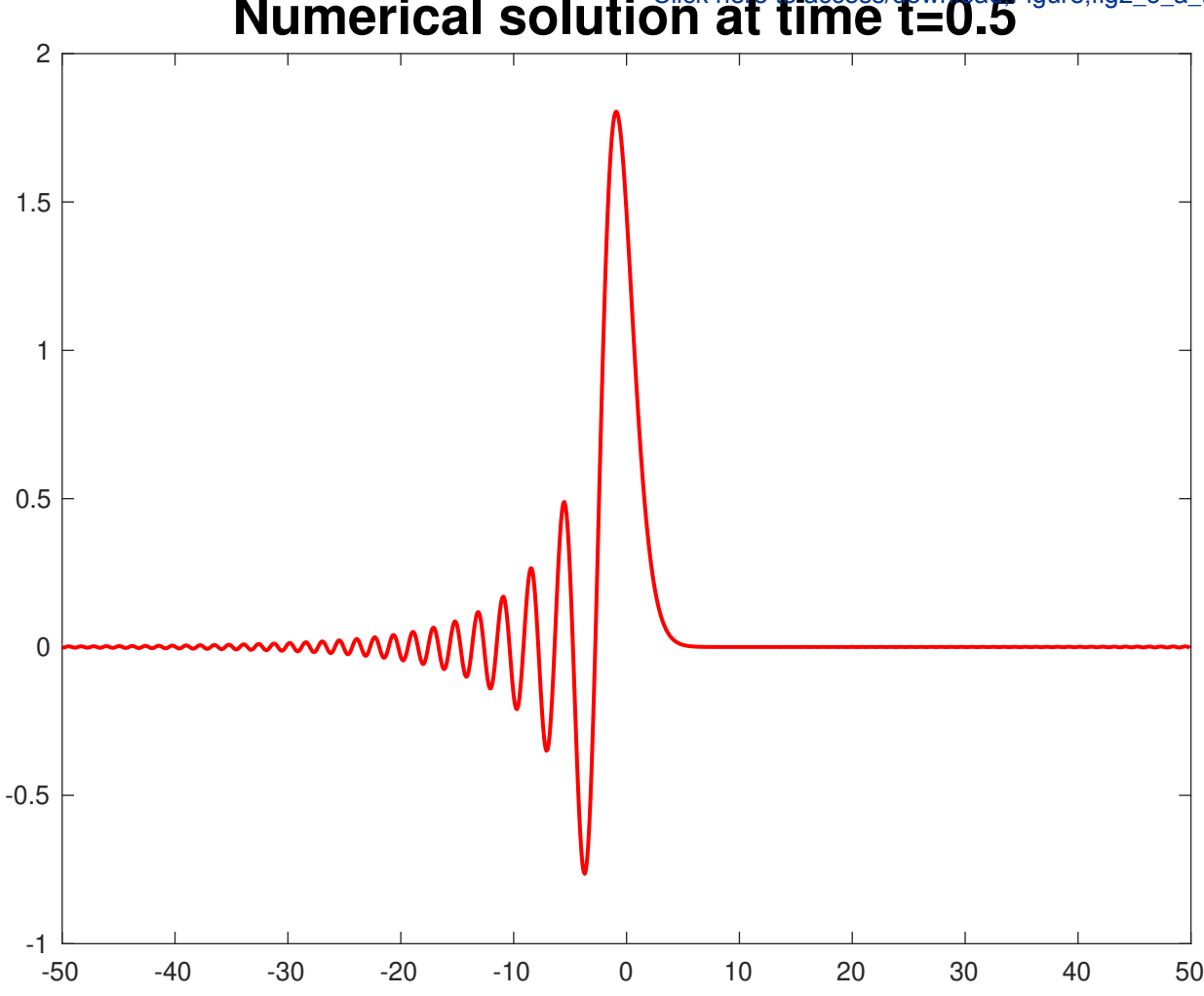

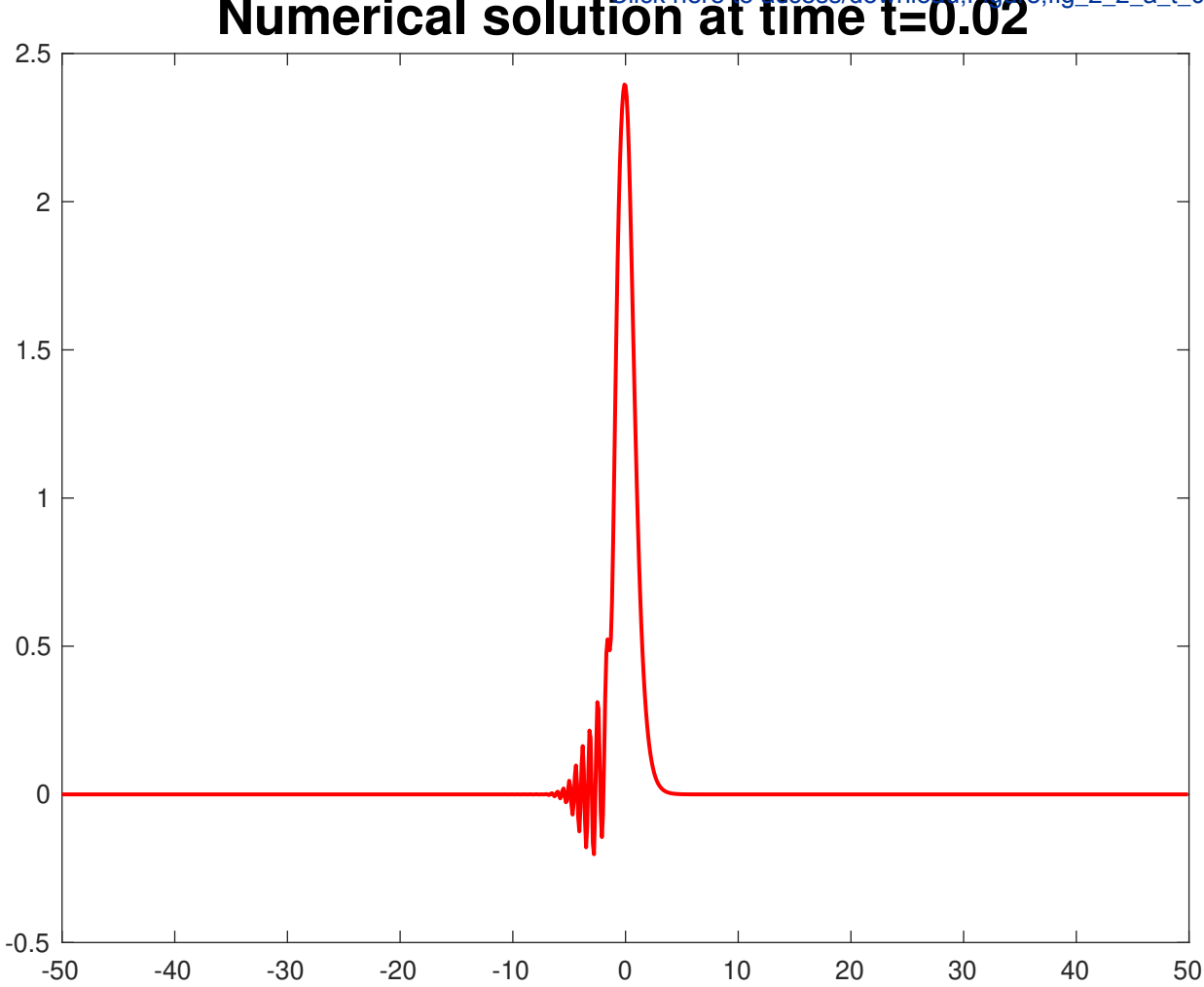

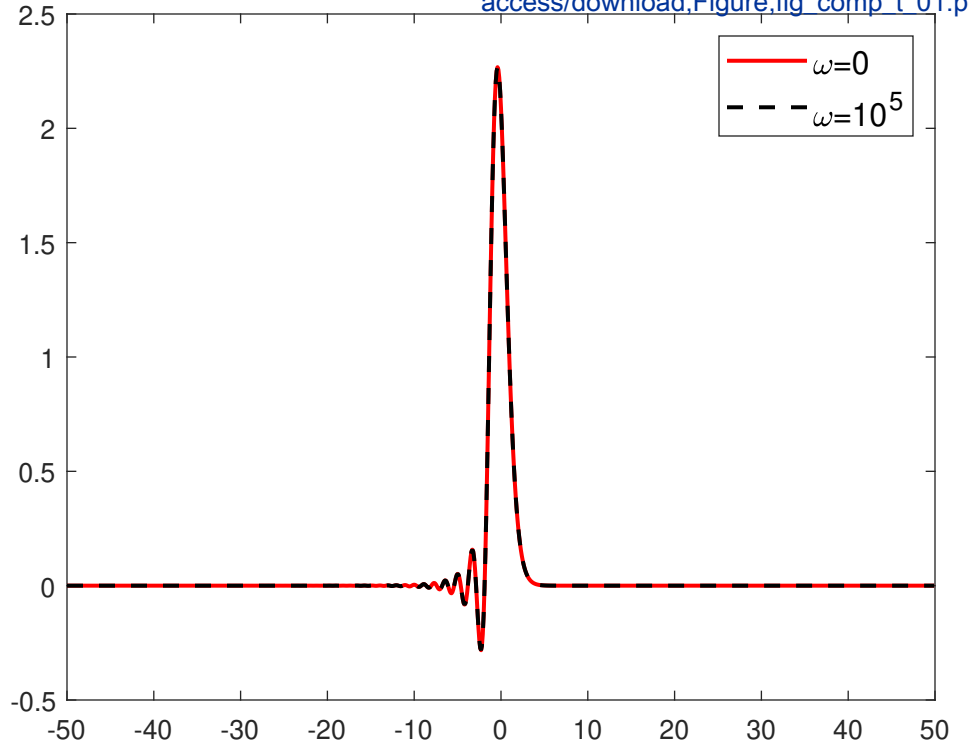
Numerical solution at t = 0.1
Click here to
access/download;Figure;fig_comp_t_01.pd
ω=0
ω=10^5
2.5
2
1.5
1
0.5
0
-0.5
-50
-40
-30
-20
-10
0
10
20
30
40
50

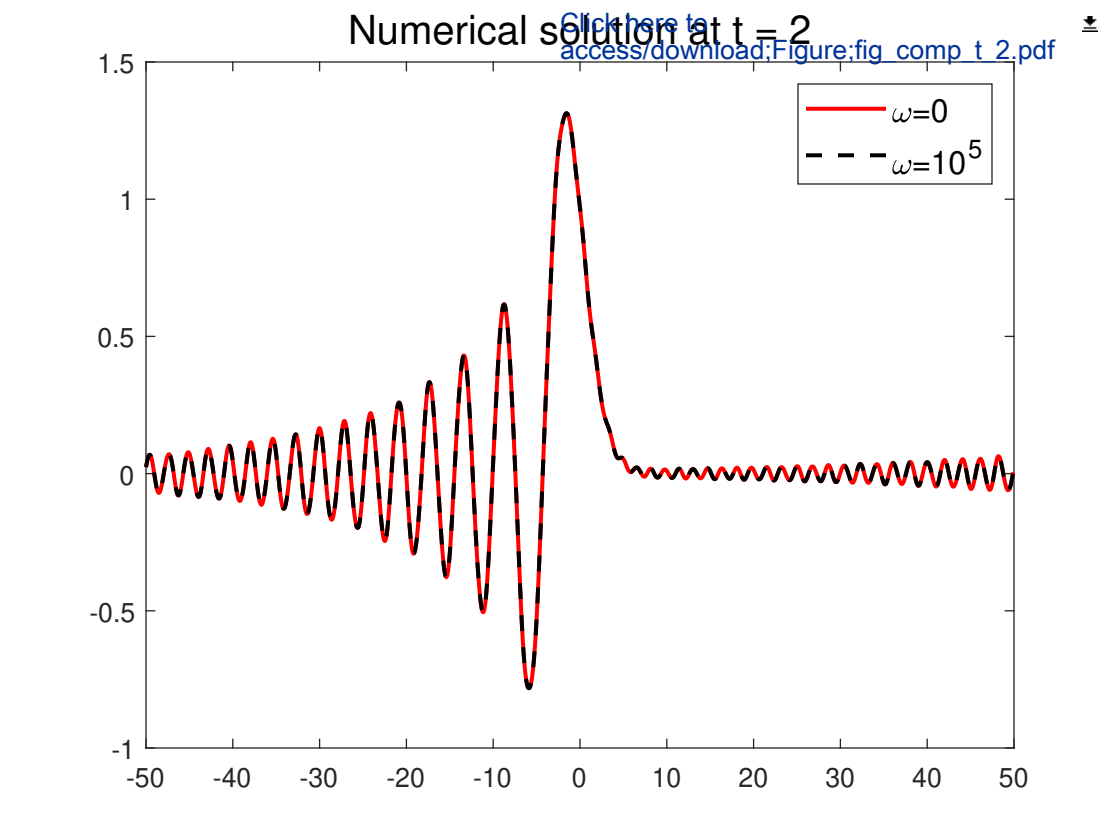
Numerical solution at t = 2
Click here to access/download;Figure;fig_comp_t_2.pdf
ω=0
ω=10^5
1.5
1
0.5
0
-0.5
-1
-50
-40
-30
-20
-10
0
10
20
30
40
50

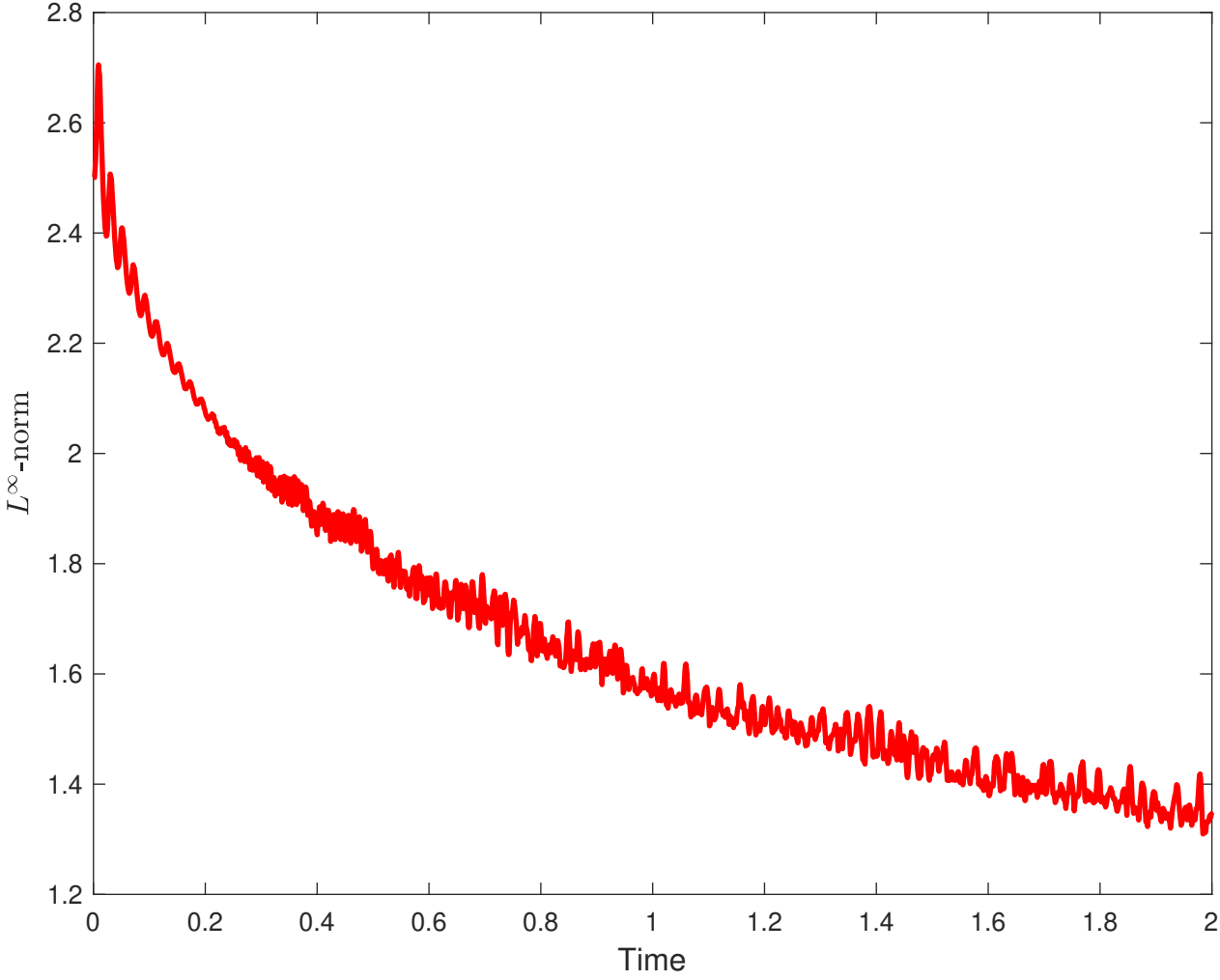

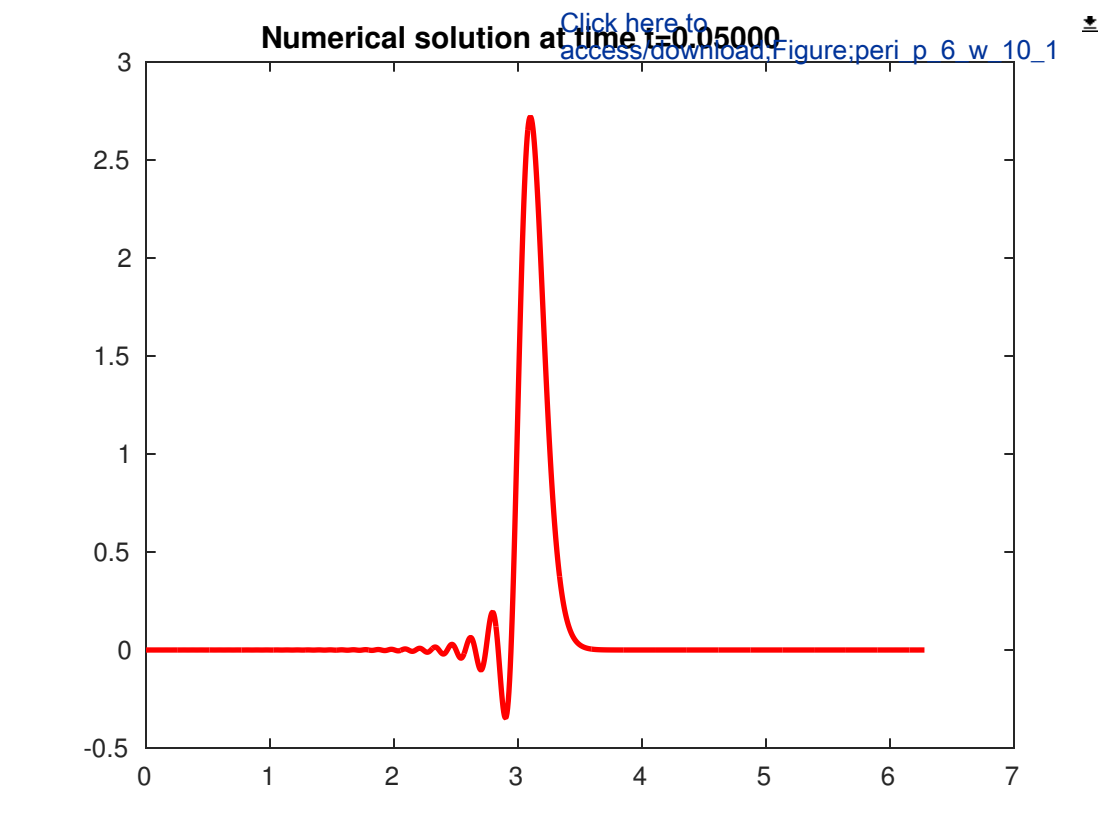
Numerical solution at time t=0.05000
Click here to
access/download;Figure;peri_p_6_w_10_1
3
2.5
2
1.5
1
0.5
0
-0.5
0
1
2
3
4
5
6
7

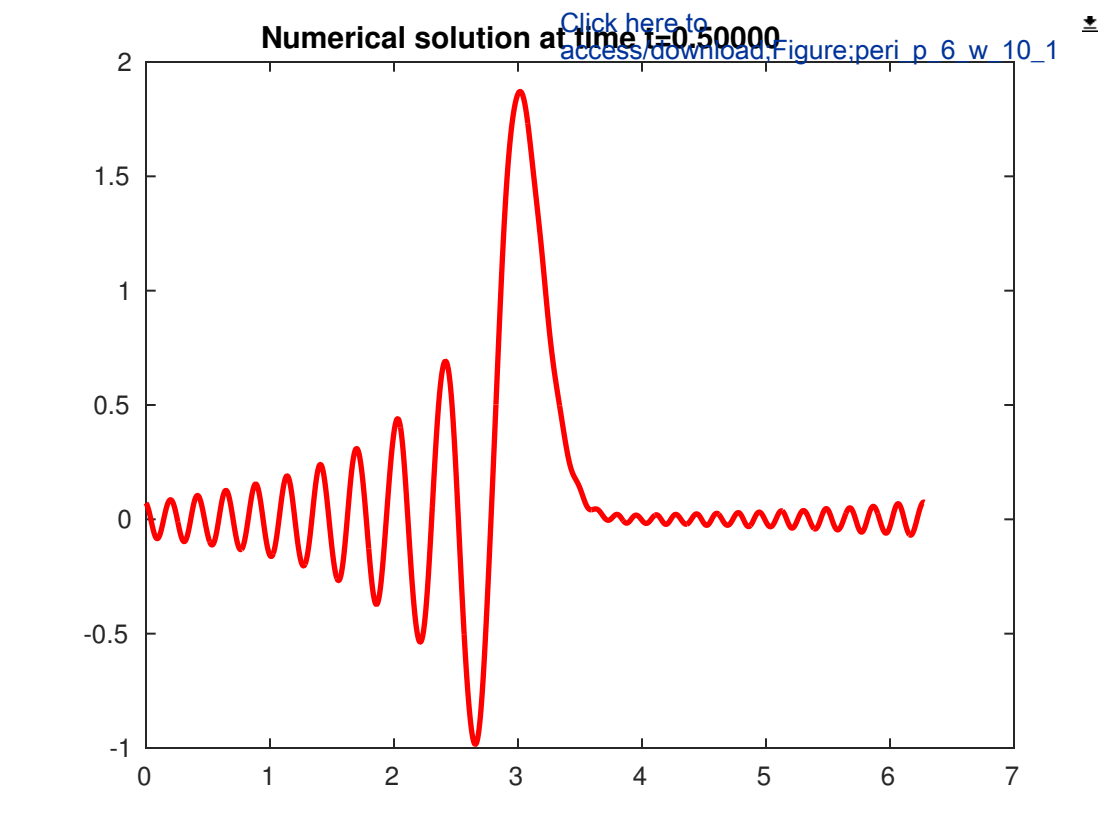
Numerical solution at time t=0.50000
Click here to access/download;Figure;peri_p_6_w_10_1
2
1.5
1
0.5
0
-0.5
-1
0
1
2
3
4
5
6
7

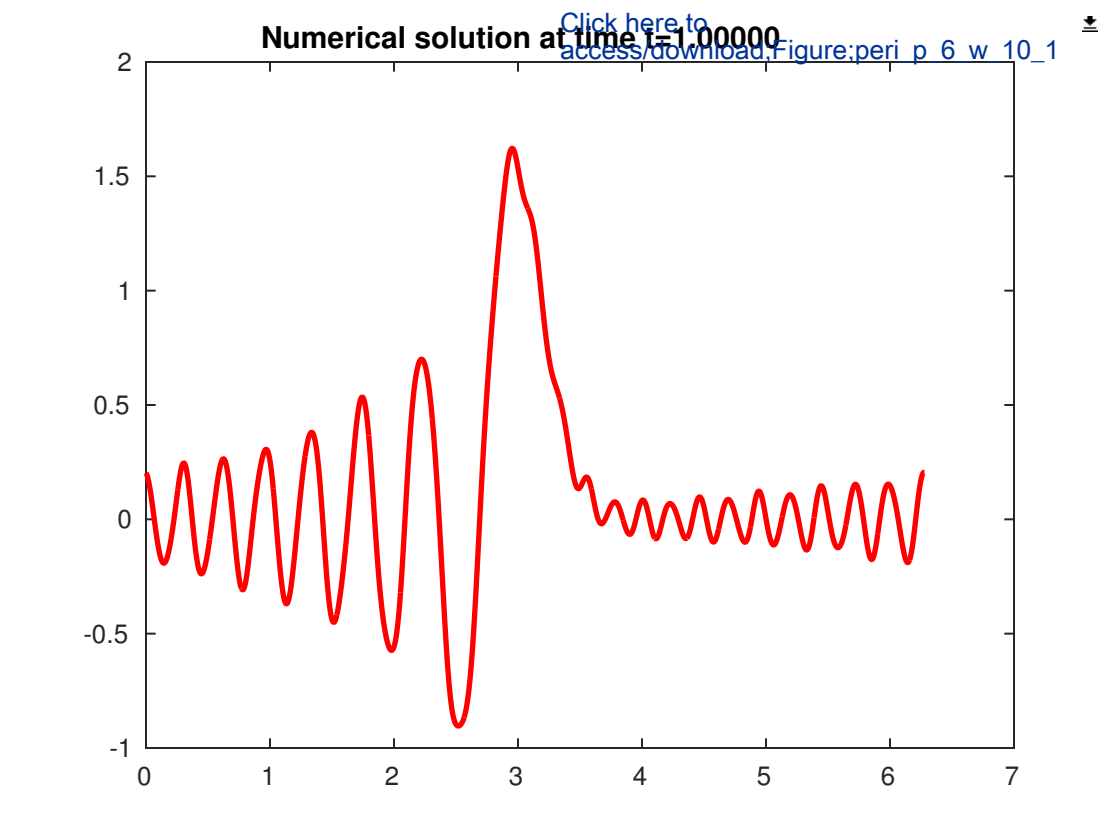
Numerical solution at time t= 1.00000
Click here to access/download;Figure;peri_p_6_w_10_1
2
1.5
1
0.5
0
-0.5
-1
0
1
2
3
4
5
6
7

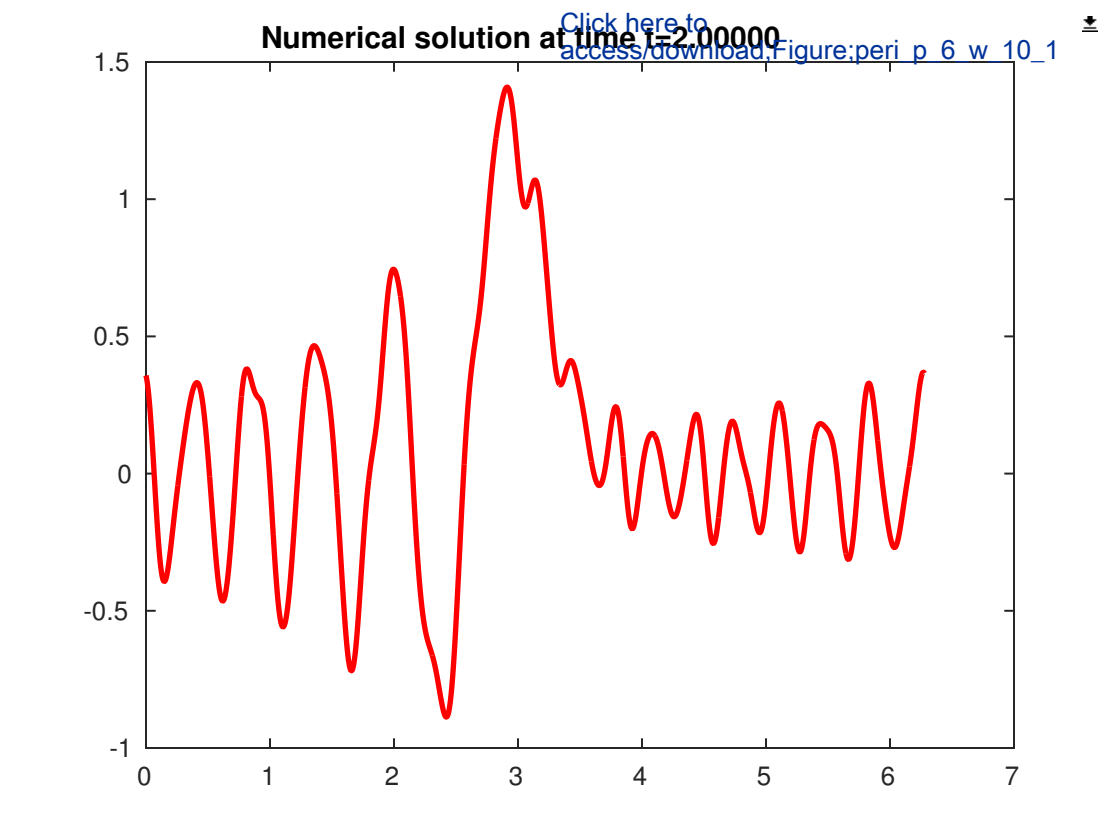
Numerical solution at time t=2.00000
Click here to access/download;Figure;peri_p_6_w_10_1
1.5
1
0.5
0
-0.5
-1
0
1
2
3
4
5
6
7

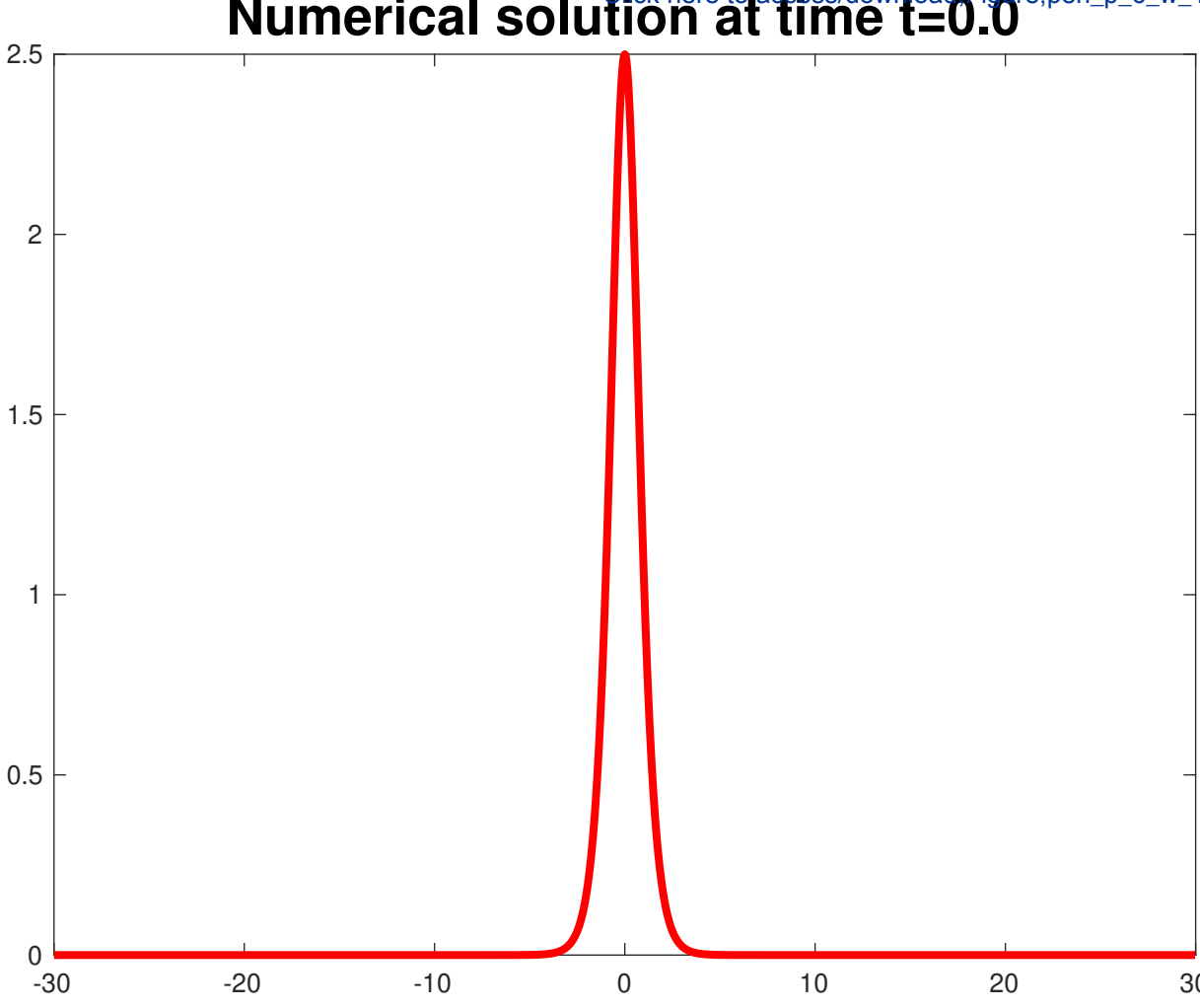

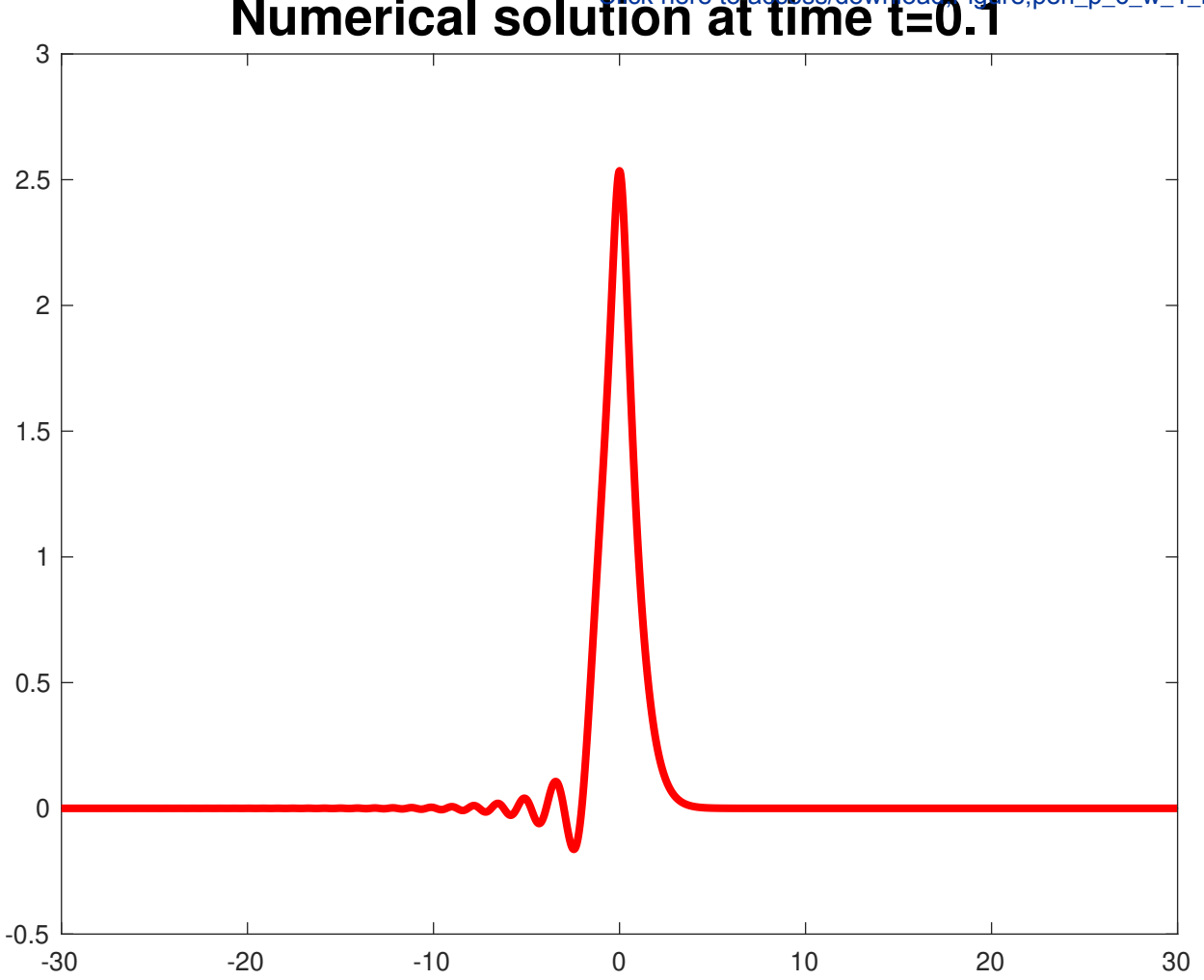

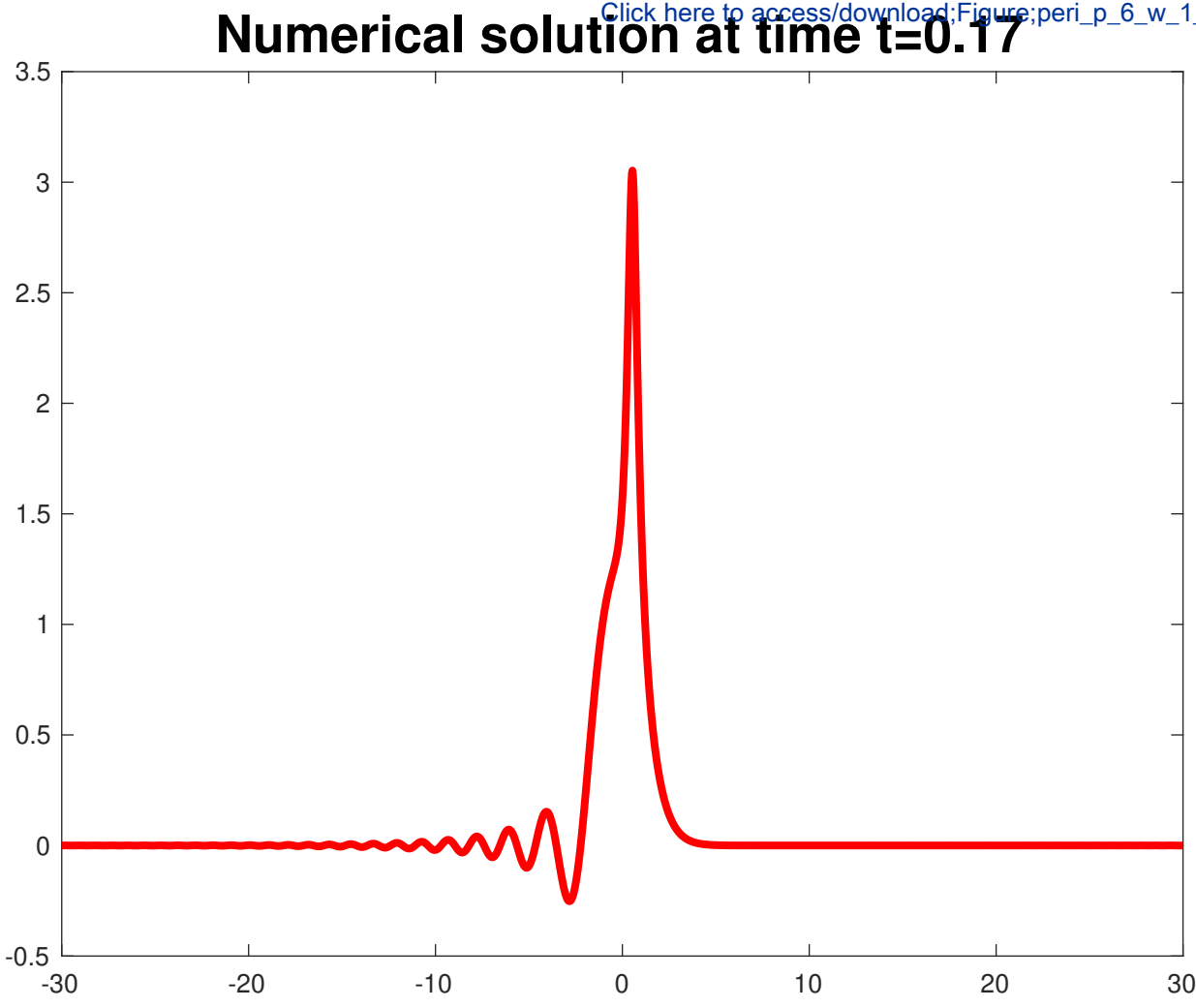

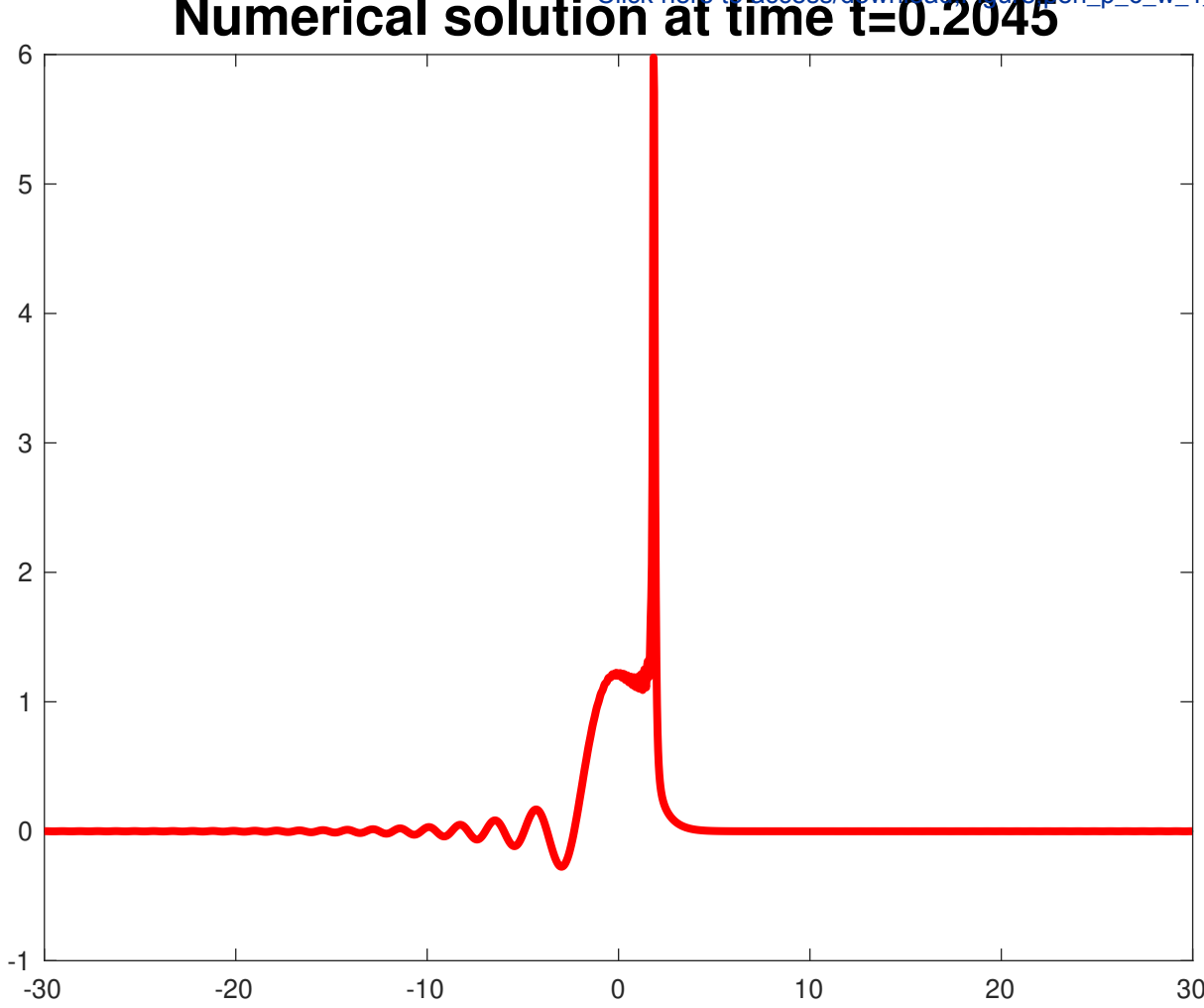

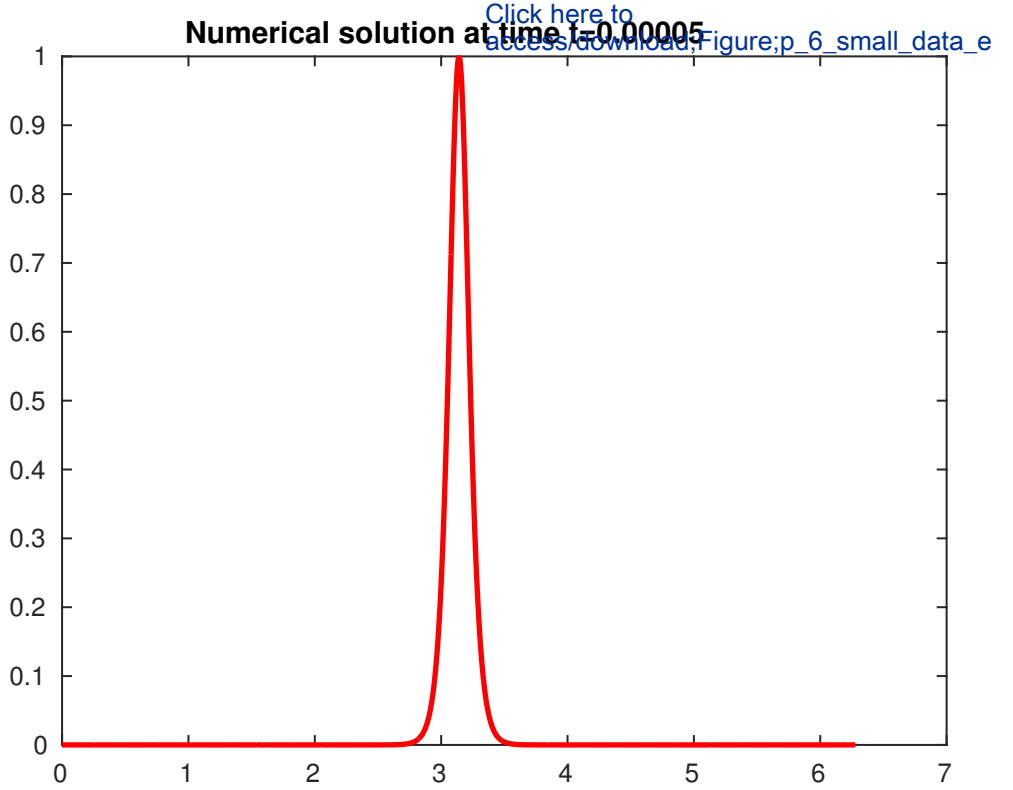
Numerical solution at time t=0.00005
Click here to
access/download;Figure;p_6_small_data_e
1
0.9
0.8
0.7
0.6
0.5
0.4
0.3
0.2
0.1
0
0
1
2
3
4
5
6
7

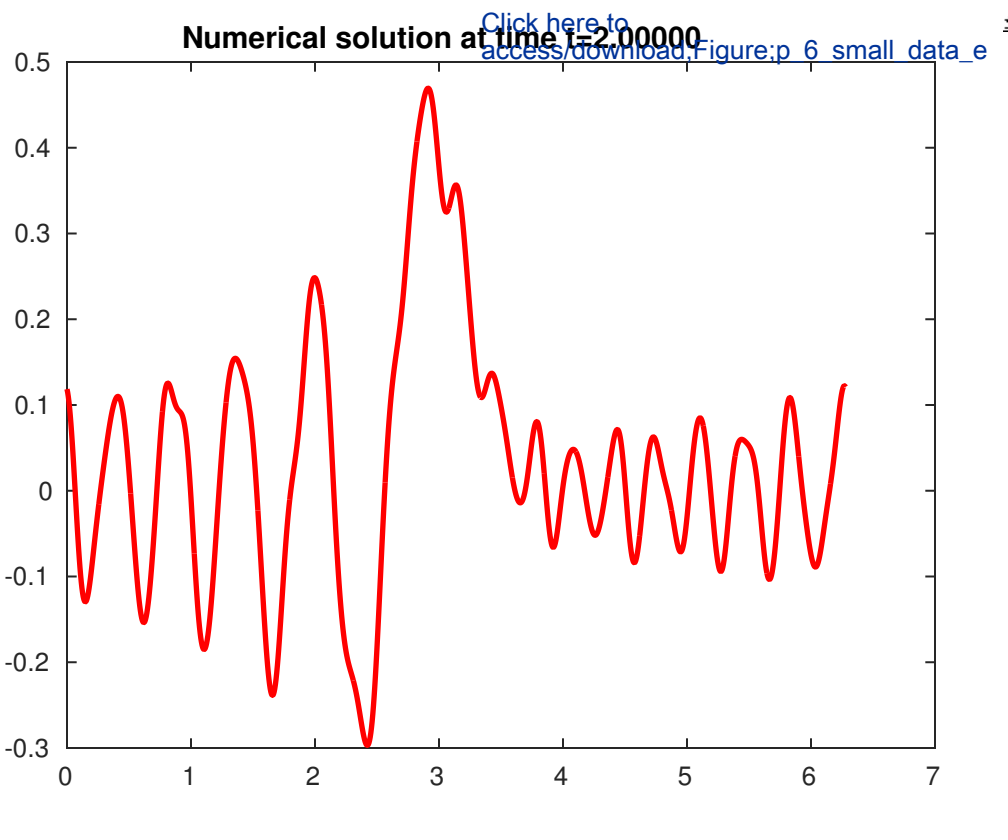
Numerical solution at time t=2.00000
Click here to
access/download;Figure;p_6_small_data_e
0.5
0.4
0.3
0.2
0.1
0
-0.1
-0.2
-0.3
0
1
2
3
4
5
6
7

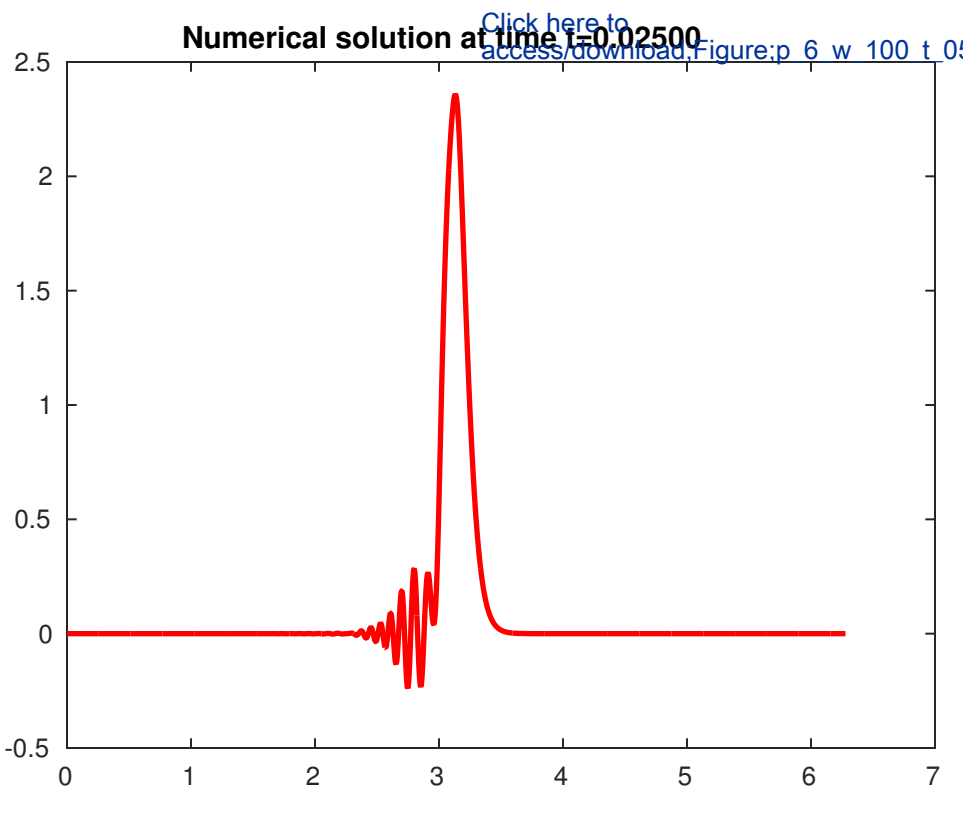
Numerical solution at time t=0.02500
Click here to access/download;Figure;p_6_w_100_t_05.
2.5
2
1.5
1
0.5
0
-0.5
0
1
2
3
4
5
6
7

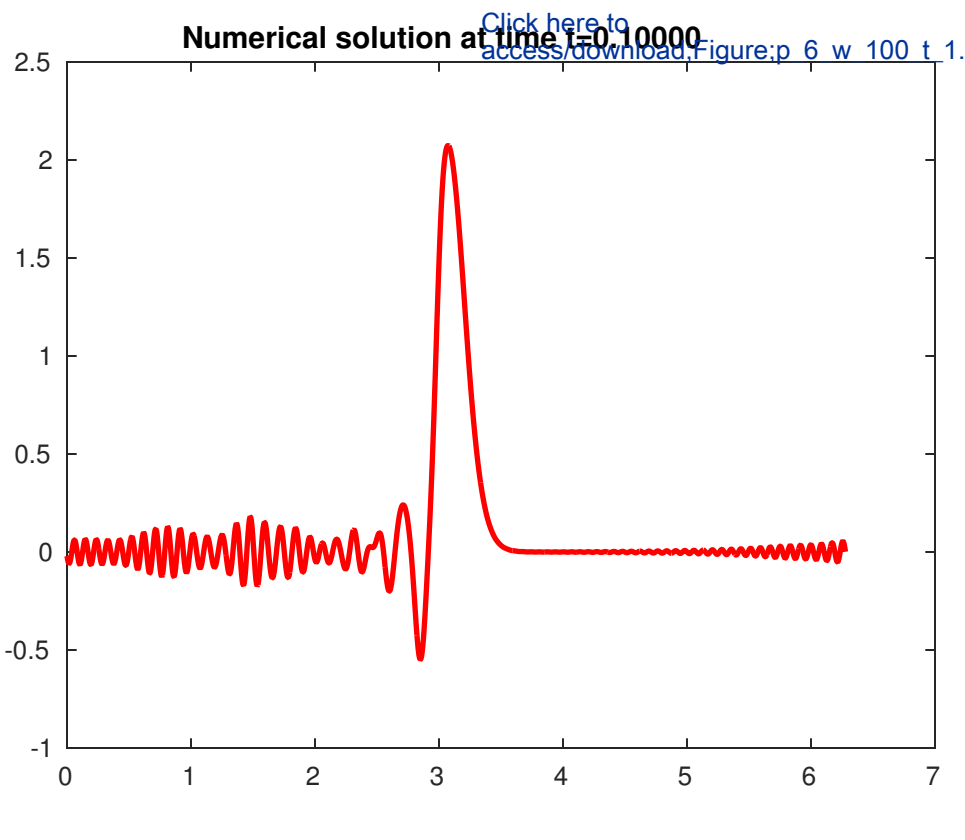
Numerical solution at time t=0.10000
Click here to access/download;Figure;p_6_w_100_t_1.p
2.5
2
1.5
1
0.5
0
-0.5
-1
0
1
2
3
4
5
6
7

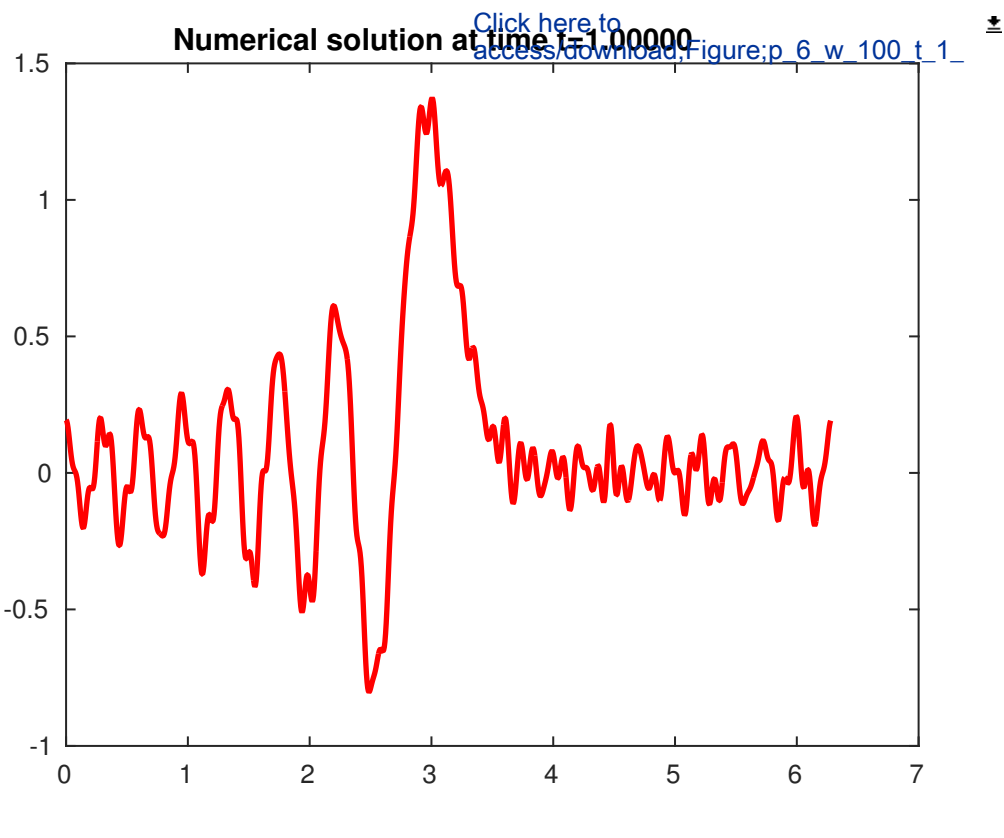
Numerical solution at time t=1.00000
Click here to access/download;Figure;p_6_w_100_t_1_
1.5
1
0.5
0
-0.5
-1
0
1
2
3
4
5
6
7

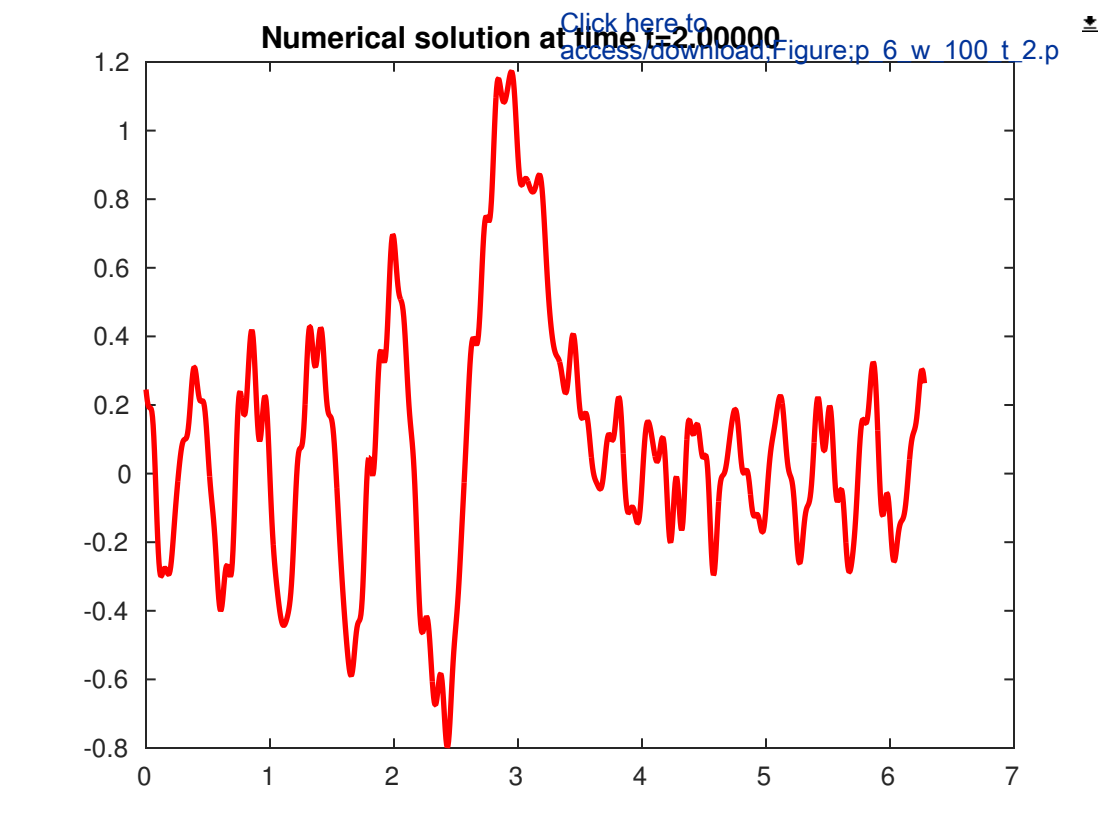
Numerical solution at time t=2.00000
Click here to
access/download;Figure;p_6_w_100_t_2.p
1.2
1
0.8
0.6
0.4
0.2
0
-0.2
-0.4
-0.6
-0.8
0
1
2
3
4
5
6
7

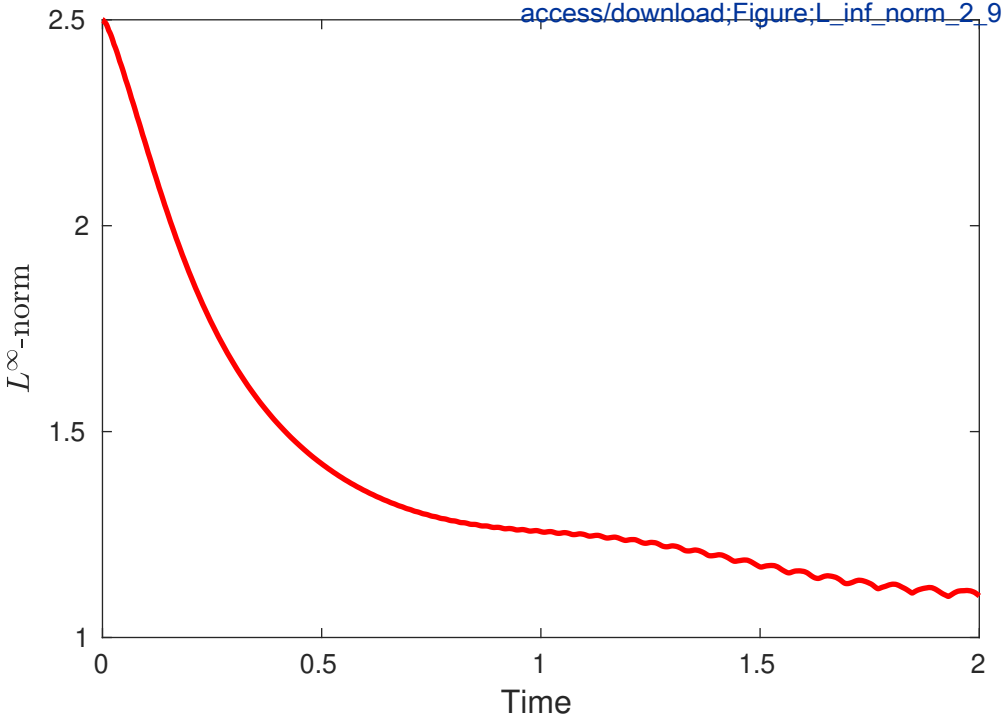

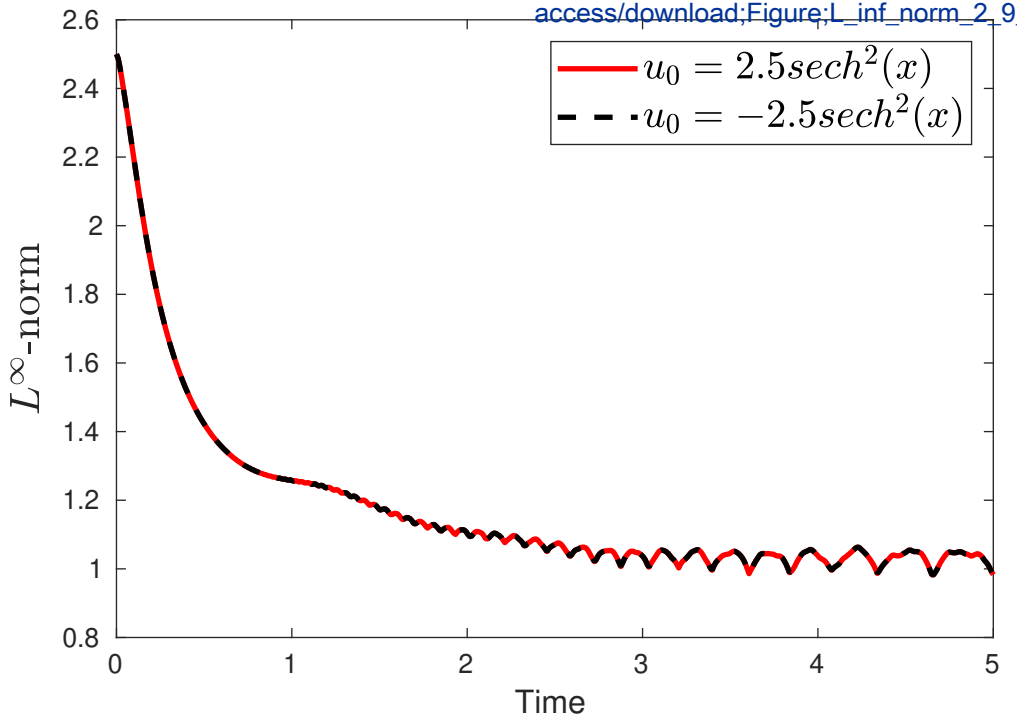

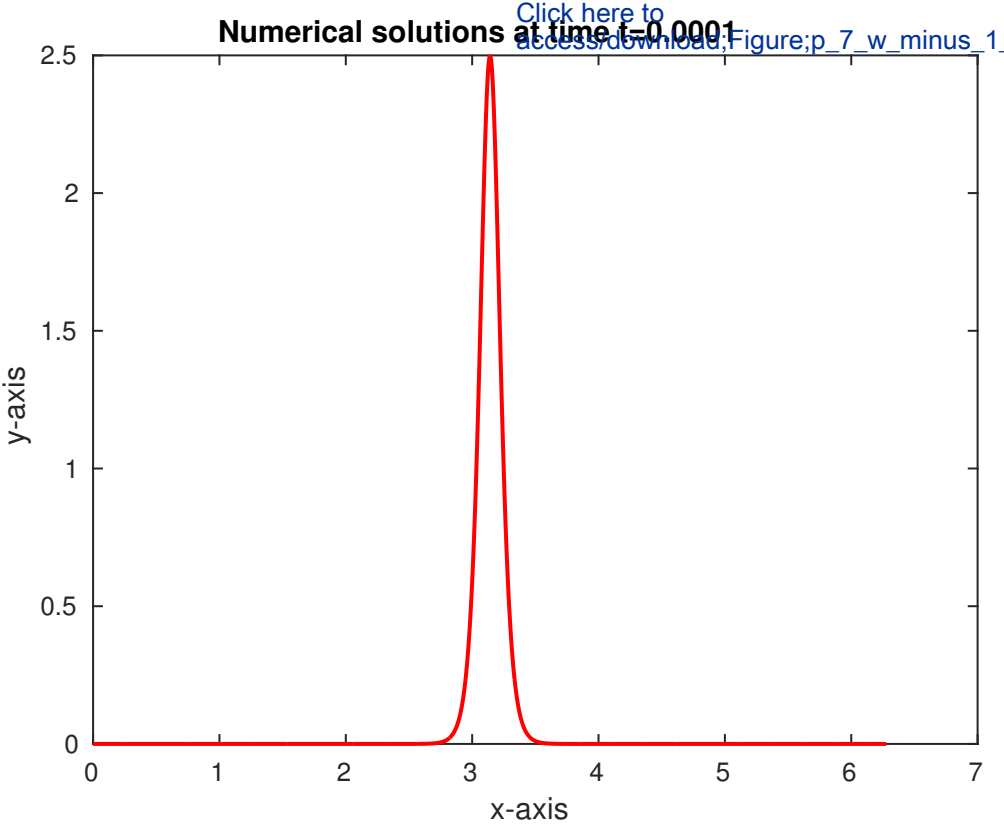

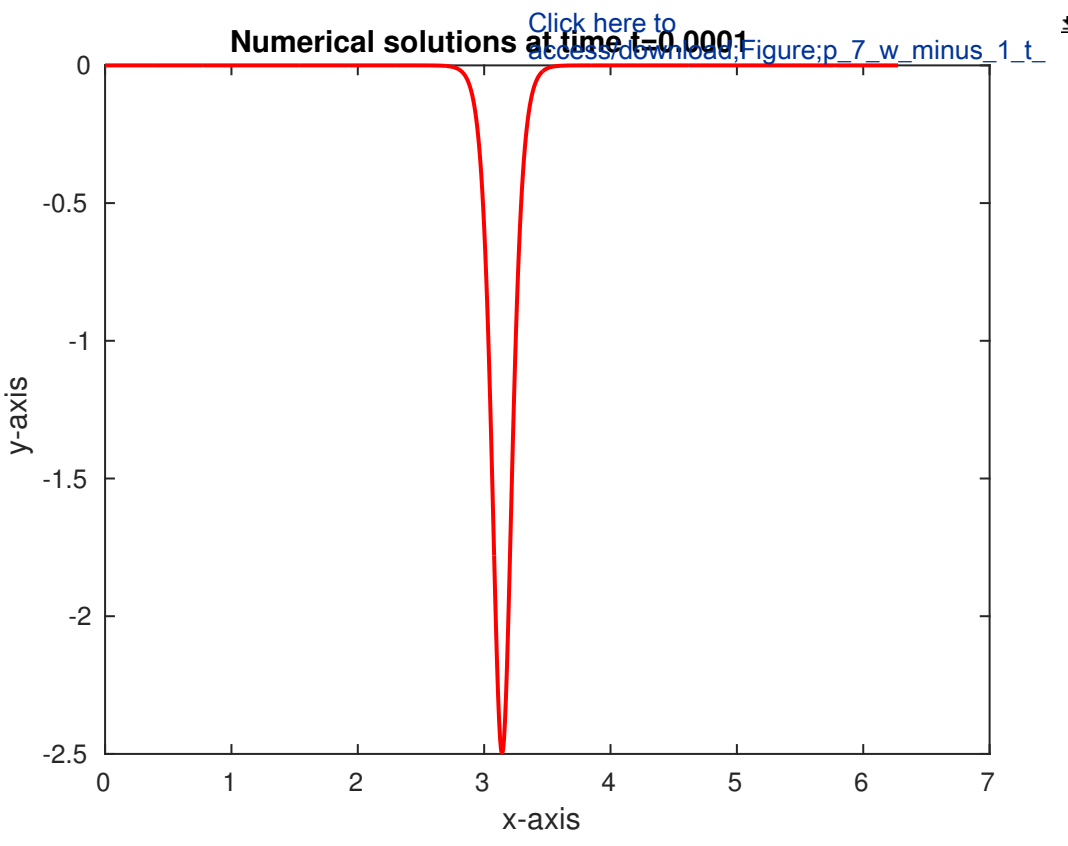
Click here to access/download;Figure;p_7_w_minus_1_t_
Numerical solutions at time t=0.0001
0
-0.5
-1
-1.5
-2
-2.5
y-axis
0
1
2
3
4
5
6
7
x-axis

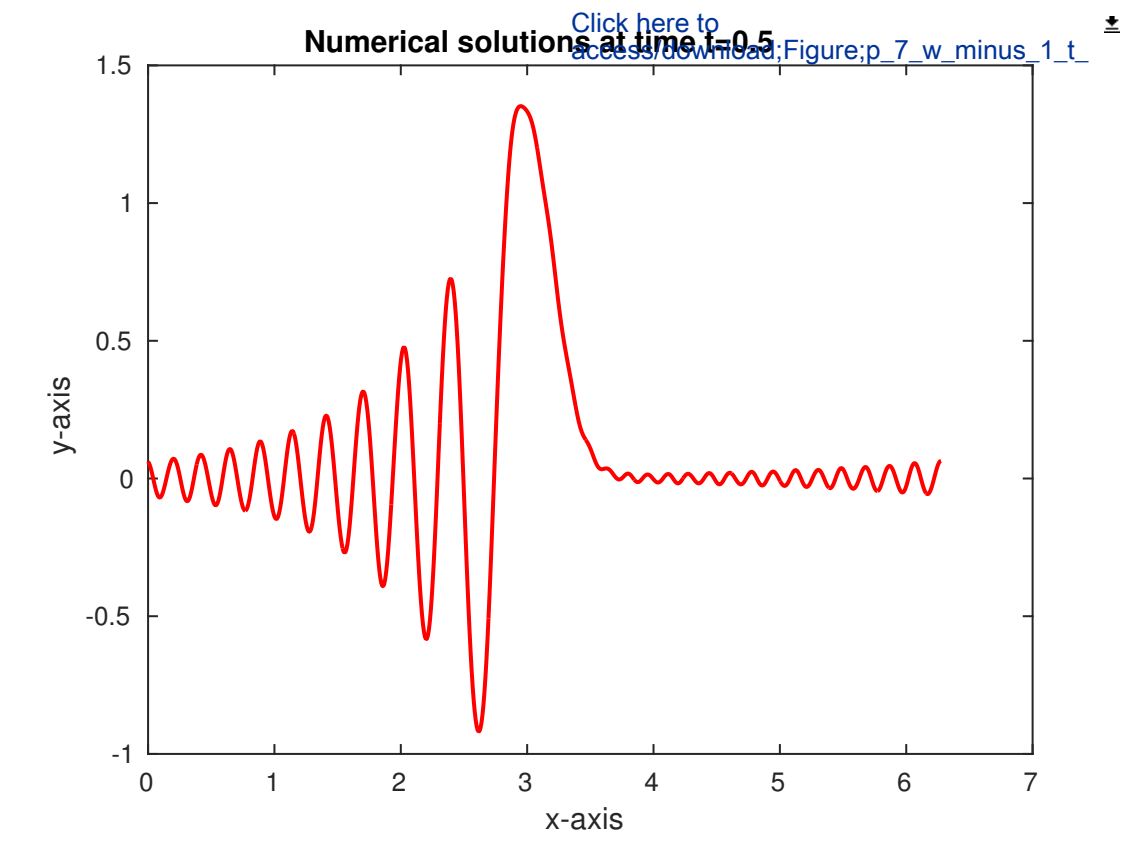
Click here to access/download;Figure;p_7_w_minus_1_t_
Numerical solutions at time t=0.5
1.5
1
0.5
0
-0.5
-1
y-axis
0
1
2
3
4
5
6
7
x-axis

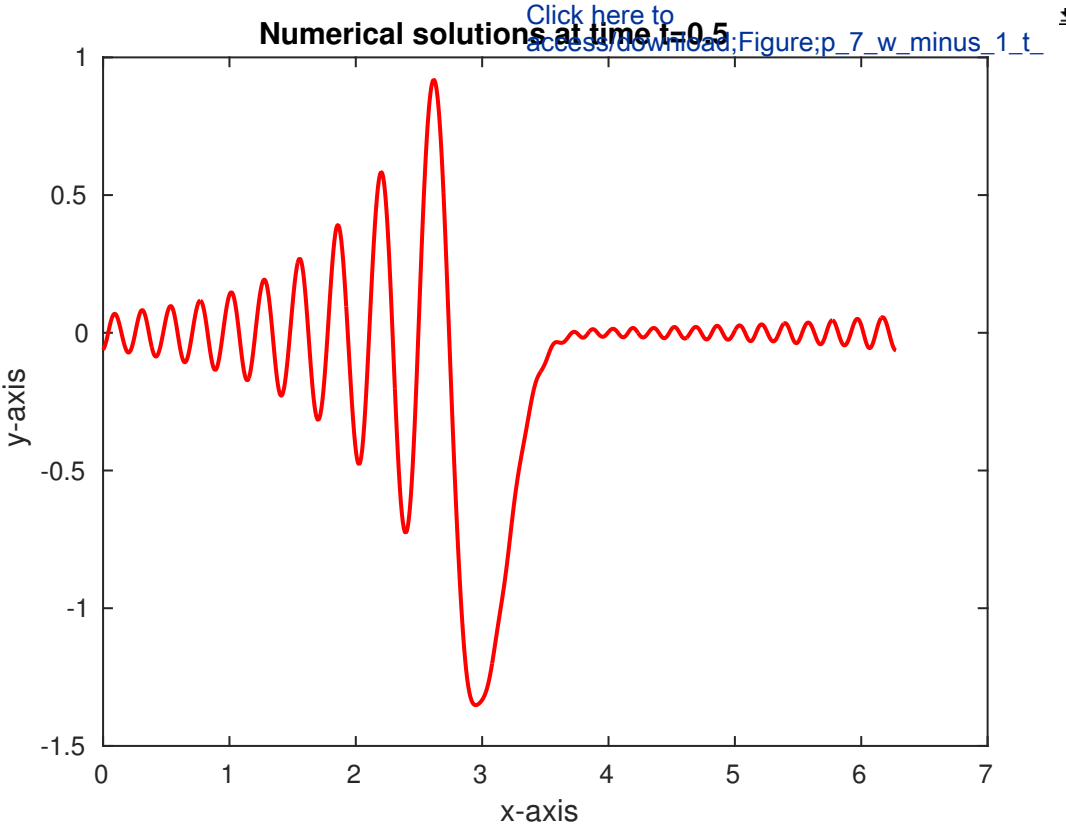
Click here to access/download;Figure;p_7_w_minus_1_t_
Numerical solutions at time t=0.5
y-axis
x-axis
1
0.5
0
-0.5
-1
-1.5
0
1
2
3
4
5
6
7

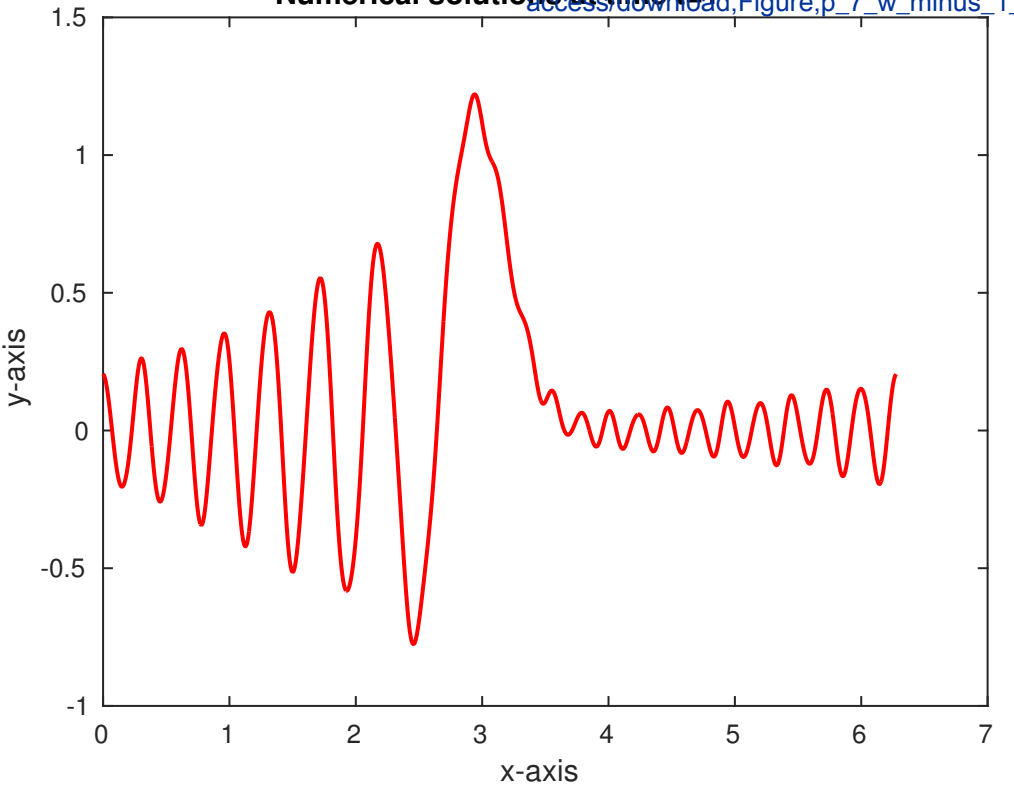

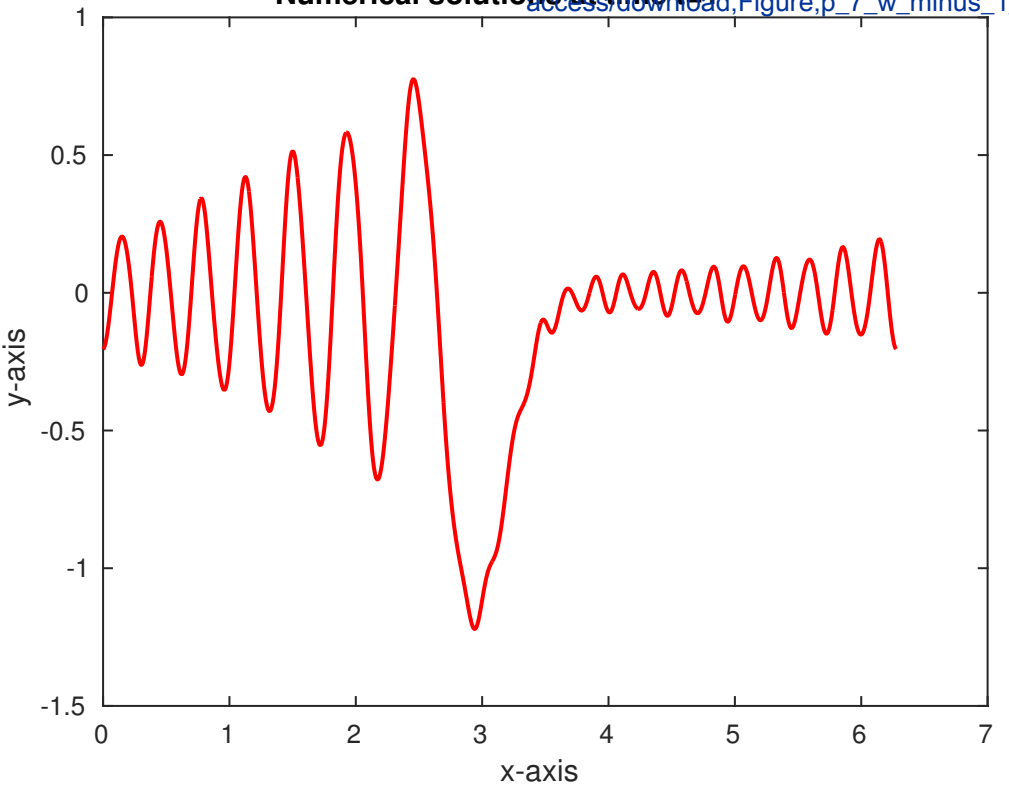

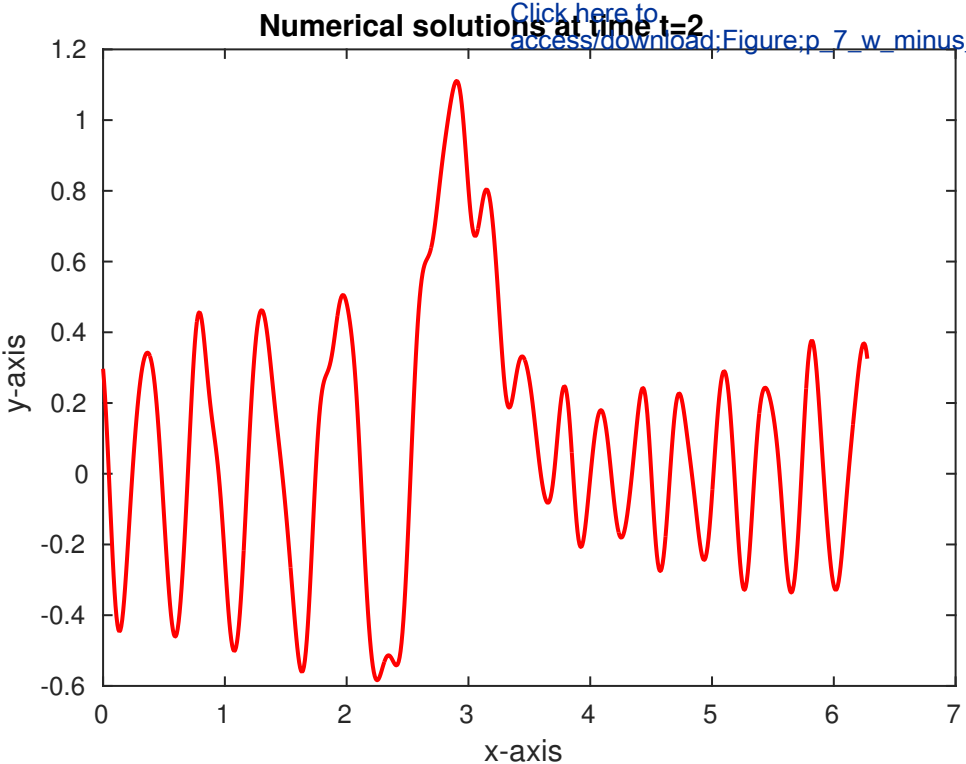

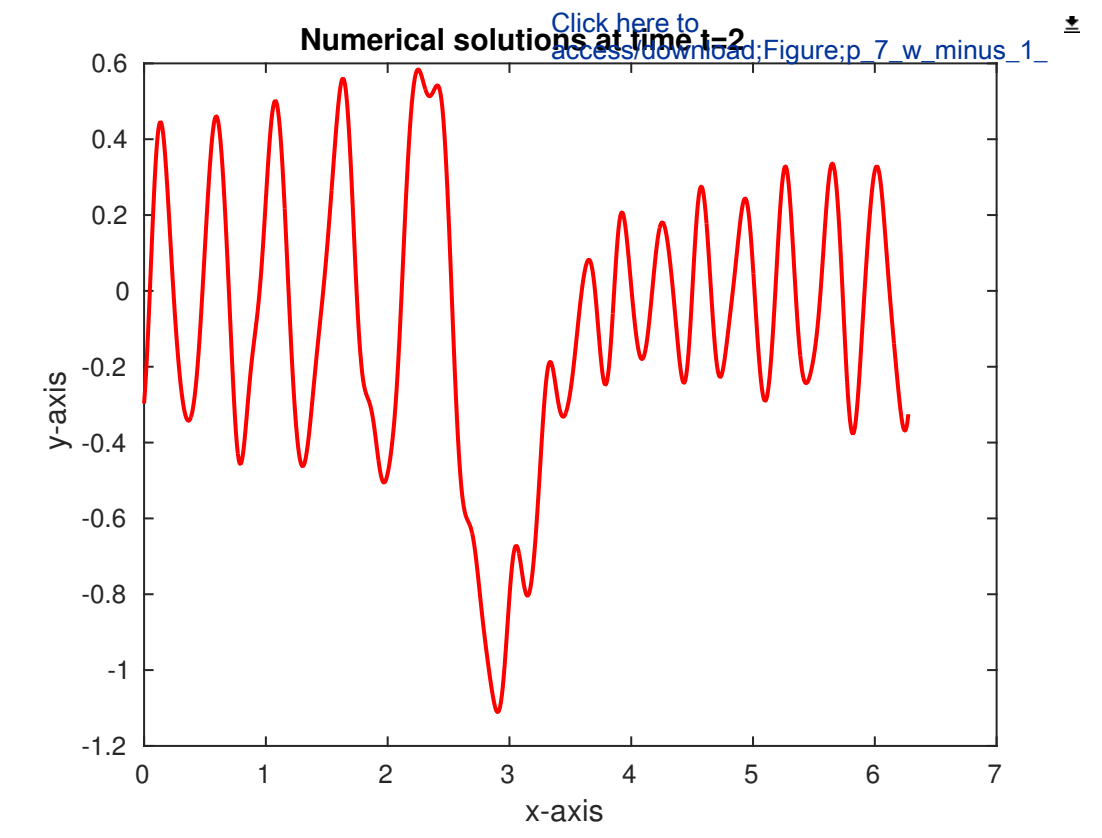
Click here to access/download;Figure;p_7_w_minus_1_
Numerical solutions at time t=2
0.6
0.4
0.2
0
-0.2
-0.4
-0.6
-0.8
-1
-1.2
y-axis
0
1
2
3
4
5
6
7
x-axis

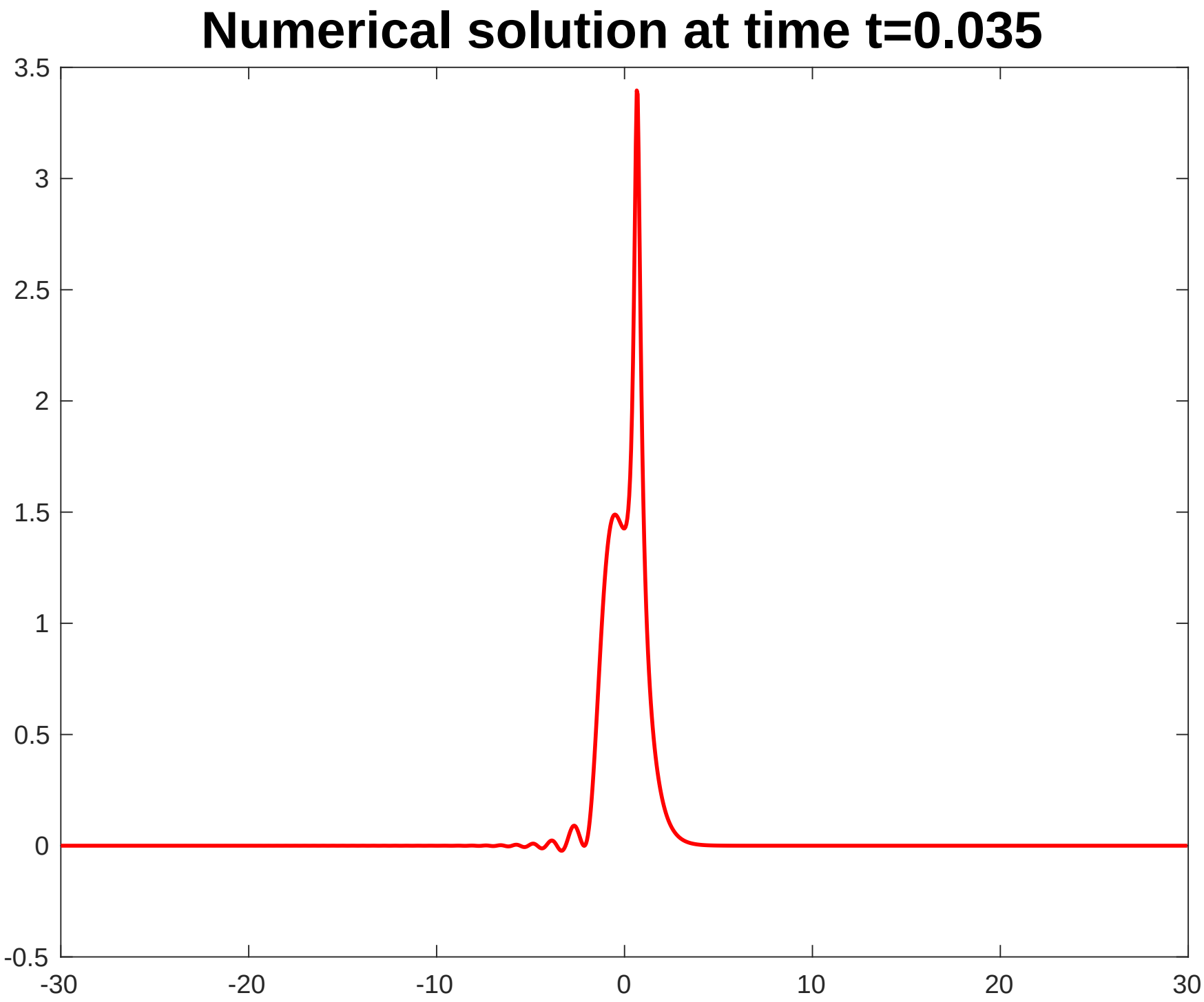

Click here to access/download/figure/new_negative_1_0035.pdf

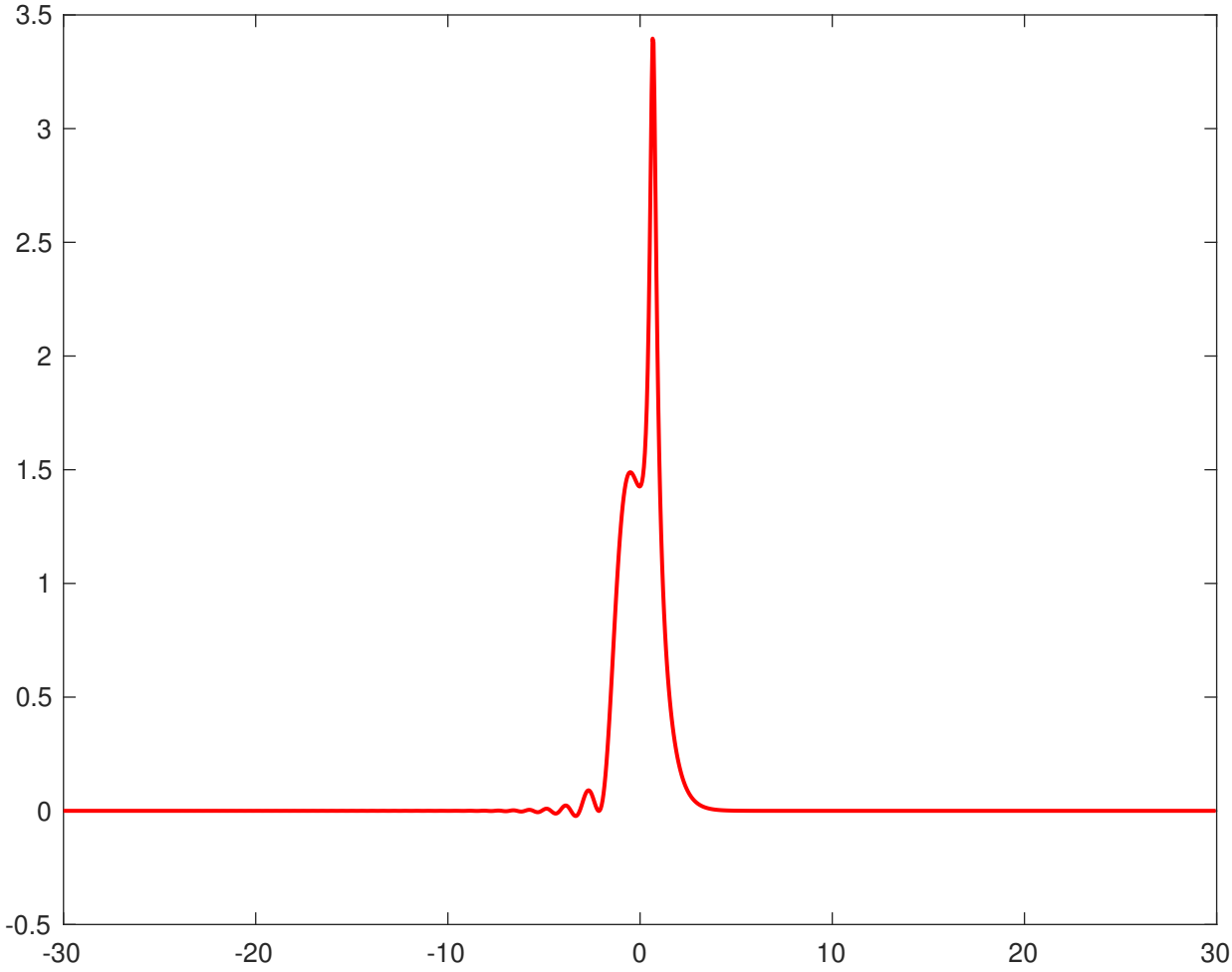

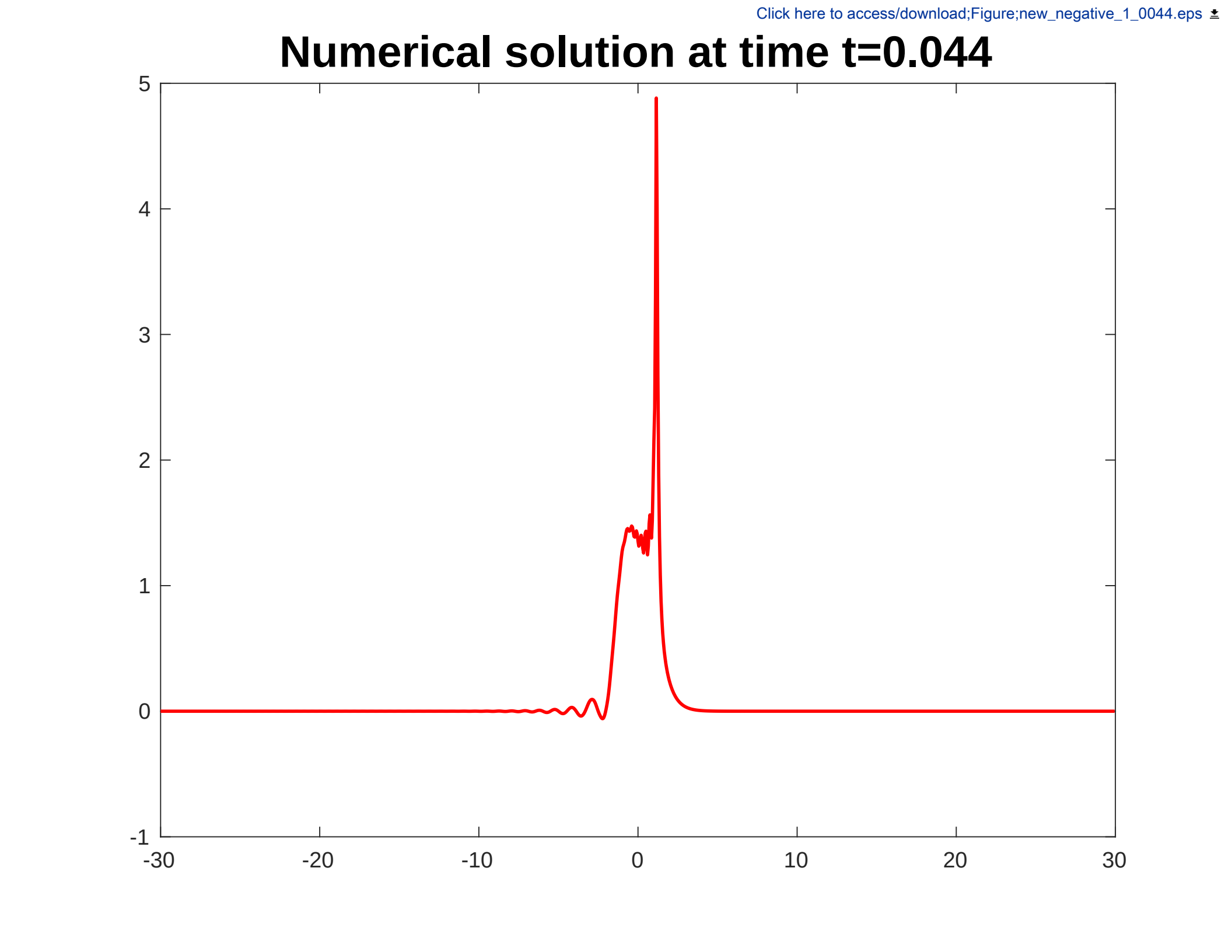

Click here to access/download/figure/new_negative_1_0044.pdf

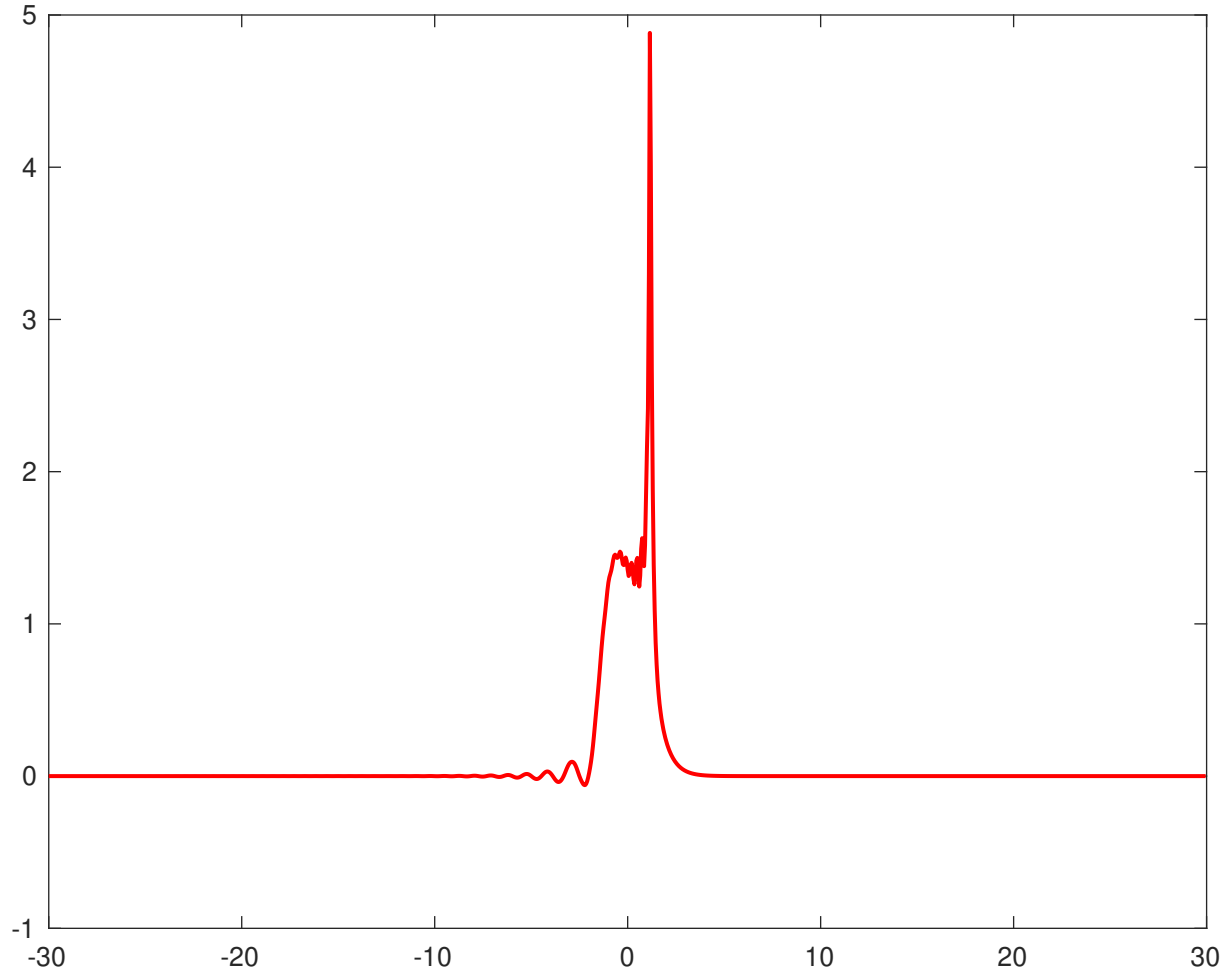

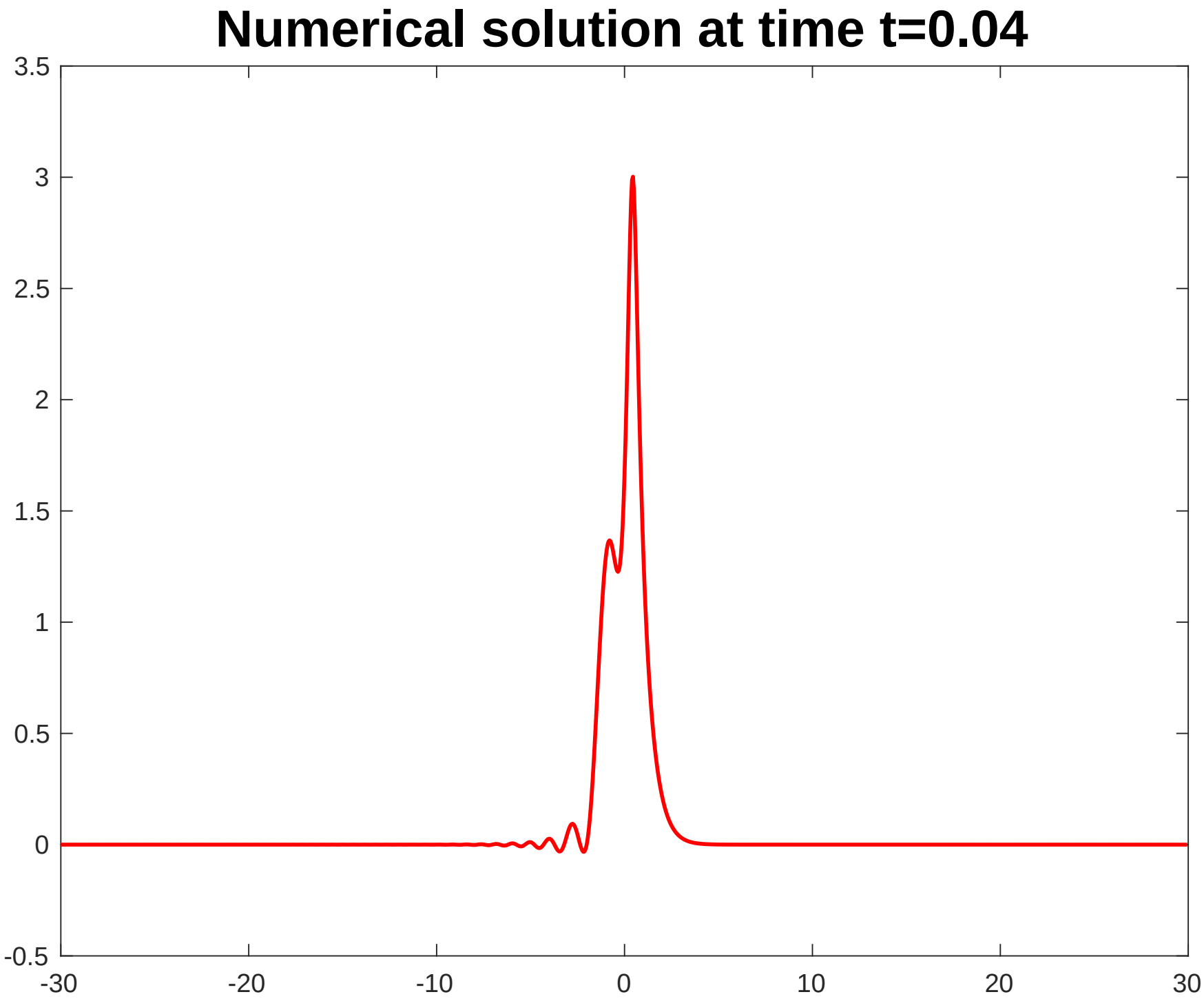

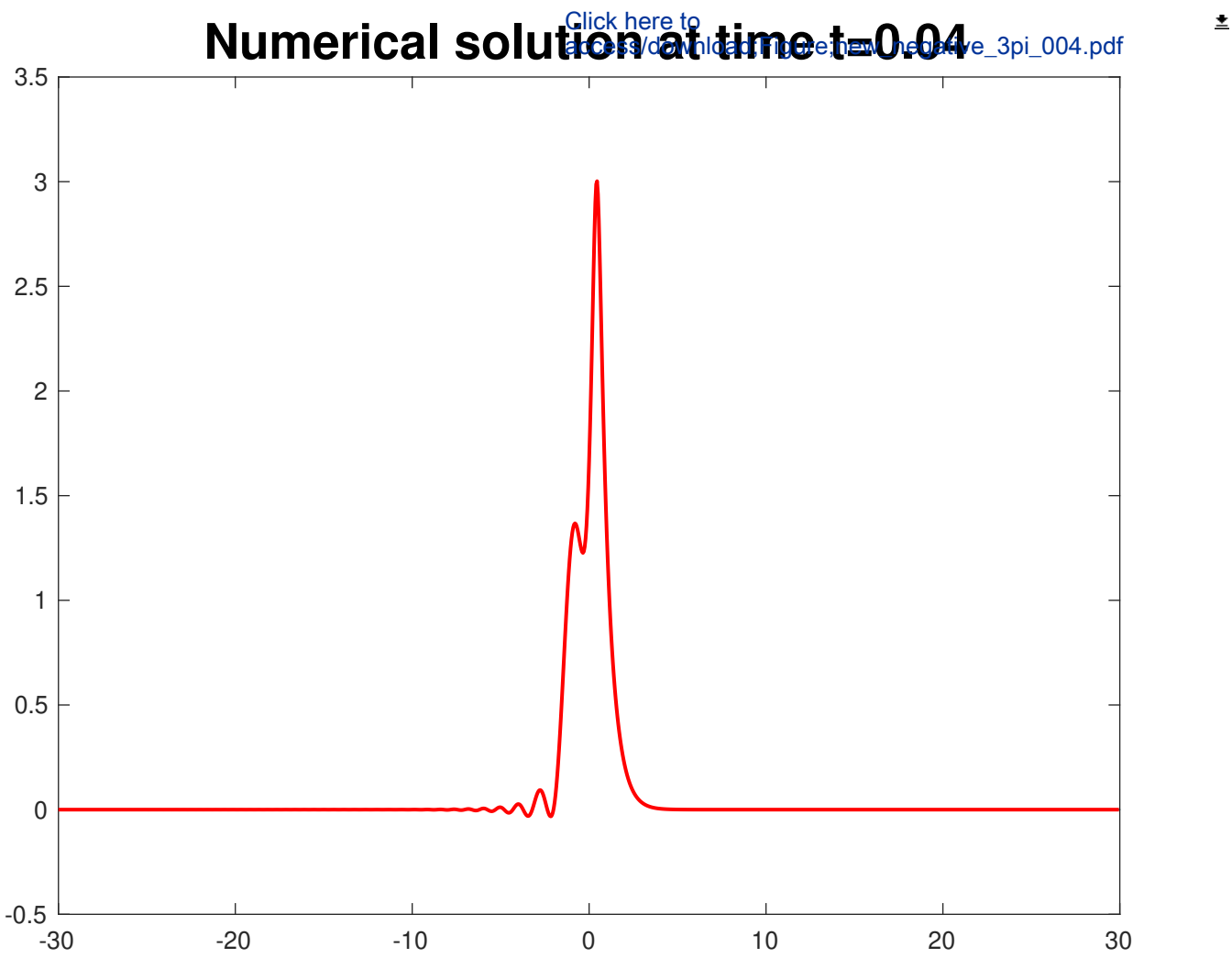
Click here to
access/download Figure new negative_3pi_004.pdf
Numerical solution at time t=0.04
3.5
3
2.5
2
1.5
1
0.5
0
-0.5
-30
-20
-10
0
10
20
30

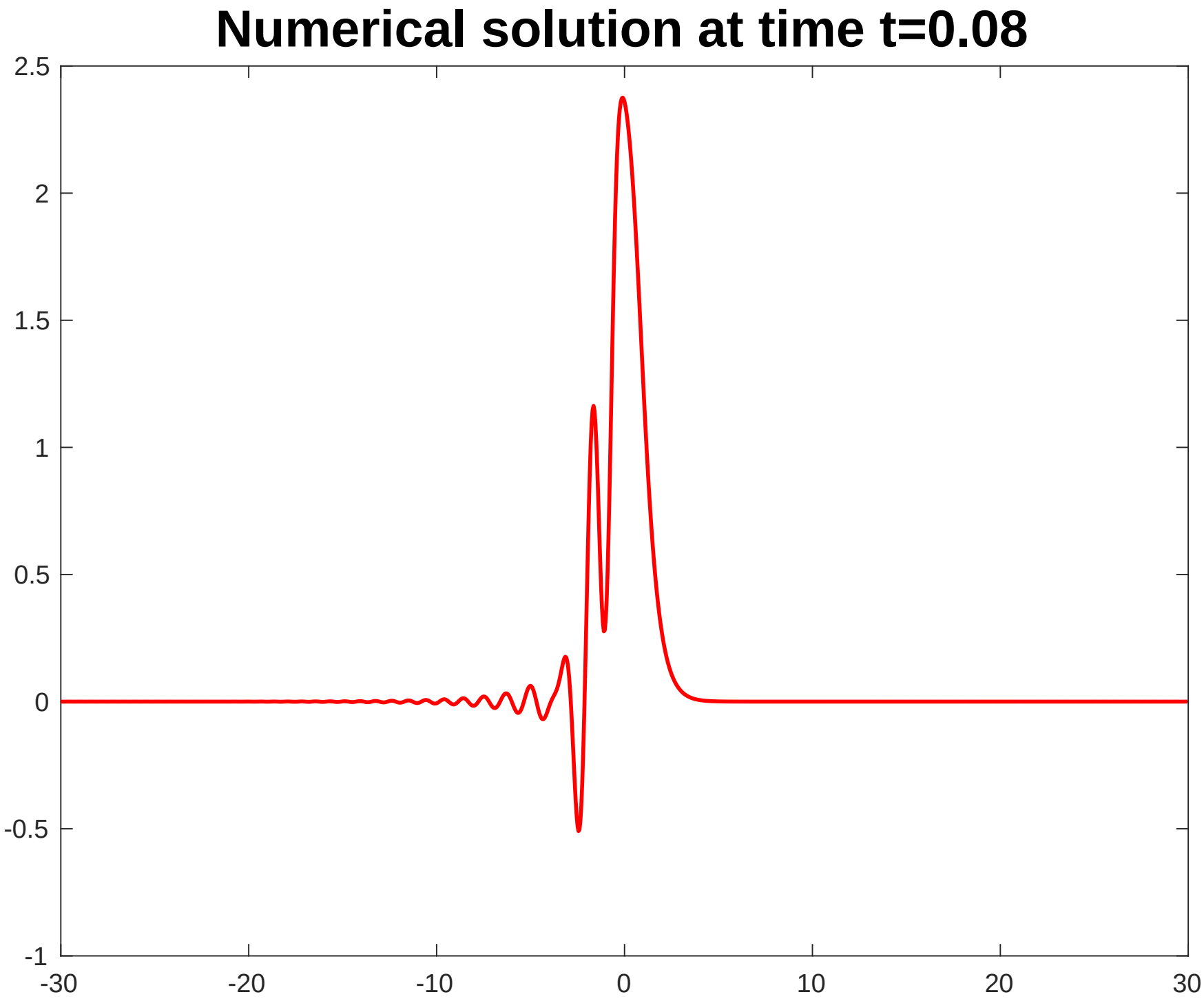

Click here to access/download Figure new_negative_3pi_008.pdf

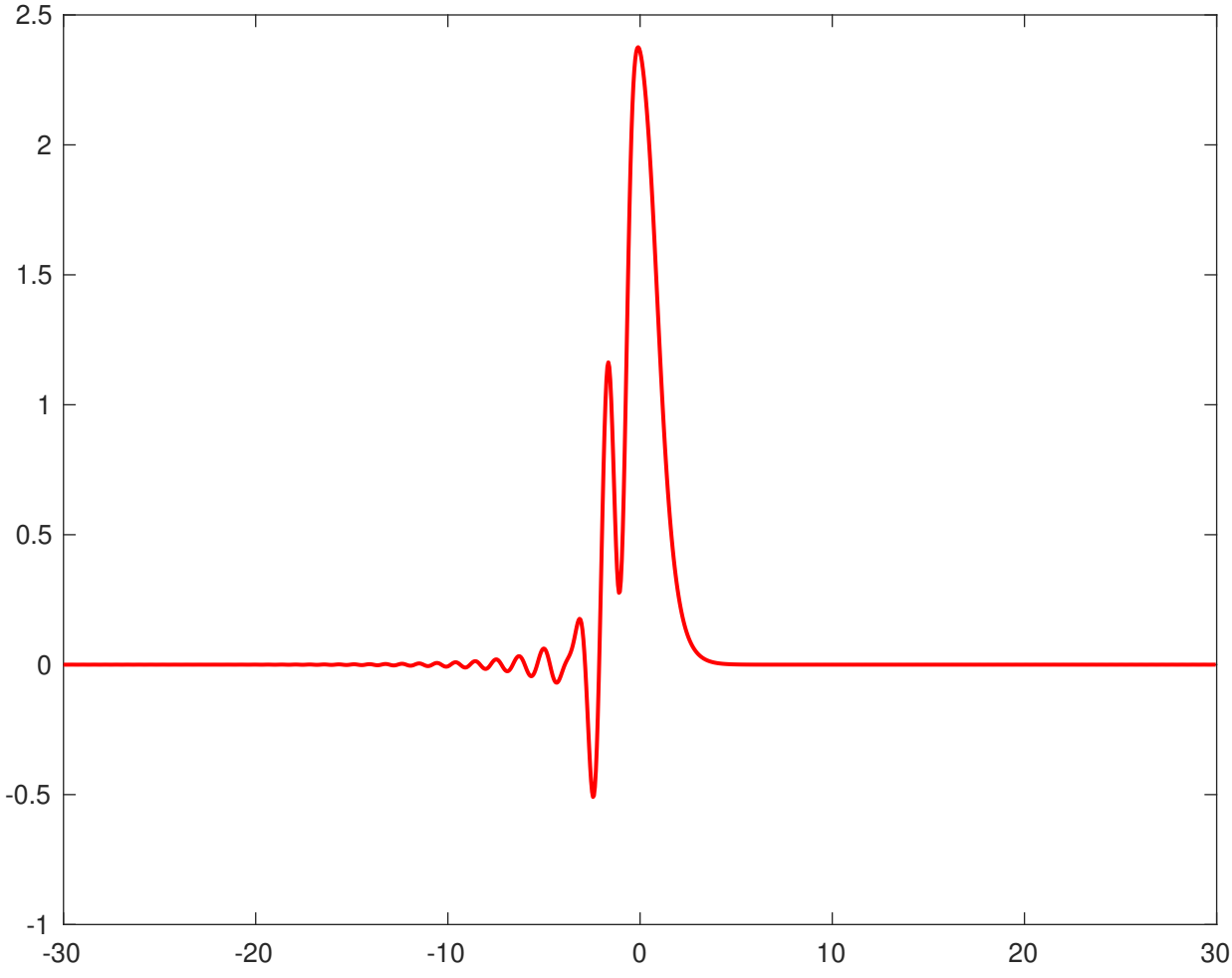

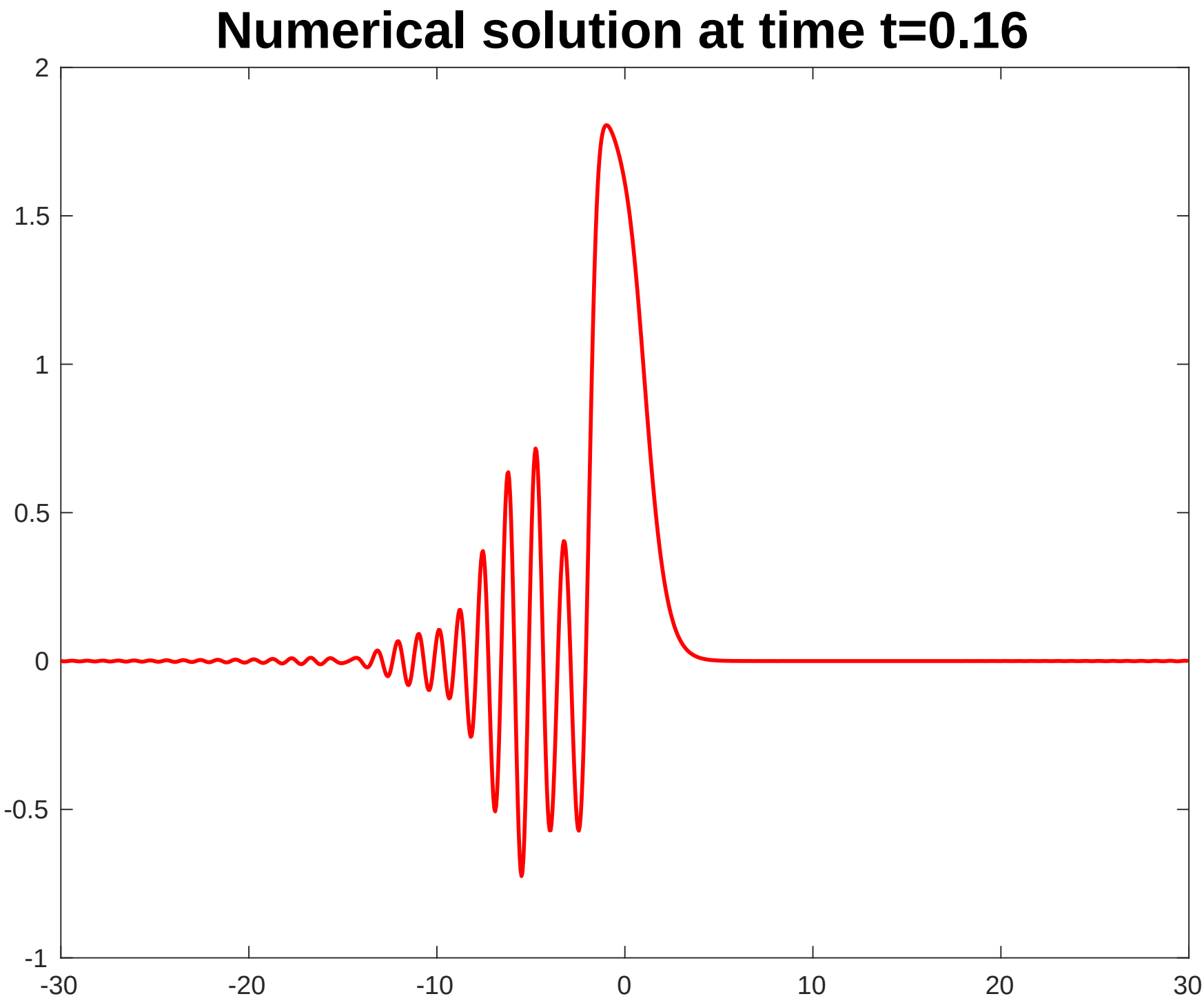

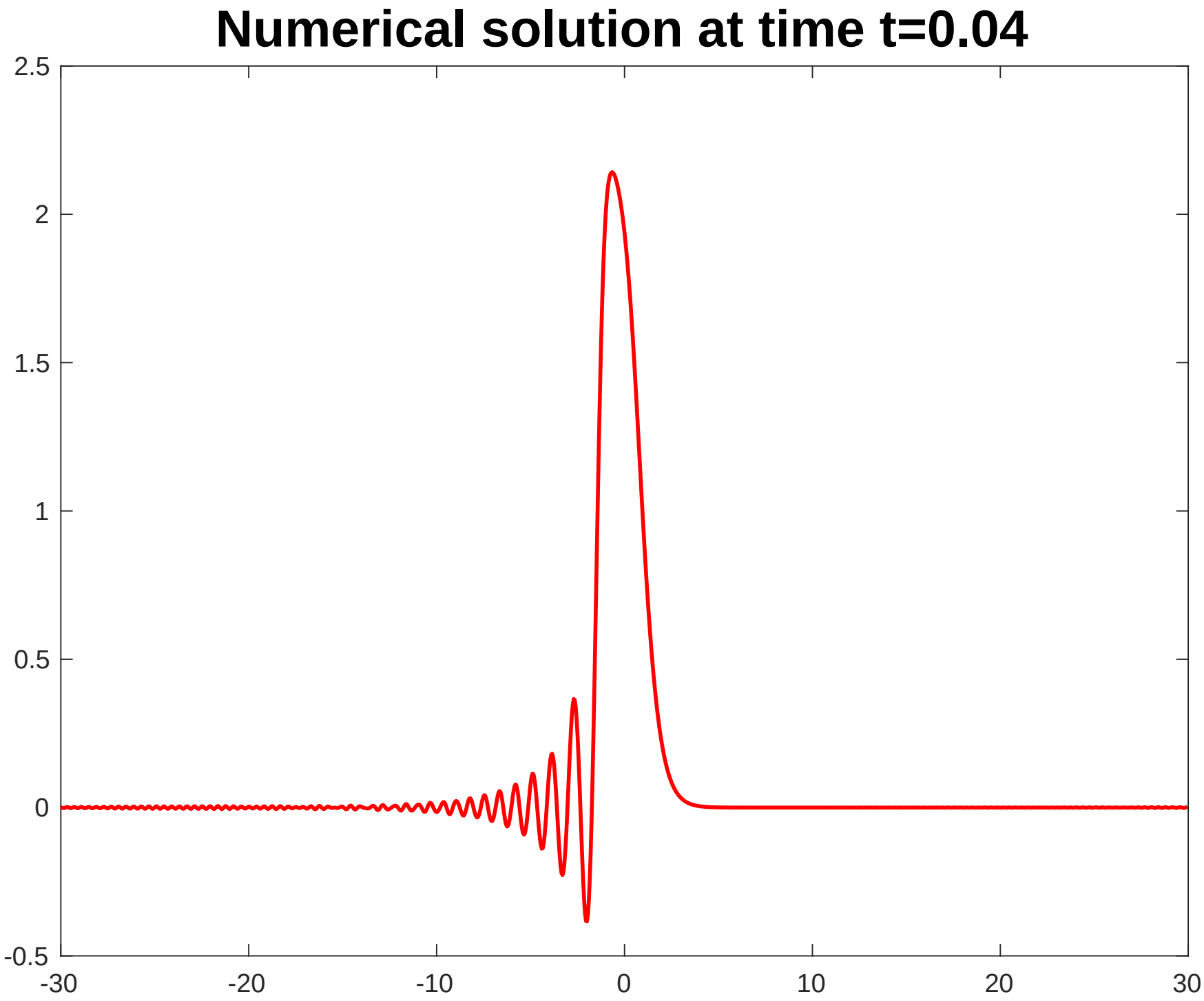

Click here to access/download Figure new_negative_500pi_004.pdf

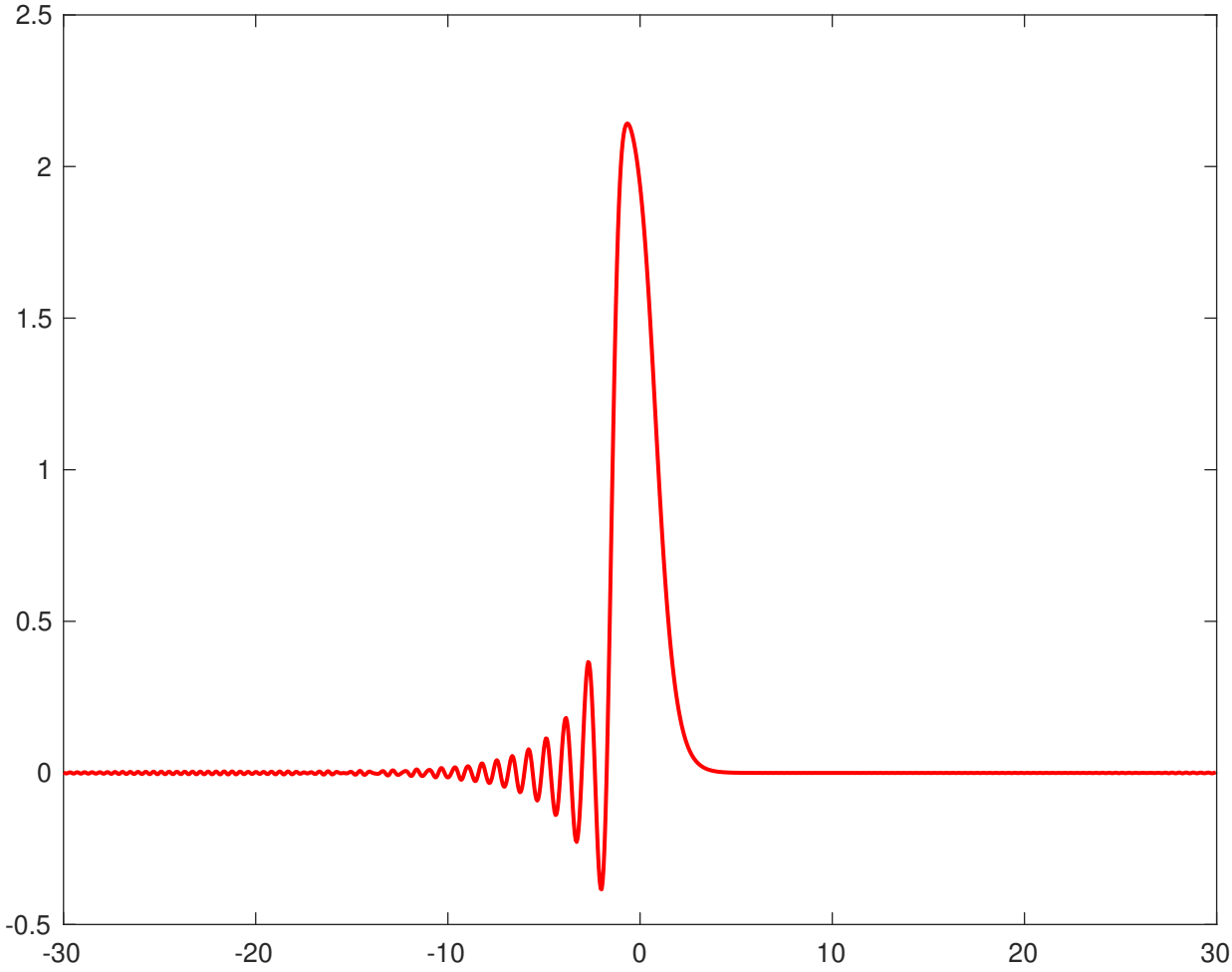

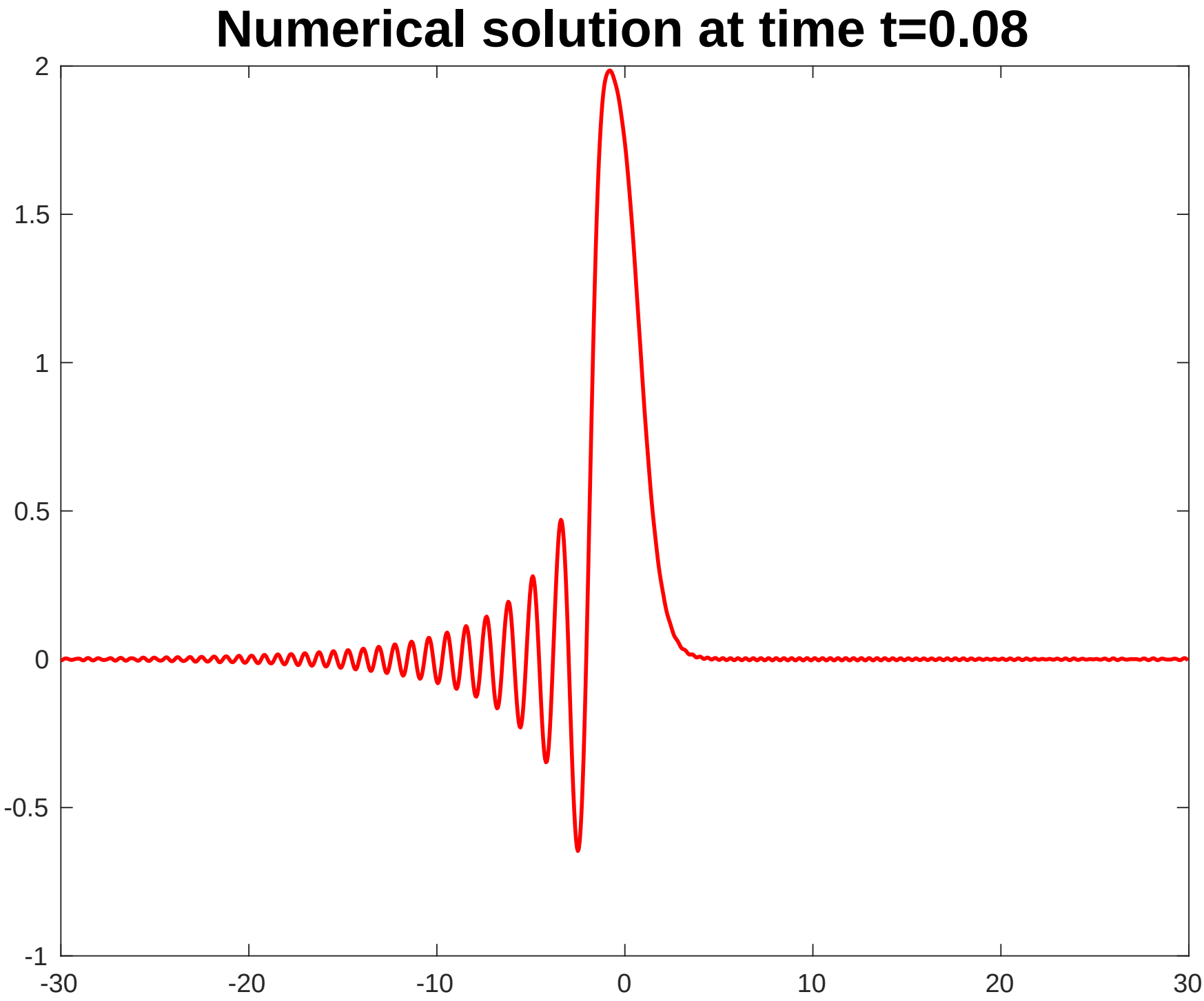

Click here to access/download Figure new_negative_500pi_008.pdf

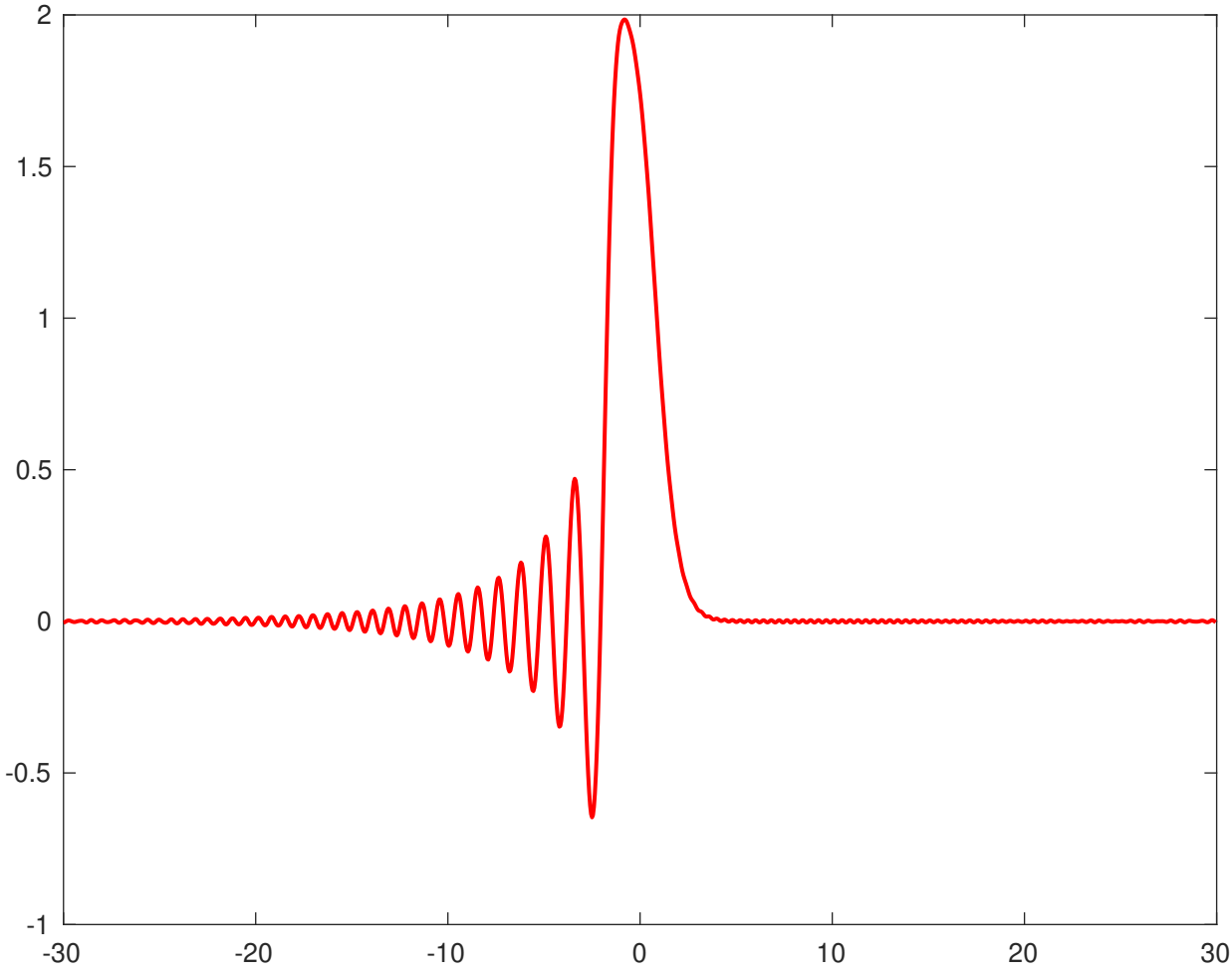

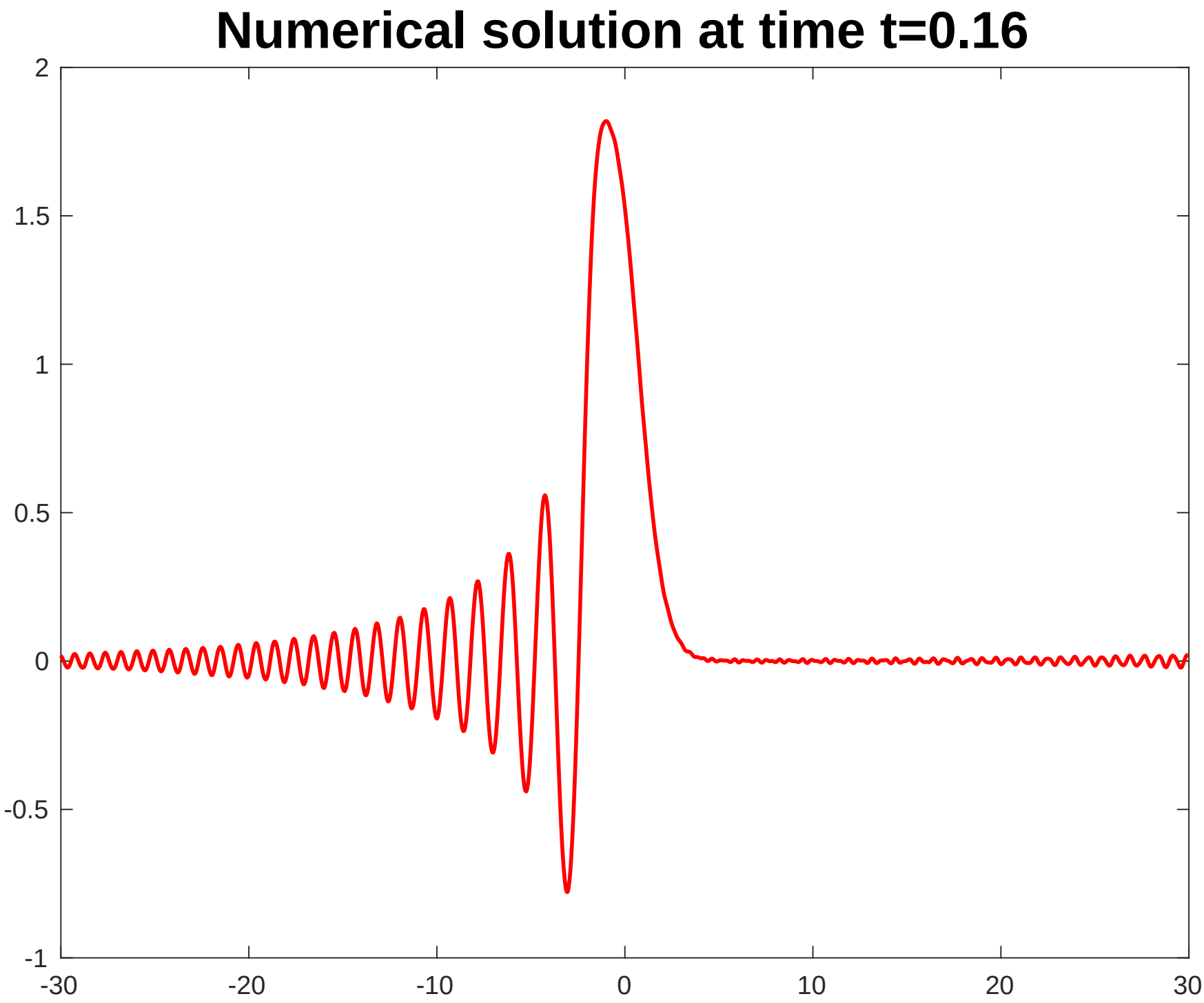

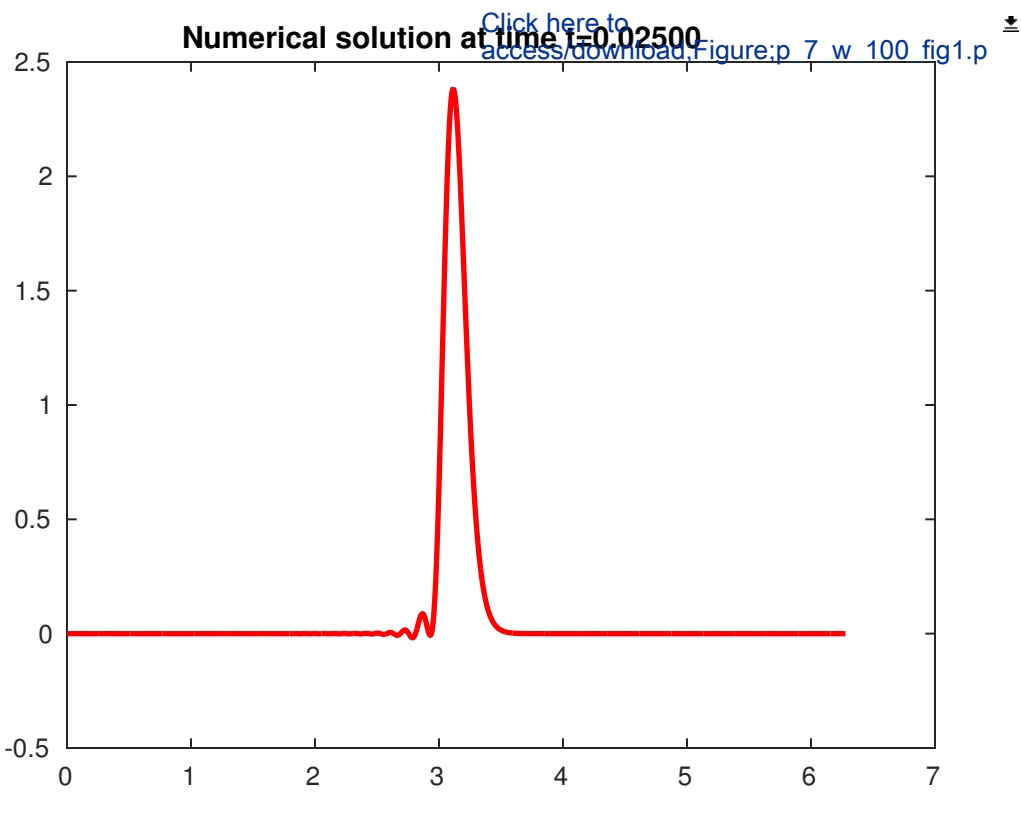
Numerical solution at time t=0.02500
Click here to
access/download;Figure;p_7_w_100_fig1.p
2.5
2
1.5
1
0.5
0
-0.5
0
1
2
3
4
5
6
7

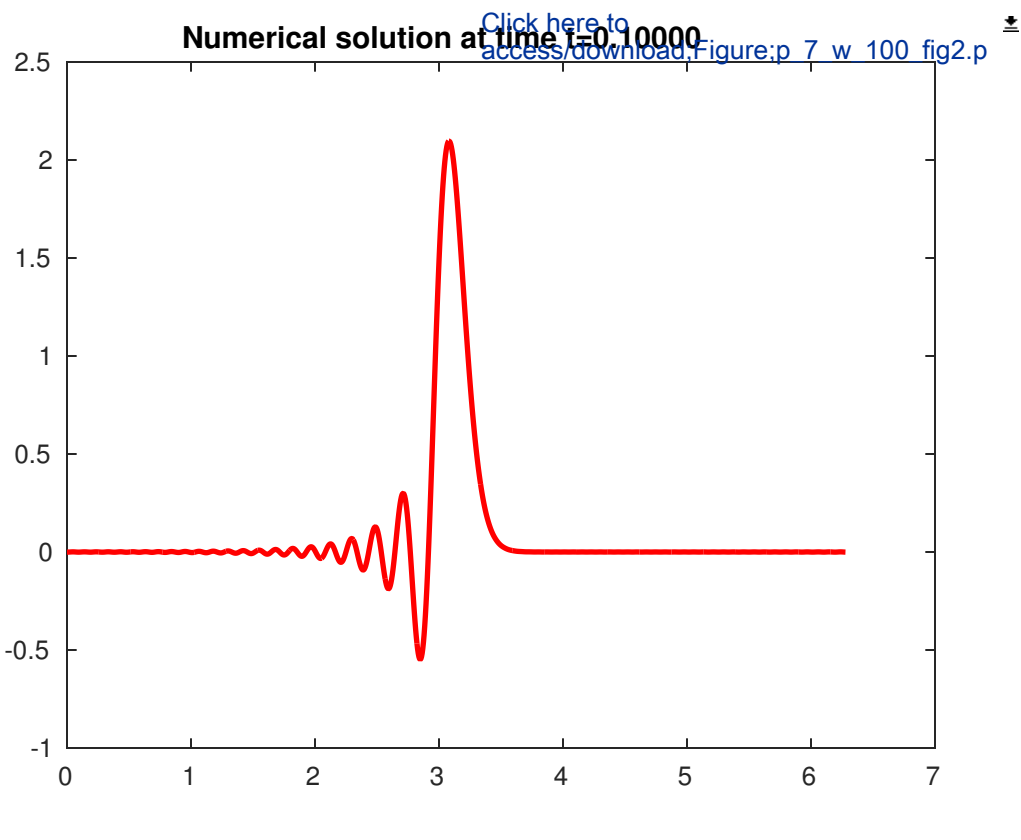
Numerical solution at time t=0.10000
Click here to
access/download;Figure;p_7_w_100_fig2.p
2.5
2
1.5
1
0.5
0
-0.5
-1
0
1
2
3
4
5
6
7

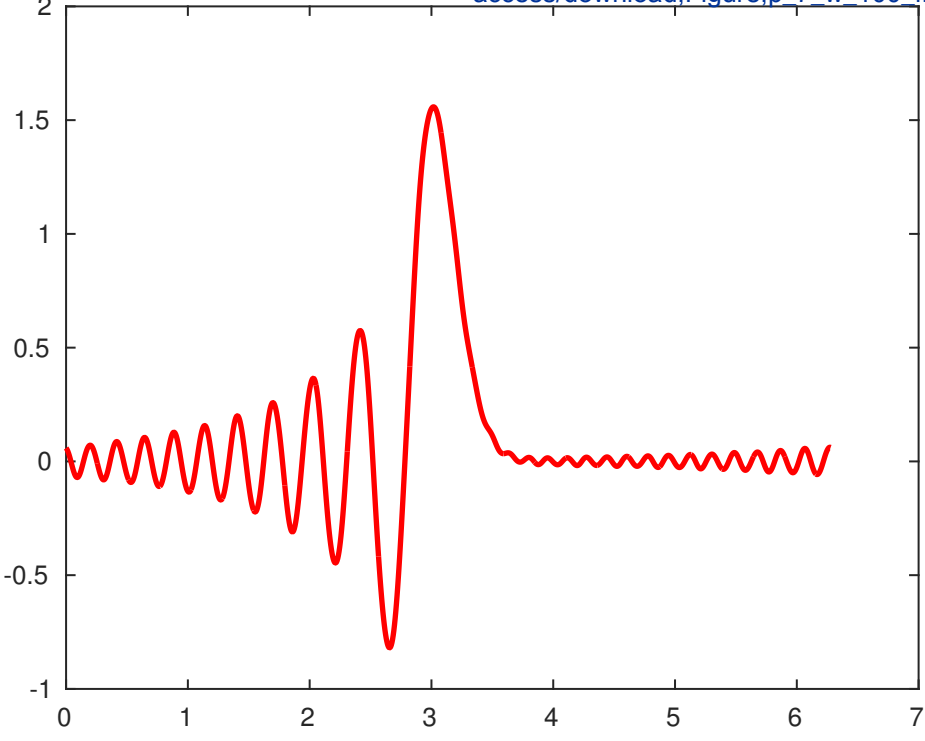

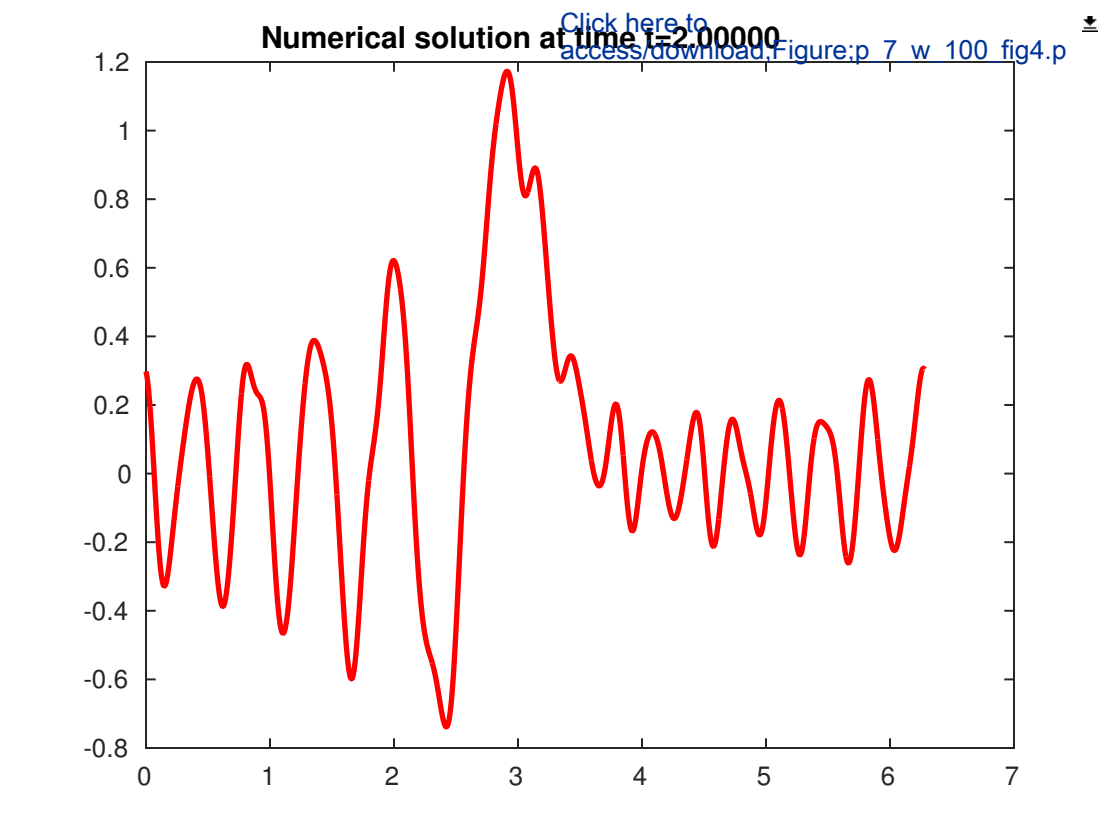
Numerical solution at time t=2.00000
Click here to
access/download;Figure;p_7_w_100_fig4.p
1.2
1
0.8
0.6
0.4
0.2
0
-0.2
-0.4
-0.6
-0.8
0
1
2
3
4
5
6
7

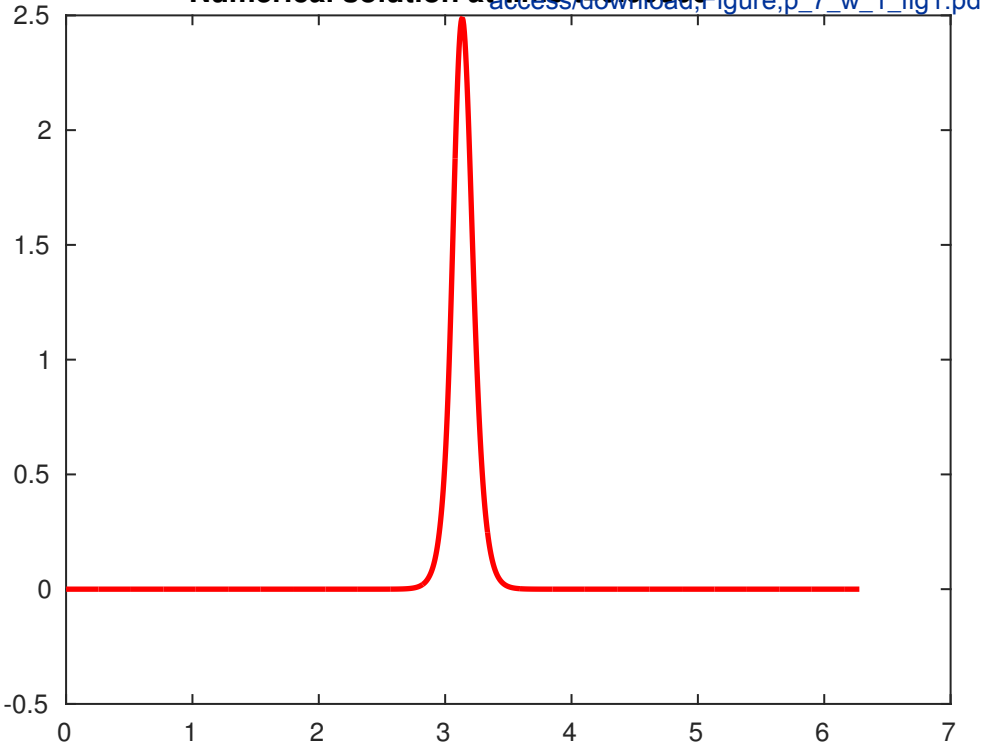

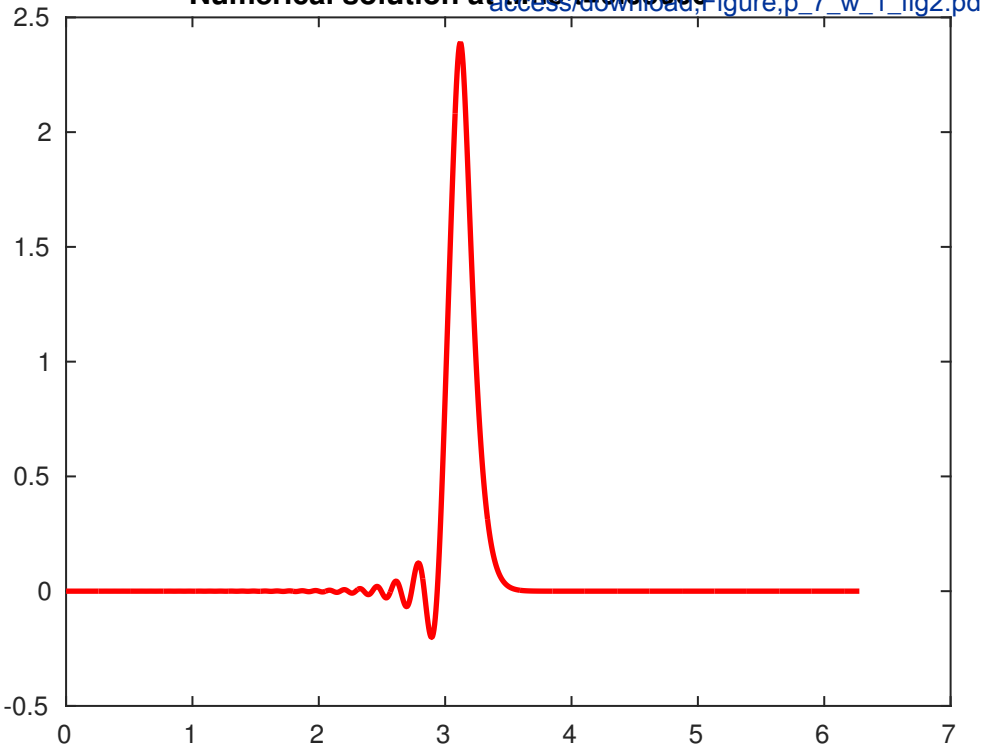

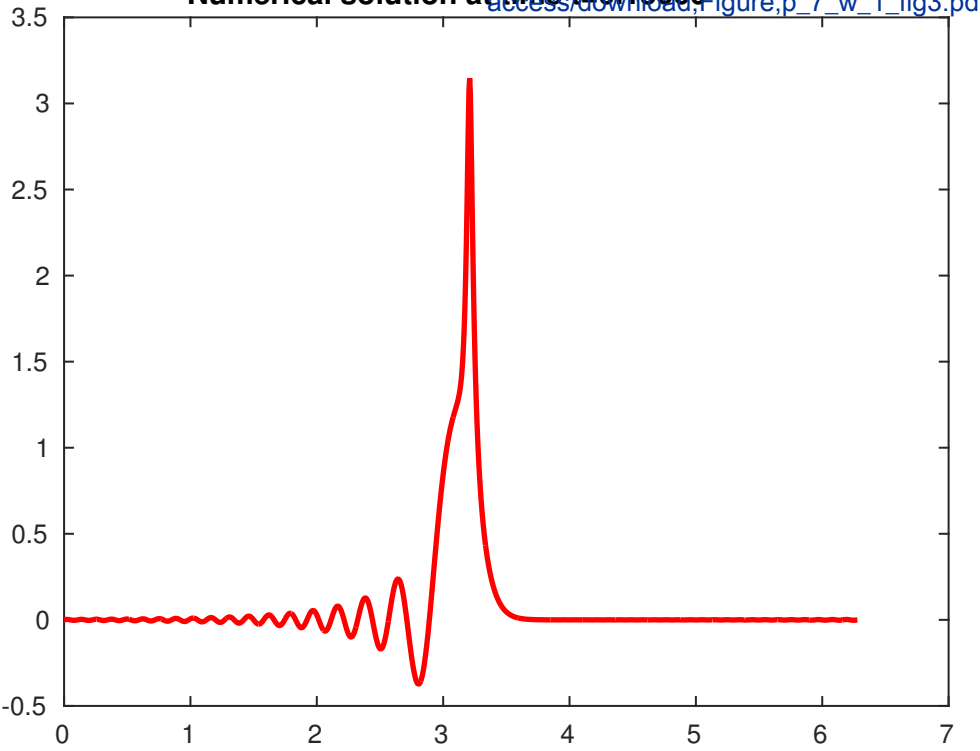

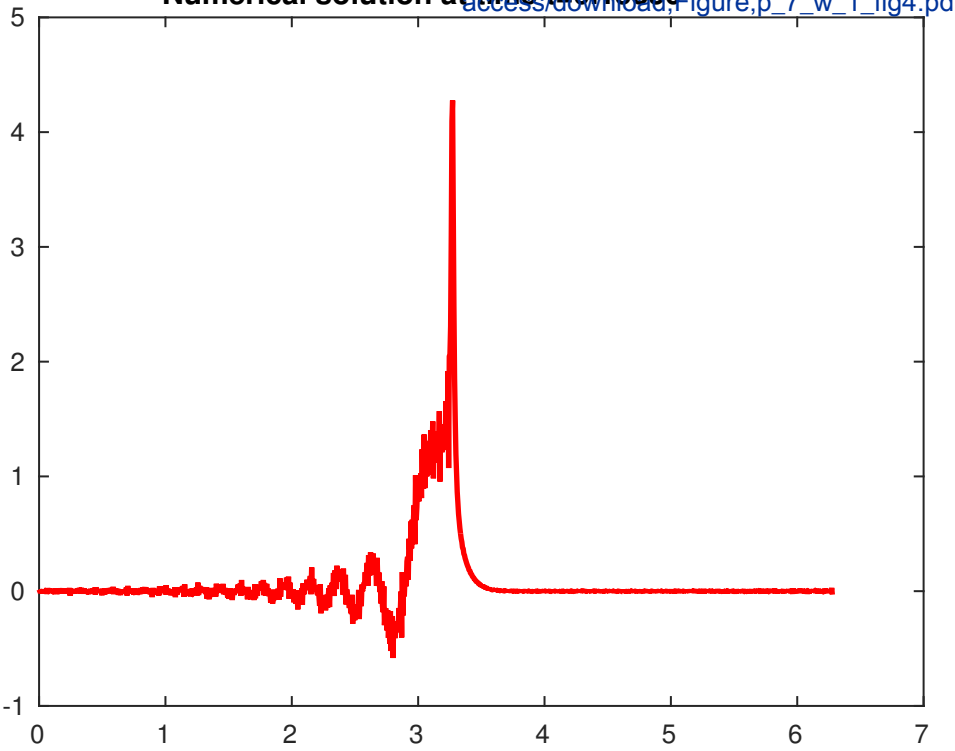

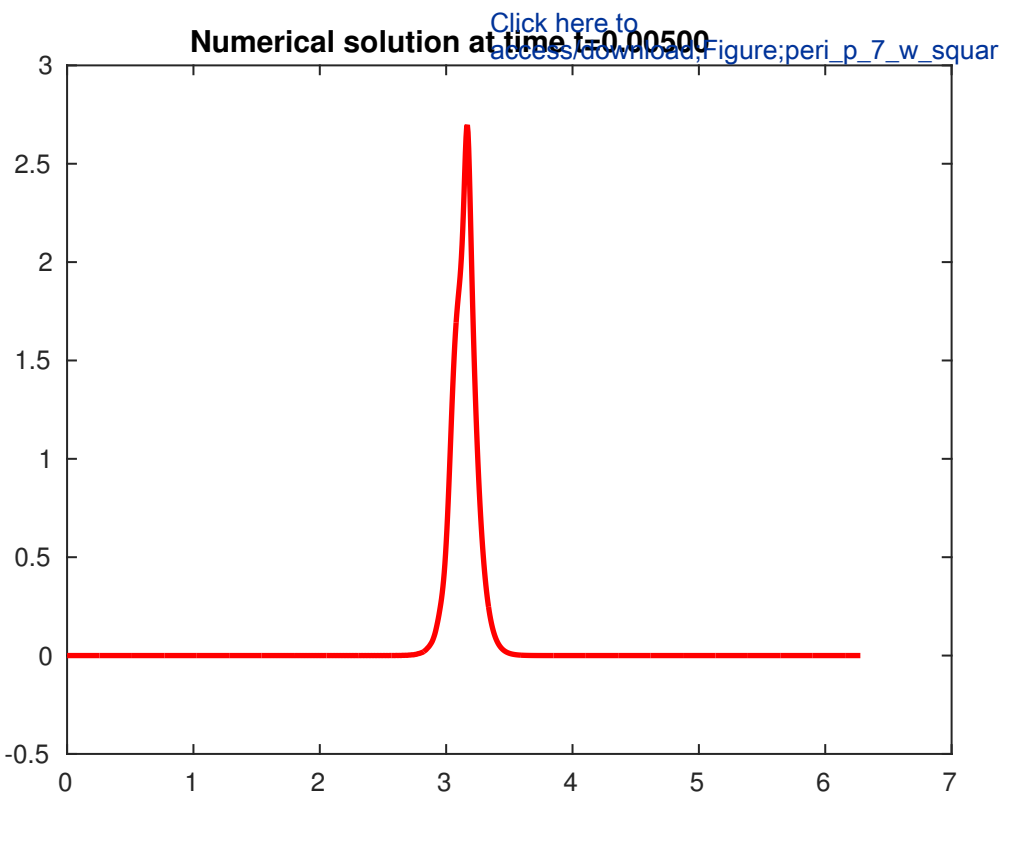
Numerical solution at time t=0.00500
Click here to
access/download;Figure;peri_p_7_w_squar
3
2.5
2
1.5
1
0.5
0
-0.5
0
1
2
3
4
5
6
7

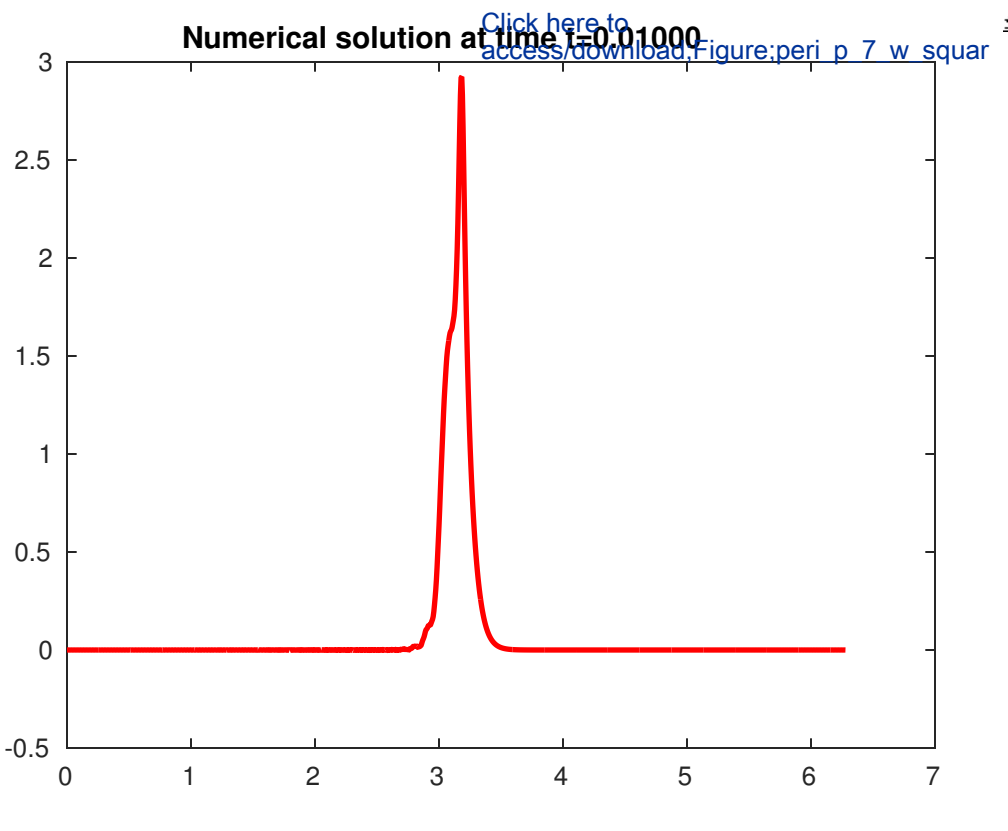
Numerical solution at time t=0.01000
Click here to access/download;Figure;peri_p_7_w_squar
3
2.5
2
1.5
1
0.5
0
-0.5
0
1
2
3
4
5
6
7

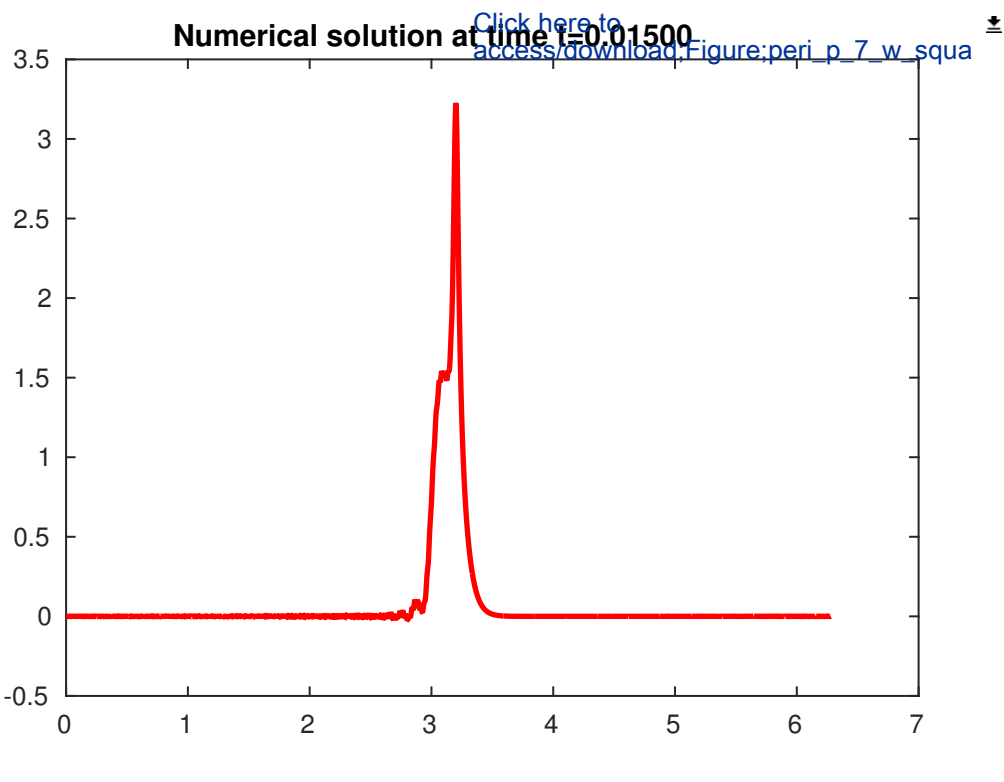
Numerical solution at time t=0.01500
Click here to access/download;Figure;peri_p_7_w_squa
3.5
3
2.5
2
1.5
1
0.5
0
-0.5
0
1
2
3
4
5
6
7

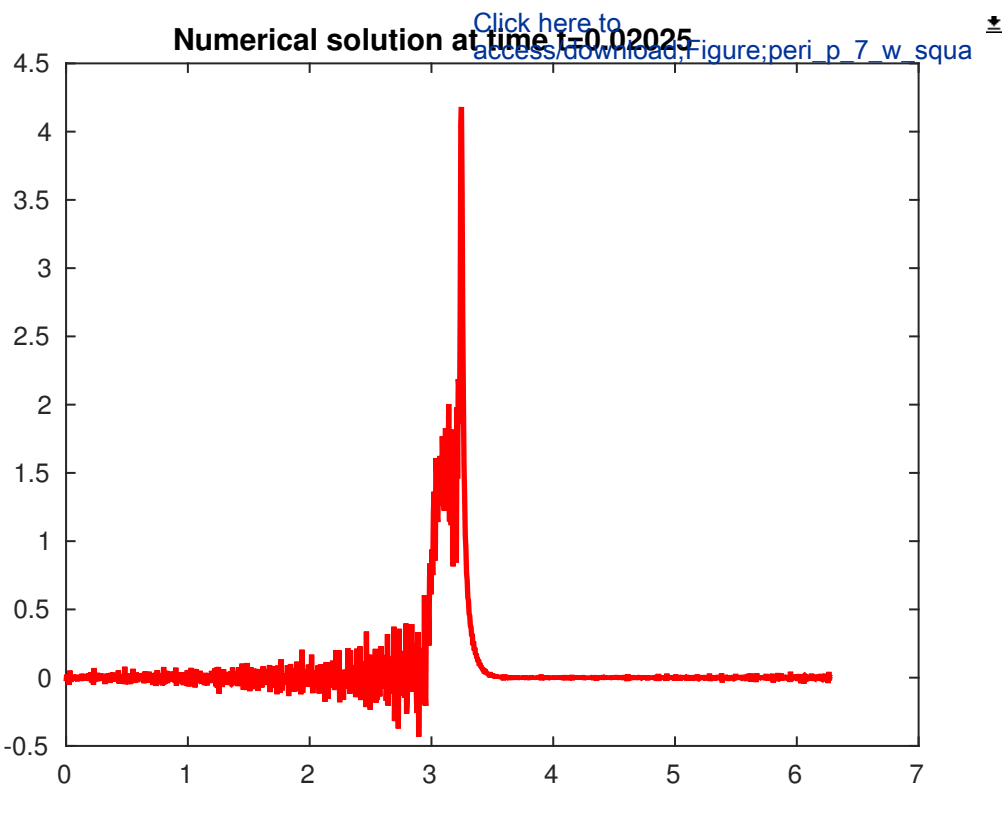
Numerical solution at time t=0.02025
Click here to access/download;Figure;peri_p_7_w_squa
4.5
4
3.5
3
2.5
2
1.5
1
0.5
0
-0.5
0
1
2
3
4
5
6
7

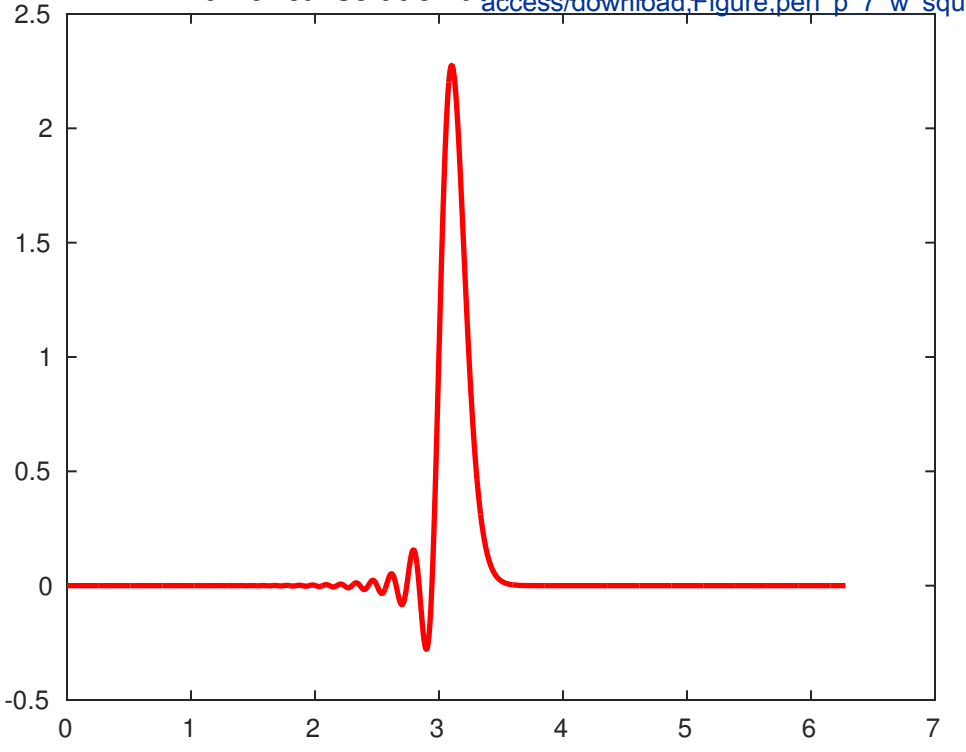
Numerical solution at time t=0.05000
Click here to
access/download;Figure;peri_p_7_w_squar
2.5
2
1.5
1
0.5
0
-0.5
0
1
2
3
4
5
6
7

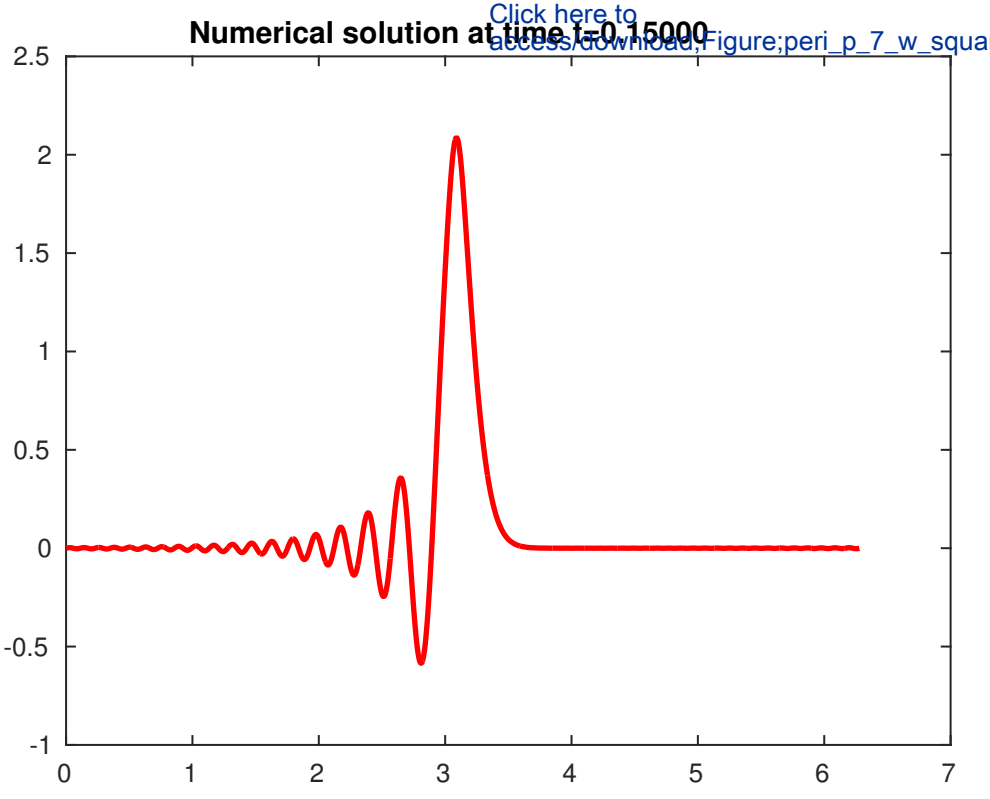
Click here to
access/download;Figure;peri_p_7_w_squar
Numerical solution at time t=0.15000
2.5
2
1.5
1
0.5
0
-0.5
-1
0
1
2
3
4
5
6
7

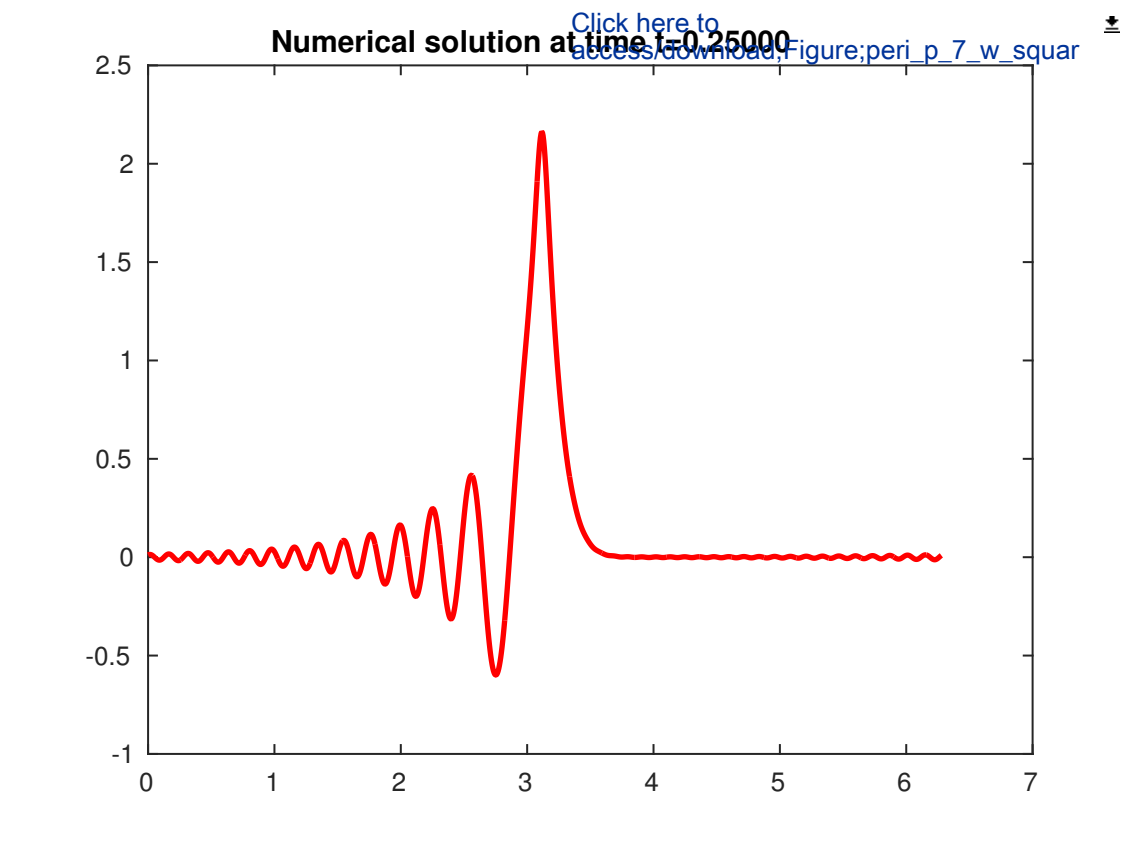
Numerical solution at time t=0.25000
Click here to access/download;Figure;peri_p_7_w_squar
2.5
2
1.5
1
0.5
0
-0.5
-1
0
1
2
3
4
5
6
7

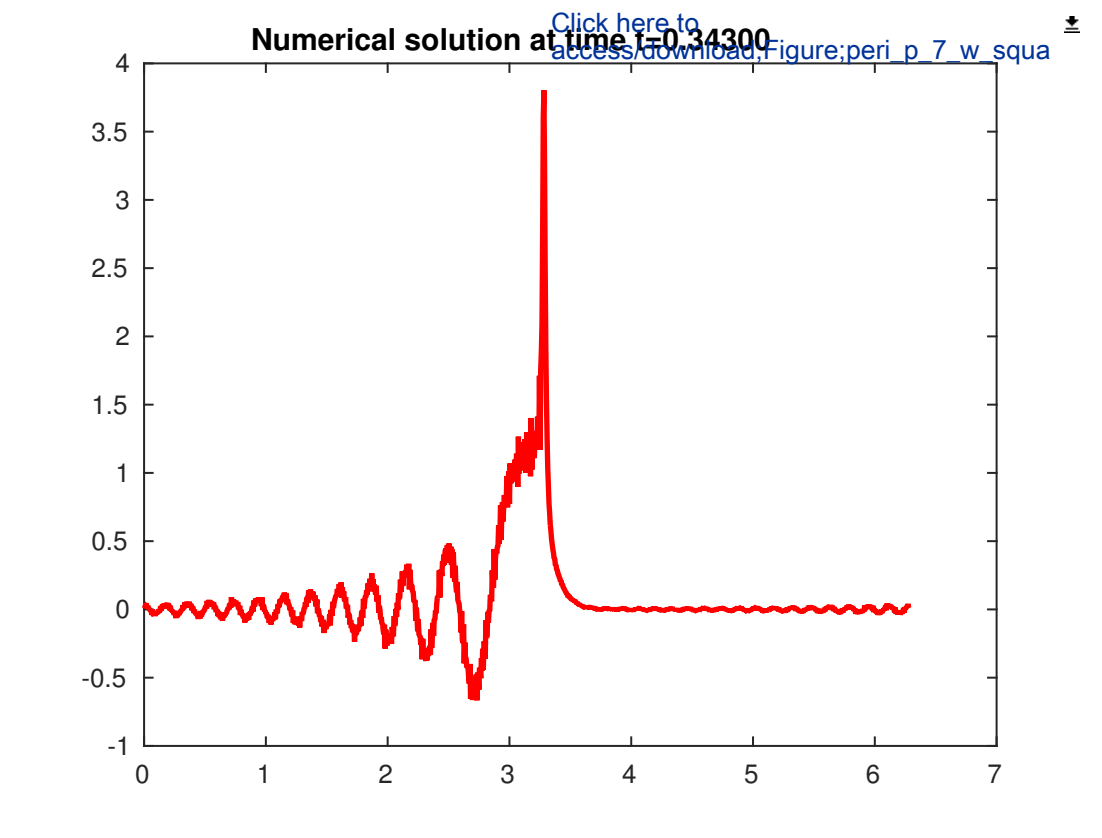
Numerical solution at time t=0.34300
Click here to access/download;Figure;peri_p_7_w_squa
4
3.5
3
2.5
2
1.5
1
0.5
0
-0.5
-1
0
1
2
3
4
5
6
7

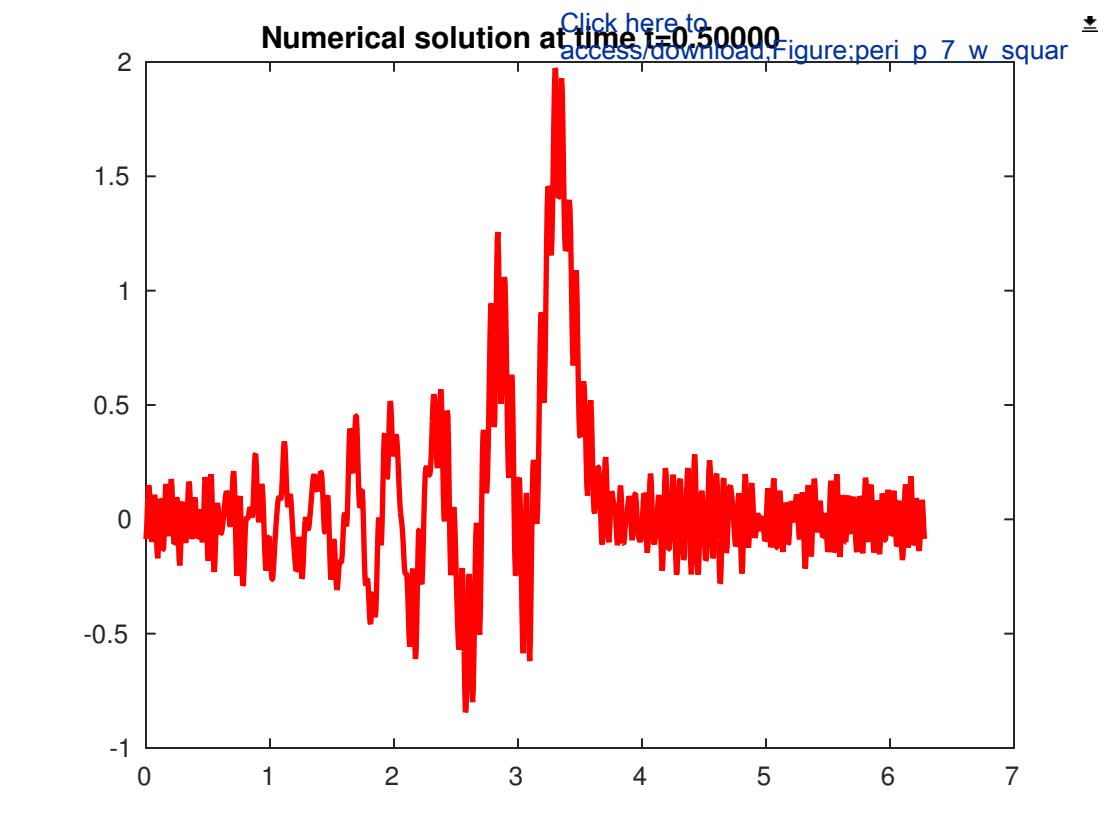
Numerical solution at time t=0.50000
Click here to access/download;Figure;peri_p_7_w_squar
2
1.5
1
0.5
0
-0.5
-1
0
1
2
3
4
5
6
7

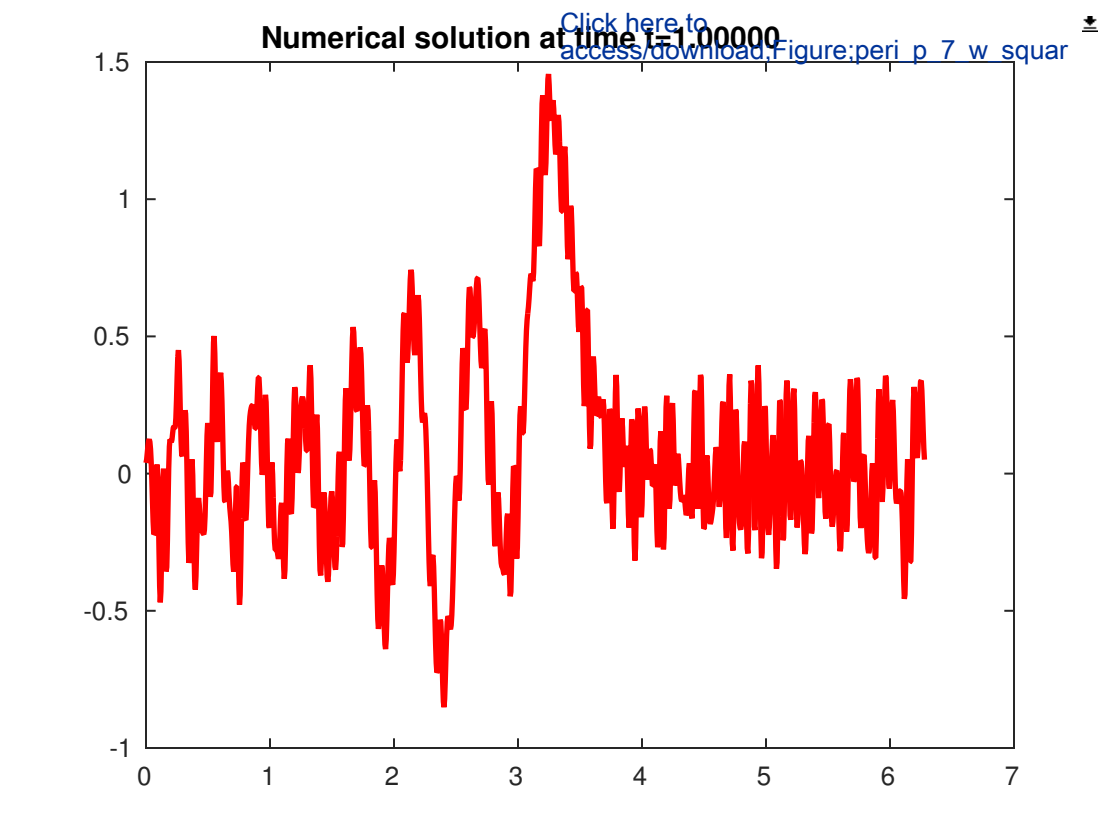
Numerical solution at time t= 1.00000
Click here to
access/download;Figure;peri_p_7_w_squar
1.5
1
0.5
0
-0.5
-1
0
1
2
3
4
5
6
7

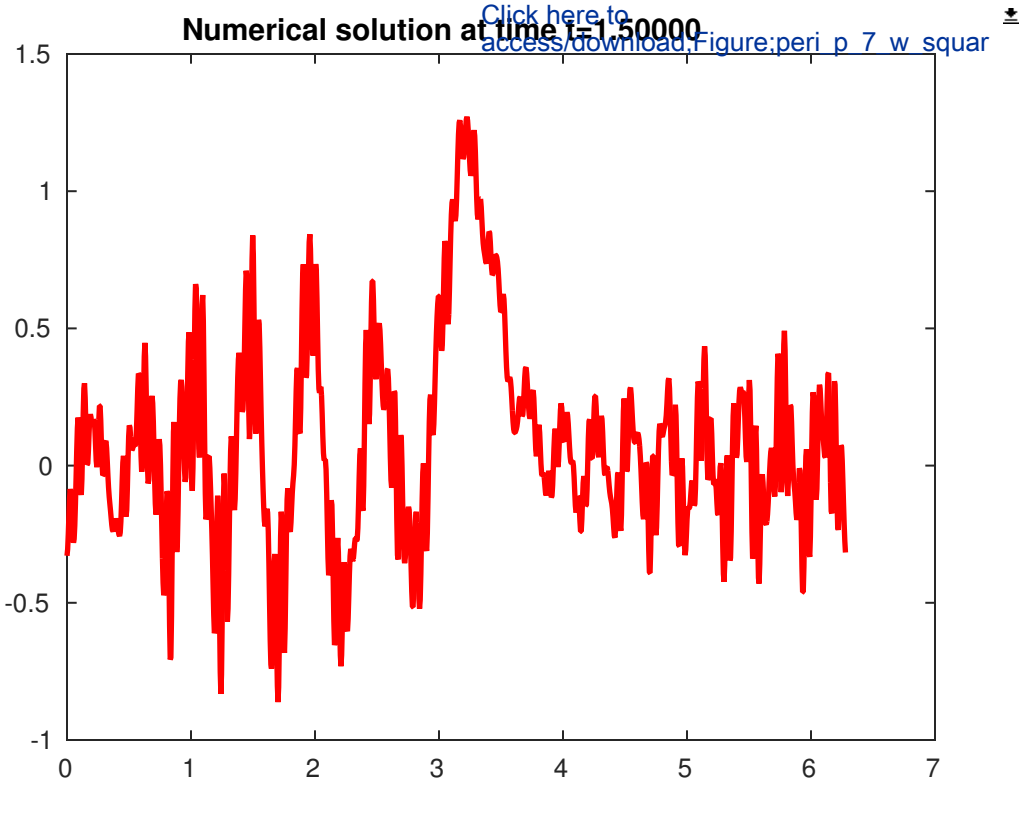
Numerical solution at time t= 1.50000
Click here to access/download;Figure;peri_p_7_w_squar
1.5
1
0.5
0
-0.5
-1
0
1
2
3
4
5
6
7

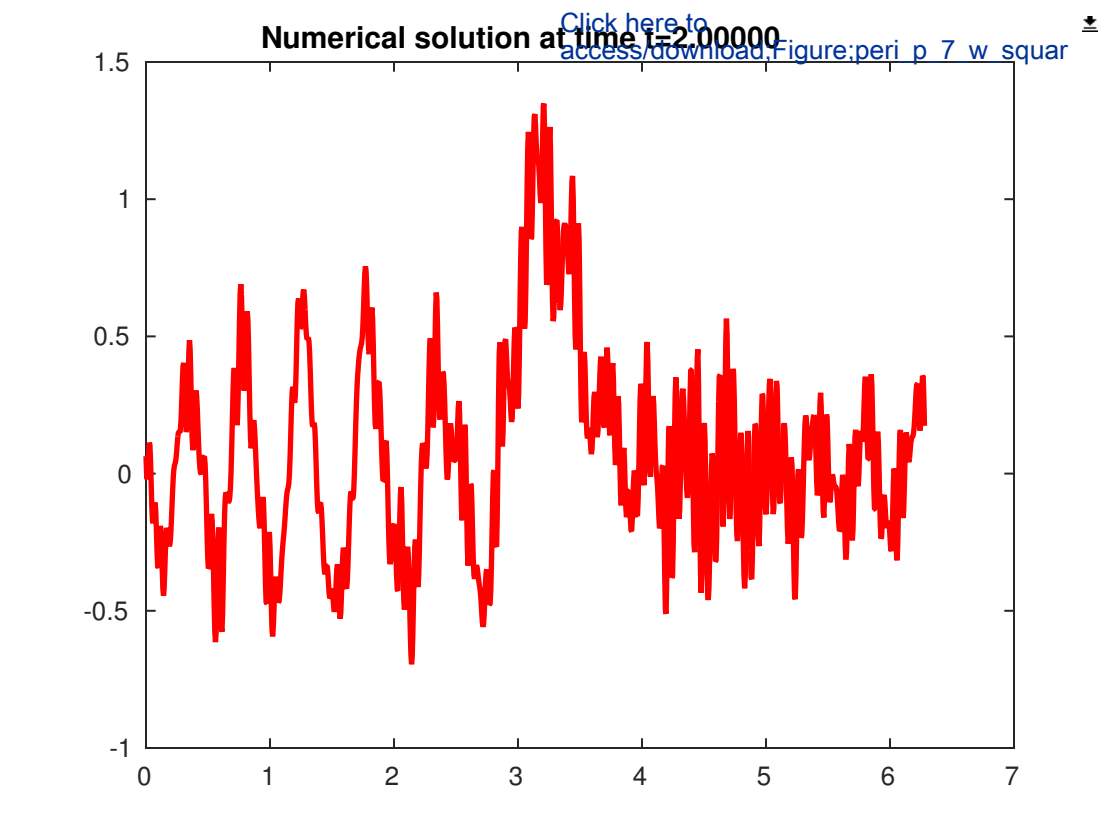
Numerical solution at time t=2.00000
Click here to access/download;Figure;peri_p_7_w_squar
1.5
1
0.5
0
-0.5
-1
0
1
2
3
4
5
6
7

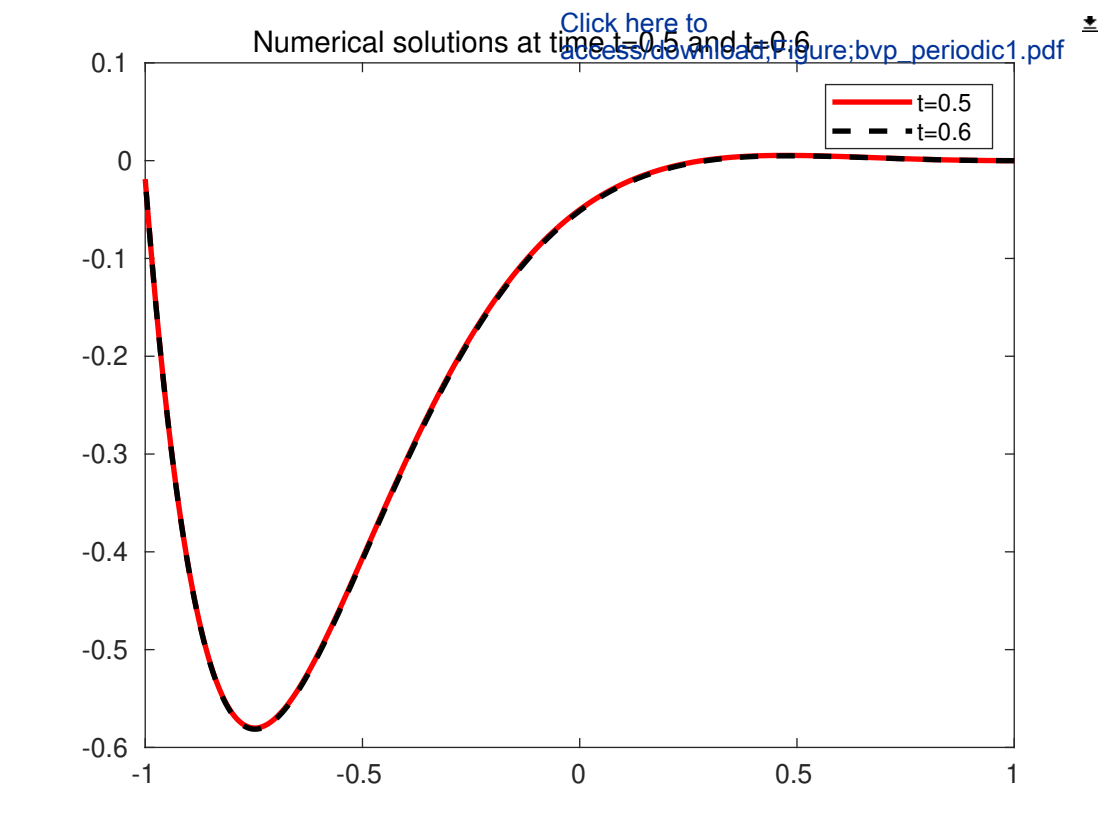
Click here to
access/download;Figure;bvp_periodic1.pdf
Numerical solutions at time t=0.5 and t=0.6
t=0.5
t=0.6
0.1
0
-0.1
-0.2
-0.3
-0.4
-0.5
-0.6
-1
-0.5
0
0.5
1

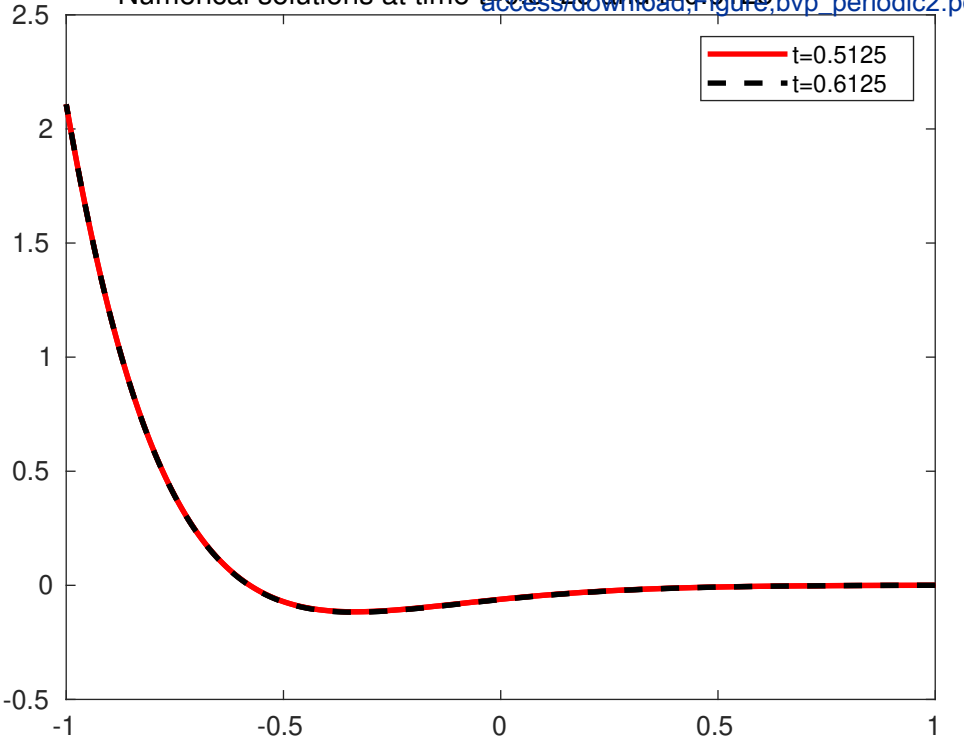

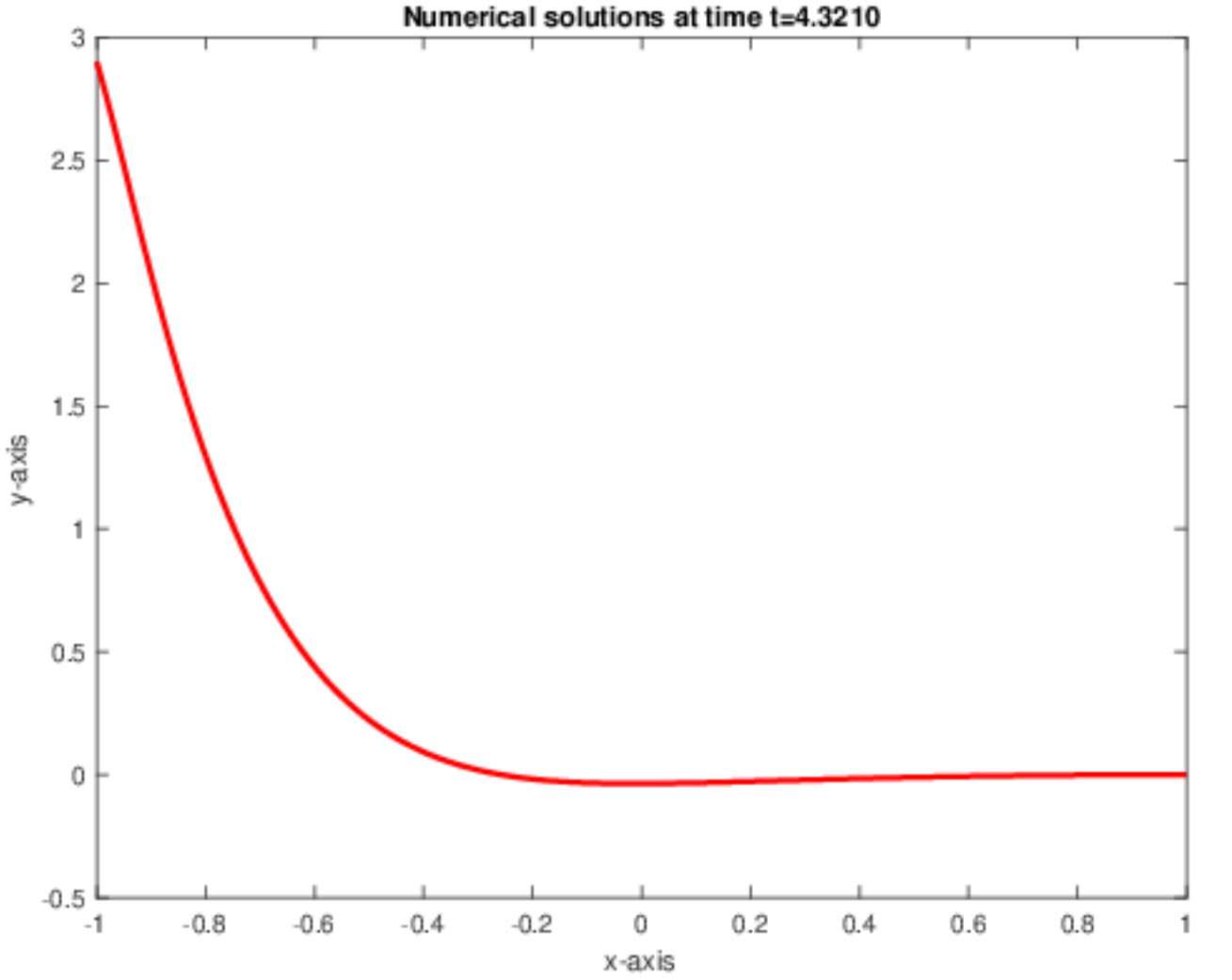

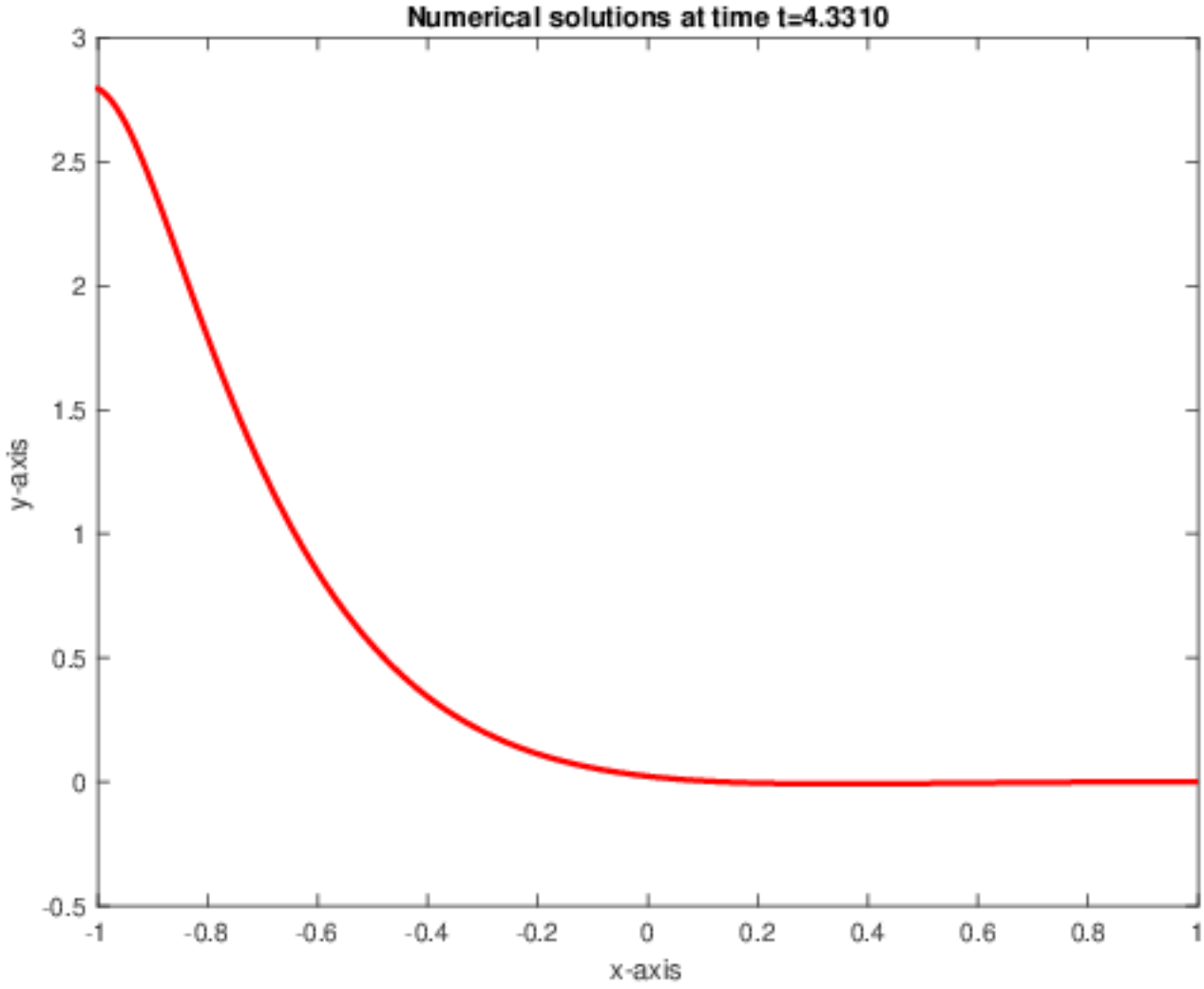

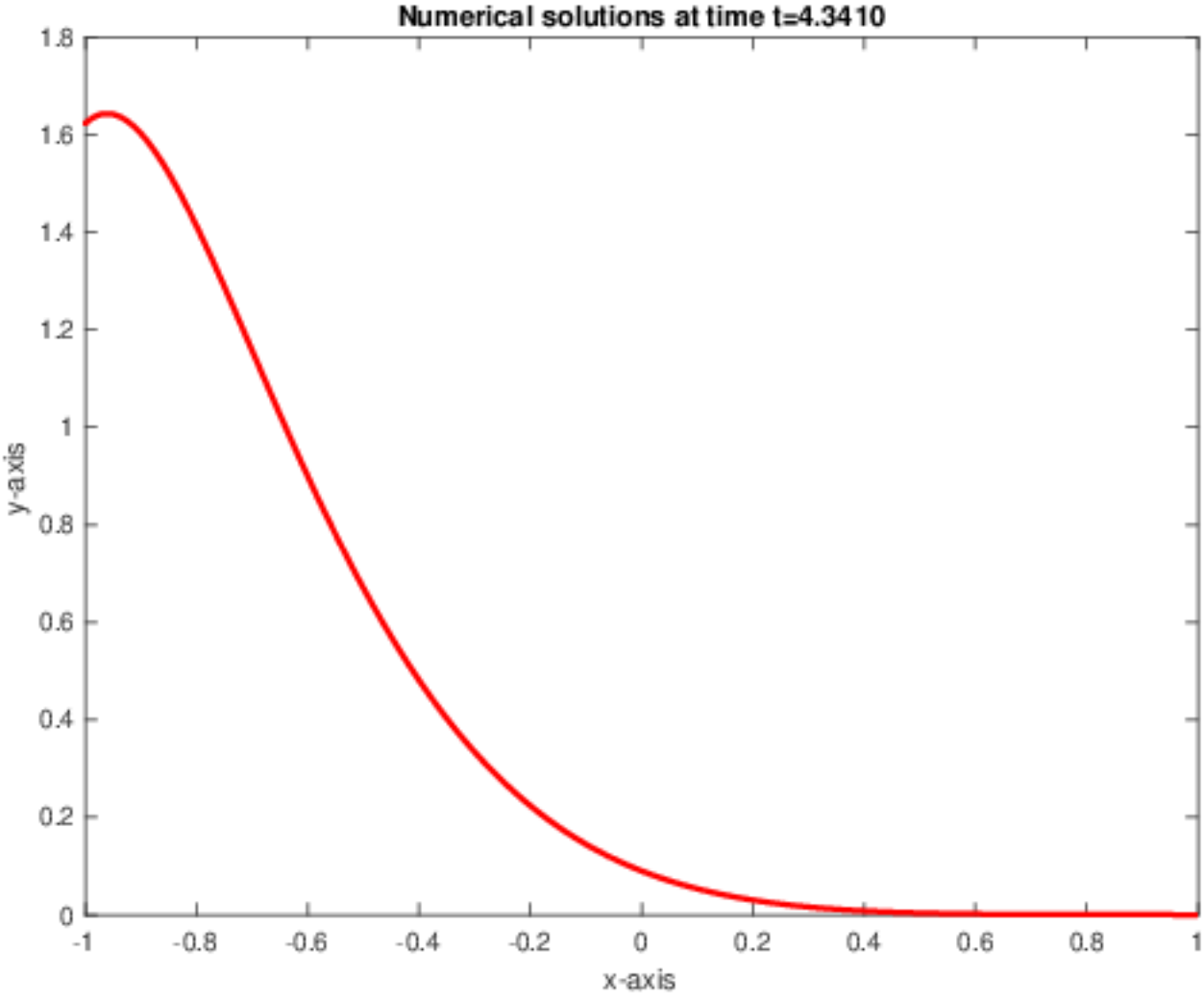

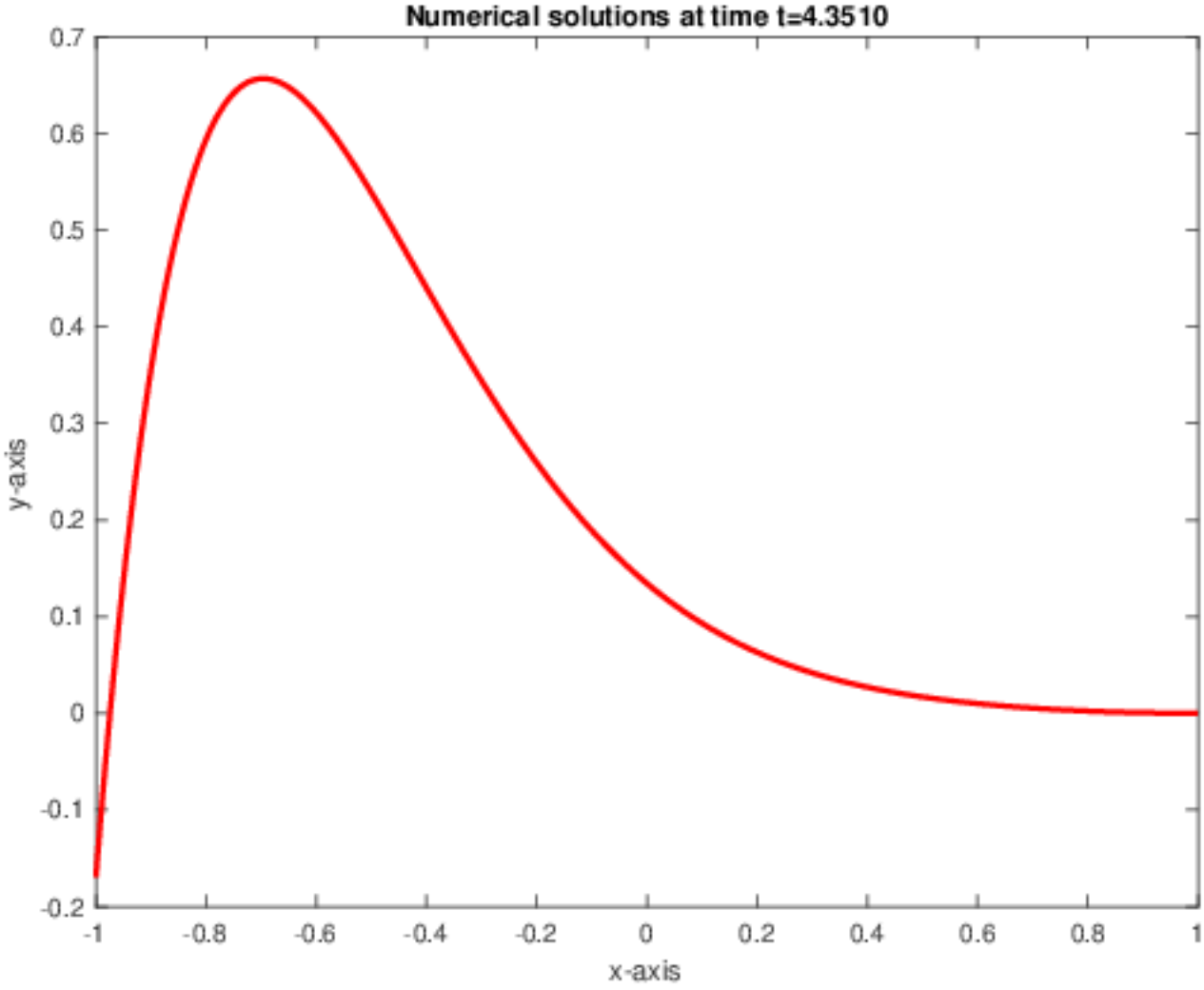

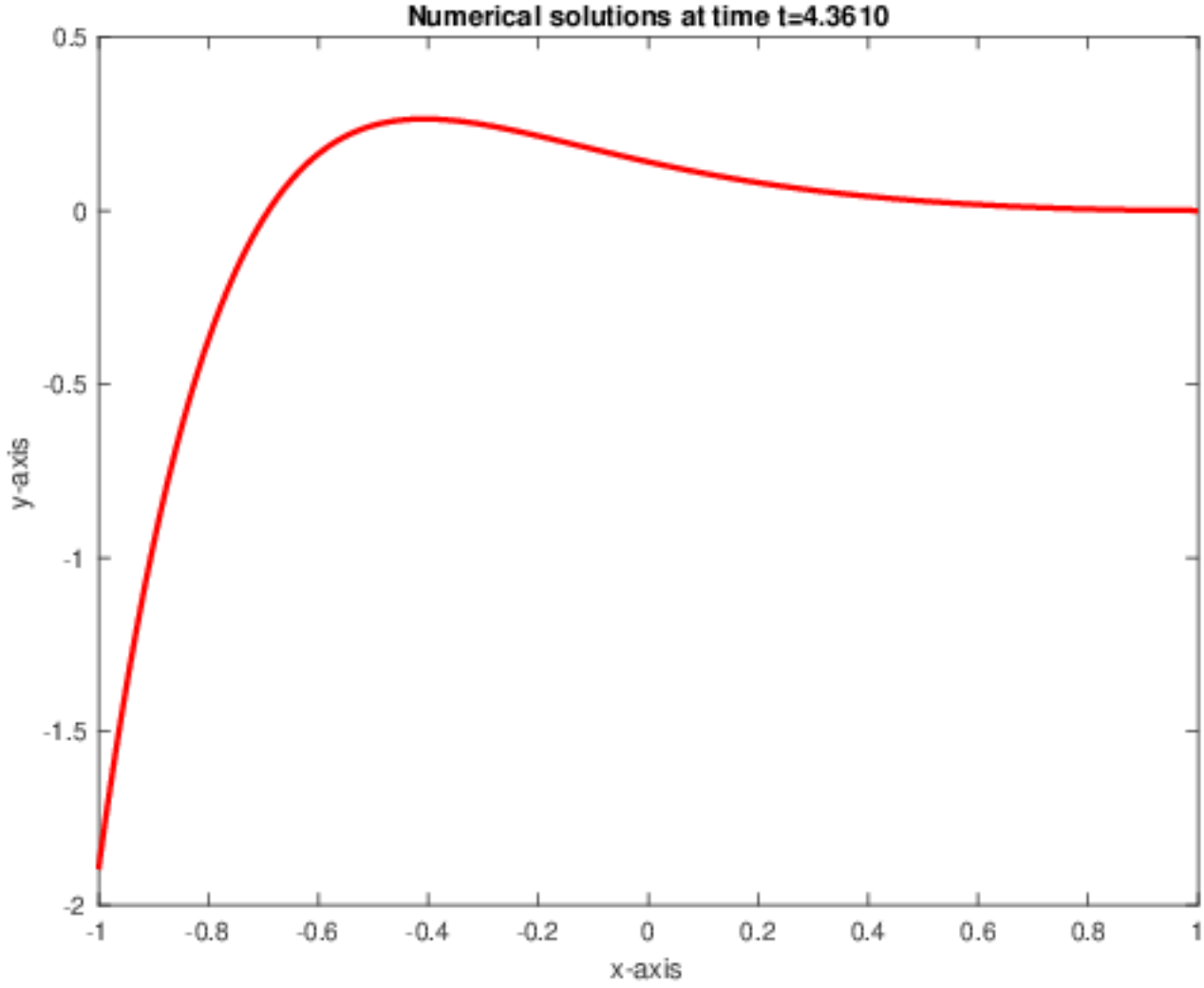

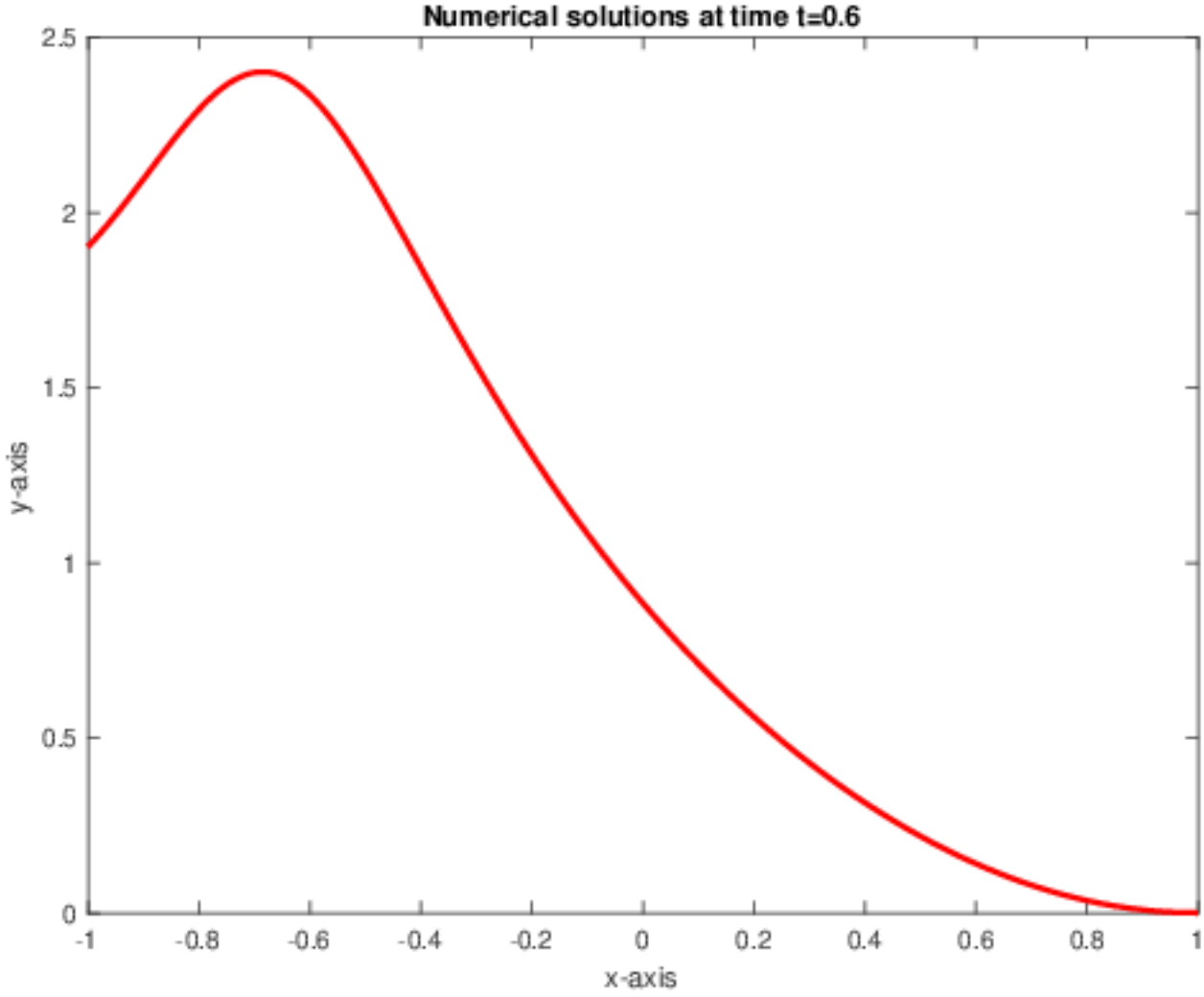

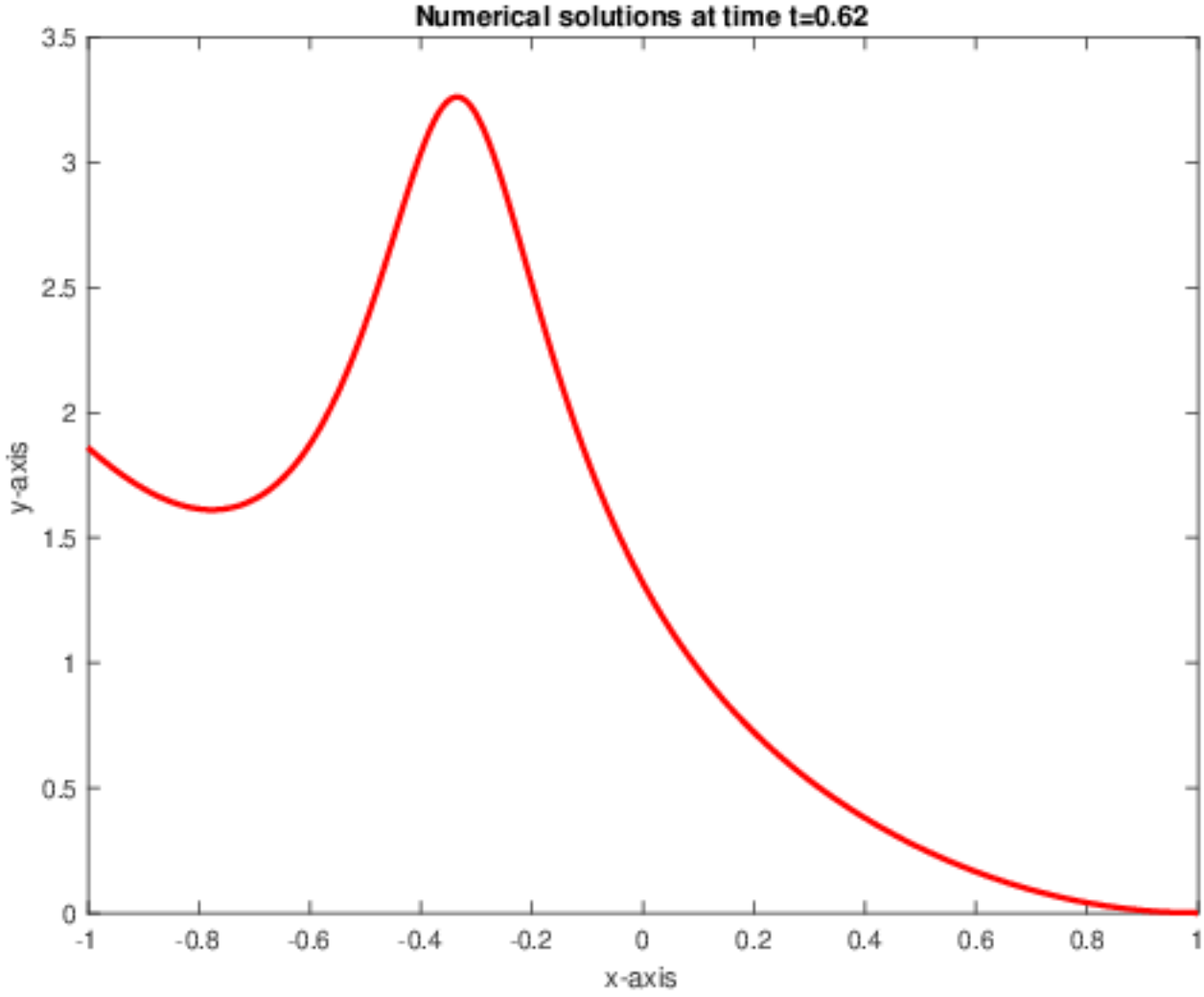

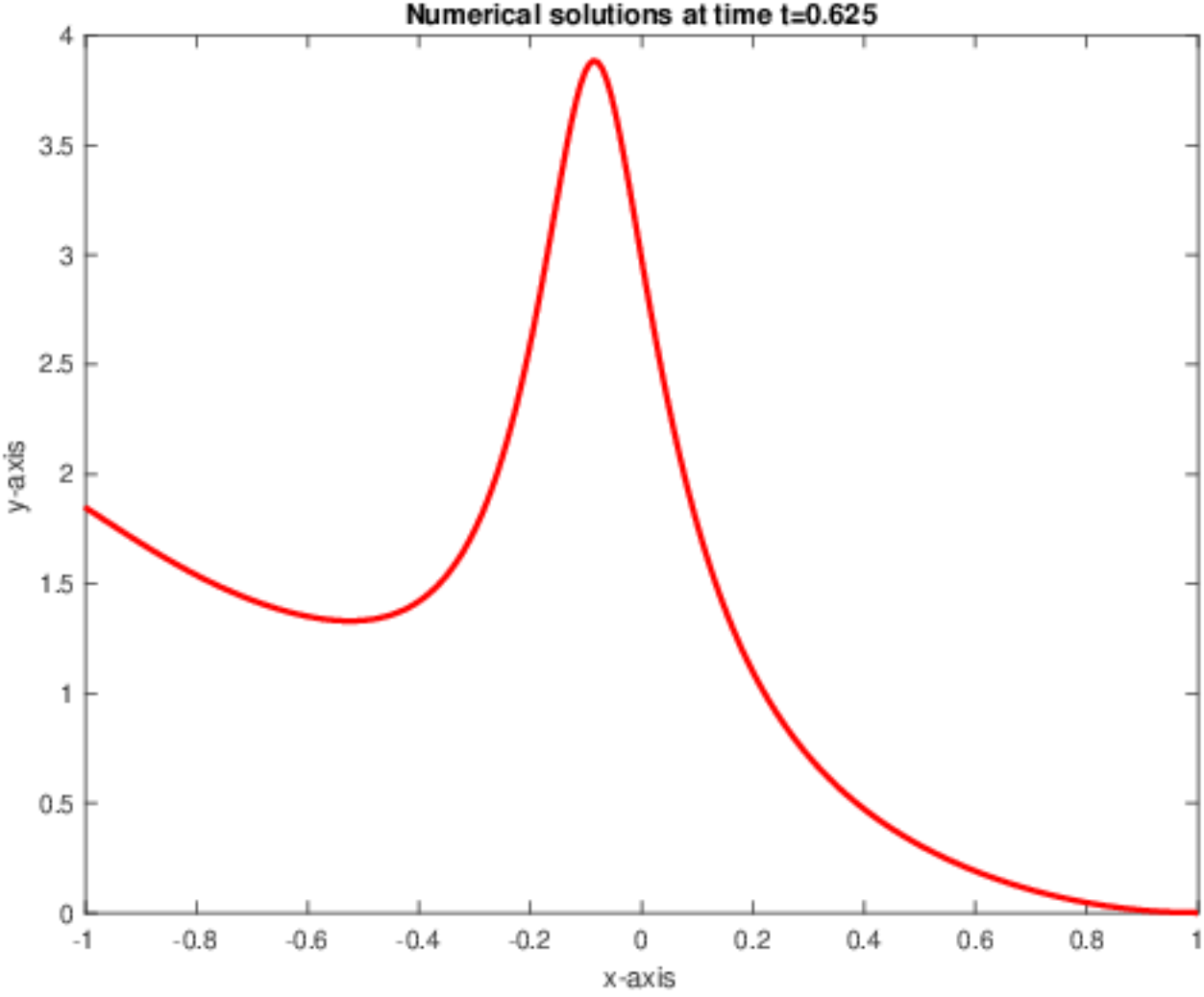

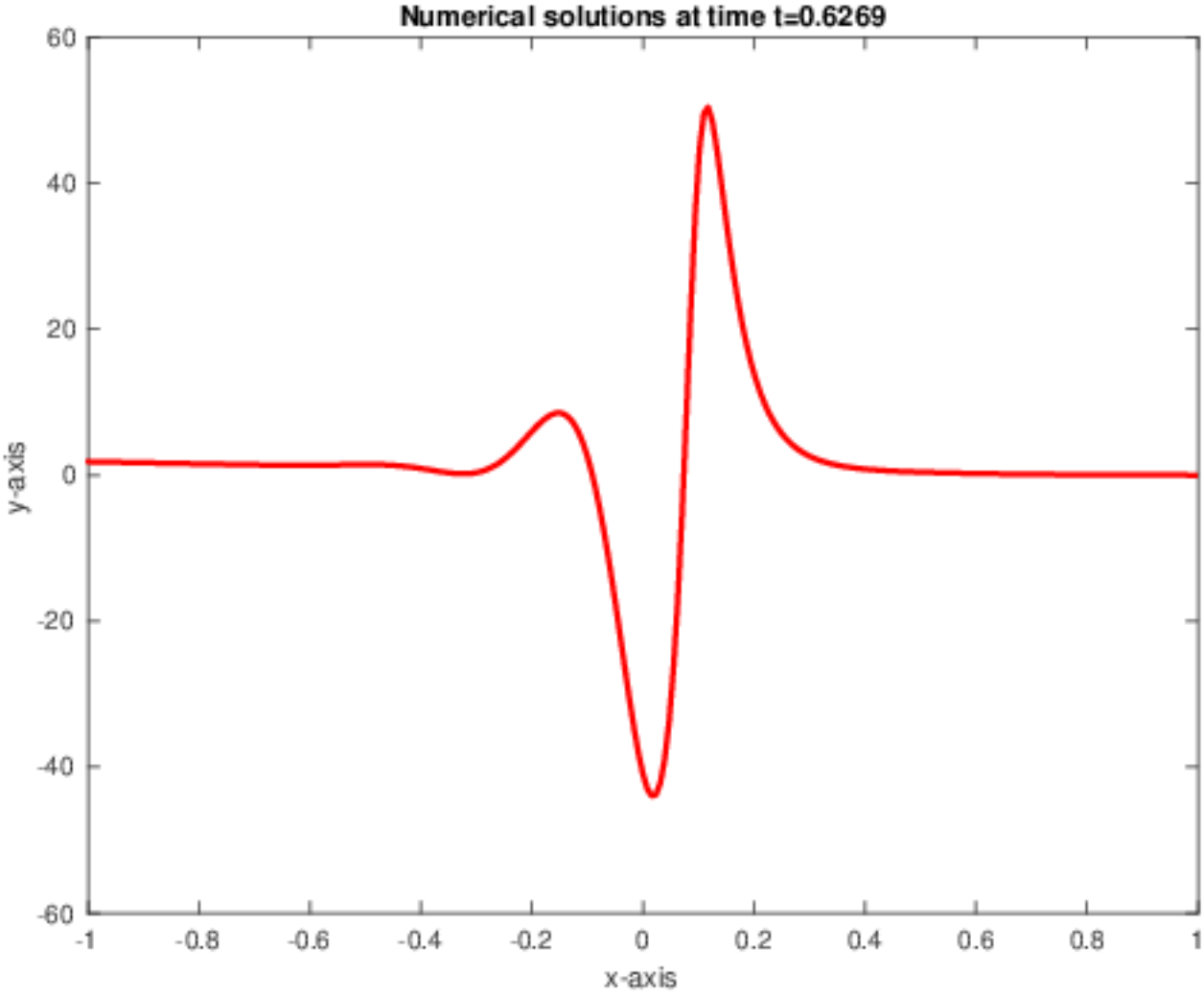

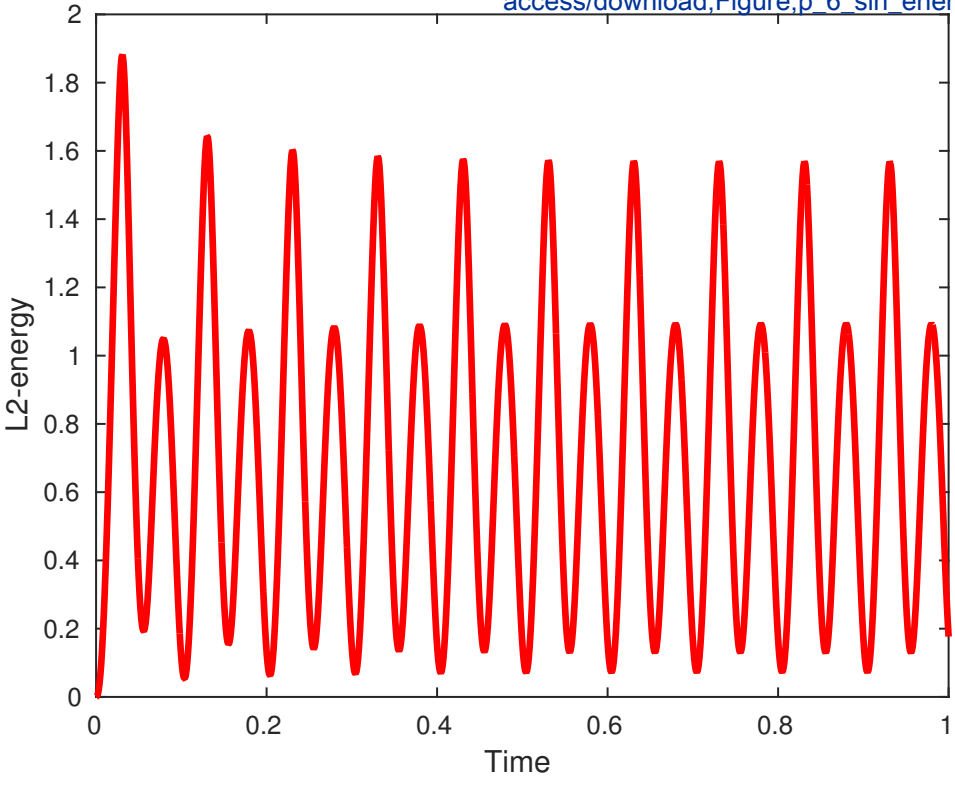

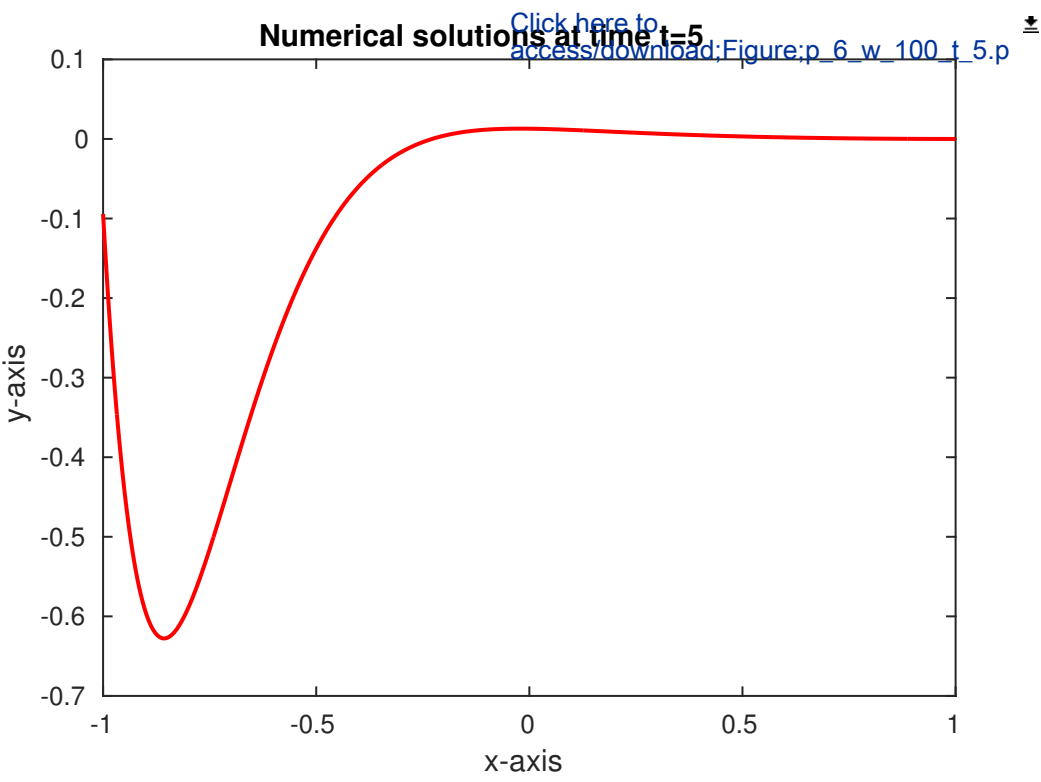
Numerical solutions at time t=5
Click here to access/download;Figure;p_6_w_100_t_5.p
0.1
0
-0.1
-0.2
-0.3
-0.4
-0.5
-0.6
-0.7
y-axis
-1
-0.5
0
0.5
1
x-axis

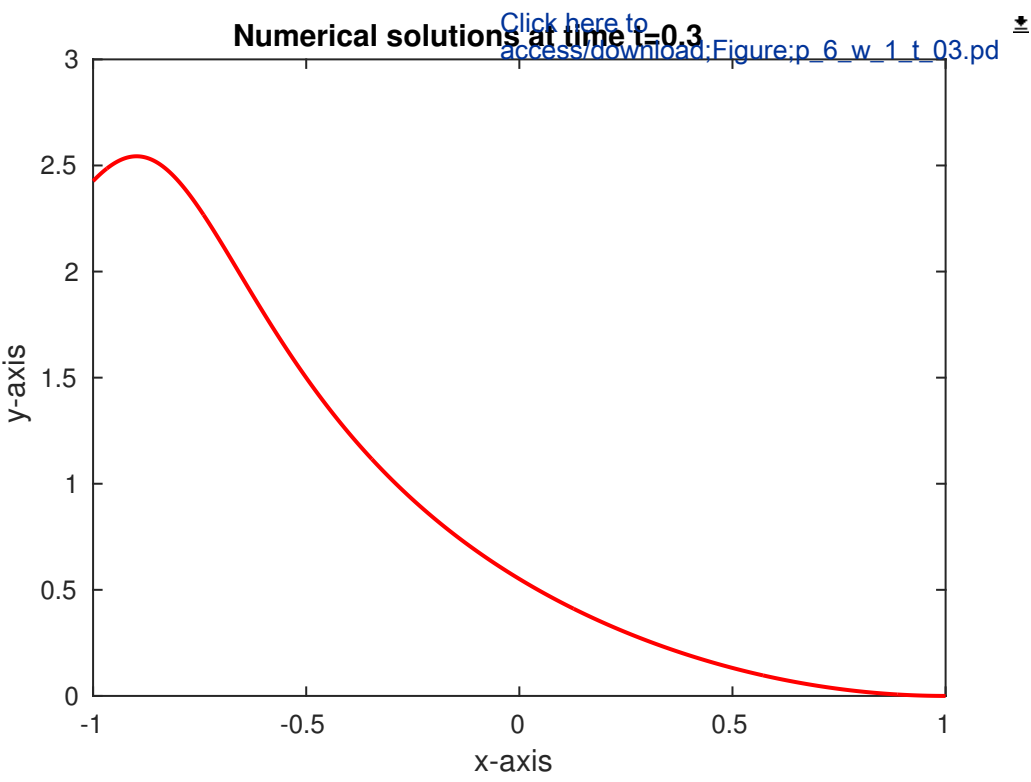
Numerical solutions at time t=0.3
Click here to access/download;Figure;p_6_w_1_t_03.pd
3
2.5
2
1.5
1
0.5
0
y-axis
-1
-0.5
0
0.5
1
x-axis

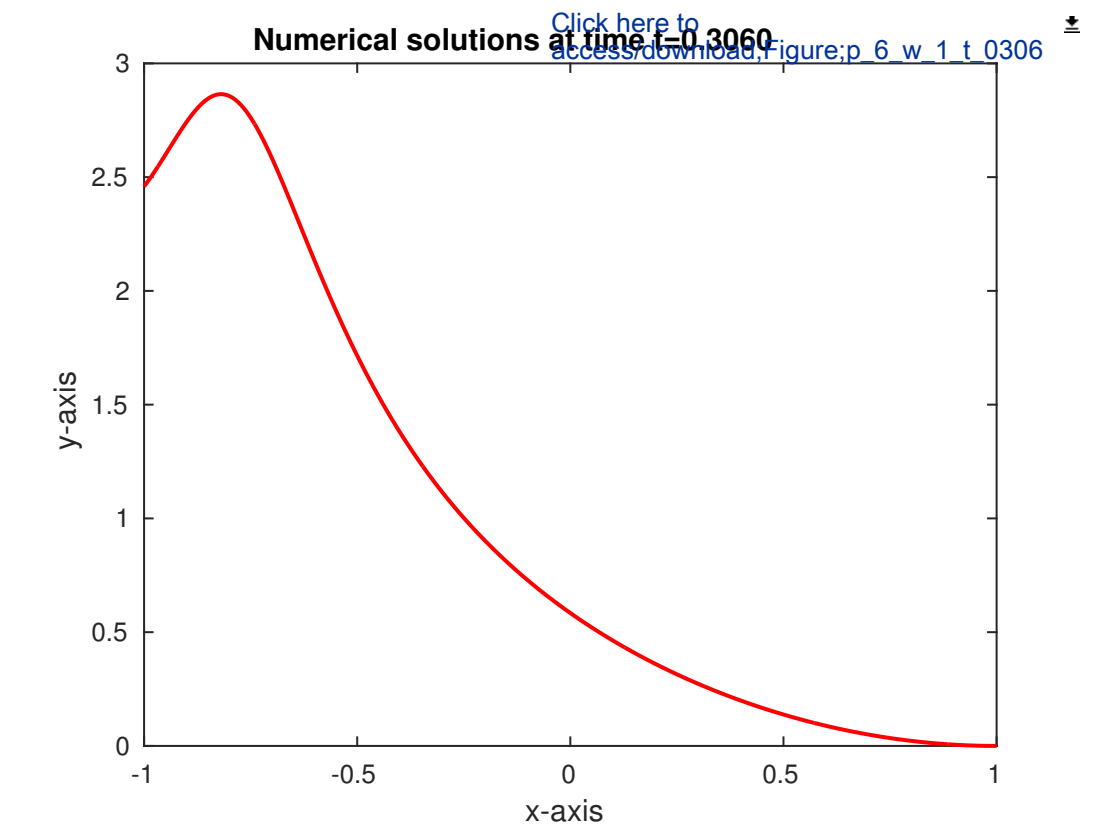
Numerical solutions at time t=0.3060
Click here to access/download;Figure;p_6_w_1_t_0306
y-axis
x-axis
3
2.5
2
1.5
1
0.5
0
-1
-0.5
0
0.5
1

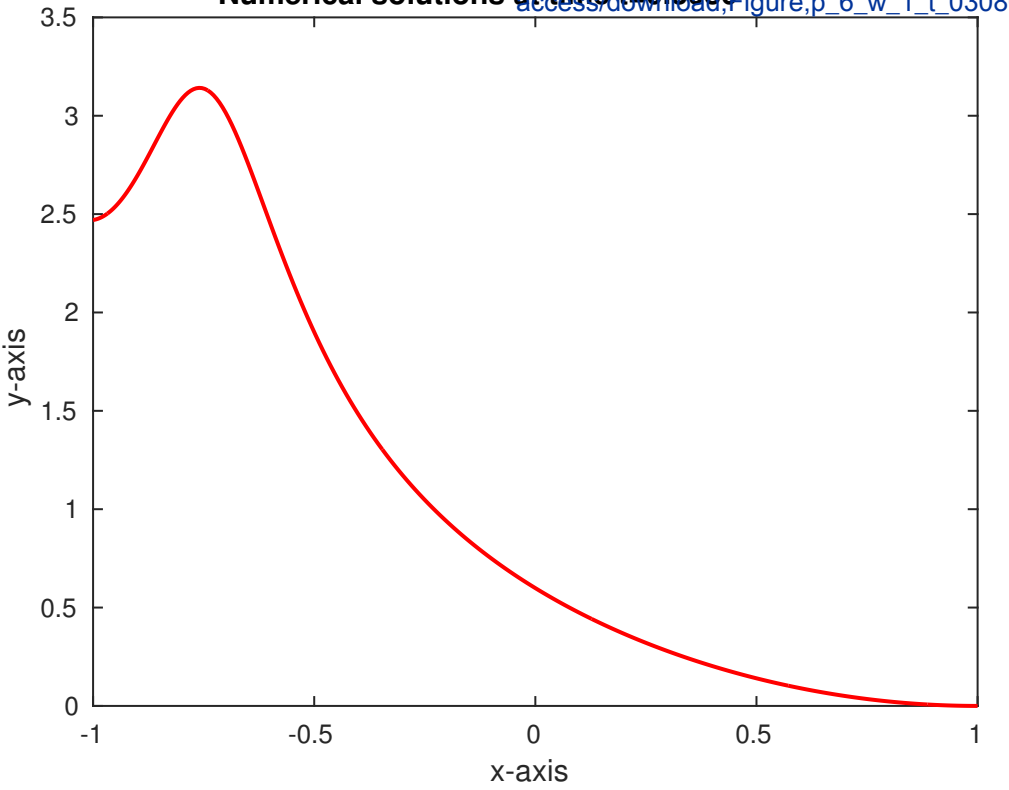

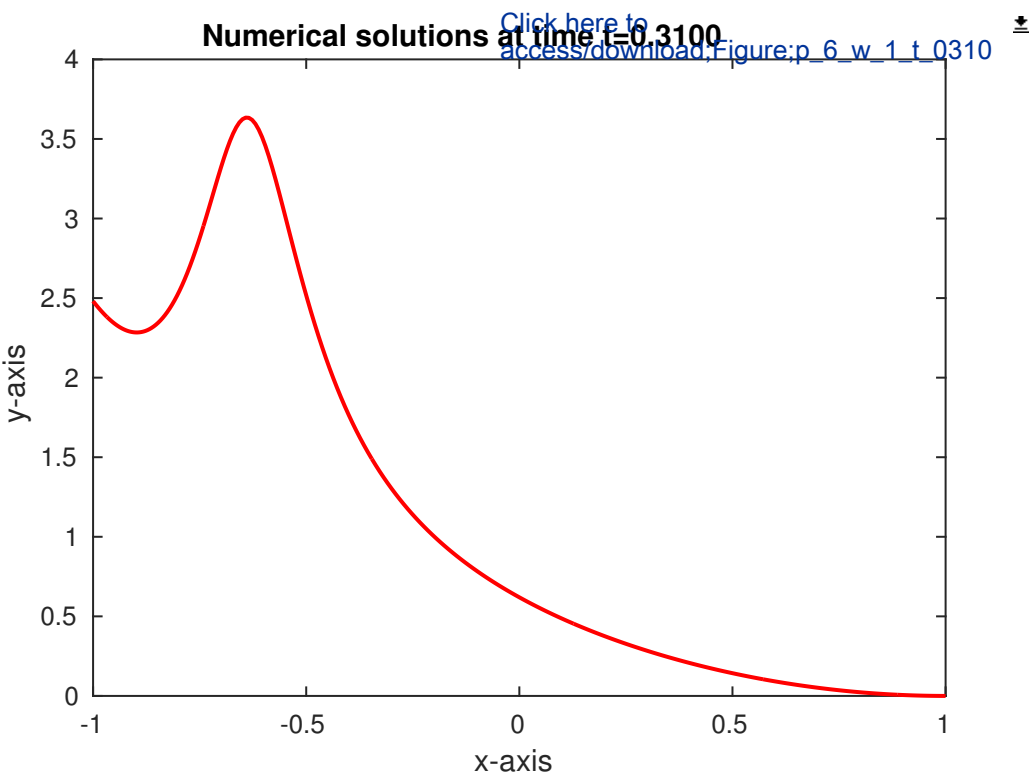
Numerical solutions at time t=0.3100
Click here to access/download;Figure;p_6_w_1_t_0310
y-axis
x-axis
4
3.5
3
2.5
2
1.5
1
0.5
0
-1
-0.5
0
0.5
1

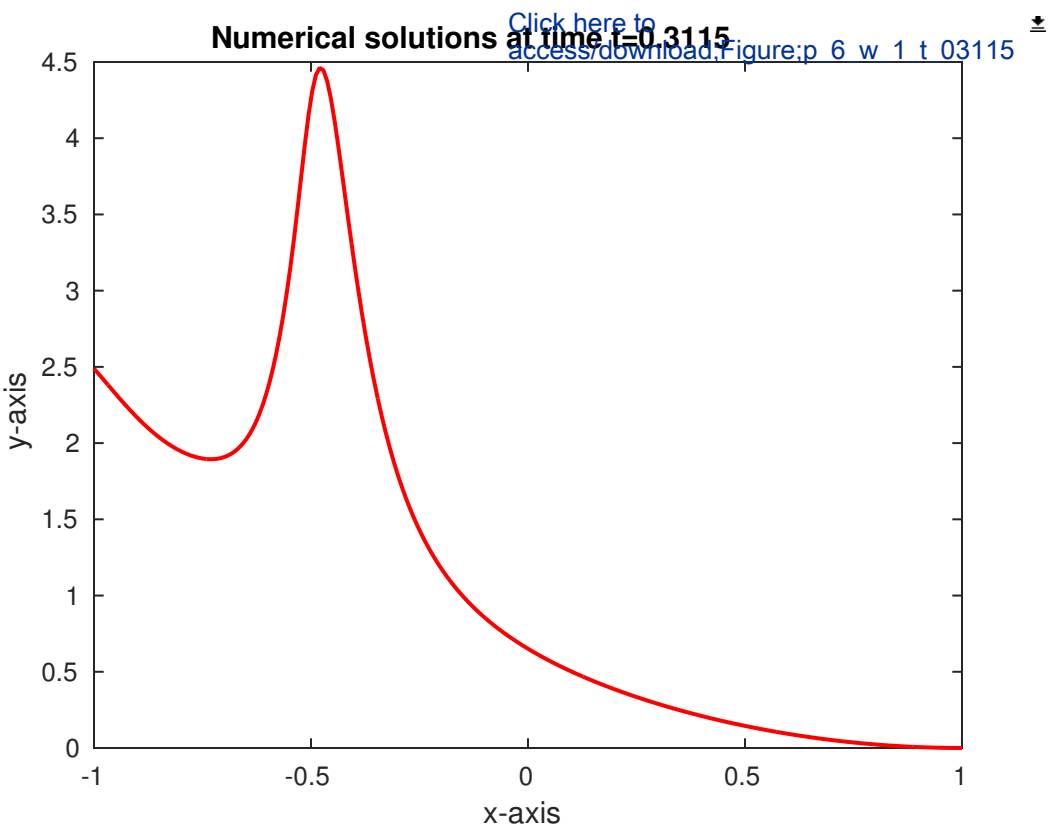
Numerical solutions at time t=0.3115
Click here to
access/download;Figure;p_6_w_1_t_03115
y-axis
x-axis
4.5
4
3.5
3
2.5
2
1.5
1
0.5
0
-1
-0.5
0
0.5
1

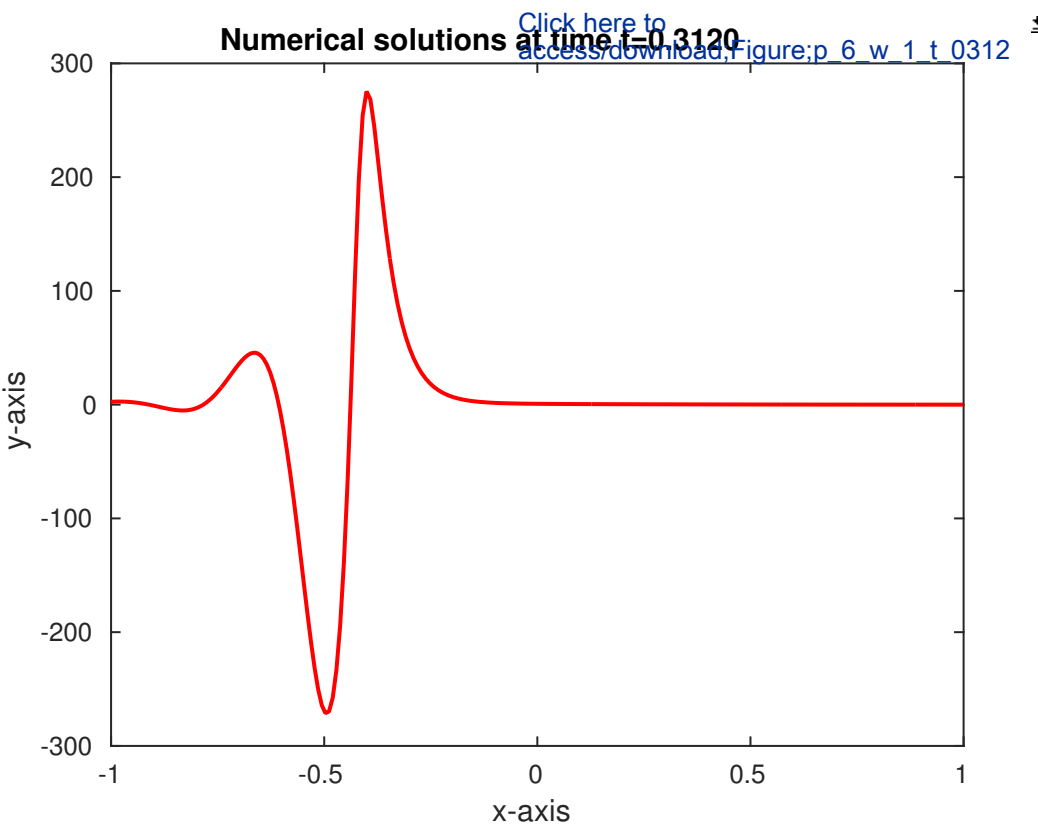
Numerical solutions at time t=0.3120
Click here to access/download;Figure;p_6_w_1_t_0312
300
200
100
0
-100
-200
-300
y-axis
-1
-0.5
0
0.5
1
x-axis

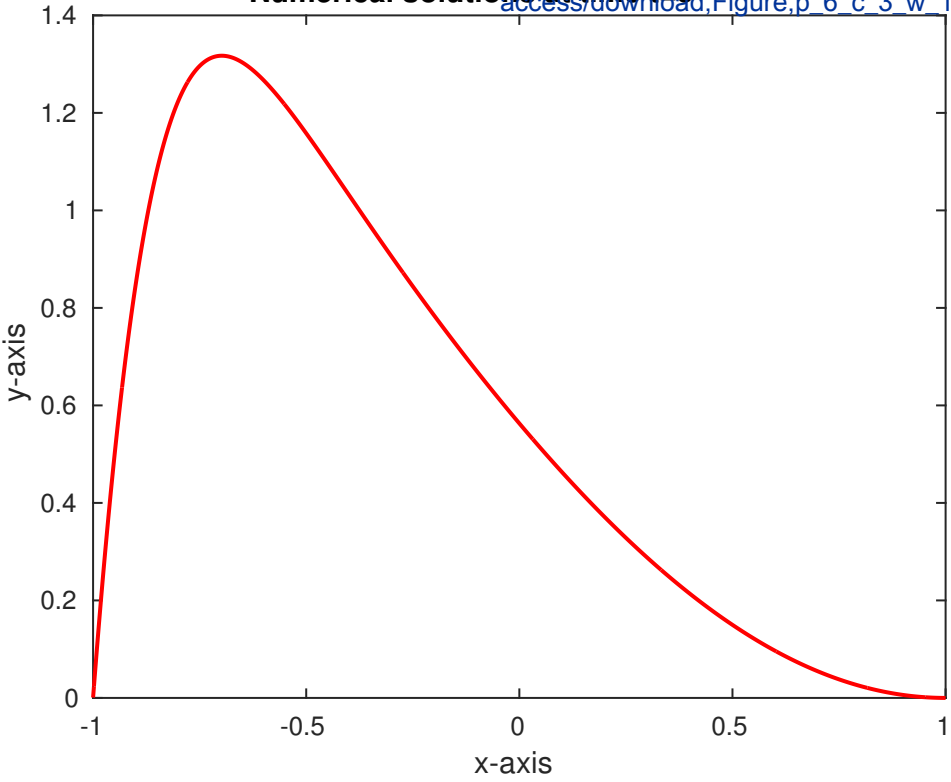

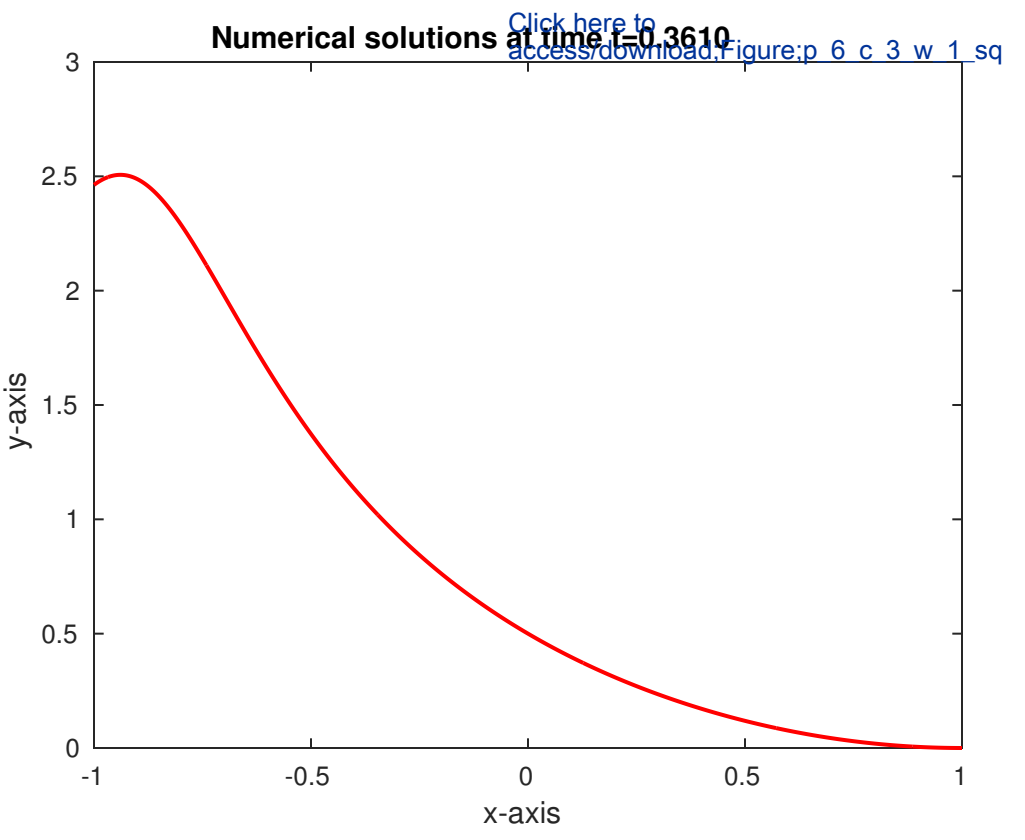
Click here to
access/download;Figure;p_6_c_3_w_1_sq
Numerical solutions at time t=0.3610
3
2.5
2
1.5
1
0.5
0
y-axis
-1
-0.5
0
0.5
1
x-axis

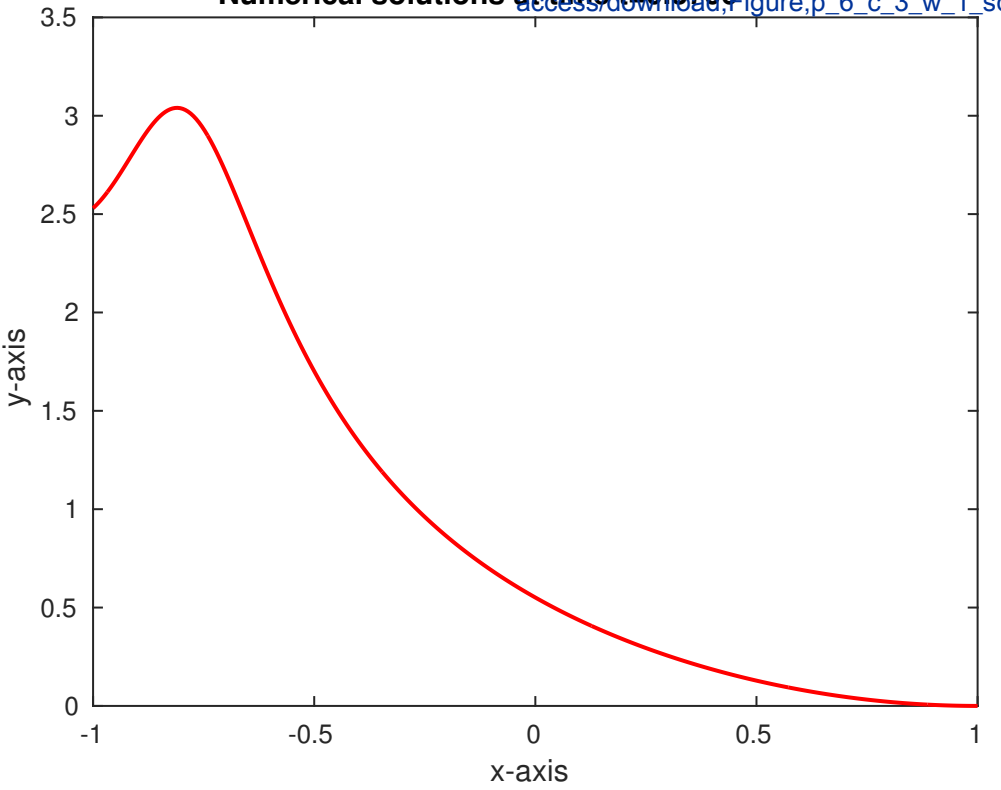

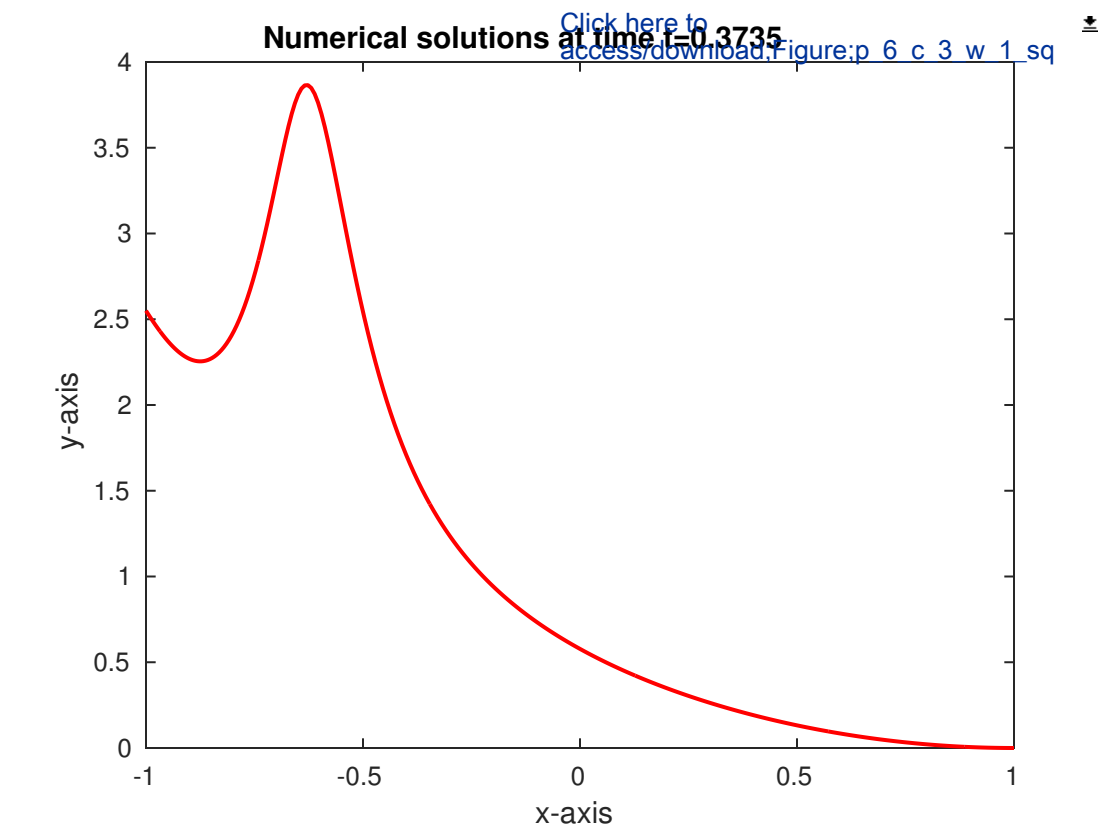
Numerical solutions at time t=0.3735
Click here to access/download;Figure;p_6_c_3_w_1_sq
y-axis
x-axis
4
3.5
3
2.5
2
1.5
1
0.5
0
-1
-0.5
0
0.5
1

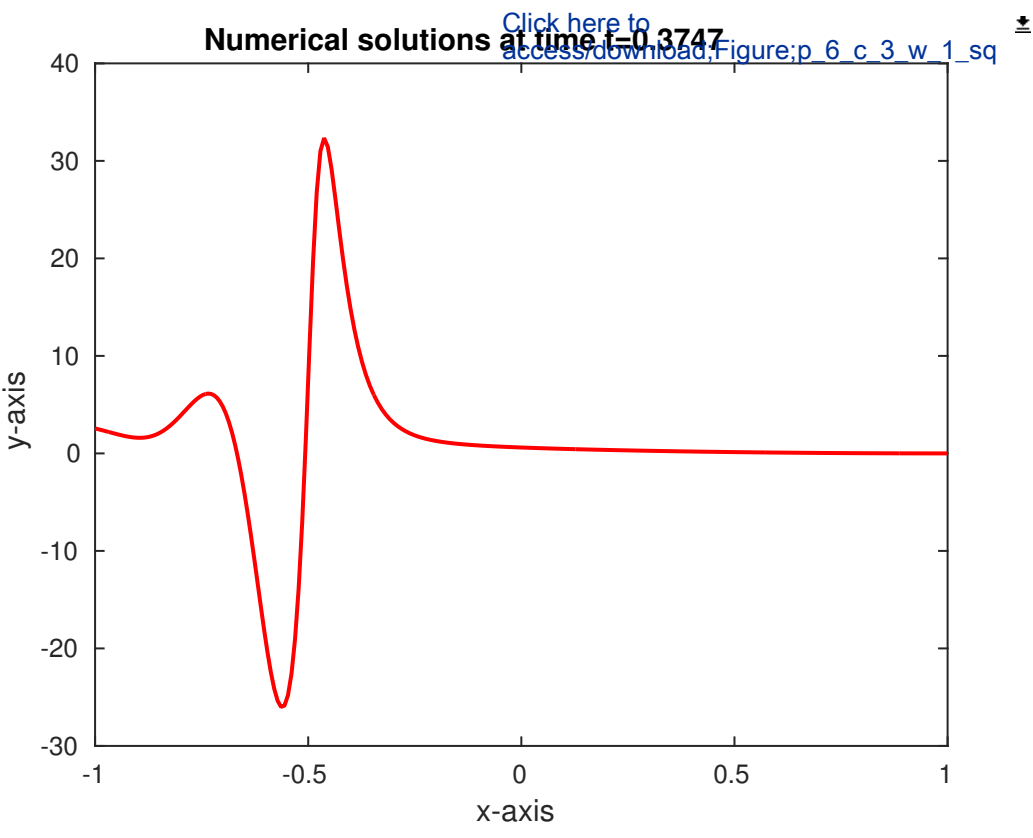
Numerical solutions at time t=0.3747
Click here to access/download;Figure;p_6_c_3_w_1_sq
40
30
20
10
0
-10
-20
-30
-1
-0.5
0
0.5
1
y-axis
x-axis

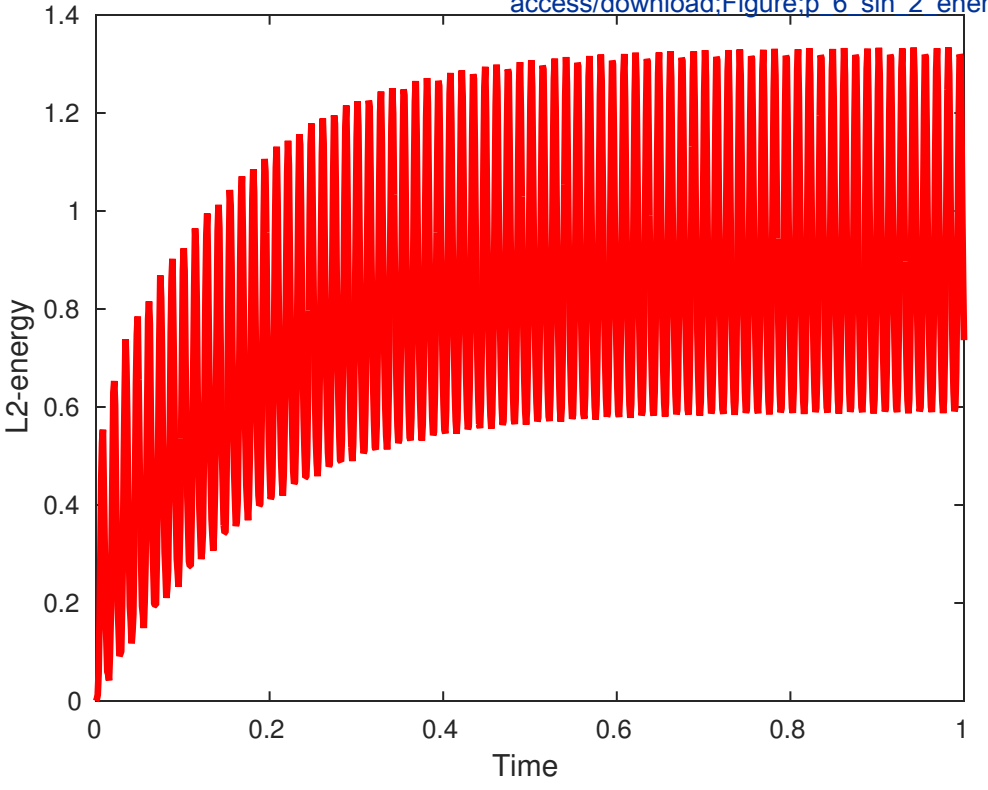

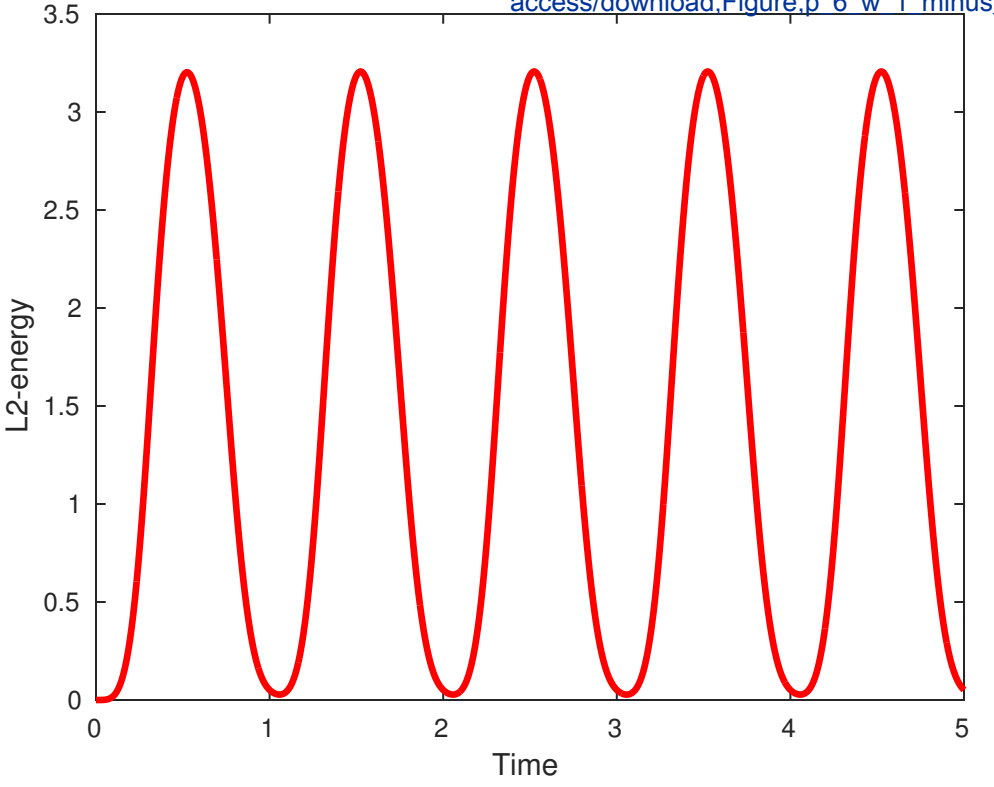

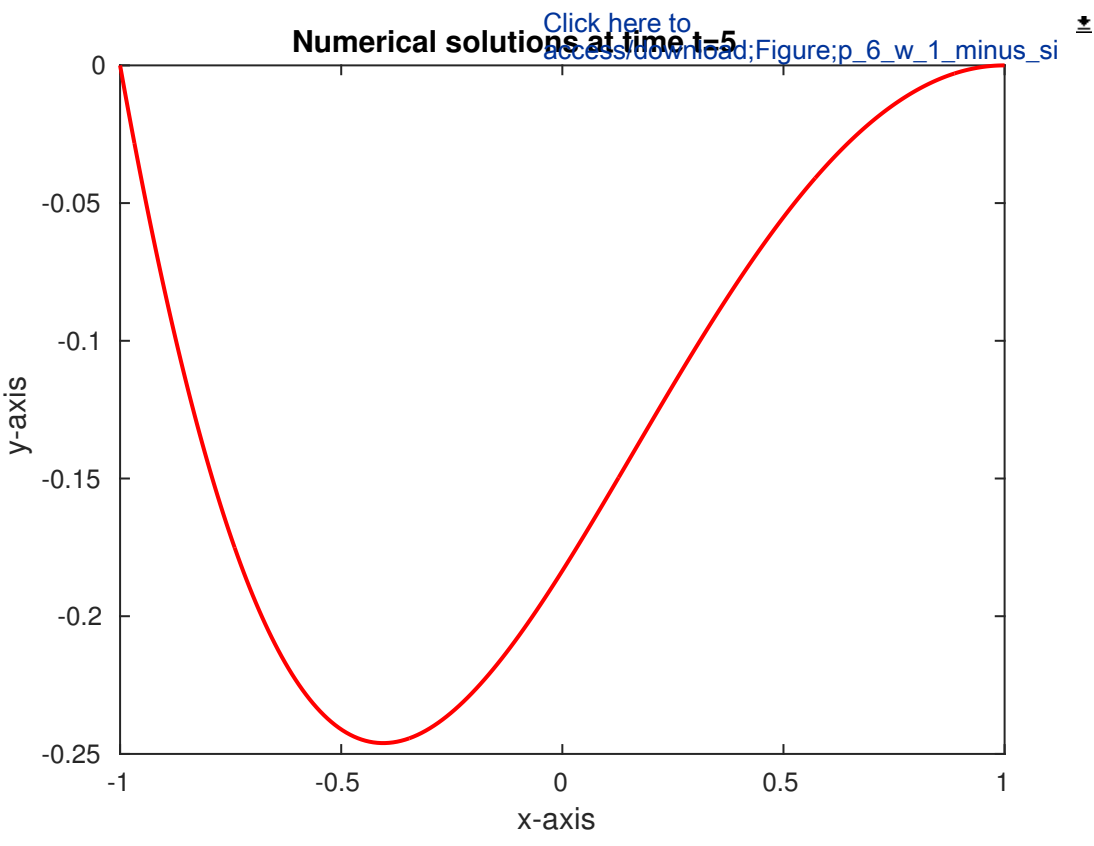
Click here to access/download;Figure;p_6_w_1_minus_si
Numerical solutions at time t=5
0
-0.05
-0.1
-0.15
-0.2
-0.25
y-axis
-1
-0.5
0
0.5
1
x-axis

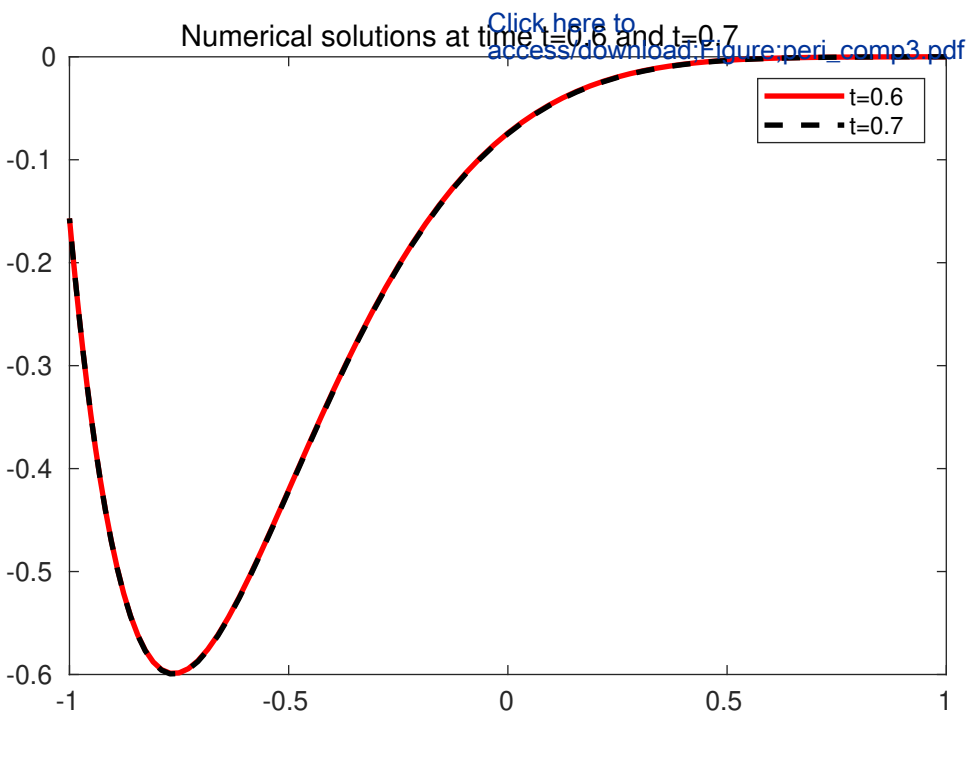
Numerical solutions at time t=0.6 and t=0.7
Click here to access/download:Figure:peri_comp3.pdf
t=0.6
t=0.7
0
-0.1
-0.2
-0.3
-0.4
-0.5
-0.6
-1
-0.5
0
0.5
1

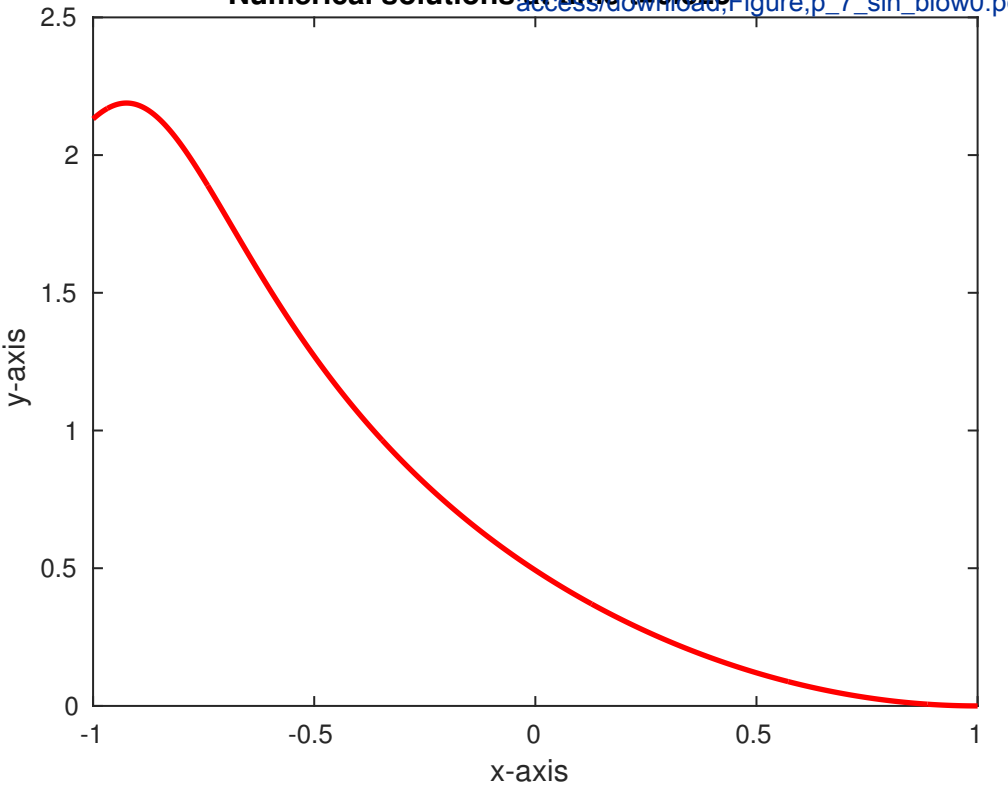

Click here to
access/download/Figure;p_7_sin_blow1.pdf

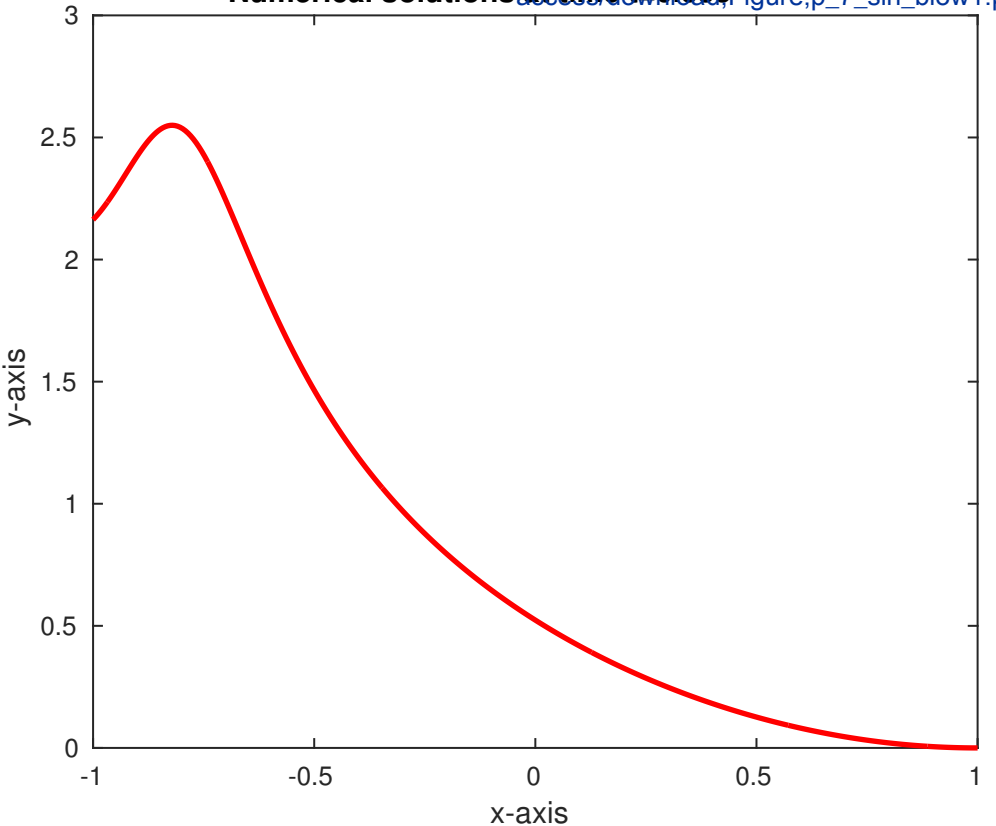

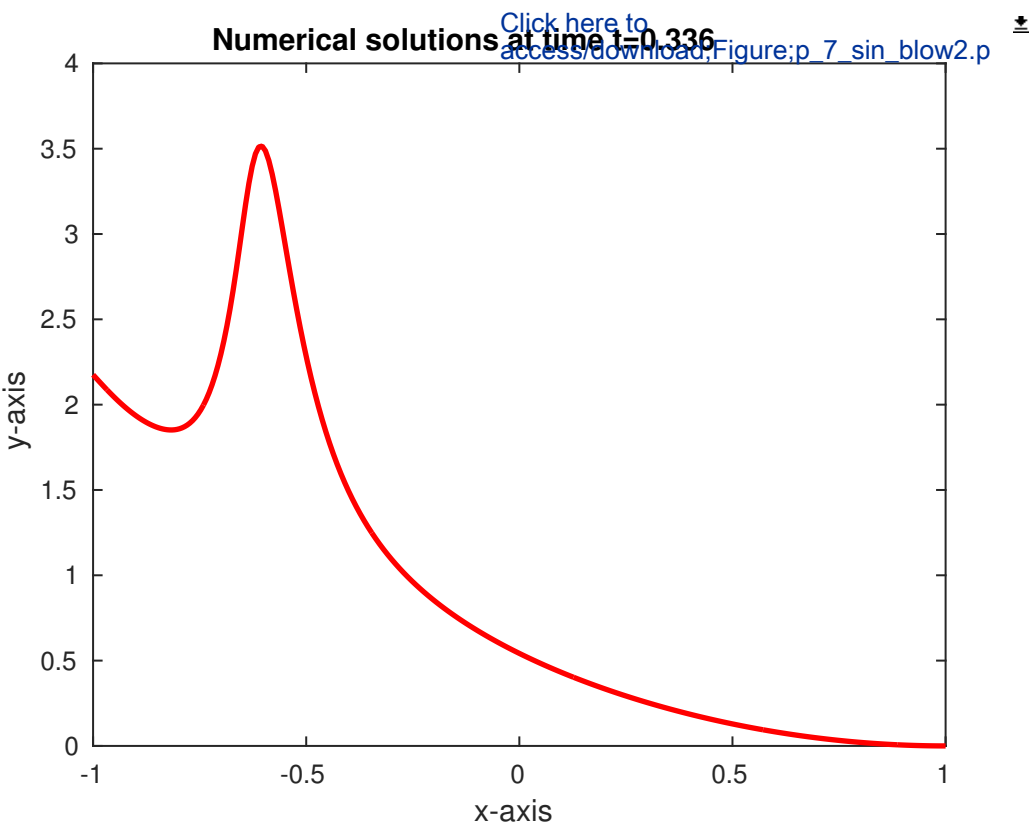
Numerical solutions at time t=0.336
Click here to
access/download;Figure;p_7_sin_blow2.p
y-axis
x-axis
4
3.5
3
2.5
2
1.5
1
0.5
0
-1
-0.5
0
0.5
1

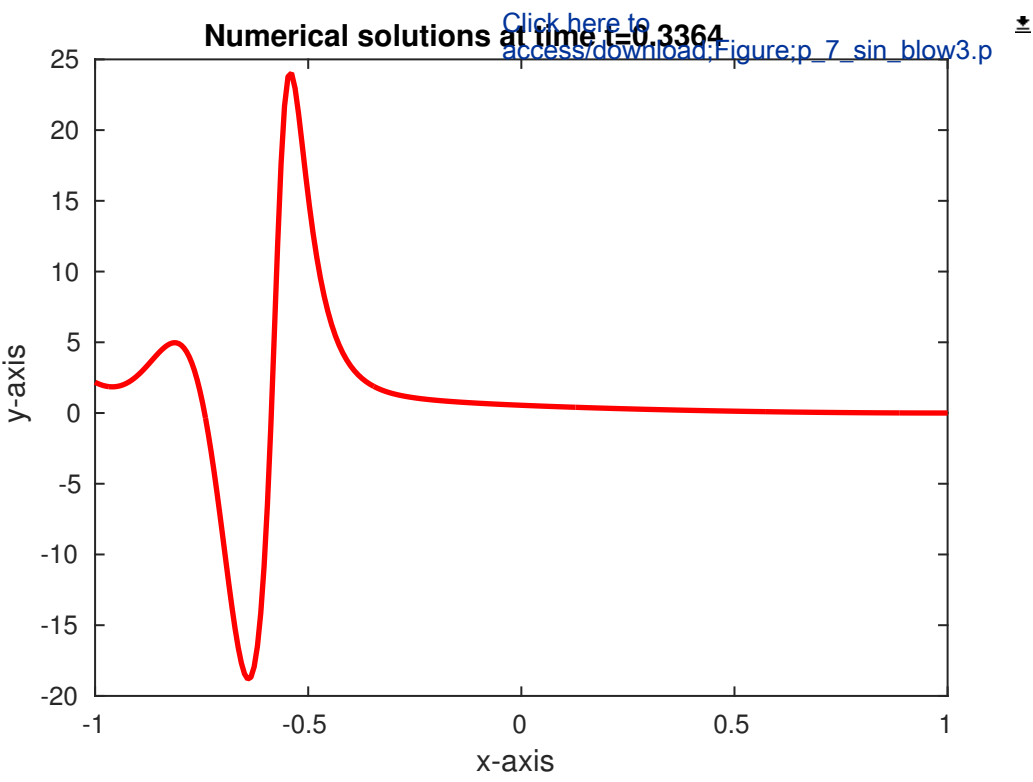
Numerical solutions at time t=0.3364
Click here to access/download;Figure;p_7_sin_blow3.p
25
20
15
10
5
0
-5
-10
-15
-20
y-axis
-1
-0.5
0
0.5
1
x-axis

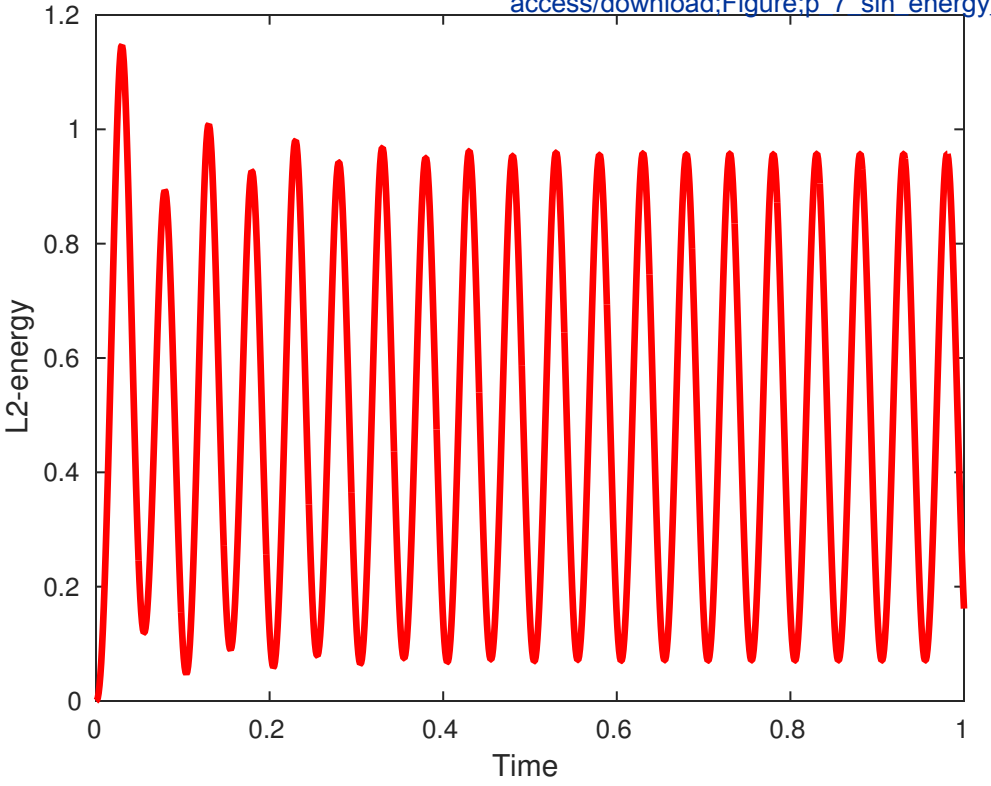

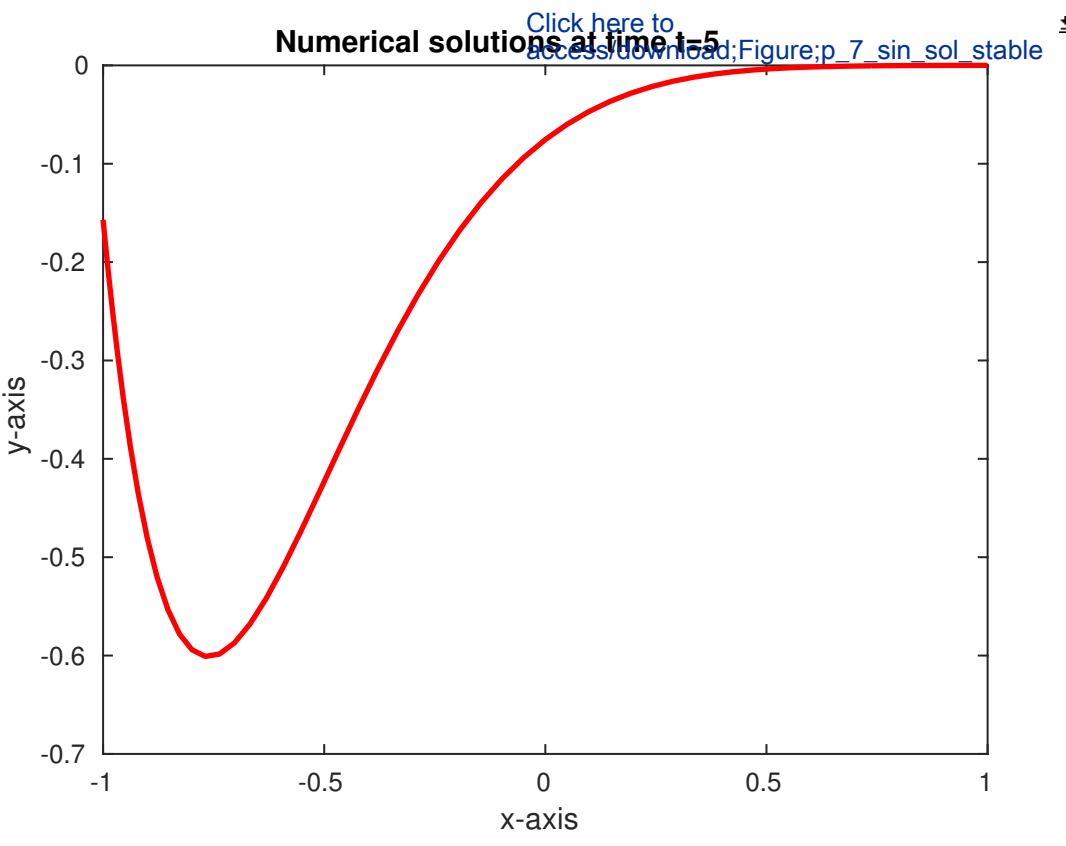
Click here to access/download;Figure;p_7_sin_sol_stable
Numerical solutions at time t=5
0
-0.1
-0.2
-0.3
-0.4
-0.5
-0.6
-0.7
y-axis
-1
-0.5
0
0.5
1
x-axis

Click here to
access/download/Figure/compare_transition02.pdf

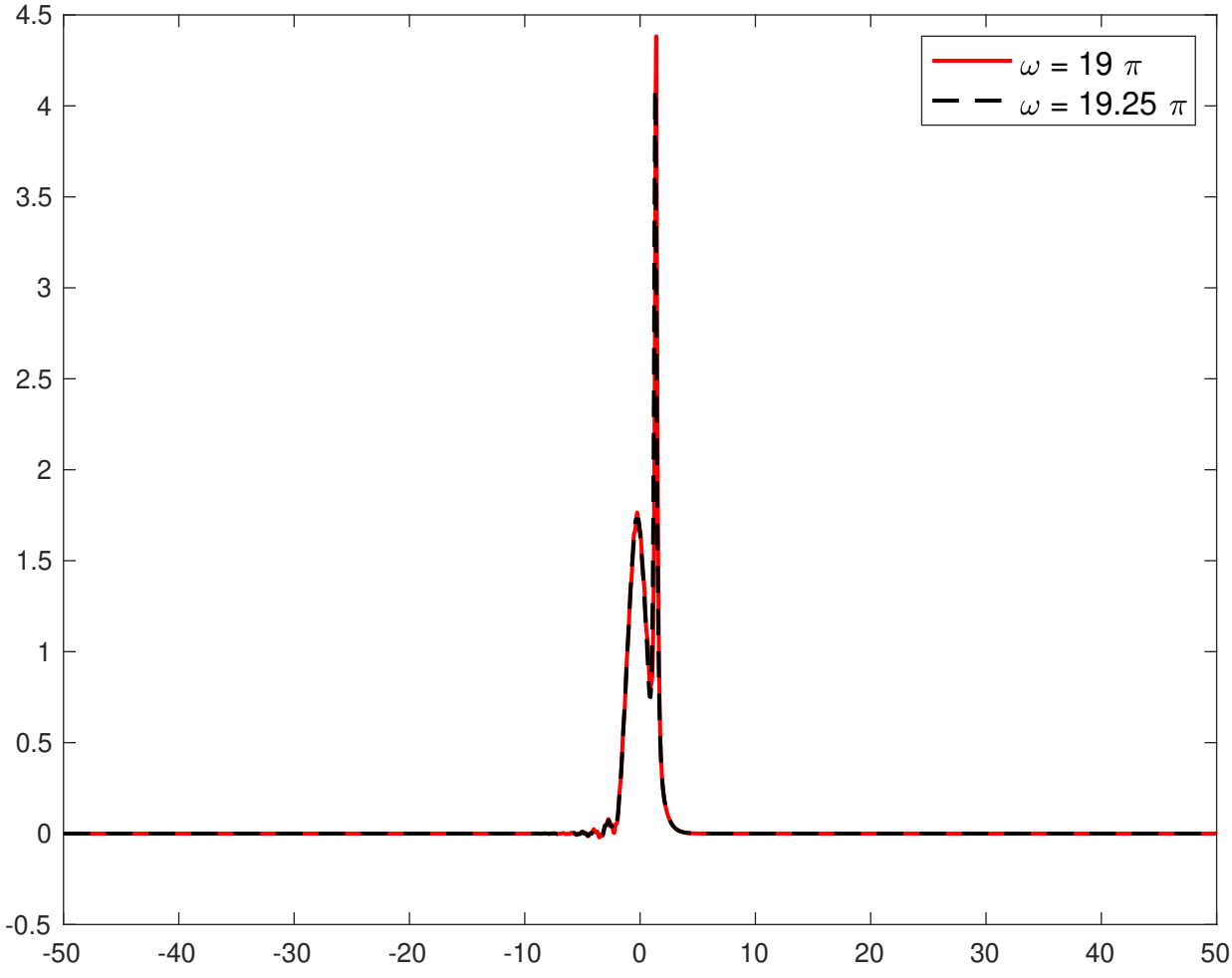

Click here to
access/download/Figure/compare_transition03.pdf

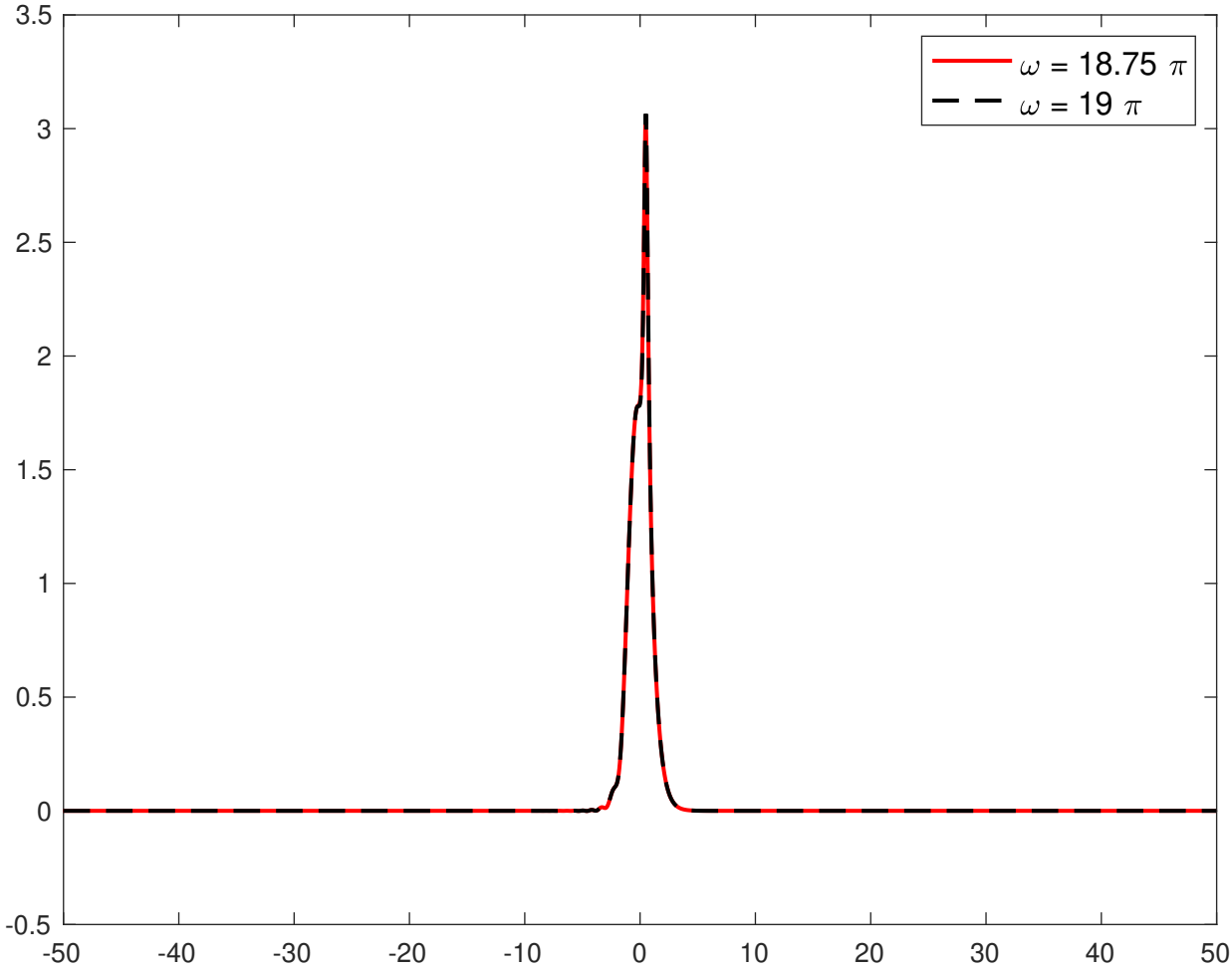

Click here to
access/download Figure compare_transition04.pdf

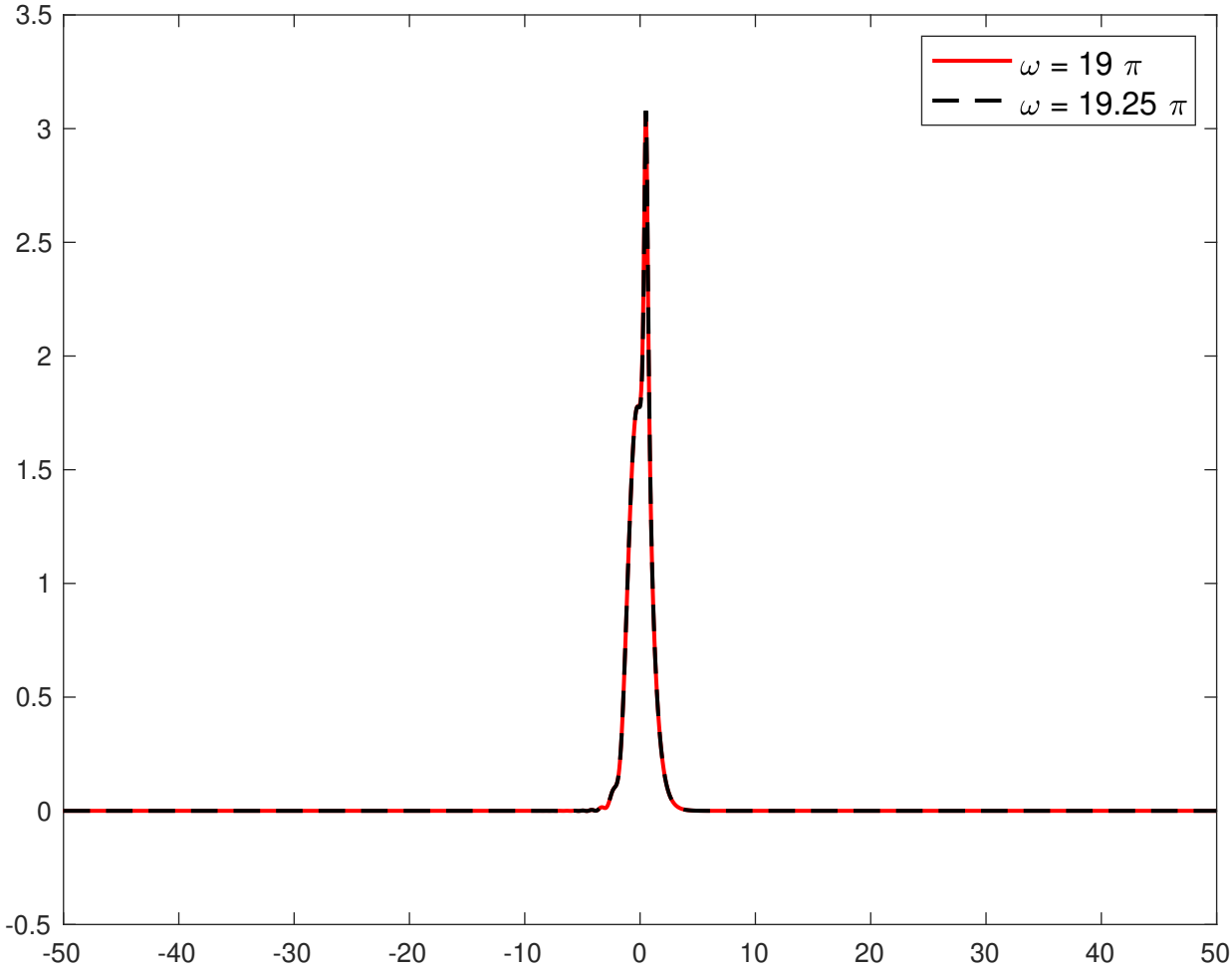

Click here to
access/download Figure compare_transition05.pdf

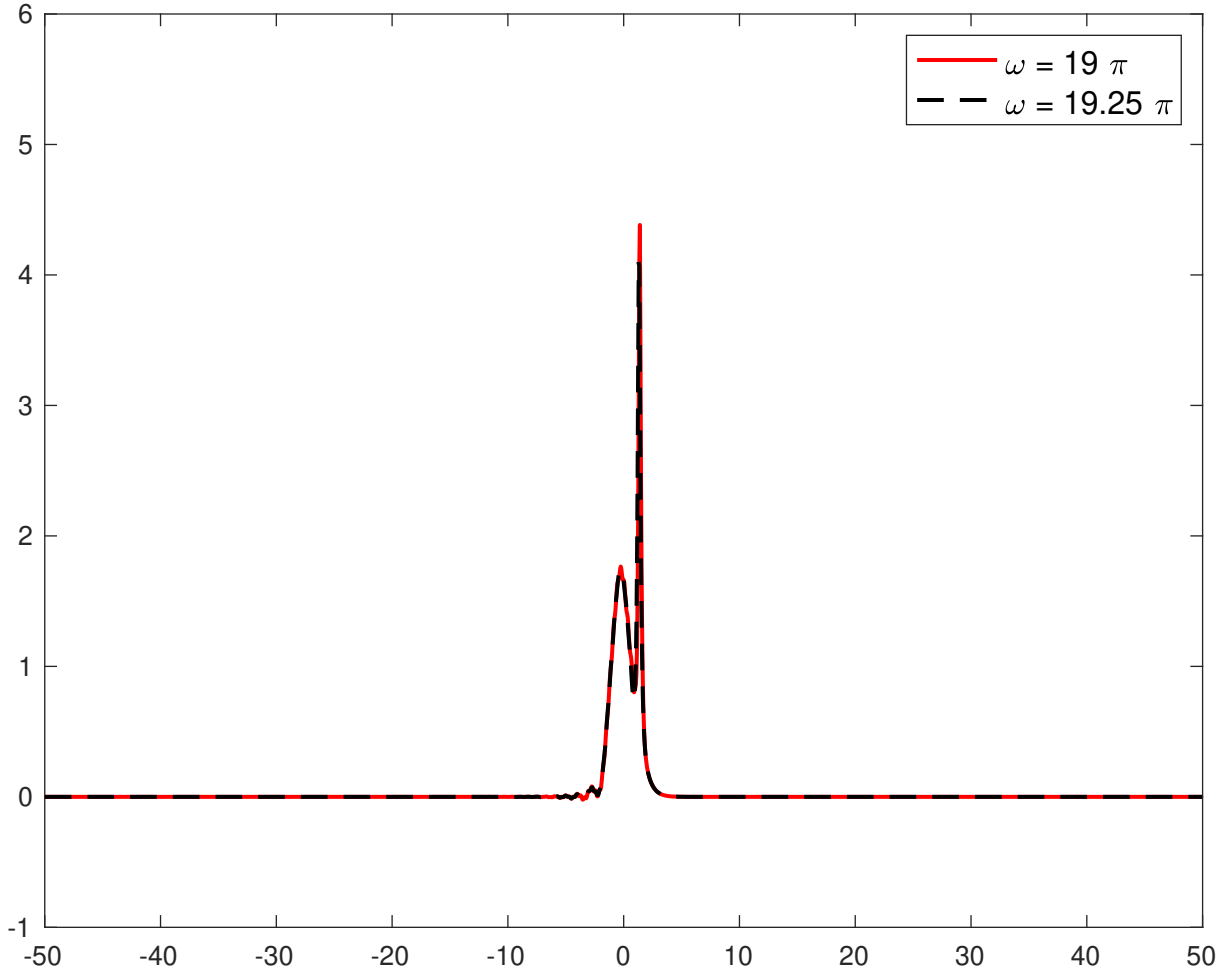

Click here to access/download Figure;blowup_compare_003.pdf

Numerical solutions at time t=0.03

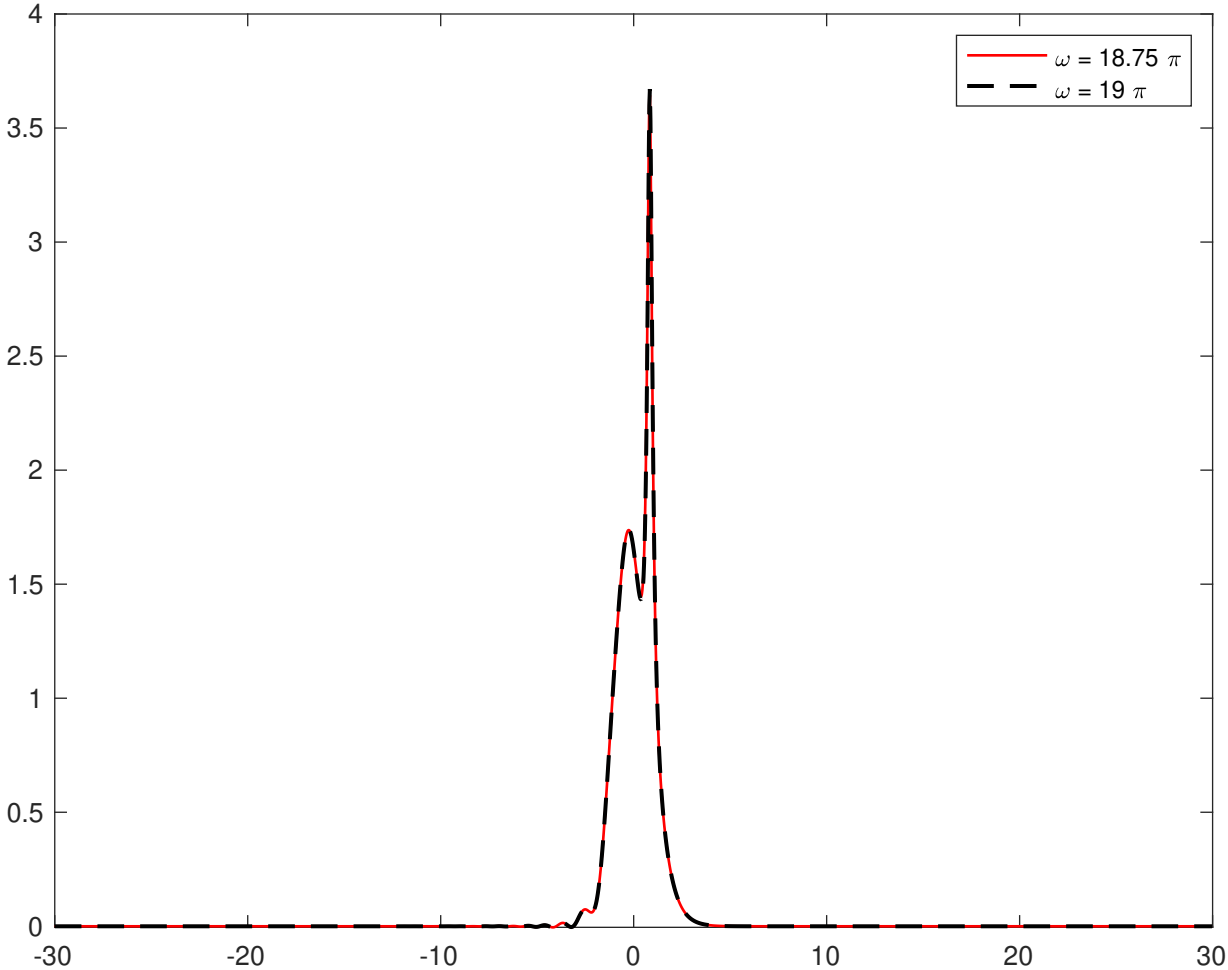

Click here to access/download Figure;blowup_compare_004.pdf

Numerical solutions at time t=0.04

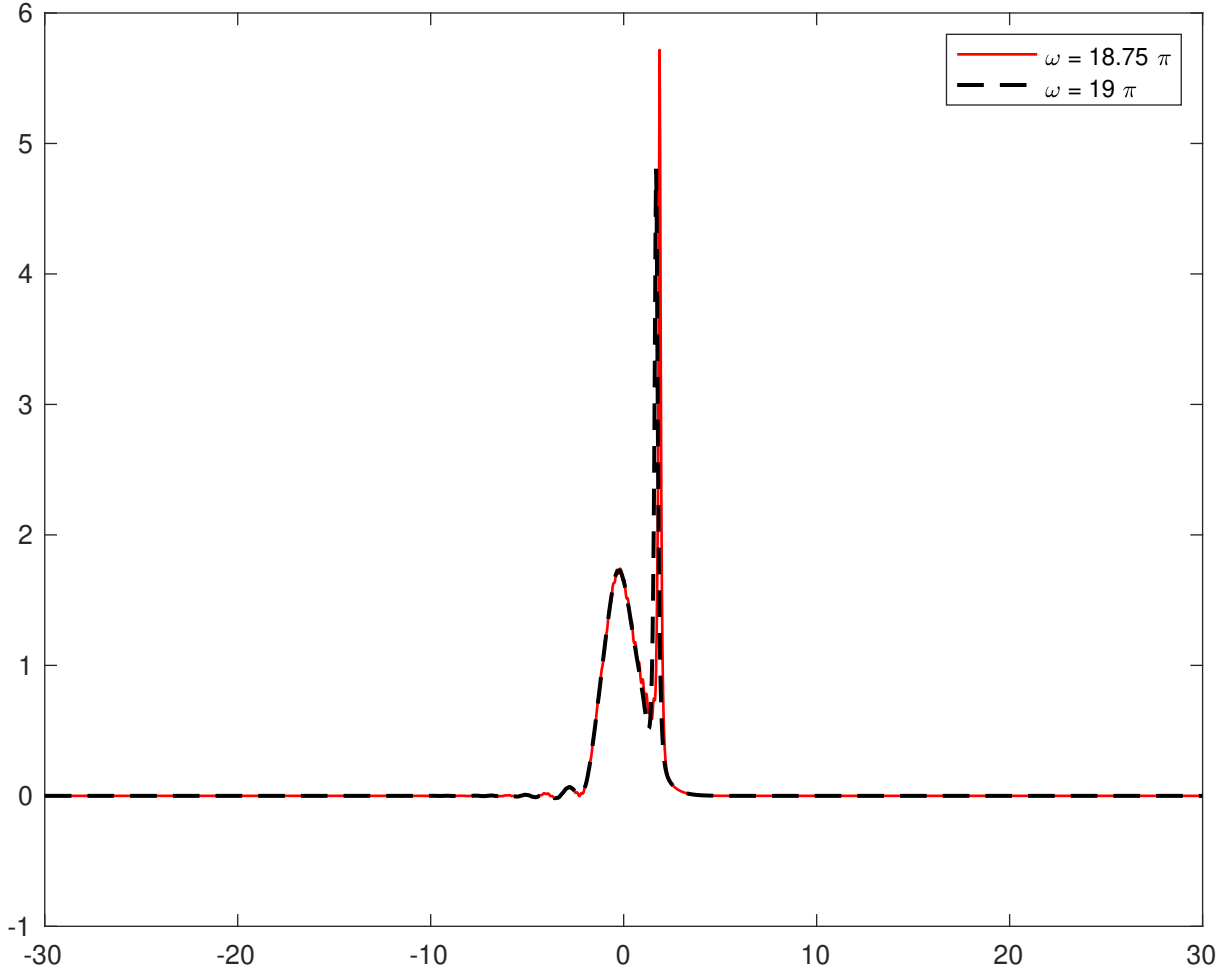

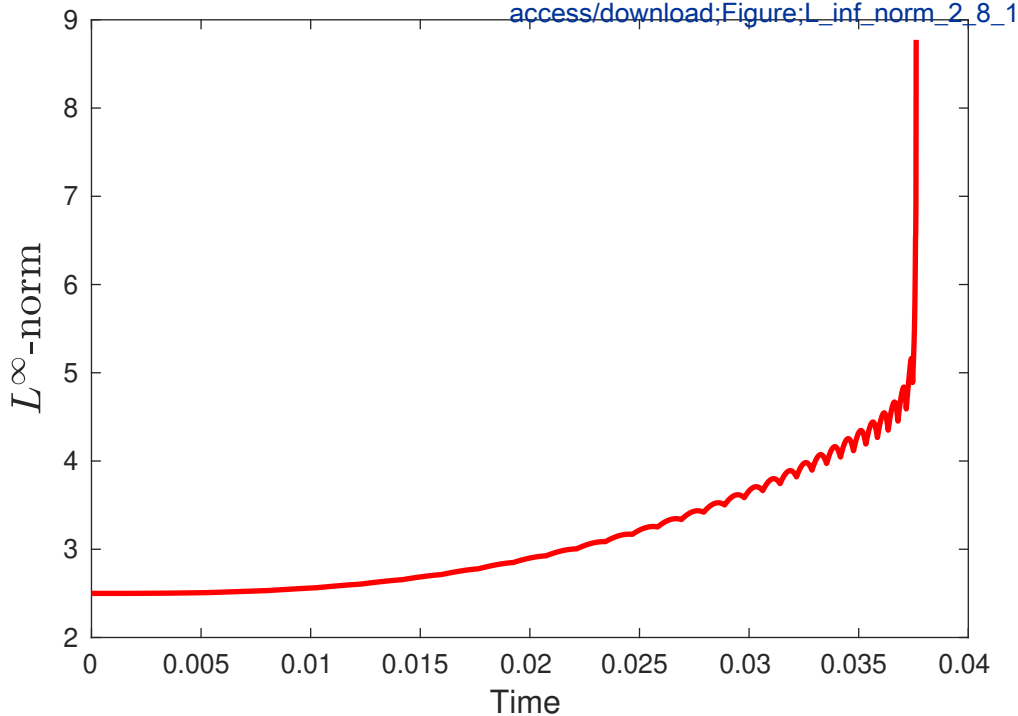

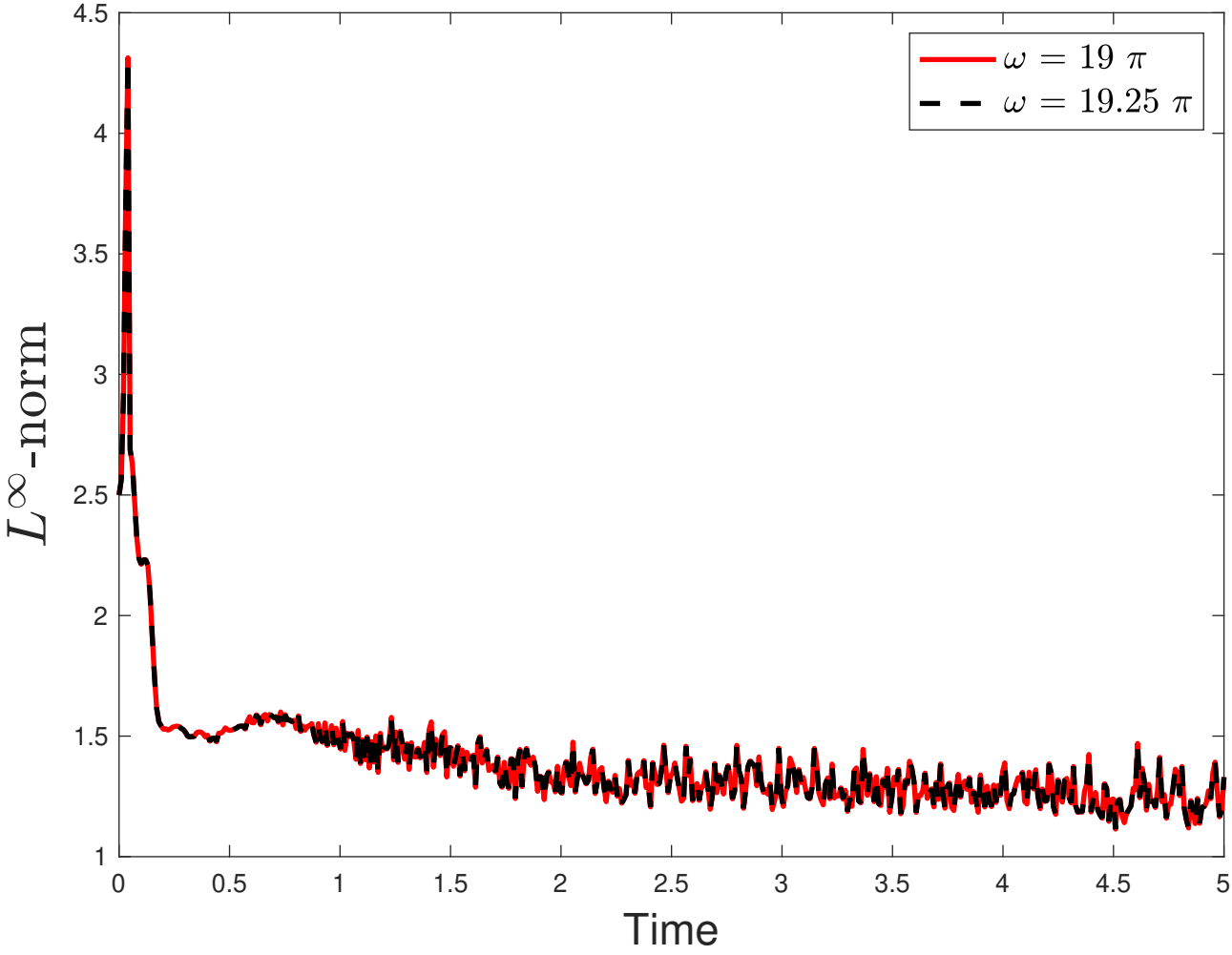

Numerical solutions at time t=0.0403

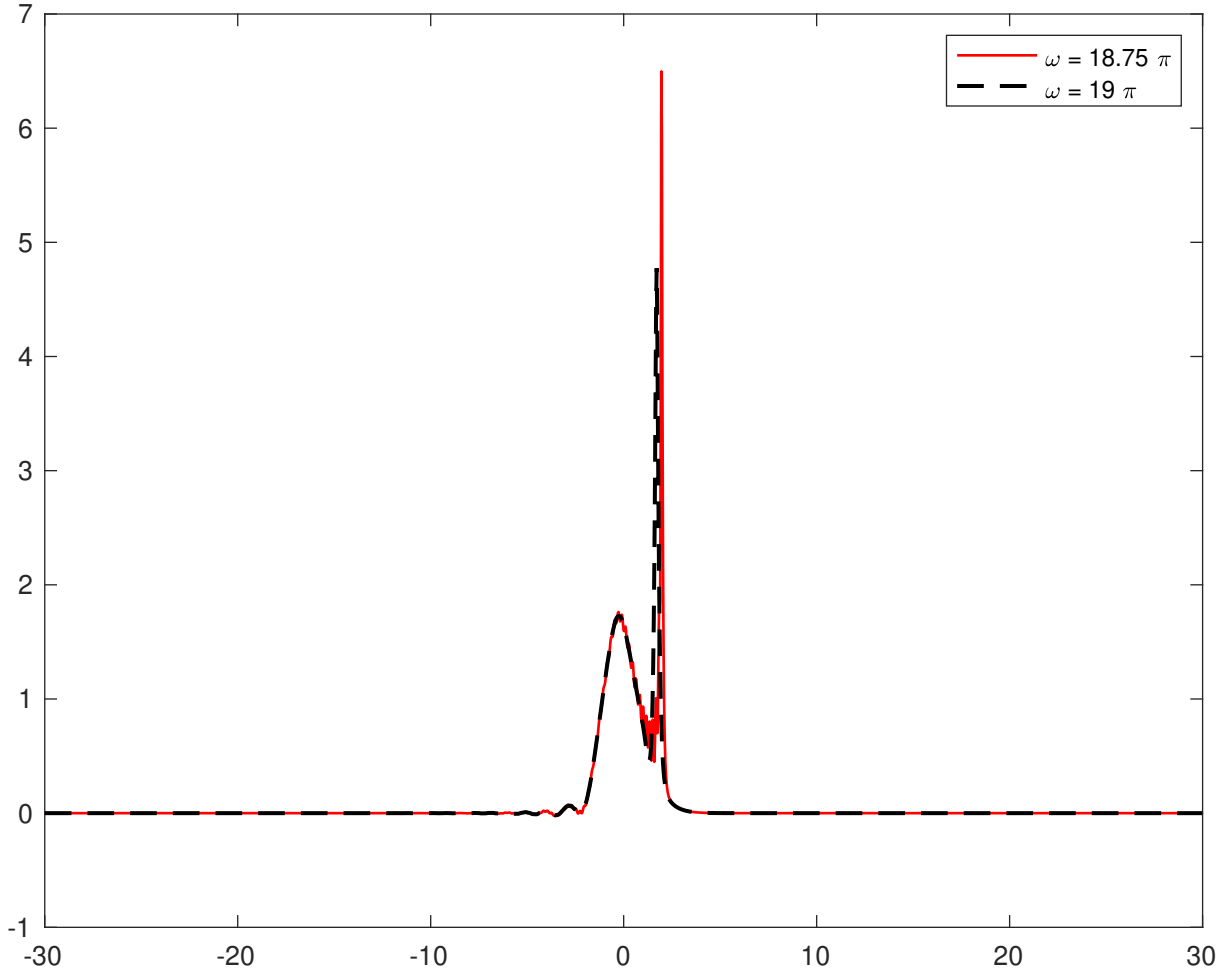

Click here to
access/download pdf file: compare_transition01.pdf

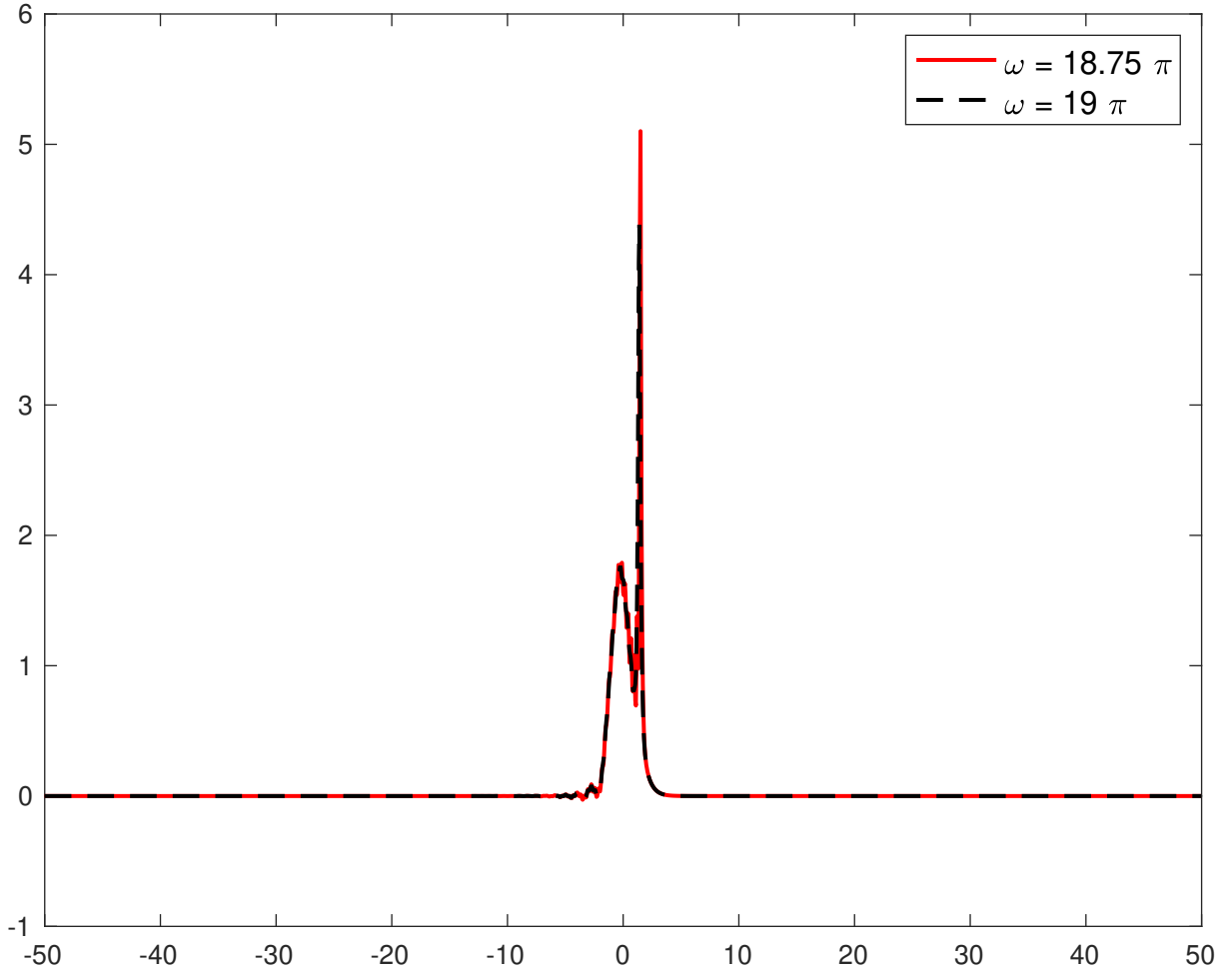

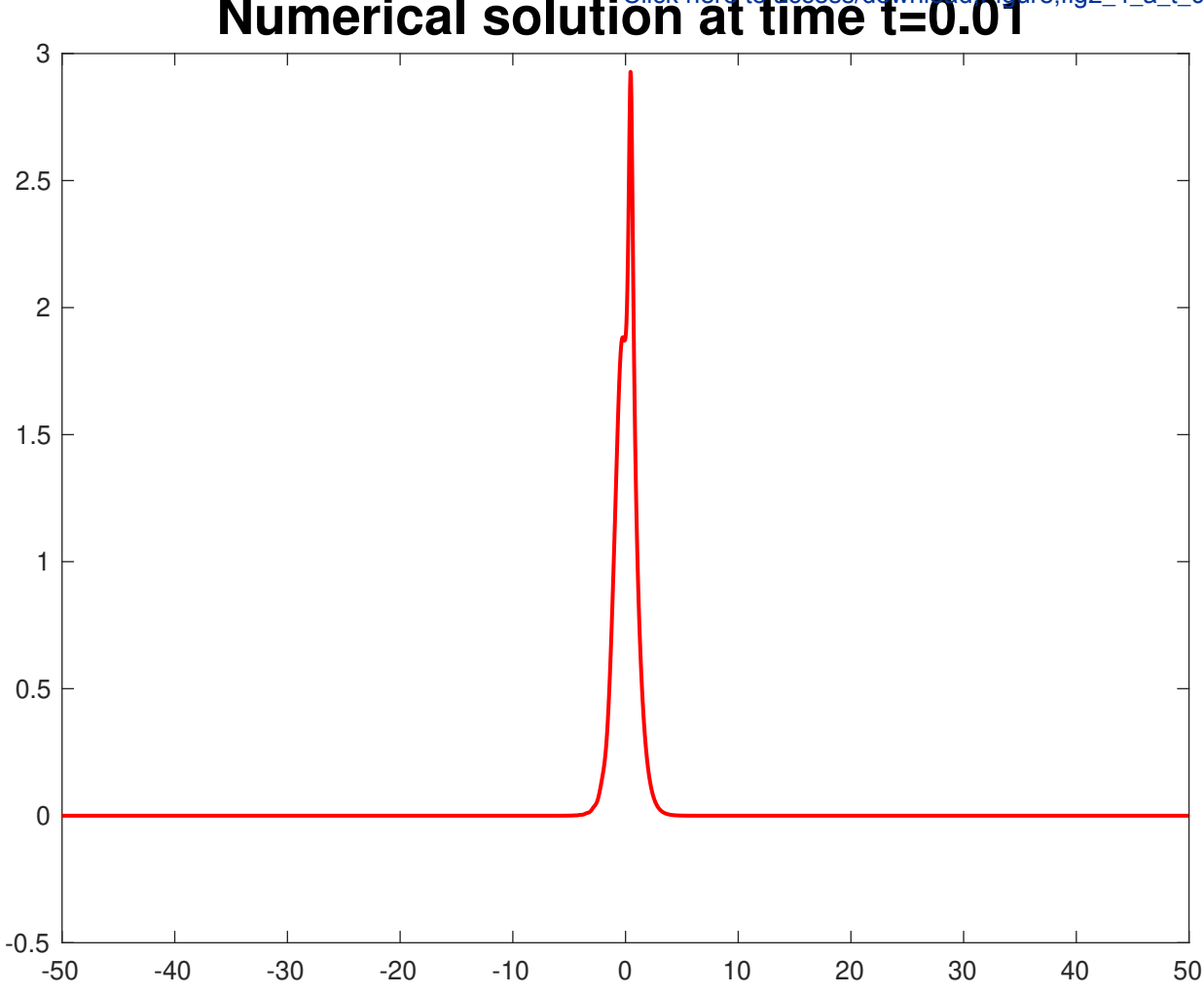

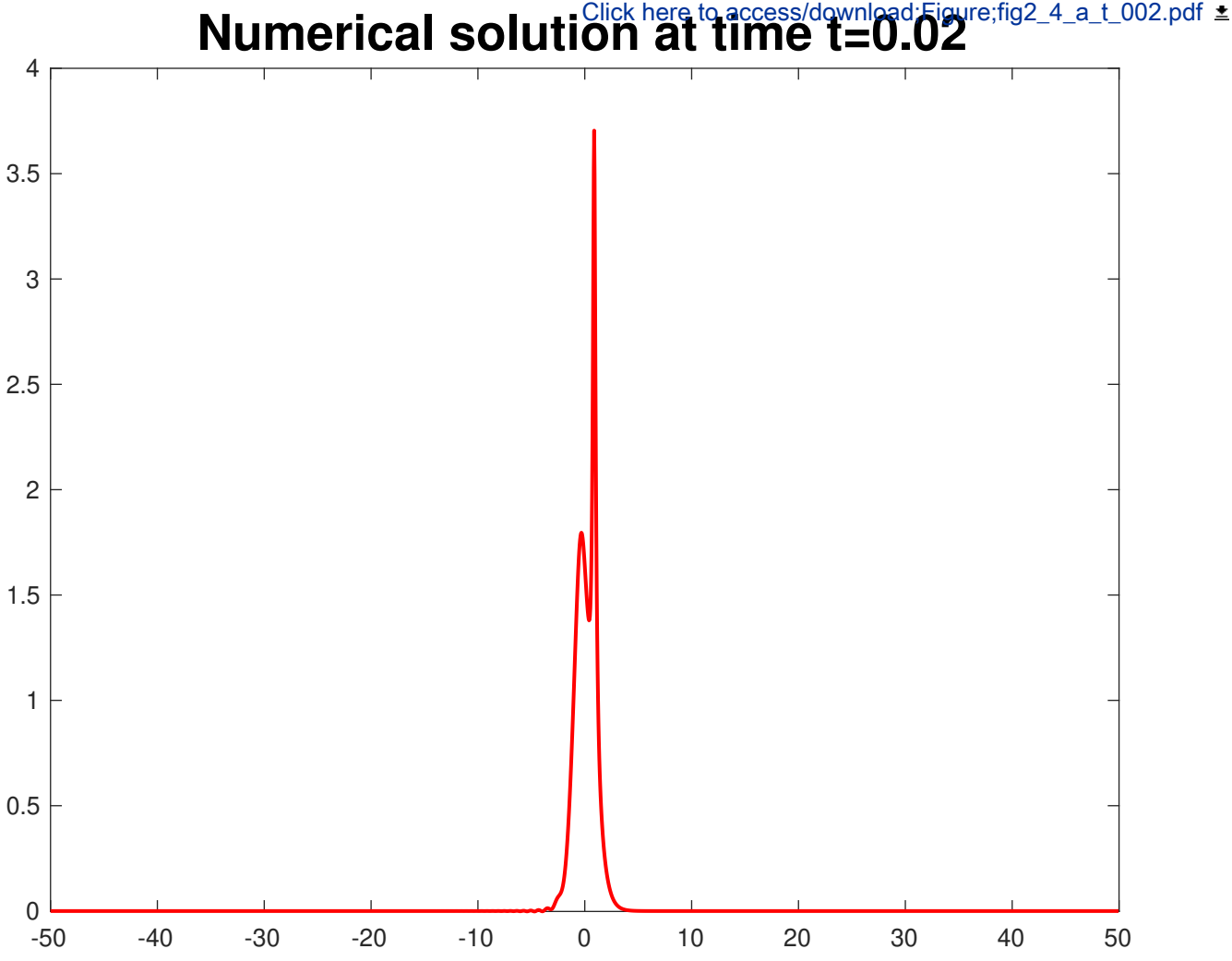

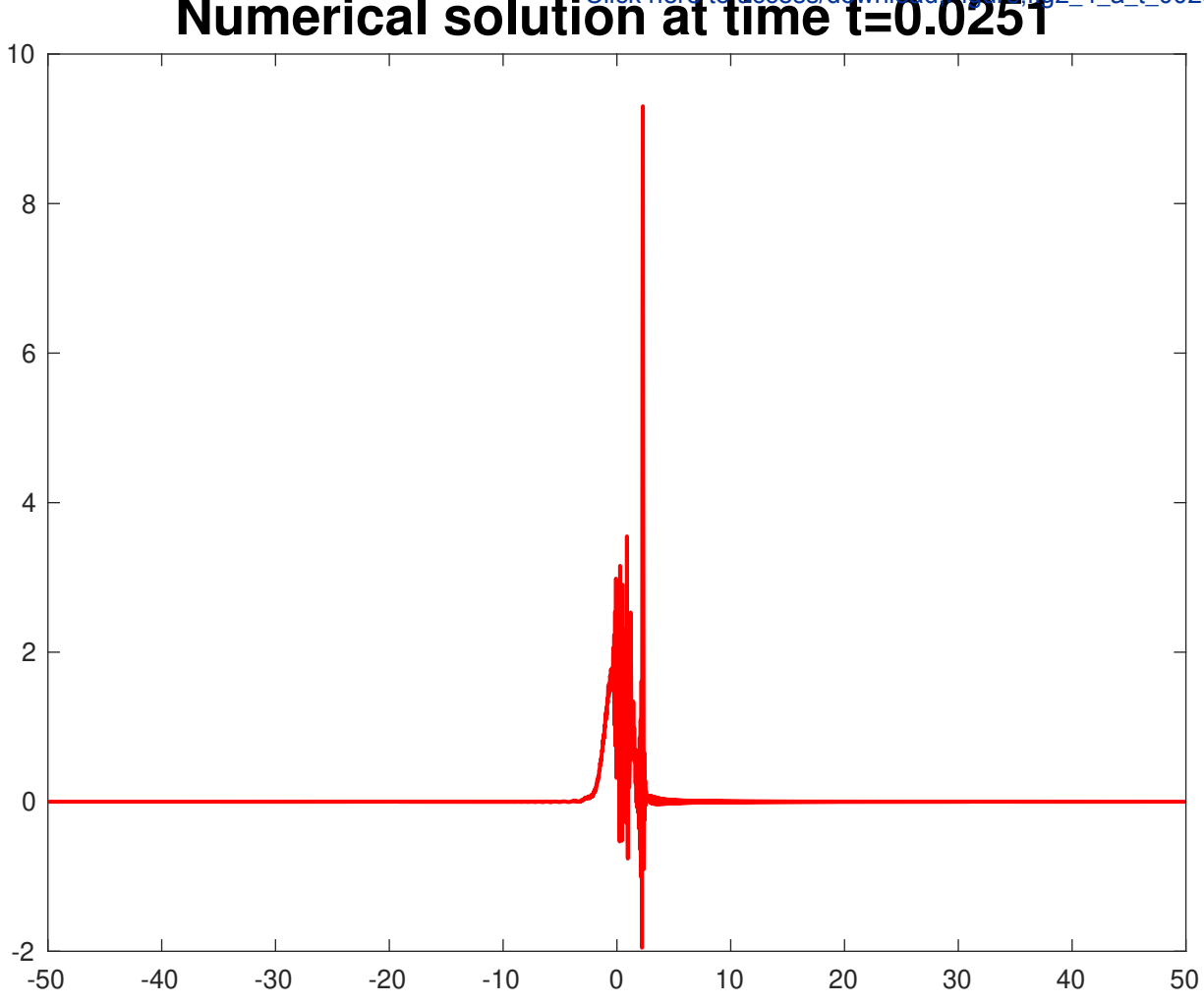

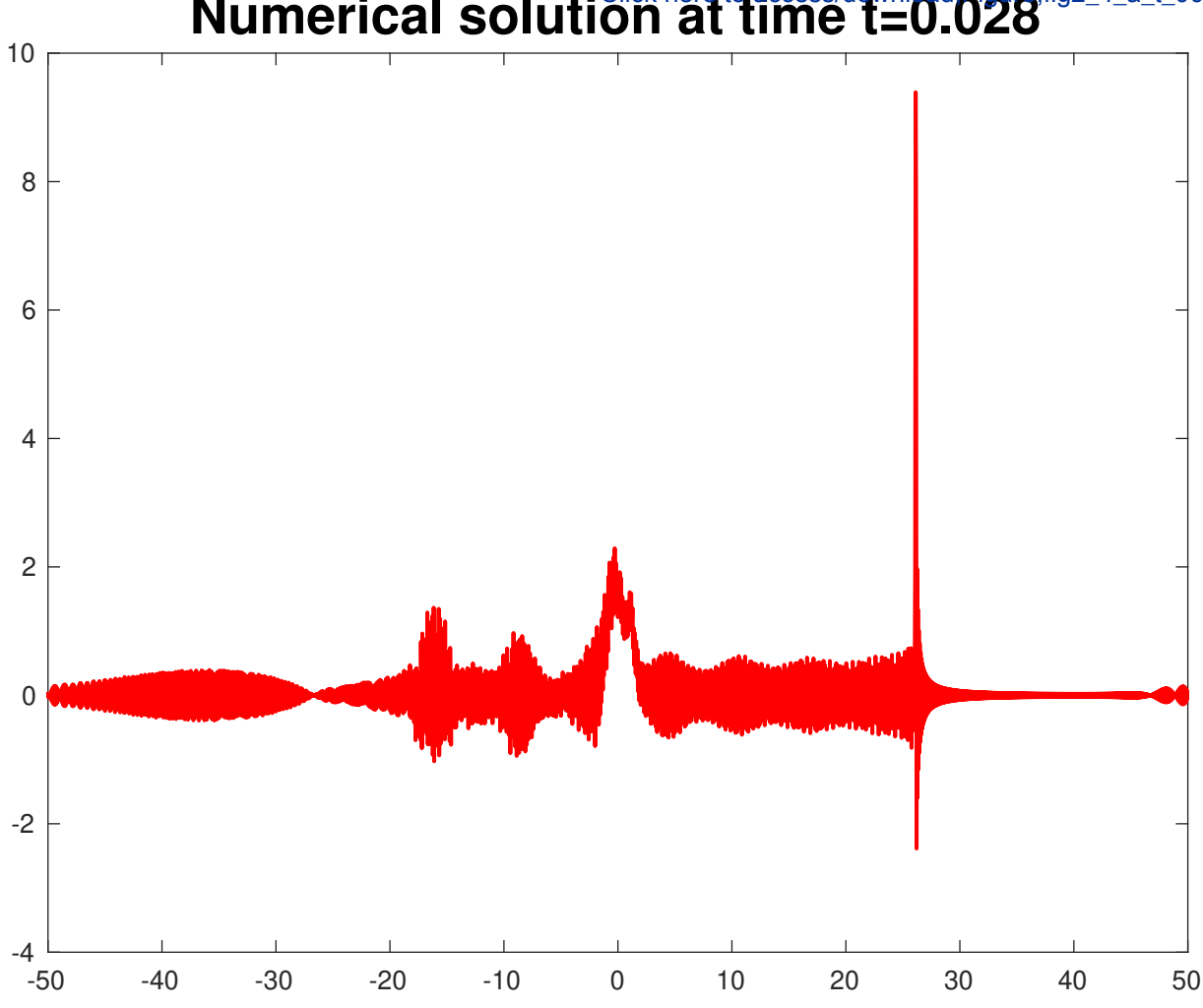

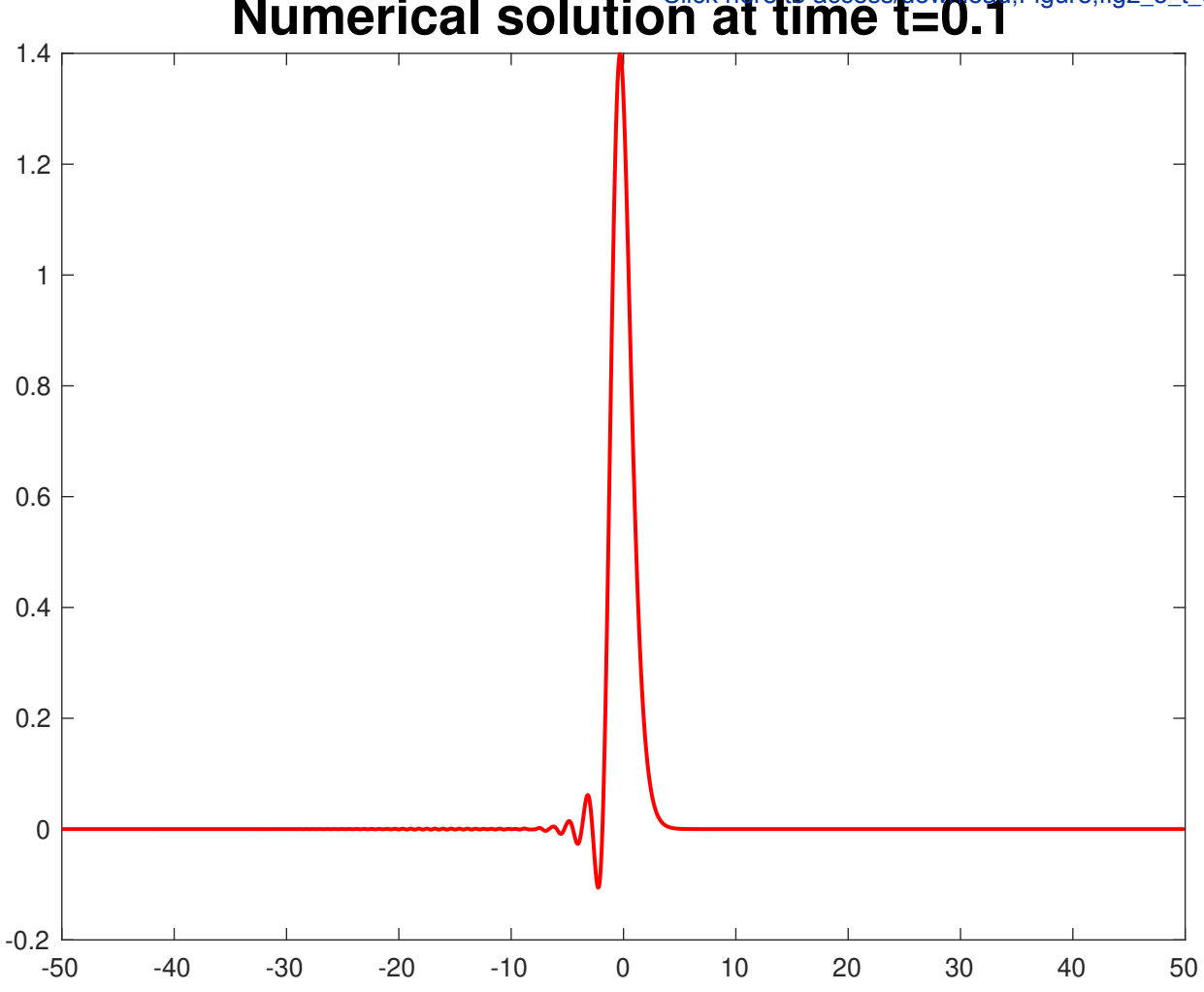

Dear Editor,

We would like to thank you for handling the review of our manuscript entitled "*Numerical study of the generalized Korteweg-de Vries equations with oscillating nonlinearities and boundary conditions*" and for the careful and constructive comments. During the revision, we have addressed every suggestion/comment in the review. We have highlighted all the changes in red to make them easy to track. As a result of the revision, we believe that our paper has been strengthened further. Our point-by-point response to the individual review comments can be found in what follows.

Reviewer #1:
The authors use numerical methods to verify some theoretical results and point out some interesting open problems. This article is acceptable under some minor revisions.

1. In background and motivation, there is a typo in the Gardner equation.
>>>> This has been changed in page 2
2. The figure numbers are wrong in the context.
>>>> The corrections have been made.
3. The figure numbers ((a), (b), (c), …) are different from the numbers ((A),(B),(C),..) in the captions.
>>>> The correction has been made throughout the paper.
4. There is a typo in the figure 8(f). Please replace pi by \pi.
>>>> This has been updated.
5. The figure 9 is not related to this manuscript.
>>>> The figure 9 is related to the defocusing case.

Reviewer #2:
This is a very good paper! Well written, and novel results. I recommend publication after a minor revision.

1. Before publishing, please fix the referencing of the figures. In the text, the format is "Figure 2.4" etc, while in the captions it is "Fig.3" etc.
>>>> The corrections have been made throughout the paper.

2. Maybe also refer to the paper
"Gabitov, I.R. and Lushnikov, P.M., 2002. Nonlinearity management in a dispersion-managed system. Optics letters, 27(2), pp.113-115."
which introduces similar ideas of non-constant coefficients in the nonlinear term of the Nonlinear Schrodinger Equation.
>>>> The paper, [GL02], has been added in page 6.